CULATE-REINFORCEMENT OF TITANIUM MATRIX COMPOSITES WITH BORIDES

Abdulfatai Jimoh

A thesis submitted to the Faculty of Engineering and the Built Environment, University of the Witwatersrand, in fulfilment of the requirements for the degree of Doctor of Philosophy in Engineering.

August 2010

DECLARATION

I declare that this thesis is my own, unaided work. It is being submitted for the degree of Doctor of Philosophy in Engineering at the University of the Witwatersrand, Johannesburg. It has not been submitted before for any degree or examination in any other University.

Abdulfatai Jimoh

---------- day of ----------, 2010

ABSTRACT

Several research efforts have been directed towards in-situ fabrication of titanium matrix composites (TMCs) from Ti and B_4C powder mixtures as one of the ways to improve the physical and mechanical properties of titanium and its alloys. In this perspective, the present study reports the development of in-situ particulate reinforced titanium matrix composites from TiH_2-B_4C and Ti-B_6O powder mixtures

The relationship between densification and microstructure and mechanical properties (hardness and fracture toughness) of pure Ti and in-situ reinforced titanium matrix composites have been studied in detail using pressureless and hot-pressing techniques. Titanium hydride powder was compacted into cylindrical pellets that were used to produce pure Ti through dehydrogenation and pressureless sintering technique. Various composition of TiH_2-B_4C powder mixtures were initially milled using alumina balls in a planetary mill. The milling was to achieve homogeneous mixing and distribution of the ceramic partially in the TiH_2 powder, as well as uniform distribution of reinforcing phases on the resulting Ti matrix.

Dehydrogenation and conversion of loose powder and compacts of TiH_2 powder was carried out in argon atmosphere and complete removal of hydrogen was achieved at 680 and 715^oC for loose and compacted powder respectively. Pressureless sintering of pure Ti from TiH_2 was carried out between 750-1400^oC, while pressureless sintering and hot pressing of TiH_2-B_4C was carried out in the temperature range1100-1400^oC using 30MPa for hot pressed samples in argon atmosphere. Different sintering times were considered. The microstructure and phase composition of the sintered and hot-pressed materials were characterized using scanning electron microscopy (SEM) and X-ray diffractometry (XRD). Densities of the sintered and hot-pressed materials were measured to determine the extent of densification, while Vickers hardness and indentation fracture toughness were used to measure the mechanical properties of the sintered and hot-pressed materials.

gher densification of above 99% of theoretical density compared to literature where lower densification and swelling was observed. Its Vickers hardness is higher than that of commercial Ti sintered under the same conditions.

Titanium matrix composites (TMCs) with different volume content of in-situ formed reinforcements $(TiB + TiC)$ *were successfully produced. The amount of reinforcements formed increases with increased amount of* B_4C *used in the starting powder mixtures, while the amount of needle-type TiB decrease and size and amount of blocky-type TiB increase with increasing volume fraction of TiB. Dense materials and improved Vickers hardness were achieved by the hot-pressed composites especially at* 1400^oC *compared to the pressureless sintered composites under the same conditions and to the relevant literature. TMCs produced in this study show higher Vickers hardness compared to available data in the literature. The hardness was found to depend on the volume content of the reinforcing phases. However, the fracture toughness obtained is low* $(5.3MPa.m^{1/2})$ *in comparison to pure Ti but is comparable with reported data in the literature.*

The mechanisms leading to the achievement of improved densification and higher hardness and the reasons for lower fracture toughness with different sintering temperature and composition of reinforcements in the composites are critically analysed. It has been shown that pure Ti can be pressureless sintered using TiH_2 *and reinforced Ti matrix composites with improved densification and mechanical properties can be produced from* TiH_2-B_4C *powder mixtures. Further work on the comprehensive study of the mechanical properties of these composites would enhance the industrial potential of using these materials and the processing route to produce economically feasible titanium matrix composites.*

DEDICATION

To Almighty God for making this research a success and to the most important people in my life: my parents and most especially, my dear wife and my beloved children, Ayomide and Olamide.

NOWLEDGEMENTS

I cannot but continue to glorify God for all HE has done in my life and most importantly the completion of this degree. HIS truly the alpha and omega and with HIM nothing is impossible. My profound gratitude and appreciations goes to the following persons for *their valuable contributions which facilitated the completion of this research work.*

Professor I. Sigalas: For your financial assistance, effective supervision, words of encouragement and mentorship, and most importantly your moral support and fatherly love without which this study couldnôt have been easy. Prof, thank you so much!

Dr. M. Herrmann: For your excellent and effective advice, useful and expertise comments, time and constructive criticism during the laboratory work and the writing of this thesis.

Dr. S.A. Abdulkareem and Dr. Ayo Afolabi: 'For God use good people to actualize HIS design and good fortune for the creationô. I cannot but continue to thank you guys for facilitating my PhD study at University of the Witwatersrand. Truly, a friend in need is a friend in deed!

This acknowledgment wouldnôt have been completed without appreciating the good love, moral and financial assistance enjoyed from **Engr. and Mrs. Olukayode John Ayanlowo** right from the days of my first degree up till this moment.

My appreciation also goes to the management of **Federal University of Technology Minna, Nigeria** for the study fellowship opportunity granted me.

I sincerely appreciate the support of the DST/NRF Centre of Excellence in Strong Materials (CoE-SM) and Financial Aid Office of the University of the Witwatersrand.

eciation to Mr Olugbenga Johnson for his assistance in getting good hardness test and SEM images, Mr Alex Normal of School of Civil Engineering for his assistance in carrying out compaction test, support staff of the School of Chemical and Metallurgical Engineering (University of the Witwatersrand) namely, Aubrey, Shadrack, Bruce, Doctor and Theo for their assistance with specimen preparation and use of equipment.

Friendship and fellowship of Mr. Davide, Mr. Rodwell, Mr. Ronald, Mr. Simba, Mr. Philip, Mr. Enoch, Mrs. Sibo, Aunty Maria, Aunty Gladys, Mama and all staff and postgraduate students in the School of Chemical and Metallurgical Engineering is also appreciated.

Once again, I wish to thank **mum** and **dad**, for their moral and spiritual support, and for giving me good educational background upon which I build.

Finally, to my beautiful queen (**Titilayo**, alias **Mama T**). Thanks for your continued love, support, patience and endurance, above all for taking good care of the family throughout this period.

BLE OF CONTENTS

DECLARATION ii
ABSTRACT iii
DEDICATION v
ACKNOWLEDGEMENTS vi
LIST OF FIGURES xii
LIST OF TABLES xix
LIST OF TABLES xix
LIST OF SYMBOLS xxi
Chapter One 1
1.0 Introduction 1
Chapter Two 5
2.0 Literature Review 5
2.1 Metal Matrix Composites (MMCs) 5
2.1.1 Material Selection for MMCs 6
2.1.1.1 Reinforcement Selection 6
2.1.1.2 Metal Matrix Selection 7
2.2 Titanium Matrix Composites (TMCs) 7
2.2.1 Boron compounds as reinforcements for TMCs 11
2.2.1.1 Titanium Monoboride (TiB) 13
2.2.1.2 Titanium Diboride (TiB_2) 15
2.2.1.3 Titanium Carbide (TiC) 15
2.2.1.4 B_4C-Ti Composites. 16
2.3 Titanium Matrix Composite (TMC) Processing 19
2.3.1 Conventional Powder-Metallurgy 21
2.3.2 Solidification Processing 21
2.3.3 Combustion Synthesis 22
2.3.4 The Exothermic Dispersion (XD^{TM}) Process 23

MA) 25
2.3.6 Rapid Solidification Processing (RSP) 26
2.3.7 Reactive Hot Pressing (RHP) 26
2.3.8 Other Techniques 27
2.4 Thermodynamic of in situ reaction System 28
2.4.1 Ti-C system 28
2.4.2 Ti-B and Ti-TiB_2 System 29
2.4.3 Ti-B_4C System 30
2.5 Formation mechanism of in situ ceramic phases in Ti-C, Ti-B_4C System 32
2.6 Microstructural characteristics of in situ TMCs 33
2.6.1 Morphology, size and distribution of in situ reinforcements in Ti-based composites 33
2.6.2 Factor influencing particle size and morphology 34
2.6.2.1 Cooling rate of the melt 34
2.6.2.2 Synthesis temperature and holding time 35
2.6.2.3 Chemistry of matrix and reactants 35
2.6.3 Interfaces between in situ reinforcement and metal matrix 35
2.7 Mechanical properties of in situ TMCs 36
2.8 Titanium hydride as the source of titanium matrix for TMCs fabrication 41
2.8.1 Titanium hydride powders 42
2.8.2 Forms of titanium hydrides 42
2.8.3 Conversion of titanium hydride to titanium (Dehydrogenation process) 44
2.8.4 Titanium alloys and composite production from titanium hydride 48
Chapter Three 51
3.0 Experimental Procedure 51
3.1 Introduction 51
3.2 Materials and Chemicals 51
3.3 Materials and Characterization 51
3.4 Equipment Description 54
3.4.1 Particle size analyzer 54

RF) 55
3.4.3 Thermogravimetric analyzer (TGA)/Differential thermal analyzer (DTA) 55
3.4.4 Planetary ball mill 56
3.4.5 Rotary evaporator 57
3.4.6 Tube furnace/ Oxygen getter furnace 57
3.4.7 Uniaxial hot press 59
3.4.8 Capsule 60
3.5 Sample preparation 60
3.5.1 Mixing of TiH_2 -B_4C and Ti-B_6Opowders 61
3.5.2 Compaction test 62
3.6 Sintering and dehydrogenation processing of powders 63
3.6.1 Pressureless sintering of commercial titanium powder 63
3.6.2 Conversion of TiH_2 to Ti through dehydrogenation and pressureless sintering. 64
3.6.3 In situ synthesis of TMC through dehydrogenation and pressureless sintering of blended TiH_2-B_4C powder mixtures. 65
3.6.4 In situ synthesis of TMC through hot ï pressing of blended TiH2-B4C powder mixtures. 66
3.6.5 Nomenclature of pressureless sintered and hot pressed samples 67
3.7 Characterization of dehydrogenated and sintered samples 68
3.7.1 X-Ray Diffraction (XRD) 68
3.7.2 Density measurements 69
3.7.3 Polishing of the samples 70
3.7.4 Scanning Electron Microscopy (SEM)/ Energy Dispersive X-Ray (EDX) and Optical Microscopy 72
3.7.5 Hardness (Hv) and measurements 72
Chapter Four 74
4.0 Experimental Results 74
4.1 Introduction 74
4.2 Characterization of the starting powders. 74

ressureless sintering of TiH_2. 75
4.3.1 Dehydrogenation of TiH_2. 75
4.3.2 Pressureless sintering of TiH_2 and Ti compact 76
4.4 Mixing and characterization of TiH_2-B_4C powders for titanium matrix composite (TMC)..... 82
4.5 In situ synthesis of titanium matrix composite (TMC) from TiH_2 and B_4C powder mixture 87
4.5.1 Pressureless sintering of TiH_2-B_4C for Ti matrix composites 88
4.5.2 Hot-pressing of TiH_2-B_4C for Ti matrix Composites..... 98
4.5.3 Hot-pressing of Ti-B6O for Ti matrix composite 110
Chapter Five 119
5.0 Discussion of results..... 119
5.1 Introduction..... 119
5.2 Compaction and dehydrogenation behaviour of commercial TiH_2 powder. 119
5.3 Relationship between densification and microstructure. 122
5.3.1 Pressureless sintered materials..... 122
5.3.2 Hot pressed composite materials..... 132
5.4 Relationship between hardness and microstructure 137
5.5 Ti-B_6O composites 147
Chapter Six 150
6.0 Conclusions and Recommendations..... 150
Reference 155
Appendices 169
Appendix A: *Calculation of Stoichiometric amount of TiH_2 and B_4C powder*..... 169
Appendix B: *Particle size distribution of starting powders:* 175
Appendix C: *XRD patterns of used starting powders and sintered samples:* 176
Appendix D: *SEM micrographs of sintered and hot pressed samples* 178

IST OF FIGURES

Figure 2. 1: Ti-B phase diagram (source: Gorsse *et al.*, 1998) 12
Figure 2. 2**:** Ti-C phase diagram (Source: Vallauri *et al.*, 2008)..... 16
Figure 2. 3: Schematic Representation of four methods of producing titanium matrix composites (Source: Ranganath. 1997)..... 20
Figure 2. 4: Schematic diagram of XD process for producing metal and Intermetallic-matrix composites (Source: Ranganath. 1997)..... 25
Figure 2. 5 The change of Gibbs free energy qG as a function of temperature for reaction in equation 2.2, 2.3 and 2.4 (Source: Cai *et al.*, (2006)..... 30
Figure 2. 6: Change of Gibbs free energy qG as a function of temperature for reactions (2.5) and (2.6) (Source: Zhang *et al.*, (1999)..... 31
Figure 2. 7: Variation of compressive yield strength with temperature for 15 vol. % TiB/Ti and 15 vol. %(TiB+ TiC)/Ti composites and unreinforced Ti. (Source: Ma *et al.*, 2000). 38
Figure 2. 8: Variation of steady-state creep rate with applied stress for unreinforced Ti (solid symbol) and 25 vol. % Ti2C/Ti composite (open symbol) (Source: Ranganath *et al.*, 1996) 40
Figure 2. 9: Ti-H phase diagram (Source: Sandim *et al.*, 2005) 44
Figure 2. 10: DTA plots of TiH_2 powders milled for different times: (a) as-received (b) 1 h, and (c) 4 h. (Source: Bhosle *et al.*, 2003) 46
Figure 2. 11: DTA/TGA plot for 4 h milled TiH_2 powder: (a) weight percent and (b) temperature difference (Source: Bhosle *et al.*, 2003) 46
Figure 2. 12: TGA curves for TiH_2 powder for heating rates varying from 5 to 20^{o}C/min (Source: Sandim *et al.*, 2003) 48
Figure 3. 1: SEM micrograph of (a) titanium (b) titanium hydride (c) boron carbide and (d) boron suboxide powder. 52
Figure 3. 2: Particle Size Analyzer (Malvern Mastersizer 2000) 54
Figure 3. 3: TGA/DTA machine (run under argon atmosphere)..... 55
Figure 3. 4: Planetary ball mill, PM100 56
Figure 3. 5: Rotary Evaporator..... 57

oxygen getter furnace 58
Figure 3. 7: Uniaxial hot pressing machine used for the sintering of composites..... 59
Figure 3. 8: Drawing of capsule used 60
Figure 3. 9: Comparison of the compaction behaviour of as received commercial titanium hydride 63
Figure 3. 10: Temperature profile for pressureless sintering of comm. Ti. 64
Figure 3. 11: Temperature profile for dehydrogenation and pressureless sintering of titanium hydride compacts 65
Figure 3. 12: Temperature profile for hot pressing of TiH_2-B_4C mixture to form titanium matrix composites 67
Figure 3. 13: Schematic representations of a Vickers indent. 72
Figure 4. 1: XRD patterns of dehydrogenated (a) TiH_2 powder at 680 ^oC and (b) TiH_2 compact at 715 ^oC. 76
Figure 4. 2: XRD patterns of pressureless sintered comm. Ti at (a) 1200 ^oC and (b) 1400 ^oC 78
Figure 4. 3: XRD patterns of dehydrogenated and pressureless sintered TiH_2 powder and compacts at various sintering temperatures. 79
Figure 4. 4: SEM micrographs of as sintered TiH_2 at (a) 750^oC, (b) 900^oC, (c)1000^oC,(d) 1200^oC (e) 1400^oC (f) light micrograph of etched sintered Ti obtained from TiH_2 at 1400^oC; sintered commercial Ti at (g) 1200^oC and (h)1400^oC for reference. 81
Figure 4. 5: EDS graphs of as sintered TiH_2 samples at(c) 1400^oC 82
Figure 4. 6: XRD patterns of mixed TiH_2 and B_4C powders at initial state of (a) 10 vol. % reinforced TMC (b) 20 vol. % reinforced TMC of (c) 40 vol. % reinforced TMC and (d) 60 vol. %reinforced TMC (e) 80 vol. % reinforced TMC 85
Figure 4. 7: SEM of mixed TiH_2 and B_4C powders (green body) of (a) 10 vol. % reinforced TMC (b) 20 vol. % reinforced TMC (c) 40 vol. % reinforced TMC (d) 60 vol. % reinforced TMC (e) 80 vol. % reinforced TMC; EDX of mixed TiH_2 and B_4C powders (green body) of (a) 10 vol. % reinforced Ti matrix composite. 87

ressureless sintered 10 vol. % TMC at (a) 1100^{0}C (b) 1200^{0}C (c) 1300^{0}C and (d) 1400^{0}C..... 92
Figure 4. 9: XRD patterns of pressureless sintered 20 vol. % TMC at (a) 1100^{0}C (b) 1200^{0}C (c) 1300^{0}C and (d) 1400^{0}C..... 93
Figure 4. 10: XRD patterns of pressureless sintered 40 vol. % TMC at (a) 1100^{0}C (b) 1200^{0}C (c) 1300^{0}C and (d) 1400^{0}C..... 93
Figure 4. 11: SEM micrographs of pressureless sintered 10 vol. % TMC at (a) 1100^{0}C (b) 1200^{0}C 95
Figure 4. 12: EDS graphs of reinforcements in as sintered sample 10PLTMC1400 . 95
Figure 4. 13: SEM micrographs of pressureless sintered 20 vol. % TMC at (a) 1100^{0}C (b) 1200^{0}C..... 96
Figure 4. 14: EDS graphs of reinforcements in as sintered sample 20PLTMC1400 . 96
Figure 4. 15: SEM micrographs of pressureless sintered 40 vol. % TMC at (a) 1100^{0}C (b) 1200^{0}C..... 97
Figure 4. 16: EDS graphs of reinforcements in as sintered sample 40PLTMC1400 . 97
Figure 4. 17: XRD patterns of hot pressed 20 vol. % TMC at (a) 1100^{0}C (b) 1200^{0}C (c) 1300^{0}C and 103
Figure 4. 18: XRD patterns of hot pressed 40 vol. % TMC at (a) 1100^{0}C (b) 1200^{0}C (c) 1300^{0}C and 104
Figure 4. 19: XRD patterns of hot pressed 60 vol. % TMC at (a) 1100^{0}C (b) 1200^{0}C (c) 1300^{0}C and 104
Figure 4. 20: XRD patterns of hot pressed 80 vol. % TMC at (a) 1100^{0}C (b) 1200^{0}C (c) 1300^{0}C and 105
Figure 4. 21: SEM micrographs of hot pressed 20 vol. % TMC at (a) 1100^{0}C (b) 1200^{0}C (c) 1300^{0}Cand (d) 1400^{0}C..... 106
Figure 4. 22: EDS graphs of reinforcements in hot-pressed sample 20**HP**TMC**1400** 107
Figure 4. 23: SEM micrographs of hot pressed 40 vol. % TMC at (a) 1100^{0}C (b) 1200^{0}C (c) 1300^{0}Cand (d) 1400^{0}C..... 107

inforcements in hot-pressed sample 40HPTMC1400 108
Figure 4. 25: SEM micrographs of hot pressed 60 vol. % TMC at (a) 1100^{0}C (b) 1200^{0}C (c) 1300^{0}Cand (d) 1400^{0}C..... 108
Figure 4. 26: EDS graphs of reinforcements in hot-pressed sample 60**HP**TMC**1400** 109
Figure 4. 27: SEM micrographs of hot pressed 80 vol. % TMC at (a) 1100^{0}C (b) 1200^{0}C (c) 1300^{0}Cand (d) 1400^{0}C..... 109
Figure 4. 28: EDS graphs of reinforcements in hot-pressed sample 80**HP**TMC**1400** 110
Figure 4. 29: XRD patterns of Ti-B_6O powder mixture (80vol%Ti: 20vol% B_6O) at initial state 111
Figure 4. 30: SEM/EDS of Ti-B_6O powder mixture (80vol%Ti: 20vol% B_6O) at initial state 112
Figure 4. 31: XRD patterns of hot pressed 80Ti -20B_6O composites at (a) 1000^{o}C (b) 1100^{o}C (c) 1200^{o}C and (d) 1300^{o}C..... 114
Figure 4. 32: SEM micrographs of hot pressed 80Ti -20B_6O composites at (a) 1000^{o}C (b) 1100^{o}C (c) 1200^{o}C and (d) 1300^{o}C..... 115
Figure 4. 33: EDS micrographs of hot pressed 80Ti -20B_6O composites heat treated at 1200^{o}C (a) TiB spot (b) B_6O spot (c) Light Ti matrix phase (d) B_6O aggregate spot 116
Figure 4. 34: SEM micrographs of hot pressed 80Ti -20B_6O composites at 1000^{o}C showing cracks around unreacted B_6O particles 117
Figure 4. 35: Optical microstructure of hot pressed 80Ti -20B_6O composites at (a) 1000^{o}C (b) 1100^{o}C (c) 1200^{o}C and (d) 1300^{o}C..... 118
Figure 5. 1: Green density of compacts made from Ti and TiH_2 powders relative to theoretical densities of 4.51g/cm^3 for Ti and 3.91g/cm^3 for TiH_2. 119
Figure 5. 2: Macrograph of green compact from TiH_2 powder with broken corner at higher compaction pressure (>393MPa). 121

ıtive density of pressureless sintered samples of commercial Ti (44ε m) and Ti obtained from TiH_2 against sintering temperature.. 122
Figure 5. 4: SEM micrographs of the sintered TiH_2 at (a) 750^{o}C, (b) 900^{o}C, (c) 1200^{o}C,..... 124
Figure 5. 5: Phase diagram of Ti-B system (Source: Gorsse et al., 98) The dotted parallel lines represent the sintering temperature region under consideration..... 125
Figure 5. 6: Phase diagram of Ti-C system (Source: Vallauri et al., 2008) the dotted parallel lines represent the sintering temperature region under consideration..... 126
Figure 5. 7: Density of pressureless sintered Ti matrix composites as a function of sintering temperature. 128
Figure 5. 8: SEM micrographs of 10vol. % reinforced Ti matrix composites at (a) 1100^{0}C (b) 1400^{0}C..... 129
Figure 5. 9: SEM micrographs of 20vol. % reinforced Ti matrix composites at (a) 1100^{0}C (b) 1400^{0}C..... 129
Figure 5. 10: SEM micrographs of 40vol. % reinforced Ti matrix composites at (a) 1100^{0}C (b) 1400^{0}C..... 130
Figure 5. 11: Density of pressureless sintered Ti matrix composites as a function of volume fraction (%) of in-situ formed reinforcements (TiC + TiB). 131
Figure 5. 12: Density of hot-pressed Ti matrix composites as a function of sintering temperature..... 133
Figure 5. 13: SEM micrographs of hot-pressed 20vol. % reinforced Ti matrix composites at (a) 1100^{0}C 134
Figure 5. 14: SEM micrographs of hot-pressed 40vol. % reinforced Ti matrix composites at (a) 1100^{0}C 134
Figure 5. 15: SEM micrographs of hot-pressed 60vol. % reinforced Ti matrix composites at (a) 1100^{0}C 135
Figure 5. 16: SEM micrographs of hot-pressed 80vol. % reinforced Ti matrix composites at (a) 1100^{0}C 135
Figure 5. 17: Density of hot-pressed Ti matrix composites as a function of volume fraction (%) of in-situ formed reinforcements (TiC + TiB)..... 136

(Hv_{-5}) of pressureless sintered Ti from TiH_2 and commercial Ti against the sintering temperature. 138

Figure 5. 19: Comparison of the Vickers hardness of as sintered pure Ti from TiH_2, and commercial Ti carried out in this work against the commercial Ti of different grades sintered by Zadra *et al.*, (2008)..... 139

Figure 5. 20: Graph comparing the hardness of pressureless sintered and hot-pressed composites at 1400^{o}C in argon atmosphere. Hardness values were measured using 5kg load. 140

Figure 5. 21: SEM image of sample (a) **PL**1200**TiH_2**90 (b) 20**HP**TMC**1400** (c) 40**HP**TMC**1300** 141

Figure 5. 22: Vickers hardness (Hv-5) of pressureless sintered Ti matrix composites as a function of volume fraction (%) of in-situ formed reinforcements (TiC + TiB)143

Figure 5. 23: Vickers hardness (Hv-5) of hot-press sintered Ti matrix composites as a function of volume fraction (%) of in-situ formed reinforcements (TiC + TiB) 144

Figure 5. 24: Comparing Vickers hardness values of composites s obtained in this work and those obtained by other researchers..... 145

Figure 5. 25: Comparing the fracture toughness of some selected Ti matrix composites produced with those obtained from the literature by different author... 147

Figure 5. 26: Hot-pressed sample **HP**8Ti2B_6O**1300** (a) SEM micrograph (b) Optical micrograph..... 149

Figure B. 1: Particle size analysis of Pure B_6O powder: d (0.1) = 1.214µm, d (0.5) = 2.819 µm, d (0.9) = 6.440µm 175

Figure B. 2: Particle size analysis of commercially obtained titanium, Ti-powder: d (0.1) = 15.672µm, d (0.5) = 30.492µm, d (0.9) = 55.166µm..... 175

Figure B. 3: Particle size analysis of commercially obtained titanium hydride powder: d (0.1) = 1.925 µm, d (0.5) = 4.473 µm, d (0.9) = 9.409 µm..... 175

Figure C. 1: XRD patterns of (a) titanium (-44ε m), (b) titanium hydride and (c) boron carbide powder 176

Figure C. 2: XRD patterns of dehydrogenated TiH_2 sample at different temperatures 177

of the pressureless sintered sample 40PLTMC1200 showing equiaxed TiB and porosity 178
Figure D. 2: SEM (SE) image of the pressureless sintered sample 40PLTMC1400 showing TiB formed 178
Figure D. 3: SEM image of hot pressed sample 20HPTMC1400 showing different sizes of TiB and TiC formed 179
Figure D. 4: SEM image of hot pressed sample 40HPTMC1400 showing types of TiB formed 179
Figure D. 5: SEM image of hot pressed sample 60HPTMC1400 showing higher magnification of blocky TiB formed 180

LIST OF TABLES

Table 2. 1: Properties of ceramic reinforcements commonly used in MMCs (Source: Ibrahim *et al.*, 1991)..... 6
Table 2. 2: Summary of room temperature tensile properties of titanium matrix composites (TMCs) (Source: Ranganath, 1997). 9
Table 2. 3: Properties of ceramic reinforcements commonly used in TMCs (Source: Ranganath (1997); *Madtha *et al.*, (2008) 10
Table 2. 4: Properties of TiB reinforcement, compared with titanium and other titanium compounds..... 14
Table 2. 5: Mechanical properties of discontinuously reinforced Ti and Ti alloys having different Vol. % TiB reinforcements (Source: Chandran *et al.*, 2004) 14
Table 2. 6: Mechanical properties of 10vol. % (TiB + TiC)/Ti composites fabricated by reactive hot pressing (RHP) (Source: Ni *et al.*, 2006) 19
Table 2. 7: Tensile properties of in situ titanium matrix composites (TMCs) (Source: Tjong and Ma, 2000)..... 37
Table 2. 8: Apparent stress exponent and apparent activation energy for creep of composites (titanium matrix composites, TMCs) and unreinforced Ti. (Source: Ranganath *et al.*, 1996) 40
Table 2. 9: List of the titanium hydrides in the Ti-H phase (Source: Wang *et al.*, 2002) 43
Table 2. 10: Peak transformation temperatures during 20 K/min constant heating rate experiments in DTA. (Source: Bhosle *et al.*, 2003) 47
Table 3. 1: Materials and chemicals used during experimental work..... 53
Table 3. 2: Preparation Method for Grinding..... 71
Table 3. 3: Preparation method for Polishing..... 71
Table 4. 1: Phase composition observed during dehydrogenation of TiH_2 powder and compact. 75
Table 4. 2: Density, phase composition and mechanical property of pressureless sintered (Isothermal sintering time, 90min) sample of comm. Ti and Ti from comm. TiH_2..... 77

ty of mixed powders TiH_2, B_4C and corresponding volume % reinforcements (TiC, TiB) expected in the final TMC Composites. 83

Table 4. 4: Density, Vickers hardness and phase composition of pressureless sintered (isothermal sintering time 90min) titanium and 10vol. % reinforced titanium composites at different sintering temperatures. Assumed theoretical density = 4.54g/cm^3 89

Table 4. 5: Density, Vickers hardness and phase composition of pressureless sintered (isothermal sintering time 90min) 20vol% reinforced titanium composites at different sintering temperatures. Assumed theoretical density = 4.55g/cm^3 90

Table 4. 6: Density, Vickers hardness and phase composition of pressureless sintered (isothermal sintering time 90min) 40vol% reinforced titanium composites at different sintering temperatures. Assumed theoretical density = 4.57g/cm^3 91

Table 4. 7: Density, Vickers hardness and phase composition of hot pressed (isothermal sintering time 120min) 20vol%TMC from TiH_2-B_4C mixture at different temperatures. Assumed theoretical density = 4.55g/cm^3 98

Table 4. 8: Density, Vickers hardness and phase composition of hot pressed (isothermal . sintering time 120min) 40vol%TMC from TiH_2-B_4C mixture at different temperatures. Assumed theoretical density = 4.57g/cm^3. 99

Table 4. 9: Density, Vickers hardness and phase composition of hot pressed (isothermal sintering time 120min) 60vol%TMC from TiH_2-B_4C mixture at different temperatures. Assumed theoretical density = 4.60g/cm^3 100

Table 4. 10: Density, Vickers hardness and phase composition of hot pressed (isothermal sintering time 120min) 80vol%TMC from TiH_2-B_4C mixture at different temperatures. Assumed theoretical density = 4.62g/cm^3 101

Table 4. 11: Density and mechanical properties of Ti-B_6O composites hot pressed at different temperatures (P = 50MPa, t = 20min). Assumed theoretical density = 4.55g/cm^3 113

Table A 2. 1 : Compaction data for titanium powder 172

Table A 2. 2: Compaction data for titanium hydride powder 173

LIST OF SYMBOLS

SEM	=	*Scanning Electron Microscopy*
TMC	=	*Titanium Matrix Composite*
EDX	=	*Energy Dispersive X-ray Spectroscopy*
XRD	=	*X-ray diffraction*
ICSD	=	*International Centre for Diffraction Data*
Hv	=	*Vickers hardness*
K_{IC}	=	*Fracture toughness*
GPa	=	*GigaPascal*
MPa	=	*MegaPascal*
hr(s)	=	*hour(s)*
min(s)	=	*minute(s)*
µm	=	*micron*
wt%	=	*Weight percent*
^{o}C	=	*degrees Celsius*
K	=	*degrees Kelvin*
''w'''	=	*Whiskers*

Chapter One

1.0 Introduction

Titanium and titanium alloys are used for highly demanding applications such as in the fabrication of some of the most critical and highly-stressed civilian and military aircraft parts, in chemical processing, nuclear power plants, food processing plants and oil refinery heat exchangers (Yamada, 1996, Christoph and Manfred, 2003; Seagle, 1996; Larsson *et al.*, 1996).

This wide range of applications have been attributed to its excellent properties such as low density, high specific strength, heat resistance, corrosion resistance, low temperature resistance and excellent biocompatibility (Yu *et al.,* 1999; Han *et al.,* 2000; Grosgogeat *et al.,* 1999; Schmidt *et al.,* 1998 and Odwani *et al.,* 1998; Abdallah, 1996).

However, applications of titanium and titanium alloys to other fields are limited by several other shortcomings that include poor plastic deformation, low modulus, high friction coefficient, low thermal conductivity coefficient and low wear resistance, in addition to high cost of production (Yu *et al.,* 1999; Han *et al.,* 2000; Grosgogeat *et al.,* 1999; Schmidt *et al.,* 1998; Odwani *et al.,* 1998).

Suggestions have been made that the physical and mechanical properties of titanium can be improved through the incorporation of reinforcing compounds using the principle of metal matrix composites (MMCs) (Cai *et al.,* 2006; Saito, 2004). This is because MMCs combine the properties of ceramics and metals to produce materials with attractive properties like good shear strength, high temperature strength etc. (Ibrahim et *al.*, 1991; Tjong and Ma, 2000; Kim *et al.*, 2001). However, titanium matrix composites (TMCs) were identified as the best form of MMCs that can provide the best combination of high specific strength, rigidity, corrosion resistance,

sistance and good wear resistance required for drastic enhancement of titanium and titanium alloyôs physical and mechanical properties (Kim *et al.*, 2001; Yang *et al.*, 2006).

Titanium matrix composites (TMCs) also face challenges that include selection of an ideal reinforcement, as well as high performance processing methods (Ranganath, 1997). Among the existing reinforcements, titanium monoboride (TiB) has been judged the best compared to the existing reinforcing compounds like TiC, SiC, TiB_2, B_4C, Al_3O_4, TiN, and Si_3N_4 because of its outstanding physical and mechanical properties with linear coefficient of thermal expansion that is approximately the same as that of titanium alloys (Saito, 2004).

In the processing methods, in situ techniques where reinforcements are synthesized in Ti-matrix during sintering or casting are considered better for TMCs production than conventional techniques (ex situ) where the reinforcement are directly incorporated into a matrix (Ni *et al*., 2006). Novel processing techniques based on in situ approach has been reported to provide new opportunities for the development of titanium matrix composites (TMCs) with small grain size, uniformly distributed reinforcing particles, and improved mechanical properties (Zhang, *et al.*, 1999a; Wang *et al.*, 2006). In situ techniques have been extensively studied because of those advantageous properties but the problem of high cost, enhanced processing route and excellent performance of the final TMCs is still under investigation for proper understanding and further improvement.

Almost all reported studies on TMCs used commercial titanium powder to provide the matrix for their investigations (Ni *et al.*, 2006, Zhang *et al.*, 1999a, Radhakrishna Bhat *et al.,* 2002). The commercial titanium powder, apart from being expensive also contains some impurities (e.g. oxygen, manganese, chlorine, nitrogen, iron, silicon, magnesium etc), thereby raising concerns on the cost effectiveness and total quality (purity) of the final composites. A possible alternative source for Ti matrix could be

h can be prepared at high purity and low grain sizes with better cost-effectiveness (Saito, 2004); while B_4C powder is also a promising reinforcement ceramic material of Ti and Ti alloys for a variety of applications that require elevated hardness, good wear and corrosion resistance (Dariel *et al.*, 2002) and above all, it is a good source for TiB, TiB_2 and TiC particulate for reinforcing titanium matrix (Ranganath *et al.*, 1992; Ranganath, 1997; Radhakrishna Bhat *et al.,* 2002). Therefore, the introduction of B_4C powder would lead to a reasonable cost reduction in comparison to using commercial TiB and TiC powder separately to reinforce titanium matrix. Furthermore, the introduction of TiH_2 powder as source of titanium is expected to enhance the quality and overall cost of the final TMCs.

In light of the literature review, the present research shall consider the feasibility of producing titanium matrix composites (with TiB_2, TiB and TiC reinforcements) from titanium hydride powder (as the source of titanium matrix) and ceramic (B_4C and B_6O) powders as the precursor for the ceramic particulate reinforcement phase using in-situ techniques with pressureless sintering and hot pressing methods. This aim can be achieved by studying the simultaneous dehydrogenation and pressureless sintering of TiH_2 to form pure Ti in an argon atmosphere; this will be followed by in situ chemical reaction and characterization of TiH_2-B_4C and Ti-B_6O powder mixtures to form reinforcing phases in titanium matrix composites, followed by full characterization and analyses of morphology change and properties (e.g. density and hardness) of TMCs produced. Successful completion of these tasks is expected to lead to an economically feasible processing route for titanium matrix composites (TMCs) with improved properties when compared to the currently used one.

In achieving the above aim and objectives a detailed literature review on the principles, mechanisms, and techniques for producing TMCs are presented in Chapter 2. This will also cover challenges in the manufacturing of TMCs with the current processing route, theoretical background, thermodynamic evaluation and in situ

matrix, TiH_2, boride, and carbide. Chapter 3 presents detailed information and explanation on the starting materials, methodology, experimental equipments and techniques used in this research. Detailed experimental results and analysis of the experimental work carried out in this research are presented in Chapter 4. Chapter 5 present comprehensive discussions of the experimental results with emphasis on the effect of sintering conditions on mechanical properties such as density, hardness and microstructures, while Chapter 6 contains the conclusions drawn from the work done, as well as recommendations for future work and refinements that can be carried out on identified challenges.

Chapter Two

2.0 Literature Review

This section reviews the available research works that has been done in the area of improving the properties of titanium and its alloys using the principle of metal matrix composite (MMC).

2.1 Metal Matrix Composites (MMCs)

Metal matrix composites (MMCs) refer to a kind of synthesized material in which a rigid ceramics reinforcement is embedded in a ductile metal or alloy matrix. The synthesized material combines the excellent properties of ceramics (high strength and modulus) and metals (ductility and toughness), leading to a greater strength in shear and compression and to higher service temperature capabilities (Ibrahim et *al.*, 1991; Tjong and Ma, 2000; Kim *et al.*, 2001; and Kuebler *et al.*, 2007). Tjong and Ma (2000) reported extensively on the attractive physical and mechanical properties such as high specific modulus, strength, and thermal stability and others that can be achieved with MMCs. Interest in MMCs, for use in aerospace, automotive and other structural applications has increased over the 25 years and this has been attributed to the availability of relatively inexpensive reinforcements, and development of various processing routes which result in reproducible microstructures and properties (Tjong and Ma, 2000; Ibrahim *et al.*, 1991). A good advantage of MMC as it affects the aerospace industry is reduction in structural weight; this can be achieved not only by reducing the alloy density, but also by increasing its modulus. For instance, a 50% increase in modulus through substitution of a discontinuous silicon carbide reinforced aluminium alloy for an unreinforced wrought counterpart resulted in a 10% reduction in weight (Ibrahim *et al.*, 1991). For more understanding of the principle involved, the mechanism of reinforcement, the processing routes, current developments in fabrication of MMCs, their microstructures and mechanical properties the reader is referred to the review articles of Ibrahim *et al.* (1991) and of Tjong and Ma (2000).

2.1.1.1 Reinforcement Selection

There are necessary criteria or conditions that must be satisfied for the selection of a ceramic as reinforcement in the manufacture of good and standard metal matrix composites. Such criteria include density, melting temperature, size and shape, elastic modulus, tensile strength, thermal stability, compatibility with matrix material, coefficient of thermal expansion, and cost (Ibrahim *et al.*, 1991). Some selected properties of commonly used ceramics in MMCs are shown in Table 2.1.

Table 2. 1: Properties of ceramic reinforcements commonly used in MMCs (Source: Ibrahim *et al.*, 1991).

Metals	*Ceramic*	*Density* ($x\ 10^{-3}\ kg\ m^{-3}$)	*Expansivity* ($10^{-6}\ ^0C^{-1}$)	*Young's Modulus (GPa))(Saito, 2004)*	*Knoop Hardness (GPa)(Saito, 2004)*	*Elastic Modulus (GPa)*
Al, ,Mg,	Al_2O_3	*3.98*	*7.92*	*350*	*22.5*	*379*
Ti	*AlN*	*3.26*	*4.84*	-	-	*310*
Ti, Al, Mg, Cu	B_4C	*2.52*	*6.08*	*449*	*27.5*	*448*
Ti, Cu, Al, Mg	*Si*	*2.33*	*3.06*	-	-	*112*
Al, Mg, Cu, Ti	*SiC*	*3.21*	*5.40*	*420*	*25.0*	*430*
Ti	*TiB*	*4.56*	*11.32*			*427*
Ti, superalloys	TiB_2	*4.52*	*8.28*	*529*	*34.0*	*500*
Ti, Cu	*TiC*	*4.93*	*7.60*	*460*	*24.7*	*440*
Al, Ti	*VC*	*5.77*	*7.16*	-	-	*434*
superalloys	*WC*	*15.63*	*5.09*	-	-	*669*
Al , Ti	ZrB_2	*6.09*	*8.28*	-	-	*503*

Selection of metal or its alloy as matrix for production of MMC depends on the type, required properties and the kind of application where such composite is required. For instance, requirements of low density, with reasonably high thermal conductivity, have made aluminium and magnesium alloys the most commonly used matrices (Ibrahim et al., 1991). However, Kim et al. (2001) pointed out that among various MMCs developed, titanium matrix composites (TMCs) provide the best combination of high specific strength, rigidity, and good wear resistance required for drastic enhancement of physical and mechanical properties of titanium and titanium alloys, thus, providing the justification for selection of titanium as a matrix in the production of metal based composites.

2.2 Titanium Matrix Composites (TMCs)

Titanium matrix composites (TMCs) are advanced materials made of titanium or titanium alloy matrices mixed either with continuous or discontinuous reinforcements. They exhibit several excellent properties such as corrosion resistance, high specific strength, high specific modulus, heat resistance etc. (Yang *et al.*, 2006). There are two families of titanium matrix composites, continuously reinforced and discontinuously reinforced TMCs (Dariel *et al.*, 2002). The early work on titanium matrix composites considered continuous fibre reinforced composites and the industrial use of the composites produced was restricted to highly specialized applications (Ranganath, 1997). The reasons attributed were prohibitive cost of continuous fibres, complex fabrication routes, limited formability and high anisotropic properties of composites produced (Ranganath, 1997).

Discontinuously reinforced (particulate) TMCs have attracted more attention compared to continuous fibre reinforced composites. This is because of their properties of isotropy, easy secondary operation, improved mechanical properties,

d economic benefits (Cai *et al.,* 2006). Typical applications for discontinuous or particulate titanium matrix composites include, (i) Creep resistant engine components, (ii) Wear parts such as gears, bearings and shafts, (iii) Erosion-corrosion resistant tubing (Cai *et al.,* 2006). However, particulate titanium matrix composites (TMCs) are also faced with challenges that include selection of ideal reinforcements, as well as high performance processing methods (Ranganath, 1997). Despite highlighted properties and advantages exhibited by particulate reinforced titanium matrix composites (which enhanced their industrial applications), many complex problems still exist that affect the overall mechanical properties of the final composites. Such problems include the need to obtain a clean matrix/particle interface (Ranganath, 1997) because in TMCs, many reinforcements are unstable and different types of reaction products form depending on the reinforcing phase. It is therefore necessary to understand the factors that influence the physical and mechanical properties of the composites since they are sensitive to the type of reinforcement, method of manufacture and processing/heat treatment used (Ranganath, 1997). Table 2.2 summaries the tensile properties of various titanium matrix composites (TMCs) at room temperature as reported in the literature up to the present.

Almost all reported studies on TMCs used commercial titanium powder as the matrix for their investigations. The commercial titanium powder, apart from being expensive also contains some impurities (e.g. oxygen, manganese, chlorine, nitrogen, iron, silicon, magnesium etc- M/S Alfa Aesar, Germany), thereby raising questions on the total quality (purity) of the final composites. In the light of the above, a possible alternative source for Ti matrix could be titanium hydride (TiH_2), which can be prepared at high purity and low grain sizes (Saito, 2004). This is the main motivation behind present research considering the feasibility of using titanium hydride as the source of titanium matrix by converting it to titanium and consequently use the dehydrogenated titanium to manufacture TMCs.

erature tensile properties of titanium matrix composites (TMCs) (Source: Ranganath, 1997).

Reinfor./Ti matrix	*Vol. % Reinfor.*	*Processing methods*	*Modulus (MPa)*	*Yield. Stress (MPa)*	*Ultimate tensile strength (MPa)*	*% E*	*Reference*
Ti	*0*	*Melting*	*108*	*367*	*474*	*8.3*	Johnson *et al.*, 1991
TiC/Ti	*37*	*Melting*	*140*	*444*	*573*	*1.9*	Johnson *et al.*, 1991
TiC/Ti	*40-50*	*Induction Melting*	-	-	*1113*	*1-2*	Chen *et al.*, 1989
TiB-Ti_2C/Ti	*15*	*CAS*	*137*	*690*	*757*	*2.0*	Ranganath, 1996
Ti-6Al-4V	*0*	*Hot pressing*	-	*868*	*950*	*9.4*	Loretto and Konitzer, 1990
TiC/Ti-6-4	*10*	*Hot pressing*	-	*944*	*999*	*2.0*	Loretto and Konitzer, 1990
SiC/Ti-6-4	*10*	*Hot pressing*	-	-	*655*	*0.16*	Loretto and Konitzer, 1990
TiC/Ti-6-4	*10*	*Cold + HP*	-	*792*	*799*	*1.1*	Abkowitz and Weihrauch, 1989
TiC/Ti-6-4	*20*	*Cold + HP*	*139*	*943*	*959*	*0.3*	Shang and Ritchie, 1990
TiB_2/TiAl	*7.5*	*XD*	-	*793*	*862*	*0.5*	Christodoulou *et al.*, 1988
Ti-6Al-4V	*0*	*IM*	*110*	*923*	*1000*	*10*	Lederich *et al.*, 1994
TiB/Ti-6Al-4V	*3.1*	*IM*	*124*	*986*	*1076*	*10*	Lederich *et al.*, 1994
Ti-6Al-4V	*0*	*RSP*	*110*	*930*	*986*	*11*	Lederich *et al.*, 1994
TiB/Ti-6Al-4V	*3.1*	*RSP*	*121*	*1000*	*1107*	*7*	Lederich *et al.*, 1994
Ti-6Al-4V	*0*	*Vacuum hot press*	*120*	-	*890*	-	Smith and Froes, 1984
Si-6Al-4V	*35-40*	*Vacuum hot press*	*225*	-	*820*	-	Smith and Froes, 1984
BORISC/Ti-6-4	*35-40*	*Vacuum hot press*	*205*	-	*895*	-	Smith and Froes, 1984
B_4C/Ti-6Al-4V	*35-40*	*Vacuum hot press*	*205*	-	*1055*	-	Smith and Froes, 1984
SCS-Ti-6Al-4V	*35-40*	*Vacuum hot press*	*240*	-	*1455*	-	Smith and Froes, 1984

An ideal reinforcing compound for TMCs manufacture places special demands that must be fulfilled; such demands include: high hardness, heat resistance and rigidity, thermodynamic stability in the titanium and titanium alloys at the sintering temperature, insolubility in the titanium matrix and the titanium atoms in the reinforcing compound (minimum mutual solubility), and crystallographic stable matrix/particle boundaries (Saito, 2004; Ibrahim *et al.* 1991). It should be noted that structural efficiency of discontinuously reinforced TMCs is a function of the density, elastic modulus, and tensile strength of the reinforcing phases (Ibrahim *et al.* 1991). Chemical stability and compatibility of the reinforcements with the matrix materials are very important both during fabrication and for the end application because lack of

debonding of the reinforcement from the matrix (Ranganath, 1997; Ibrahim *et al.* 1991).

Also, lack of stability of the second phase can lead to the formation of undesirable interfacial products. Both situations can therefore lead to premature failure of the components produced from such materials during service (Ranganath, 1997; Ibrahim *et al.* 1991). Besides, the difference between the coefficients of thermal expansion of the reinforcement and matrix must be minimized in order to minimize strain accumulation, especially for composites that will be exposed to thermal cycling (Ibrahim *et al.* 1991). Some selected properties of commonly used ceramics in TMCs are shown in Table 2.3

Table 2. 3: Properties of ceramic reinforcements commonly used in TMCs (Source: Ranganath (1997);

Ceramic	*Density (g/cm^3)*	*M.Pt. (K)*	*Thermal conductivity ($J.cm^{-2}.S^{-1}.K^{-1}$)*	*Thermal Expansion ($10^{-6}\ ^0C^{-1}$)*	*Poisson's ratio*	*Elastic modulus (MPa)*	*Tensile Strength (MPa)*
B_4C	*2.51*	*2720*	*0.273-0.290*	*4.78(25-500 ^0C)*	*0.207*	*445*	*158(980 ^0C)*
*TiB**	*4.56*	-	-	*7.15-11.32(20-1380 ^0C)*	*0.11 and 0.16*	*427 and 371*	-
TiB_2	*4.52*	*3253*	*0.244-0.260*	*4.6-8.1*	*0.09-0.28*	*500*	*129*
TiC	*4.99*	*3433*	*0.172-0.311*	*6.52-7.15(25-500 ^0C)*	*0.188*	*440*	*120(1000 ^0C)*
SiC	*3.19*	*2970*	*0.168*	*4.63(25-500 ^0C)*	*0.183-0.192*	*430*	-
ZrB_2	*6.09*	*3373*	*0.231-0.244*	*5.69(25-500 ^0C)*	*0.144*	*503*	*201*

*Madtha *et al.*, (2008)

Several reinforcing phases have been used in producing TMCs and these include SiC, TiC, TiB_2, Al_2O_3, TiN, Si_3N_4, TiB, Nd_2O_3, Y_2O_3, B_4C etc. (Cai *et al.*, 2006; Xu *et*

inforcements, Titanium monoboride (TiB) has been identified as the best reinforcement for TMCs (Table 2.3) because of its chemical compatibility with Ti, outstanding physical and mechanical properties (such as high elastic modulus) with linear coefficient of thermal expansion that is approximately the same as that of titanium and titanium alloys (Saito, 2004; Xu *et al.*, 2005; Gorsse and Miracle, 2003). Similarly, TiC has been reported as having potential as a good reinforcement for TMCs because of its high hardness, high modulus and high flexural strength (Yang *et al.* (2006; Saito, 2004; Xu *et al.*, 2005). Therefore, composites combining TiB and TiC as reinforcements offer an attractive combination of excellent mechanical properties, good wear resistance, corrosion resistance etc. Yang *et al.* (2006) also confirmed that a combination of both TiC and TiB as reinforcement in TMCs is now being considered as the best reinforcement.

Review of relevant literature has shown that in addition to commercial TiB and TiC powders, commercial TiB_2 and graphite powder had also been used for the in-situ formation of stable TiB and TiC particles reinforcement (Ranganath *et al.*, 1992; Saito, 2004; Yang *et al.*, 2006). Recent researches however have shown that B_4C powder is also a promising reinforcement ceramic material of Ti alloys for a variety of applications that require elevated hardness, good wear and corrosion resistance (Dariel *et al.*, 2000), above all, it is a good source for TiB, TiB_2 and TiC particulate for reinforcing titanium (Ranganath *et al.*, 1992; Ranganath, 1997; Radhakrishna Bhat *et al.*, 2002) as will be shown in the next section.

2.2.1 Boron compounds as reinforcements for TMCs

Three boron compounds exist in the Ti-B system (Fig. 2.1). These include TiB, T_3B_4, and TiB_2 (Chandran *et al.*, 2004). Based on the phase diagram shown in fig. 2.1, the equilibrium phases of the titanium-boron system are classified into:

mperature *body-centered cubic* (beta) titanium, low-temperature *hexagonal close-packed* (alpha) titanium, and *rhombohedral* (beta) boron.

(ii) ***Intermetallic compounds*** ð TiB (monoboride) and TiB_2 (diboride), as well as Ti_3B_4 (formed only in a narrow temperature range).

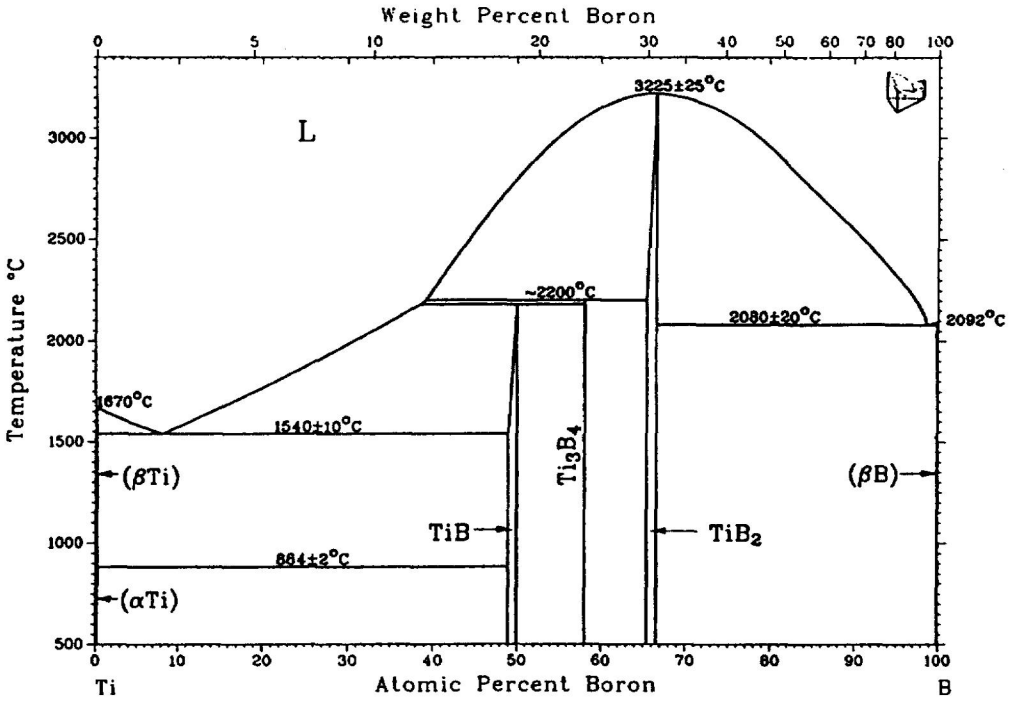

Figure 2. 1: Ti-B phase diagram (source: Gorsse *et al.*, 1998)

As seen in figure 2.1, the technically important titanium-rich section of the Ti-B binary system has a *eutectic* reaction (liquid ð > beta titanium + TiB) at 1540 °C and 1.64 wt. % B (6.88 at. % B). TiB has a tendency to rapidly segregate to the grain boundaries, and boron itself is slightly soluble with solubility of less than 1at.% in the high-temperature BCC (beta) and low-temperature HCP (alpha) titanium (***www.calphad.com/titanium-boron.html, October 2009***).

of titanium-base alloys may be increased by the precipitation of TiB intermetallic phase. However, the ductility and fracture toughness are retained only if the amount of boron is less than the eutectic composition (hypo-eutectic Ti-B alloys). It is important to emphasize that the eutectic point can shift significantly when other alloying elements are added ***(www.calphad.com/titanium-boron.html, October 2009).***

2.2.1.1 Titanium Monoboride (TiB)

The use of TiB as reinforcement is attractive because Ti and TiB are in equilibrium (Chandran *et al.*, 2004). TiB is a line compound (B27 structure) in the Ti-B system (Madtha *et al.*, 2008). It forms as a primary phase by peritectoid reaction during solidification, but the phase formed is relatively coarse and often contains internal holes. TiB has high hardness, stiffness, and strong Ti-B covalent bonding (Madtha *et al.*, 2008). Other advantages of TiB over other titanium compounds like TiC, TiN, Ti_3Si_5, and TiB_2 are the lower temperature (900-1100^{0}C) for solid state composite processing and formation of long pristine single-crystal whiskers in the titanium matrix. These enhance the stiffness and strength of the composites formed. Table 2.4 lists some of the properties of TiB reinforcement along with those of TiC, TiB_2 and TiN. Many workers had carried out different studies on TiB-Ti composites (Gorsse *et al.*, 1998; Tsang *et al.*, 1997; Saito, 1993a, b, 1995 and 2004; Abkowitz *et al.*, 2004; Ravi Chandran *et al.*, 2002; Yolton and Moll, 1996). Table 2.5 summaries the mechanical properties of TiB-Ti composites developed by these researchers.

ement, compared with titanium and other titanium compounds (Source: Chandran *et al.*, 2004)

Property	*Ti*	*TiB*	*TiB_2*	*TiC*	*TiN*
Density (g/cm^3)	*4.57*	*4.56*	*4.52*	*4.92*	*5.43*
Elastic modulus (GPa)	*110*	*371*	*540*	*450*	*390*
Coeff. of thermal exp. at RT (K^{-1})	*8.6×10^{-6}*	*7.15×10^{-6}*	*6.2×10^{-6}*	*7.95×10^{-6}*	*9.35×10^{-6}*
Vickers hardness (HVN)	*150*	*1800*	*2200*	*3200*	*2300*
Melting/decomposition temp. (^0C)	*1.668*	*2200*	*2970*	*3054*	*3220*

Table 2. 5: Mechanical properties of discontinuously reinforced Ti and Ti alloys having different Vol. % TiB reinforcements (Source: Chandran *et al.*, 2004)

Matrix composition (wt. %)	Vol. % TiB	E (GPa)	σ_y	σ_y	% E	Processing Method	Reference
Ti	15	139	842	903	0.4	VAR+hot swaging	Tsang et al., 1997
Ti (ASTM Grade-4)	0	110	480	550	15.0	Wrought	Boyer et al., 1994
Ti-6Al-4V	10	136.6	-	1,000	0.25	MA+HIPing	Godfrey et al., 2000
Ti-24Al-10Nb (at. %)	10	-	*	695	0.0	PM+HIPing	Emura et al., 1996
Ti-6Al-4V	11	144	1.315	1,470	3.1	GA+HIPing/extrusion	Yolton and Moll, 1996
Ti-5Al-2.5Fe	15	151	*	1.092	0.0	PM+HIPing	Hagiwara et al., 1992
Ti	20	148	*	673	0.0	PM	Ravichandran and Panda, 2002
Ti-6Al-4V	20	145-	1.170	-	2.5	MA+HIPing	Saito et al., 1993
Ti-4.3Fe-7Mo-1.4Al-1.4V	0	110	-	1.080	17.5	MM+CIP+sinter.+hot swaging	Saito et al., 1995
Ti-4.3Fe-7Mo-1.4Al-1.4V	10	134	-	1.380	~7	MM+CIP+sinter.+hot swaging	Saito et al., 1995
Ti-4.3Fe-7Mo-1.4Al-1.4V	20	156	-	1.640	~3	MM+CIP+sinter.+hot swaging	Saito et al., 1995
Ti-4.3Fe-7Mo-1.4Al-1.4V	30	180	-	1.820	~1	MM+CIP+sinter.+hot swaging	Saito et al., 1995
Ti-6.4Fe-10.3Mo	34	163.2	*	737	0.49	PM	Chandran et al., 2004
Ti-24.3Mo	34	171.2	*	1.105	0.85	PM	Chandran et al., 2004
Ti-53Nb	34	122.12	710	724	1.65	PM	Chandran et al., 2004
Ti-6Al-4V	20	170	1.181	1.251	0.5	PM+E	Gorsse and Miracle, 2003
Ti-6Al-4V	40	210	-	864	0	PM+E	Gorsse and Miracle, 2003

*σ_y: Yield stress, σ_y: Ultimate tensile strength, E: Elastic modulus, %E: Elongation, MA: Mechanical alloying, MM: Mechanical mixing, PM: powder metallurgy processing, GA: argon gas atomization, VAR: vacuum arc melting, CIP: cold isostatic pressing, E: extrusion, *specimen failed before yielding, ~data determined by extrapolation*

(TiB$_2$)

Titanium Diboride, TiB_2 is a covalently bonded ceramic with good properties such as high hardness, high melting point, good chemical stability, and good thermal and electrical conductivity. It is also wetted and resists molten metals and molten halides (Zhang *et al.*, 1995; Kang and Kim, 1990). A times, TiB_2 is considered as the first choice for reinforcing titanium due to the relative high values of melting point, elastic modulus, and hardness (Table 2.1 and 2.3) but the possibility of formation of TiB and T_3B_4 at the Ti- TiB_2 interface was reported to have deterred the composite development (Chandran *et al.*, 2004). TiB_2 is attractive for technological applications such as in making of wear components like mechanical seals, wire drawing and forming dies, in aerospace and in cutting tools (Ogwu and Davies, 1996). However, their poor mechanical impact resistance and moderate oxidation resistance also limit their applications (Zhang *et al.*, 1995). Despite these hindrances, several TiB_2-matrix composites have been developed-such as TiB_2-ZrO_2, TiB_2-Ti (C, N), TiB_2-B_4C and TiB_2-TiC-SiC composites (Zhang *et al.*, 1995).

2.2.1.3 Titanium Carbide (TiC)

Titanium carbide, TiC is an extremely hard refractory ceramic material. It has the highest specific strength and specific modulus (among the transition metal carbides), high melting point and relatively high electrical and thermal conductivities (Lin *et al.*, 1991). TiC has the B1 (or NaCl-type) crystal structure type where the titanium atoms are situated in a face-centered cubic closed-packed arrangement with the octahedral interstitial sites being occupied by the carbon atoms (Vallauri *et al.*, 2008). Due to the excellent physical and mechanical properties exhibited by TiC, it has been widely used as reinforcement in titanium matrix composites (TMCs) (Lu *et al.*, 2001). At the beginning, TMCs produced with TiC as reinforcement were manufactured using either powder metallurgy or casting techniques with TiC particles directly incorporated into solid or liquid matrices. Introduction of novel processing techniques based on in situ techniques already gave birth to TiC reinforced TMCs

2.2 shows the Ti-C phase diagram. Several researchers have worked on the TiC reinforced titanium matrix composites (Chen *et al.*, 1989; Konitzer and Loretto, 1989; Rawers *et al.*, 1990; Loretto and Konitzer, 1990; Shang and Ritchie, 1990; Zee *et al.*, 1991; Liu *et al.*, 1993; Alman and Hawk, 1999; Lu *et al.*, 2001). Table 2.2 shows the properties of TiC reinforced titanium composites produced by some of these researchers.

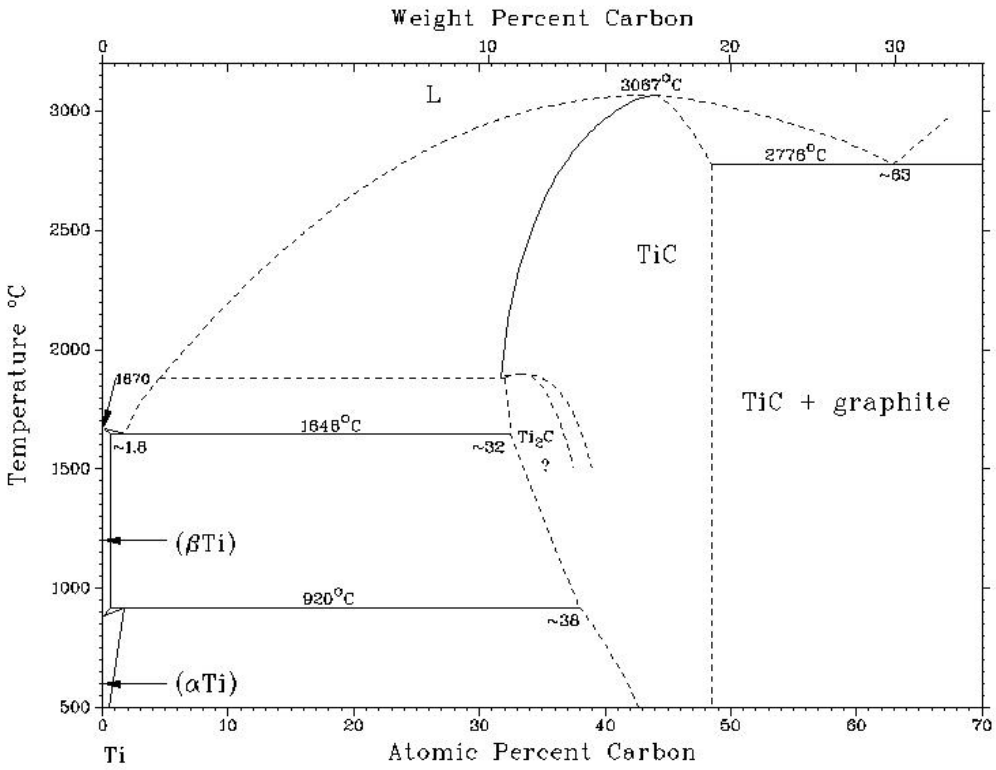

Figure 2. 2**:** Ti-C phase diagram (Source: Vallauri *et al.*, 2008)

2.2.1.4 B_4C-Ti Composites.

Boron carbide is an extremely promising material for a variety of applications that require elevated hardness, good wear and corrosion resistance (Levin *et al.*, 2000)**.** Application of B_4C in the highlighted areas is due to its excellent properties that include high hardness, high wear resistance, high melting point (Table 2.3), good

ss-section for neutron absorption and high thermal conductivity (Jianxin and Junlong, 2009). This material is reported as the third hardest (after diamond and cubic boron nitride) of the technically useful materials (Jianxin and Junlong, 2009). B_4C, currently finds application in the nuclear industry and high-temperature thermo-electric conversion but there is restriction to its wide industrial application because of low strength (about 200-400MPa), low fracture toughness (2-3 MPa $m^{1/2}$) (Jianxin and Junlong, 2009), as well as poor sinterability that results from its low self-diffusion coefficient (Yamada *et al.*, 2003). However, several B_4C based composites, such as B_4C ï SiC, B_4C ï Al, B_4C-CrB_2, B_4C-(W, Ti)C, B_4C-TiB_2, have been developed and used in various applications (Jianxin and Junlong, 2009).

Recent research focuses more attention on the use of Ti and B_4C powder in the manufacturing of in situ TMCs. This is because of the excellent and unique properties exhibited by reinforced particulate TMCs produced when combined reinforcement of particles of TiB and TiC is used, and the possibility of obtaining both reinforcements simultaneously from the reaction of B_4C and Ti powders. Some few works have been reported using Ti- B_4C systems:

In 1992, Ranganath used both conventional melting and combustion synthesis reaction to produce Ti-TiB-TiC composites from the Ti- B_4C system. Tensile testing of hot rolled sample show yield strength, $\sigma_y = 471\text{MPa}$, tensile strength, $\sigma_{TS} = 635\,\text{MPa}$, and elongation value of 1.2 %, while as-cast composite obtained $\sigma_y = 425\,\text{MPa}$, $\sigma_{TS} = 574\,\text{MPa}$, and 1.6 % with Youngôs modulus value of 148GPa. A considerable improvement in strength and modulus compared with the matrix metal, titanium ($\sigma_y = 275\,\text{MPa}$, Youngôs modulus = 116GPa) was achieved and the hot rolling of the composites results in a more uniform distribution of the reinforcing particles.

(TiB +TiC)/Ti matrix composites from Ti, B_4C and graphite powder through a novel in-situ process where traditional ingot metallurgy plus self-propagating high-temperature synthesis (SHS) techniques were used. The composites produced shown uniform distribution of TiB and TiC reinforcement in titanium alloy matrix. TiB formed grows into needle-shape, while formed TiC grows into dendritic-shaped and equiaxed-shaped particles during solidification. The reinforcements are on large scale ranging from less than 1εm to over 100εm. The authors reported that addition of graphite increased the quantity of TiC in the matrix and that the peak intensity of TiC increases with the addition of graphite. It was also reported that 10 and 20 vol. % of (TiB +TiC)/Ti composites with two different compositions (mole ratio of TiB and TiC are 4:1 and 1:1) were successfully produced.

Radhakrishna Bhat *et al.,* (2002) produced discontinuously reinforced titanium matrix composites with TiB and TiC reinforcements by hot pressing process from starting materials of Ti and B_4C powders. The initial composition used was adjusted to have a reinforcement content of 70% by volume (56%TiB and 13%TiC, i.e. 4:1) and 30% by volume Ti- matrix in the final composite. X-ray diffraction analysis confirmed the completion of the reaction and SEM studies revealed the morphology of the reinforcement formed. They concluded that composites produced with TiB + TiC reinforcement have a better strength and toughness with hardness value of 1020Hv and flexural strength value of 629 MPa that was attributed to the presence of needle shape TiB compared to composites with only TiB reinforcement in the form of TiB particulate that has inferior strength and fracture resistance with flexural strength value of 350MPa and hardness value of 1351Hv. According to them, analysis of the fracture morphology of Ti-TiB shows brittle failure, while that of Ti-TiB-TiC shows involvement of large number of needle shaped particles in the fracture process leading to higher strength and toughness

eems to be the most recent on Ti-B_4C system research for titanium matrix composites. They investigated the effect of B_4C particle size on microstructure of in situ titanium matrix composites prepared by reactive processing of Ti-B_4C system. They discovered that TiB clusters were observed in the composites when using B_4C powder of particle size 3.5ε m but none was present when using finer B_4C powders. It was reported that TiB clusters formed during sintering process can only be reduced but not removed completely by hot extrusion. They concluded that the size of B_4C particles affects the microstructure and mechanical properties of the composites formed directly, and the use of finer B_4C powders of a narrow size distribution can produce a finer size of TiB whiskers and prevent the TiB clusters from being formed during the fabrication of composites. Table 2.6 summaries the mechanical properties they obtained at room temperature.

Table 2. 6: Mechanical properties of 10vol. % (TiB + TiC)/Ti composites fabricated by reactive hot pressing (RHP) (Source: Ni *et al.*, 2006)

Sample	*B_4C particle size (μm)*	*Mechanical properties*			
		UTS (MPa)	*% E*	*Modulus(GPa)*	*Vickers hardness*
1	*3.5*	*817*	*0.55*	*140*	*452*
2	*0.5*	*950*	*0.64*	*142*	*581*

2.3 Titanium Matrix Composite (TMC) Processing

For particulate-reinforced TMCs to gain industrial viability, their processing methods must be economically feasible, reliable and must be designed in such away as to produce a composite with a microstructure that will optimize their critical properties (Ranganath, 1997). Ranganath (1997) reported that high melting point and high reactivity (especially in liquid state) of titanium have been identified as major limitations encountered in the process of manufacturing particulate-reinforced TMCs. However, despite these problems, few techniques like solidification processing,

as cold and hot isostatic pressing were reportedly used to produce particulate-reinforced composites with some success (Ranganath, (1997).

In a recent review, Xu *et al.*, (2005) reported several methods that have been used by in-situ techniques to produce TMCs. Such methods include self-propagating high-temperature synthesis (SHS), mechanical alloying (MA), powder metallurgy (PM), rapid solidification powder processing (RSP), reactive hot pressing (RHP), ingot metallurgy techniques (IM) and liquid-liquid or liquid-solid or solid-solid reactions. Among these available techniques for producing TMCs, the solidification processes are more attractive due to their simplicity, economy and flexibility (Zhang *et al.*, 1999). Fig. 2.3 shows a schematic representation of various processing routes for TMCs production.

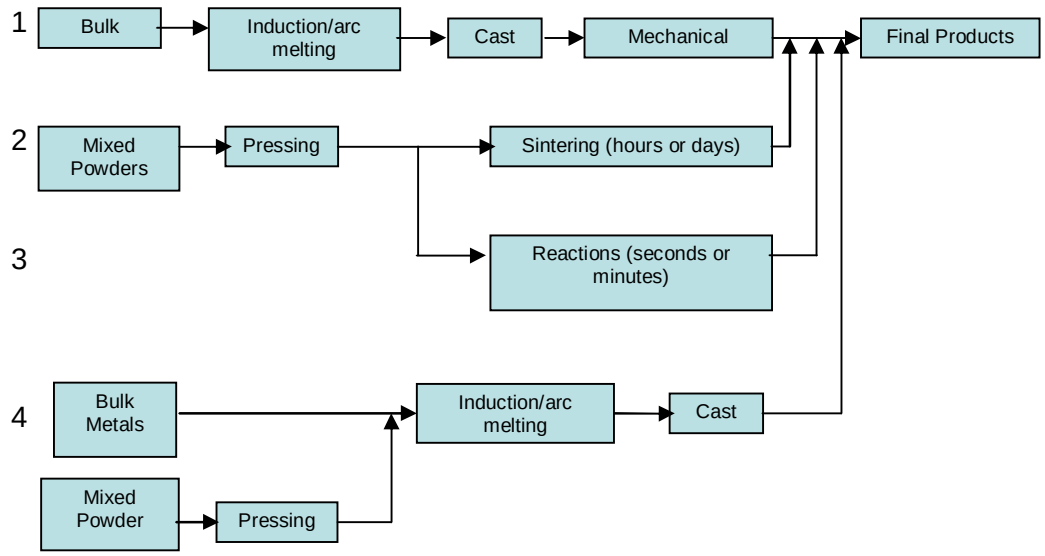

1. Conventional Melting; 2. Powder Metallurgy; 3. Combustion Synthesis; 4. Combustion-assisted Synthesis.

Figure 2. 3: Schematic Representation of four methods of producing titanium matrix composites (Source: Ranganath. 1997)

The powder-metallurgical process of fabricating composites consists of mixing matrix and reinforcing powders, cold isostatic processing (CIP), vacuum sintering and hot isostatic pressing (HIP) or hot working. The process is difficult for production of composites having relatively high reinforcement content because of difficulties in uniform mixing, cold compaction and also the size control of the reinforcements (Kim *et al.*, 2001). However, in 1993 Abkowitz *et al.* reported the use of powder metallurgy technique to fabricate titanium matrix composites (TMCs). The process has also been described as the most viable and promising route for cost effective fabrication of titanium alloy composites (Abkowitz *et al.,* (1993); Moxson et al., 1998).Based on the convinced reports on the wide acceptability of this method in the production of titanium alloy composites (because of its economic reliability and cost effective), the present study considered the method has an appropriate, a more suitable and affordable production route for TMC.

In another way, this method incorporates elemental cold-compactable titanium powder. In this elemental powder blending technique, the correct proportion of master alloy and base elemental powders are blended to obtain a uniform distribution of the required chemical composition. This processing technique has been used to produce 10-20 vol. % TiC particulate-reinforced Ti-6Al-4V composites (Shang and Ritchie, 1990; Liu *et al.*, 1993; Ranganath, 1997), as well as TiB-Ti composite (Abkowitz et al., 2004). Major advantages of this technique are that no additional expensive tools are required and raw material utilization can be maximized. However, the cost of investment is still on the high side when compared to conventional and other emerging techniques. Table 2.2 and 2.5 summarized the properties of composites developed using this method.

2.3.2 Solidification Processing

This is another processing route for manufacturing particulate reinforced titanium composites. The method is not frequently used like other methods in the production of particulate reinforced TMCs because of problems like high reactivity of titanium with the reinforcements in the liquid state and difficulties in the melting and casting of titanium and its alloys. However, Chen *et al.* (1989) reported that there were few successful efforts in this direction, which include the production of Ti-TiC composite by mixing graphite powder and titanium through the induction melting route. Another attempt was in the production of stable high temperature titanium Diboride reinforcements through addition of boron to gamma TiAl alloys (Zee *et al.*, 1991; Ranganath, 1997). See table 2.2 for some of the properties achieved by fabricated composites using this processing route.

2.3.3 Combustion Synthesis

Combustion synthesis or Self-propagating high temperature synthesis (SHS) is another processing technique that involves using the energy released during exothermic reaction for the production of TMCs. This route involves exothermic chemical reactions and the heat liberated is so adequate to sustain the reaction by the rapid propagation of a combustion front without further addition of energy (Subrahmanyam *et al.,* 1989). High enthalpy of reaction is the major requirement for the propagation of a reaction in a self-sustaining mode. According to Ranganath (1997), the combustion synthesis process involves mixing and compaction of powders of the constituent elements into a green compact, followed by igniting a portion of the green compact with a suitable heat source. According to him, this permits the use of low temperature initiation of high temperatures, rather than bulk heating over a long period at lower temperature. He also reported that the heat source for this process could be electrical sparks, lasers, heater wires, conventional furnaces, other reactions etc. The major reported advantage of this processing technique over other processing routes is the self-generation of energy (unlike sintering and plasma

for costly equipment unnecessary (Subrahmanyam *et al.,* 1996; Ranganath, 1997). SHS has also been reported to be useful in the production of near-net shape components and high purity products because of the possibility of all volatile impurities evaporating at very high temperatures.

Subrahmanyam *et al.* 1996 also reported that with slight modification combustion synthesis route can be used to produce titanium matrix composites. Over 350 individual reinforcing phases were reported to have been synthesized through this modification with majority being intermetallic and ceramic compositions. The main problem with this method is intrinsic porosity generation; where products formed expand due to the molar volume change from reactants to reaction products, that resulting in the generation of intrinsic porosity. Christodoulou, *et al.*, (1988b) and Ranganath (1994) said such porosity can be reduced substantially by exothermic dispersion (XD) and combustion-assisted synthesis methods. Literature shows that combustion synthesis has been successfully used to produce TiC, TiB, TiC-TiB and Al-TiB_2 composites (Ranganath and Subrahmanyam, 1991).

2.3.4 The Exothermic Dispersion (XD^{TM}) Process

Martin Marietta Corporation was reported to have developed XD process, which considered as the first step in making materials for conventional metalworking processing-casting, forging, extrusion, rolling and so on (Christodoulou *et al.*,1988; Ranganath, 1997). XD technology involves blending and compaction of elemental powders, followed by igniting the compact that initiated the exothermic reaction and generation of sustainable energy that produces the composites (meaning that the process is based on sustained high temperature synthesis). Figure 2.4 shows the schematic diagram of XD process for producing metal and Intermetallic- matrix composites (Christodoulou *et al.*, 1988; Ranganath, 1997). For instance, XD technology was used for the production of TiAl-TiB_2 composites, where elemental powders (boron, titanium and aluminium) were blended and consolidated into a

ited; the flame front passes through the green compact and spontaneously forms titanium aluminide and titanium diboride. It was reported that because of in situ development of reinforcements, the process eliminates oxide formation that could have weaken the interface between the reinforcement (TiB_2) and the matrix (Christodoulou *et al.*, 1988; Ranganath, 1997). The same authors also reported that TiB_2 particles introduced via XD process offer substantial grain refinement and improved microstructural uniformity compared to un-reinforced TiAl. XD processing is expected to find wide application in the fabrication of compressor cases, vanes, missile fins, turbine disk, shaft housing and turbocharger wheels. Although the XD process is reported to be very cheap it has some limitations such as chemical and thermal stability of the dispersed phase, another possible problem may arise when the reaction between composite forming elements are less exothermic (Christodoulou *et al.*, 1988). See Ranganath (1997) and Christodoulou *et al.* (1988) for more information on this processing method. Composites developed using this method as well as some of their key properties are shown in table 2.2.

XD process has been successfully used to produce variety of metal matrix composites (MMCs) with Ti, TiAl, and Ti_3Al as matrices and borides, nitrides, and carbides as reinforcements but there is no mention of using the processing method to generate TMC composites from Ti and B_4C mixture.

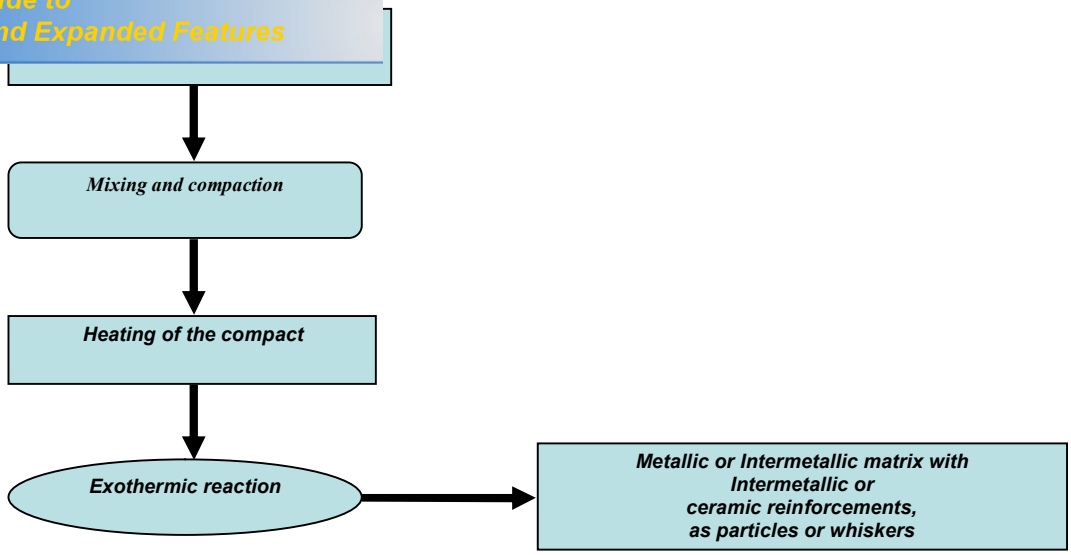

Figure 2. 4: Schematic diagram of XD process for producing metal and Intermetallic-matrix composites (Source: Ranganath. 1997)

2.3.5 Mechanical Alloying (MA)

MA is a solid state powder processing method which involves repeated cold drawing and fracture of particles resulting from high energy ball-sample collision (Tjong and Ma, 2000). In this process, the starting constituent phases (powder mixture) are subjected to mechanical milling techniques (e.g. ball milling), after which the milled powder mixture is heat treated at the desired temperature. This method can be used to produce fine-grained alloyed powder particles in metal-metal and metal-ceramic composite system (Benjamin, 1970; 1974; 1976). MA method has been extensively used to produce in situ ceramic particle reinforced MMCs (Tjong and Ma, 2000). Lu *et al.,* (1998) used the MA method to investigate the possibility of forming in situ TiB_2 particulate from elemental Ti and B powders in a system diluted with Al. They reported that a low volume concentration of TiB_2 phase is formed in situ after an extensive period of milling (>40h).

rocessing (RSP)

RSP route combines Ingot metallurgy (IM) and a rapid solidification technique to produce in situ MMCs. For instance, rapid solidification processing (RSP) of Ti-B or Ti-Si alloys accompanied by high cooling rates has been shown to be very effective in producing in situ Tiï based composites that contain large volume fractions of reinforcing particles (Soboyejo *et al.*,1991). In the preparation of in situ Ti-based composites via the RSP route, rapidly solidified powders of Ti alloys containing B or Si are initially produced by the plasma arc melting/centrifugal atomization (PAMCA) technique (Peng *et al.*, 1989). More so, RSP route has been used by Tong *et al.*, (1995; 1998) to fabricate in situ TiC particulate reinforced Al-based composites. In situ formed TiC particles of 40-80nm were reported to be distributed uniformly in the Al matrix with a grain size of 0.3-0.85ε m (Tong *et al.*, 1998a,b). The main advantage of RSP is its ability to produce alloy compositions not obtainable by conventional processing methods. Besides, RSP materials have excellent compositional homogeneity, small grain sizes, and homogeneously distributed fine precipitates or dispersoids.

2.3.7 Reactive Hot Pressing (RHP)

RHP refers to a process in which ceramic reinforcement is in situ formed through chemical reaction between elements or between element and compound during hot pressing of mixture powders (Tjong and Ma, 2000). Lu *et al.* (1999) and Li *et al.* (1993) successfully prepared in situ TiB_w whisker reinforced Ti-6Al-4V composites by means of RHP. Powder mixtures containing Ti, Al-V master alloy, and TiB_2 were initially hot pressed at 1473K in a vacuum. Pressed billets were subjected to hot extrusion at 1323K. They reported that TiB_w whiskers with a diameter of 0.1-3.5ε m and aspect ratio of 10-20 were in situ generated through the reaction between Ti and TiB_2. In a similar manner, Sahay *et al.* (1999) used the RHP route to prepare TiB/Ti composites containing high volume content of TiB_w whiskers (30-92%). They

inant phase for the composites containing less than 86 vol. % of reinforcing particles. In the case of TiB/Ti composites with TiB above 86 vol. %, a significant amount of TiB_2 phase remains. In another development, Ma *et al.* (2000) examined the possibility of producing in situ TiB particle reinforced Ti composites by means of RHP route from four different mixtures of Ti-B, Ti-TiB_2, Ti-B_4C and Ti-BN. The powders from these mixtures were first blended thoroughly and then cold compacted. The green compacts were then degassed in a vacuum and hot pressed at 1523K for 1h. XRD analysis confirmed the presence of TiB phase generated in the composites from four mixtures. Additional TiC phase was detected in the composite from Ti-B_4C mixture, while certain amount of TiB_2 remains in the Ti-TiB_2 mixture, indicating an incomplete conversion of TiB_2 to TiB. It was also reported that no titanium nitride were detected in the Ti-BN mixture.

2.3.8 Other Techniques

Several other techniques such as direct reaction synthesis (DRS), flux-assisted synthesis (FAS), reactive spontaneous infiltration (RSI), directed melt/metal oxidation (DIMOX) and reactive squeeze casting (RSC) were reportedly used to fabricate other MMCs (See Tjong and Ma, 2000) but have not yet been used for the fabrication of TMCs. In 1991, Thompson and Nardone reported that in situ reinforced Ti-matrix composites were successfully fabricated by plasma melting a powder agglomerate of Ti alloys and zirconium diboride. TEM analysis of the sample identified that the reinforcement formed during the plasma melting process was titanium boride (TiB) in the form of whiskers with <100 µm diameter and an aspect ratio of 10-50. Dearnley and Roberts (1990) also produced Ti based composite with SiC, B_4C and TiB_2 reinforcements using vacuum plasma spraying.

Ravichandran *et al.* (1995) used perfected shock wave consolidation technique to process SiC particulate reinforced Ti composites. Fully dense composite compacts that are free from interfacial reactions and macroscopic cracks were developed. No

of this method for the fabrication of in situ reinforced particulate TMCs.

2.4 Thermodynamic of in situ reaction System

Several different processing techniques have been developed and successfully used to fabricate in situ TMCs as discussed in section 2.3. In a similar manner, the thermodynamic feasibility of these in situ reactions involved in fabricating in situ Ti based composites had been considered by many researchers. This section therefore reviews the thermodynamic analysis of the major reactions involved in the in situ formed reinforced TMCs. The systems considered are basically Ti-C (graphite), Ti-B, Ti-TiB_2, and Ti-B_4C.

2.4.1 Ti-C system

In situ TiC reinforced Ti matrix composites have been fabricated from Ti and C by means of combustion assisted casting (CAC) and several other routes as discussed under section 2.2.1.3 and 2.3. The thermodynamic feasibility of the reaction has been reported in terms of enthalpy, æH, and Gibbs free energy, æG by Zhang *et al.,* (1999) and Cai *et al.* (2006). According to their report, in situ TiC reinforcement can be synthesized through the reaction in equation 2.1

$$Ti + C \rightarrow TiC \text{ ---------- (2.1)}$$

The reaction formation enthalpy, æH, and Gibbs free energy, æG, for the reaction between Ti and C was calculated using thermodynamic data from Knacke *et al.* (1991) and the variations of æH and æG with temperature for the reaction 2.1 was also investigated (Lu *et al.*,1999). All authors reported that, æG for the reactions are negative for the temperature ranges that were investigated (350-1600K), indicating

ation of TiC are thermodynamically feasible. More so, the æH values obtained are very large as also been reported by Tjong and Ma (2000), indicating that the reaction is favoured to occur with high quantity of heat been released (exothermic) during the reaction.

2.4.2 Ti-B and Ti-TiB_2 System

In the case of system involving Ti and B, the possible reactions that can occur as reported by Cai *et al.*, (2006) are:

$$Ti + B \rightarrow TiB \text{ ---------- (2.2)}$$

$$Ti + 2B \rightarrow TiB_2 \text{ ---------- (2.3)}$$

Fig. 2.5 shows the generated Gibbs free energy versus temperature for reactions represented by equ.2.2 and 2.3 respectively. The figure shows that æG for reaction in equ.2.3 is much less than that for reaction in equ.2.2. Although both TiB_2 and TiB are probable reinforcements, however, TiB_2-reinforced TMCs cannot be synthesized by in situ reaction because TiB_2 is not stable when there is an excess of Ti (Zhang *et al.,* 1999; Tjong and Ma, 2000 and Cai *et al.,* 2006). Thus, TiB_2 is transformed to TiB as shown in the reaction represented by equ.2.4.

$$Ti + TiB_2 \rightarrow 2TiB \text{ ---------- (2.4)}$$

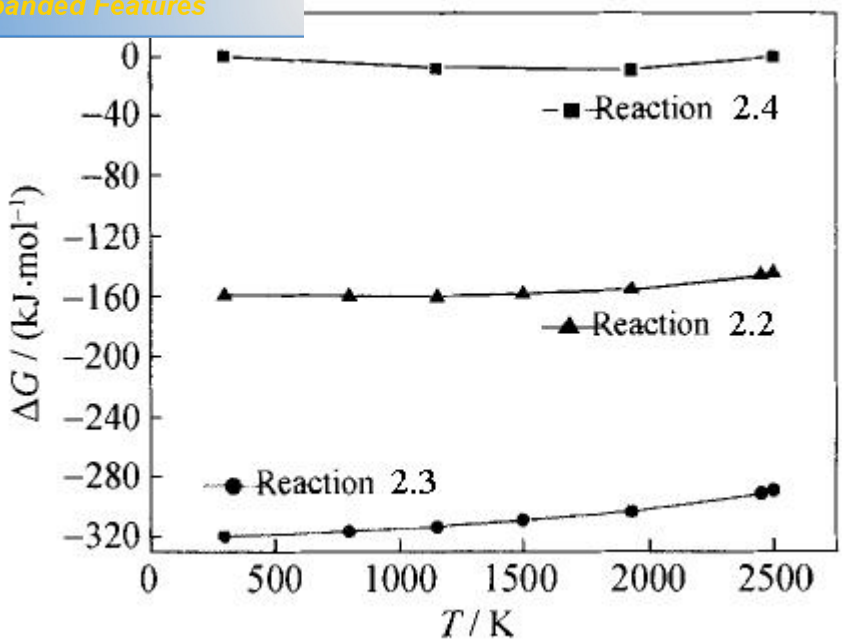

Figure 2. 5 The change of Gibbs free energy qG as a function of temperature for reaction in equation 2.2, 2.3 and 2.4 (Source: Cai *et al.*, (2006)

2.4.3 Ti-B_4C System

Ranganath *et al.* (1992), Zhang *et al.* (1999) and Cai *et al.* (2006) successfully fabricated TiB and TiC mixture -reinforced Ti matrix composites (TMCs) from Ti-B_4C mixture by means of the CAC route. Ma *et al.* (2000) also succeeded in fabricating a (TiB+TiC)/Ti composite from Ti-B_4C mixture by means of the RHP route. These researchers agreed that TiC, TiB and TiB_2 can be synthesized by the chemical reaction between Ti and B_4C and that the possible reactions that occur are:

$$5Ti + B_4C \rightarrow 4TiB + TiC \text{ ---------- (2.5)}$$

$$3Ti + B_4C \rightarrow 2TiB_2 + TiC \text{ ---------- (2.6)}$$

The reaction formation enthalpy, æH and Gibbs free energy, æG for the reactions in equ.2.5 and 2.6 was calculated by Zhang *et al.* (1999) using thermodynamic data

results of æG are shown in fig.2.6 (Zhang *et al.*, 1999; Cai *et al.,* 2006). Fig. 2.6 shows that æG of the two reactions, equ.2.5 and equ.2.6 are all negative, which indicate that both reactions can take place. More so, the calculated reaction formation enthalpy, æH of each of the two reactions is all very large, which indicates that quite a lot of heat is released during the reactions (exothermic). Zhang *et al.* (1999) also reported that the calculated adiabatic temperatures T_{ad} of the two reactions are 3628K and 3193K respectively. These values are far greater than the experimental value, $T_{ad} \geq 2500$ proposed by Merzhanov (1990), thus indicating that the reactions can be sustained by themselves (i.e. SHS can occur but only in concentrated systems). Subsequent fabrication of TiB and TiC reinforced Ti matrix composites from Ti-B_4C mixture using RHP by Radhakrishna Bhat *et al.* (2002) further explains and proves that the thermodynamic calculations are correct and can be used to support further experiments. SEM analysis of the TMCs produced shows both needle-like and spherical reinforcement particles that enhanced the strength and toughness of the TMCs.

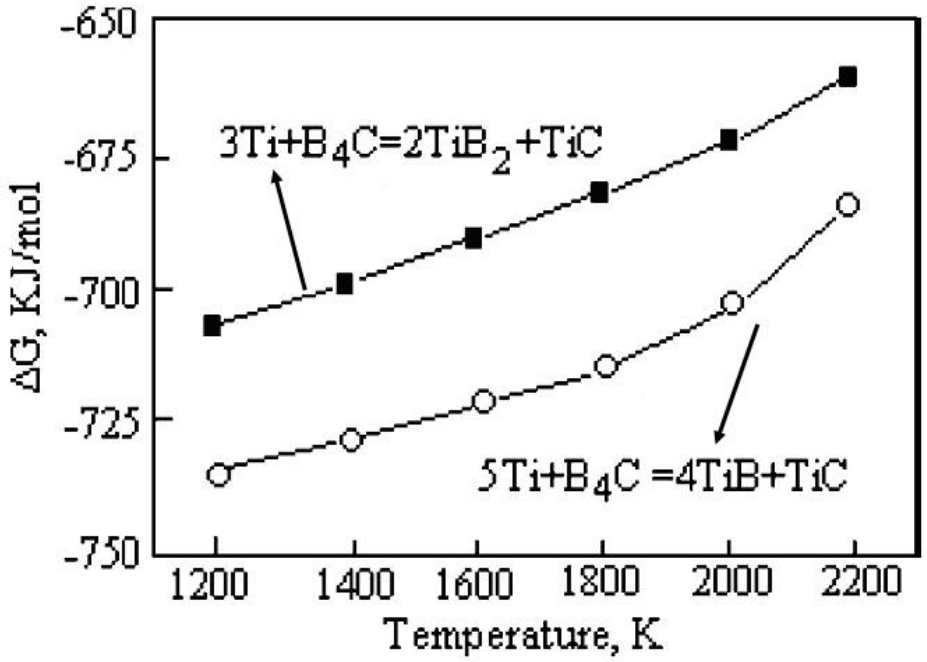

Figure 2. 6: Change of Gibbs free energy qG as a function of temperature for reactions (2.5) and (2.6) (Source: Zhang *et al.*, (1999).

2.5 Formation mechanism of in situ ceramic phases in Ti-C, Ti-B_4C System

Formation mechanism of in situ ceramic phases (reinforcements) in titanium matrix composites involves several different, or combinations of mechanisms that include: Solution-precipitation, solid-liquid interface reaction, combination mechanism of solid-liquid reaction and solution-precipitation, solid-solid interfacial reaction in metal melt, and solid diffusion reaction. The reader is referred to the review article of Tjong and Ma (2000) for more detailed information and explanation on each of the mechanisms enumerated above.

In a related development, Lu *et al.* (2001) described formation mechanism of TiC reinforcement at higher temperature and classified it into two, diffusion mechanism and dissolution-precipitation mechanism. The growth mechanism is diffusion when the processing temperature is lower than liquid phase line, while it is precipitation mechanism if the temperature is higher than the liquid phase line.

However, Tjong and Ma (2000) reported that during the processing of TMCs from Ti-B_4C mixture, especially when the combustion assisted cast (CAC) route is used, the temperature of the melt is so high that the TiC and TiB reinforcements synthesized by SHS undergo disintegration and dissolution from the Ti melt by means of nucleation and growth. Thus, the size and morphology of the in situ reinforcements are controlled by the solidification paths. Available literature shows that much work still needs to be done on the mechanism formation of in situ reinforced TMCs.

2.6.1 Morphology, size and distribution of in situ reinforcements in Ti-based composites

In situ TiC reinforced TMCs have been fabricated through combustion assisted cast (CAC) routes by several researchers and TiC particles generated in TMCs are generally three-dimensional (3-D) dendrites (Tjong and Ma, 2000). In similar work, Lu *et al.* (1999) and Zhang *et al.* (1999) reported that the formation of this dendritic TiC reinforcements in the cast structure of combustion assisted cast (CAC) processed TMCs is mainly attributed to over-cooling of the composition during solidification. Swain *et al.* (1994) pointed out that TiC has a cubic structure. Thus, when TiC nucleates, the growth rate in symmetric crystal planes is similar, therefore leading to the formation of equiaxed spherical particles. This claim has been proven to be correct by the in situ formation of equiaxed spherical TiC particles in the Al matrix composites developed by several other workers (Tjong and Ma, 2000).

In another development, Li *et al.* (1993) reported that TiB_w whiskers developed in the reactive HP-processed TiB/Ti composite were in the form of elongated needles with a roughly hexagonal cross-section. They reported that the TiB_w whiskers have a cross-sectional size of 1-2ε m, aspect ratio of ~20, and that the growth direction of the TiB whiskers is parallel to $[0\ 1\ 0]_{TiB}$. In a similar manner, Ranganath *et al.* (1996a, b) reported the formation of rod-like TiB in the CAC-processed (TiB +Ti_2C)/Ti composites. The rod-like TiB has a cross-sectional size of 2-6ε m and aspect ratio of 10-15. They were of the view that the faster growth rate of TiB along the [0 1 0] direction than normal to the (1 0 1) and (1 0 0) planes could possibly be responsible for a needle or rod-like morphology. This claim was also supported by the formation of rod-like TiB reinforcements in TMCs as reported by Li *et al.* (1993), Tjong and Ma (2000), and Lu *et al.* (2001)

In a more recent development, Ma *et al.* (2000) developed in situ TMCs through reactive HP route from Ti-B, Ti-TiB_2, Ti-BN, and Ti-B_4C mixture with rod-like TiB reinforcements in situ formed in all the composites (Tjong and Ma, 2000). The microstructure of TiB/Ti and (TiB +TiC)/Ti formed was characterized by numerous rod-like reinforcements. In addition to the TiB whiskers, some fine TiC particles are dispersed in the TMCs fabricated. The TiB whiskers in the TiB/Ti composite have a diameter of ~10εm and a length of 40-400εm, while those in the (TiB +TiC)/Ti composite have a diameter ~6εm and a length of 25-250εm. TiB exhibits a rod like shape, while TiC has spherical shape. It was also pointed out that the spherical TiC particulates in RHP-processed TMCs are quite different from dendritic reinforcements formed in CAC-processed composites (Ranganath *et al.*, 1992; Tsang *et al.*, 1996; Tsang *et al.*, 1997; Lu *et al.*, 1999; Zhang *et al.*, 1999).

2.6.2 Factor influencing particle size and morphology

The main factors that can significantly influences the particle size and morphology of the final TMCs include: cooling rate of the melt, synthesis temperature and holding time, as well as chemistry of matrix and reactants.

2.6.2.1 Cooling rate of the melt

Effect of cooling rate of melt on the reinforcement and final TMCs was studied by Lin *et al.*, (1991) and Tjong and Ma (2000). They fabricated in situ TMCs using CAC route and were able to reveal that faster cooling yields smaller dendrites of TiC, encourages the formation of TiC dendrite arrays, and decreases the stoichiometry of the TiC materials. Good examples of the effect of cooling rate of the melt on the final TMCs are reported by Tong *et al.*, (1998). The effect of cooling rate of melt needs further investigation with respect to other processing routes using different starting materials for TMCs fabrication, so that the effect better be understood.

ture and holding time

In 1998, Nukami investigated the relationship between holding time and TiC particle radius at various temperatures. He reported that the size of the TiC particles tends to increase with increasing synthesis temperature and holding time. Similarly, Chu and Premkumar (1993) reported that there is a drastic difference in the size of the TiC particles generated in the samples that reacted with carbon-bearing gas for 5min and the samples that reacted with carbon-bearing gas for 30min at the same temperature of 1533K. The TiC particles in the former sample are as small as 2ε m, while the TiC particles in the latter samples are as large as 10ε m. This indicates that there is coarsening of the in situ particles with increasing holding time.

2.6.2.3 Chemistry of matrix and reactants

Zhang *et al.* (1999) fabricated (TiB +TiC)/Ti composites from Ti-B_4C using CAC route and they showed that the addition of Al exerts a significant effect on primary TiC structure. They however, reported that there is a trend for the primary TiC to grow into an equiaxed grains and generate a fine structure after the addition of Al. In a similar way, Ma *et al.* (2000) fabricated TiB/Ti and (TiB +TiC)/Ti composites from Ti-TiB_2 and Ti-B_4C mixtures, respectively, under identical processing conditions. The reactants in both cases, TiB_2 and B_4C, have the same particle size of 3ε m but the in situ formed TiB whiskers in the Ti-B_4C mixture are much smaller than those in Ti-TiB_2 mixture.

2.6.3 Interfaces between in situ reinforcement and metal matrix

Li *et al.*, (1993) worked on the ultrafine structure of reactive hot pressing -processed TiB_w/Ti-6Al-4V composite by using high-resolution electron microscopy. They reported that an orientation relationship exists between Ŭ-Ti or ɓ-Ti and TiB. Three

ientation relationships (ORs) were reported to exist between ß-Ti and TiB: **OR I:**

$(1\,0\,0)_{TiB} \| (1\,10)_{\beta-Ti}$, $[0\,1\,0]_{TiB} \| [0\,1\,0]_{\beta-Ti}$

OR II:

$(1\,0\,0)_{TiB} \| (1\,1\,0)_{\beta-Ti}$, $[0\,1\,0]_{TiB} \| [0\,0\,1]_{\beta-Ti}$

OR III:

$(1\,0\,0)_{TiB} \| (1\,1\,\bar{2})_{\beta-Ti}$, $[0\,1\,0]_{TiB} \| [1\,1\,1]_{\beta-Ti}$

Also, there is a unique orientation relationship between Ŭ-Ti and TiB:

$$(0\,0\,1)_{TiB} \| (0\,0\,0\,1)_{\alpha-Ti}, \qquad [0\,1\,0]_{TiB} \| [1\,1\,\bar{2}\,0]_{\alpha-Ti}$$

See Tjong and Ma (2000) for more details on the orientation relationship of the Ti and TiB.

2.7 Mechanical properties of in situ TMCs

Homogeneity of reinforcements and titanium matrix in a TMC is very important for high-performance engineering applications such as those in the automotive and aircraft industries (Tjong and Ma, 2000). Uniform distribution of reinforcement in TMCs is very essential to achieve effective load-bearing capacity of the reinforcement, while non-uniform distribution of reinforcement could bring about lower ductility, strength and toughness of the composites. In situ method of fabricating TMCs generate fine ceramic particles that are uniformly distributed in the Ti matrix, leading to significant improvement in the yield strength, stiffness, creep and wear resistance of the materials.

Table 2.3 shows the tensile properties of typical in situ TiC particle and /or TiB whisker reinforced titanium matrix composites (TMCs) fabricated by different authors (Ranganath *et al.*, 1992; Tsang *et al.*, 1996; Tsang *et al.*, 1997; Ranganath *et al.*, 1996). The table shows that both strength and modulus of the TMCs are higher

anium. The values of these properties increase with increasing particle content up to a limit because increasing the particle content to 25 vol. % and beyond results in a decrease in the strength of TMCs. However, according to the results in Table 2.7, the ductility of the TMCs is reduced significantly with increasing particle content and it is obvious that TiB_w whisker exhibit a much larger reinforcing effect on the titanium matrix than the TiC particle.

Table 2. 7: Tensile properties of in situ titanium matrix composites (TMCs) (Source: Tjong and Ma, 2000)

Materials	*Ultimate tensile strength (MPa)*	*Yield stress (MPa)*	*% E*	*E (GPa)*	*Reference*
Pure Ti	*467*	*393*	*20.7*	*109*	*Tsang et al., 96*
10 vol.% TiC/Ti	*697*	*651*	*3.7*	*-*	*Tsang et al., 96*
5 vol.% TiB/Ti	*787*	*639*	*12.5*	*121*	*Tsang et al., 97*
10 vol.% TiB/Ti	*902*	*706*	*5.6*	*131*	*Tsang et al., 97*
15 vol.% TiB/Ti	*903*	*842*	*0.4*	*139*	*Tsang et al., 97*
15 vol.% (TiB + Ti_2C)/Ti	*757*	*690*	*2*	*-*	*Ranganath et al., 96*
25 vol.% (TiB + Ti_2C)/Ti	*680*	*635*	*<0.2*	*-*	*Ranganath et al., 96*
10 vol.% (TiB + TiC)/Ti	*817*	*-*	*0.55*	*140*	*Ni et al., 06*
25 vol.% (TiB + TiC)/Ti	*635*	*471*	*1.2*	*-*	*Ranganath et al., 92*

he compressive properties of in situ TMCs prepared by RHP route. They generated a graph that shows the variation of compressive yield strength with temperature of the composites and unreinforced titanium at strain rates of $7x10^{-4}S^{-1}$ (Fig.2.7). The figure shows that the strength of the composite is significantly higher than that of unreinforced titanium at temperatures ranging from 623 to 923 K. These authors also revealed that the strength of (TiB + TiC)/Ti composite fabricated from the Ti-B_4C system is significantly higher than that of TiB/Ti composite produced from a Ti-TiB_2 system. However, they suggested that the high strength of (TiB + TiC)/Ti composite could emanate from the presence of smaller reinforcements since the strength of the composites generally increases with decreasing size of the reinforcements.

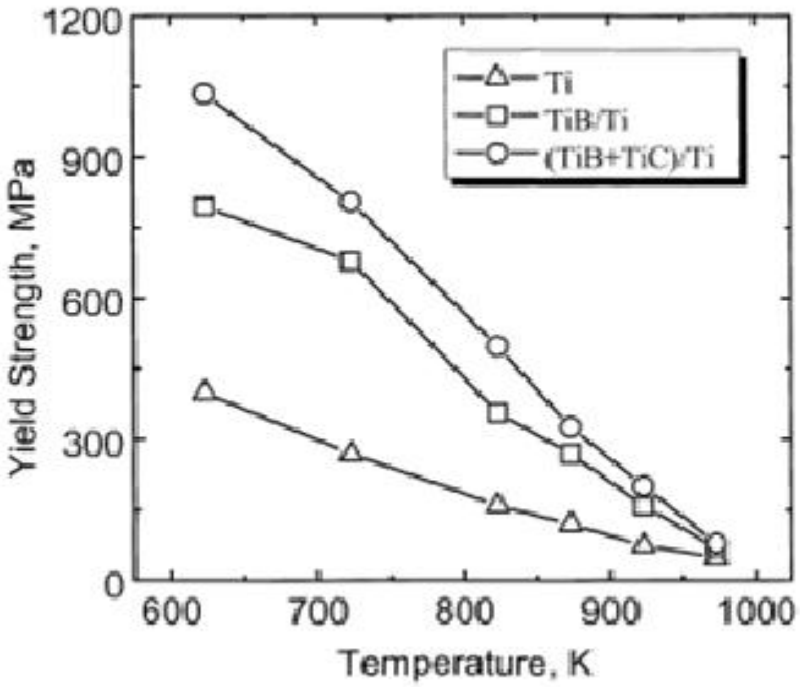

Figure 2. 7: Variation of compressive yield strength with temperature for 15 vol. % TiB/Ti and 15 vol. %(TiB+ TiC)/Ti composites and unreinforced Ti. (Source: Ma *et al.*, 2000).

The creep properties of particulate-reinforced titanium matrix composites (TMCs) are very important especially for high temperature applications (Ranganath, 1997).

hat much study have not been done on the creep properties of the titanium matrix composites. However, few reported studies on the creep behaviour of TMCs are mentioned below:

In 1993, Zhu *et al.* conducted a preliminary study on the tensile creep behavior of TiB_2 and TiC-particulate reinforcedTi-6Al-4V composite at temperature from 500-650^{0}C and stresses from 230-700MPa. Their results shows that the creep strain rates of TiB_2 and TiC reinforced composites were lower than those of the matrix alloy by two and one order of magnitude respectively. They further submitted that the creep fracture of composites in a high stress region was caused mainly by the debonding of the interface of TiB_2/ matrix and TiC/matrix and the cleavage of TiB_2 and TiC particles. However, the stress and temperature dependence of creep rates in this Ti-based composite agree with that for unreinforced Ti alloy.

In another development, Soboyejo *et al.* (1994) carried out an investigation on the high temperature creep properties of in situ TiB_w/Ti-Al-V composite at 813 and 923K using RSP method. Their results show that TiB reinforcements decrease the creep rate by approximately two to three orders of magnitude when compared with the ingot metallurgy produced matrix alloy. However, the creep rates of the in situ composites are approximately one-order of magnitude lower than those of monolithic PM alloy. They concluded that deformation restrain and pinning/locking of grain boundaries by TiB reinforcements are the two most likely creep resistance mechanisms.

In 1996, Ranganath and Mishra investigated the steady-state compressive creep behavior of Ti_2C/Ti and (TiB + Ti_2C)/Ti composites at 823-923K. Their results show that steady-state creep rate of composites is two to three orders of magnitude lower than unreinforced Ti in the temperature range investigated. Fig.2.8 shows the variation of creep rate with stress for unreinforced Ti and 25 vol. % Ti_2C/Ti composite, while Table 2.8 summarizes the apparent stress exponent and apparent activation energy for creep of the investigated materials.

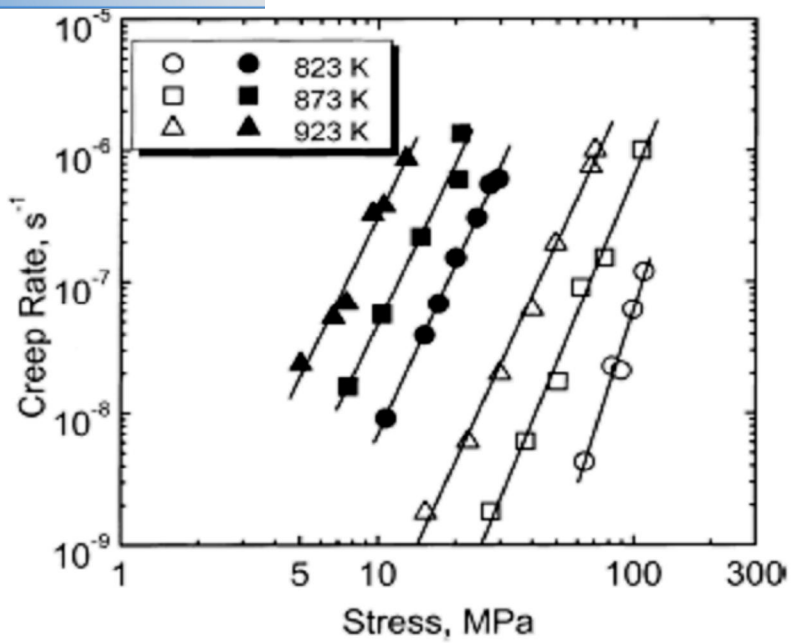

Figure 2. 8: Variation of steady-state creep rate with applied stress for unreinforced Ti (solid symbol) and 25 vol. % Ti2C/Ti composite (open symbol) (Source: Ranganath *et al.*, 1996)

Table 2. 8: Apparent stress exponent and apparent activation energy for creep of composites (titanium matrix composites, TMCs) and unreinforced Ti. (Source: Ranganath *et al.*, 1996)

Materials	*Apparent stress exponent*			*Apparent activation energy (KJ/mol)*
	823 K	*873 K*	*923 K*	
Ti	*4.3*	*4.1*	*4.1*	*236*
10 vol.% (TiB + Ti_2C)/Ti	*4.9*	*4.9*	*4.8*	*284*
15 vol.% (TiB + Ti_2C)/Ti	*7.2*	*4.7*	*4.1*	*336*
25 vol.% Ti_2C/Ti	*6.1*	*4.7*	*4.3*	*353*

es of stress exponent are higher for all composites than for unreinforced Ti at 823K, whereas the difference in value is not significant at 873 and 923 K. More so, the value of apparent activation energies for creep is significantly higher than that for Ti, and increases with increasing volume fraction of reinforcements. They suggested that creep deformation of unreinforced Ti is governed by the climb-controlled creep mechanism.

In a recent review, Tjong and Ma (2000) studied compressive creep behavior of in situ 15 vol. % TiB/Ti and 15 vol. % (TiB + TiC)/Ti composites at 873-923 K. They reported that the creep rate of the composites is about one-order of magnitude lower than that of unreinforced Ti. They however, reported that the creep resistance of the (TiB + TiC)/Ti composite is higher than that of the TiB/Ti composite. The higher creep resistance of (TiB + TiC)/Ti composite were attributed to smaller size of reinforcements. They further reported that both investigated composites exhibit identical stress exponents of 4.5-4.7 at 873-923 K, which are close to those of 15 vol. % (TiB + Ti_2C)/Ti composite (4.8-4.9) reported by Ranganath *et al.*, (1996).

2.8 Titanium hydride as the source of titanium matrix for TMCs fabrication

Many reported studies on TMCs fabrication used commercial Ti powder as the metal matrix. Apart from the expensive nature of commercial Ti powder, it also contains impurities (e.g. oxygen, manganese, chlorine, nitrogen, iron, silicon, magnesium etc- M/S Alfa Aesar, Germany). This generates a big question mark on the economic viability and the total quality (purity) of the final TMCs produced. Saito (2004) pointed out that titanium hydride powder is more cost-effective and contains little impurity when compared to commercial hydride-dehydride titanium powder mostly used for TMCs fabrication. This point serves as the basis of the motivation for considering TiH_2 as the alternative source of Ti matrix for TMCs fabrication.

This is a brittle form of metallic hydrides which forms when metallic (titanium) pieces (e.g. machining turning, sponge fines or selected scraps) are embrittled by gaseous hydrogen yielding the corresponding titanium hydrides (Sandim, *et al.*, 2005). Titanium hydrides exhibit the characteristic of angular morphology and also exhibit tetragonal structures at ambient conditions within a wide range of temperatures compared to other metal hydrides (Sandim, *et al.*, 2005; Vennila *et al.*, 2008). In the area of application, titanium hydride is used as an excellent catalyst in reversible dehydrogenation of other hydrides and carbon nanotubes (Kumar *et al.*, 2007; Bashkin *et al.*, 2000), as a bonding material to attach diamond surface to metals (Dillon et al., 2001), and as a catalyst in preparation of titanium compounds (Reilly and Wiswall, 1974). It is also used for the formation of ceramic and glass seals from a mixture of active metal titanium or titanium hydride in powder form and titanium coatings (Vennila *et al.*, 2008). In a very relevant application, the brittle hydride can be milled, sieved, and dehydrogenated in vacuum at high temperatures to obtain titanium powders (Vennila *et al.*, 2008).

2.8.2 Forms of titanium hydrides

Titanium hydrides have different forms that include Ŭ, ɓ, and ŭ-phases as shown in the Ti-H phase diagram (Fig.2.9), depending on the hydrogen concentration, temperature, and applied pressure (Numakura and Koiwa, 1984; Woo *et al.*, 1985). The literature shows that the accurate determination of the hydrogen site position in the crystal structure of these phases by XRD is difficult due to the small scattering factor of hydrogen (Sandim *et al.*, 2005) but some structural models reported in the literature were obtained from neutron diffraction measurements. The ŭ-phase has a CaF_2-type crystal structure with possibility of vacancies being created in the F-site when the H: Ti ratio is smaller than 2. For smaller hydrogen concentrations, a phase transition to Ŭ-phase has been observed with Ŭ-Ti crystal structure while, ɓ-phase that

s has a ɓ-Ti crystal structure (Sandim *et al.*, 2005). Several numbers of hydrides of Ti have been mentioned in the literature but the well-documented phases are TiH_2, $TiH_{1.924}$, TiH, and $TiH_{0.71}$ (Wang *et al.*, 2002; Crane *et al.*, 1971; Numakura and Koiwa, 1984). Table 2.9 shows the list of titanium hydride in the Ti-H phase.

Table 2. 9: List of the titanium hydrides in the Ti-H phase (Source: Wang *et al.*, 2002)

Ti/H phases	*Matrix*	*a = b/ Å*	*c/Å*	*V per atom(Å^3)*	*ΔV/V (%)*	*H/(H+Ti): at.% (x in TiHx)*	*Note*
α	*hcp*	*2.951*	*4.683*	*17.65*	*0*	*<0.12*	*Solid solution*
β	*bcc*	*3.30*	*3.30*	*18.13*	*2.5*	*~12(0.14)*	*T>883^{0}C*
TiH(γ)	*tetra.*	*4.199*	*4.576*	*20.17*	*14.3*	*1-3(<0.03)*	*Meta-stable*
TiH_2(δ)	*fcc*	*4.44*	*4.44*	*21.88*	*24.0*	*<55(1.22)* *<55(1.22)*	*Mix. With α phase* *Single phase*
TiH_2(ε)	*fct*	*4.528*	*4.279*	*21.93*	*24.2*	*~66(1.94)*	*T<20^{0}C*
TiH_x (ω)	*bcc Hex. distorted*	*4.620*	*2.828*	*-*	*-14.7*	*(0.33)*	*P:42-60 kbar*
TiH_x	*fcc Orth. distorted*	*A:4.354 B:4.18*	*4.02*	*18.23*	*3.3*	*(0.71)*	*Formed at 45-65kbar, 555-730K; Quenched<90 K*

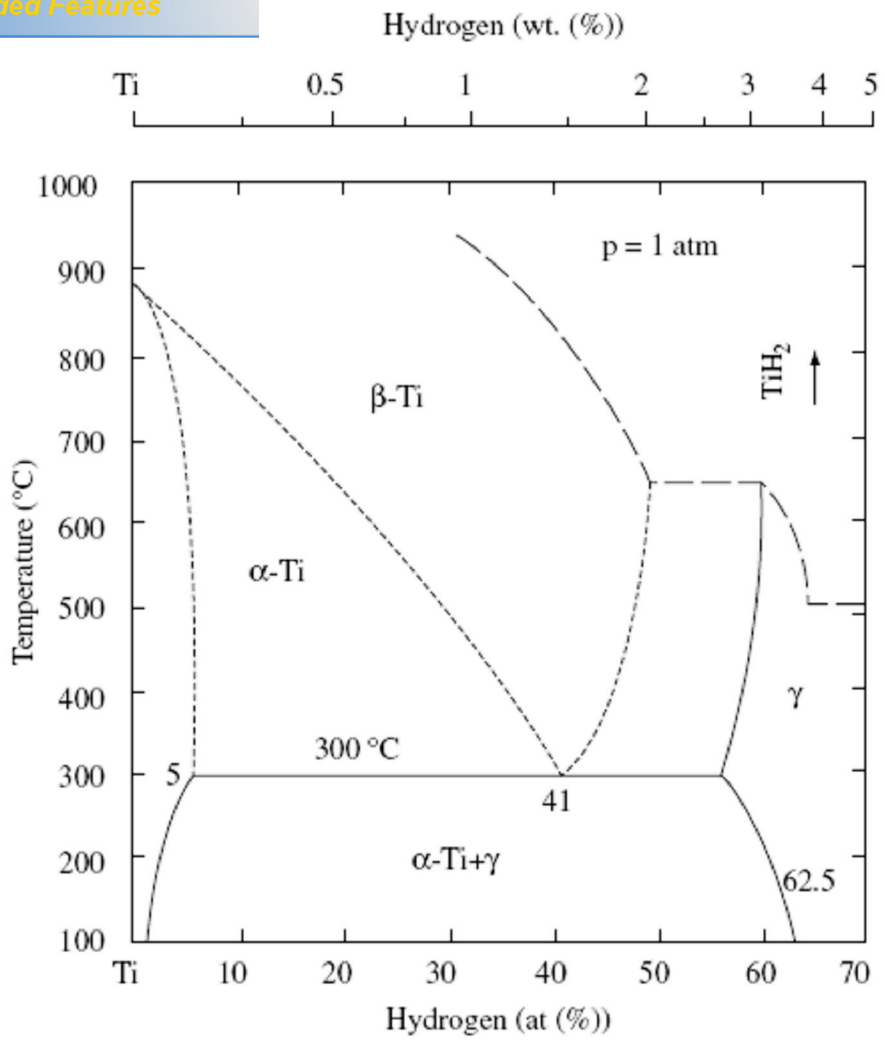

Figure 2. 9: Ti-H phase diagram (Source: Sandim *et al.*, 2005)

2.8.3 Conversion of titanium hydride to titanium (Dehydrogenation process)

Several studies have confirmed the possibility of converting titanium hydride powder to titanium powder through dehydrogenation process at temperatures between 450 - 650^{0}C (Sandim et al., 2005) and between 700 -800^{0}C (Bhosle et al., 2003). Zhang and Kisi (1997) and Padurets and Shilov (1997) carried out studies on the decomposition of TiH_2 by means of thermal-analysis techniques. Zhang and Kisi compared the dehydrogenation of nanocrystalline TiH_2 produced by reaction milling with commercially available TiH_2 powder by using thermogravimetric analysis (TGA).

the dehydrogenation rate is higher for ultrafine TiH_2 (obtained through reaction milling) compared to micron-sized TiH_2 powders (obtained commercially). They also attributed this to the large surface energy associated with a nanoscale crystal size.

In another report, Bhosle *et al.* (2003) investigated the dehydrogenation of nanocrystalline TiH_2 and consequent consolidation to form dense Ti by a combination of thermal analysis, X-ray diffraction (XRD), and transmission electron microscopy (TEM) under vacuum. They showed through DTA/TGA analysis that the dehydrogenation of TiH_2 to form Ti occurs as a two-step process (Fig.2.10 and 2.11) involving the formation of an intermediate phase, TiH and that the dehydrogenation temperature for the transformation decreases with increasing milling time (Table 2.10) and a consequent decrease in particle size. They further pointed out that consolidation of Ti components from titanium hydride through in situ dehydrogenation experiments by vacuum annealing using a powder metallurgy (P/M) route is very possible. The results of their work also reveal that the kinetics of dehydrogenation is controlled by the surface area of the particles and sintering temperature, that the reduction in surface area of powders particles by cold compaction retards dehydrogenation process and results in higher temperatures for the dehydrogenation completion. They finally reported that dehydrogenation under vacuum occurs at a faster rate as compared to that in an argon atmosphere.

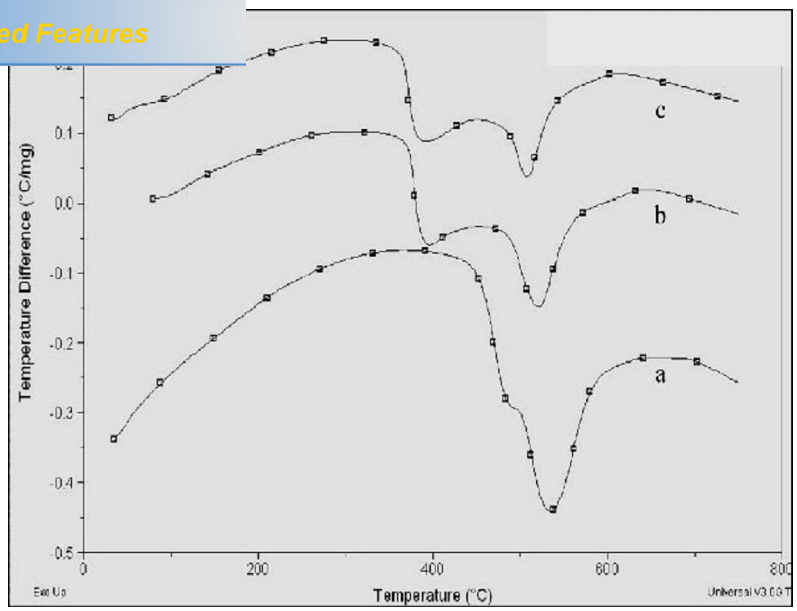

Figure 2. 10: DTA plots of TiH_2 powders milled for different times: (a) as-received (b) 1 h, and (c) 4 h. (Source: Bhosle *et al.*, 2003)

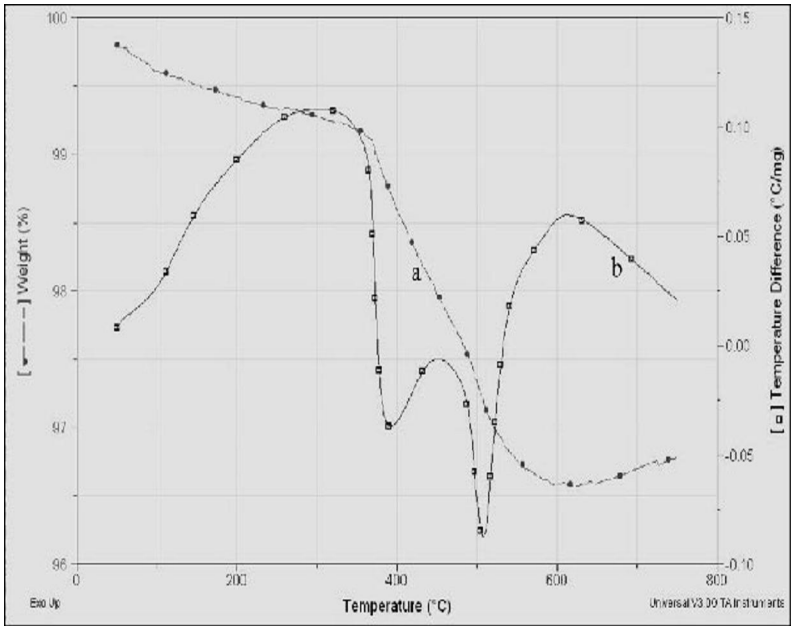

Figure 2. 11: DTA/TGA plot for 4 h milled TiH_2 powder: (a) weight percent and (b) temperature difference (Source: Bhosle *et al.*, 2003)

mperatures during 20 K/min constant heating rate experiments in DTA. (Source: Bhosle *et al.*, 2003)

Milling Time	Peak transformation temperature (^{0}C)	
	Peak 1	Peak 2
As-received TiH_2	480	540.23
TiH_2 milled for 1h	397.00	521.01
TiH_2 milled for 4h	392.18	508.39

In a more recent development, Sandim *et al.* (2005) examined the thermal decomposition of titanium hydride powder (ŭ-phase) to titanium (Ŭ-phase) by means of TGA and high-temperature X-ray diffraction (HTXRD). The results of their TGA show that the decomposition of the titanium hydride powder carried out in high vacuum becomes significant at about 450^{0}C and above 500^{0}C the decomposition was completed in times shorter than 50minutes. They also reported that onset temperature for hydrogen release from ŭ-TiH_2 depends on the heating rate in TGA (Fig. 2.12). More so, the final amount of the hydrogen in the transformed powder investigated for up to 800 ^{0}C was found to be dependent on the applied heating rate because the lower heating rates enable larger residence time favouring a more pronounced degassing (Sandim *et al.*, 2005).

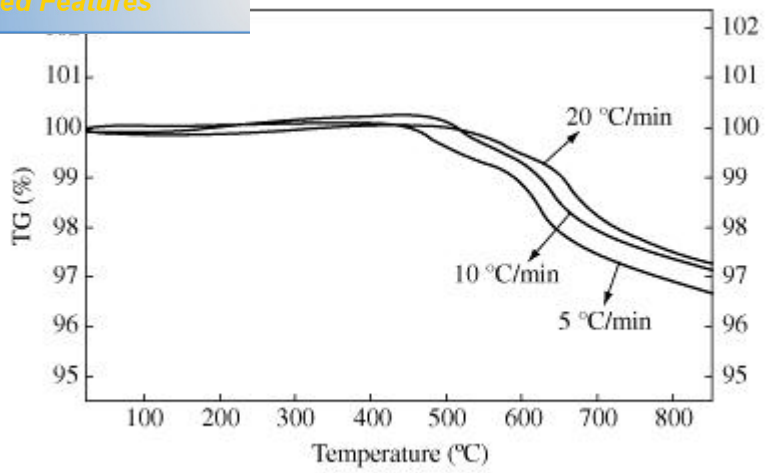

Figure 2. 12: TGA curves for TiH_2 powder for heating rates varying from 5 to 20°C/min (Source: Sandim *et al.*, 2003)

However, Bhosle *et al.* (2003) reported that even though dehydrogenation of the highest-hydrogen containing phase, TiH_2, has been studied by many researchers, the sequence of transformation leading to the formation of Ti is still not understood. This implies that a lot still needs to be done, in terms of the mechanism and kinetics of the transformation of titanium hydride powder to titanium power. Many researchers are still working in this direction with the aim of acquiring the necessary knowledge for a better understanding of the dehydrogenation process, its significance for improving the known applications of Ti-H compounds and solid solution, and also in order to develop new applications.

2.8.4 Titanium alloys and composite production from titanium hydride

Reasonable levels of success have been recorded by several workers in the transformation of titanium hydride to titanium powder and even dense titanium as reported in section 2.9.4. Efforts are directed towards using titanium hydride to synthesize titanium alloys and possibly titanium matrix composites. Although a significant break through has not been recorded in this area the reported feasibility and possibility of producing titanium alloys and composites from titanium hydride

iveness, economic viability and quality (purity) of material has made several serious researchers to pursue these goals and few attempts have been reported.

In one of such attempts, Ivasishin *et al.*, (2005) examined the microstructure and properties of titanium alloys synthesized from hydrogenated titanium powders with different hydrogen contents (0.2 to 3.9 wt %). They synthesized Ti-6Al-4V alloy with 99±0.5% relative density using blended elemental powder metallurgy (BEPM) with simplest press-and-sinter approach. The effect of hydrogen contents on the microstructure, residual porosity and mechanical properties (tensile and fatigue) of the synthesized alloys was examined and it was shown that the synthesized alloy exhibited chemically homogeneous fine-grained microstructure independently of hydrogen content. Increase in hydrogen content of the starting powder provides higher density of synthesized material and made sintered density less sensitive to a molding pressure. The only shortcoming is that decrease in hydrogen content of the starting material resulted in slight increase in porosity (up to 2%). Although the slight increase in the porosity did not cause any noticeable effect on the tensile properties of the synthesized alloy, it significantly affected its fatigue properties. They reported that the mechanical properties of the synthesized dense alloy were matching the properties achieved with conventional ingot metallurgy.

No further study was reported until when Adam *et al*. (2008) reported that they used powder metallurgy process to produce titanium alloy products from hydrogenated titanium powder. Direct powder rolling (DPR) process was used to produce titanium and titanium alloy flat products (plates, sheets, foils) from hydrogenated titanium powder. A master alloy was blended (BE method) with hydrogenated titanium powder to achieve the required chemistry. The mixed powders were compacted to flat products of near final thickness by DPR and subsequently sintered under vacuum. They produced near full density titanium alloys with optimized microstructures and properties equivalent to those of the ingot metallurgy.

In the case of titanium composites fabrication from titanium hydride, there has never being any reported literature to the best knowledge of this author. It is therefore a worthwhile effort to research into such an area of application of titanium hydride.

In conclusion, it was realized that a wide variety of composite production processing methods are available to serve various commercial needs. The appropriate choice of which technique to use depends on the specific application and what is an acceptable cost for such an application. This review shows that significant work has been done in the area of in situ reinforcement of titanium matrix composites using different types of reinforcement. Fewer works have been reported on the in situ reinforcement of titanium matrix composites using Ti-B_4C powders as starting materials, although the available literature shows that physical and mechanical properties of TMCs are significantly improved when in-situ techniques combined with TiB and TiC particulates are used during fabrication. However, many questions still remain if a proper understanding of this field is to be obtained. For instance, the detailed reaction mechanism and kinetics of reaction between B_4C and Ti powder are not yet fully understood. More so, almost all the available literature used commercial Ti powder as metal matrix in producing TMCs raising questions about the cost effectiveness and purity of the final composites produced. The extensive review carried out in the present study shows that no research work has been reported on the use of another source of titanium like titanium hydride powders as metal matrix based and available review indicates the possibility of using titanium hydride as an alternative source of titanium matrix in the TMCs fabrication.

Therefore, the present research shall examine the feasibility of using TiH_2 and B_4C powders as starting materials for the production of in situ reinforced titanium matrix composites using a powder metallurgical (PM) processing method together with simple powder consolidation and sintering (pressureless and hot pressing).

Chapter Three

3.0 Experimental Procedure

3.1 Introduction

This chapter provides detailed description of the starting materials, chemicals, equipments, methodology (procedures used in the experimental part of this research work), as well as characterization of the starting materials and sintered samples in terms of phase identification, composition, morphology of the phases, density and hardness.

3.2 Materials and Chemicals

The starting materials used in this research work include titanium, titanium hydride (TiH_2), boron carbide (B_4C) powders (all commercially obtained from M/S Alfa Aesar, Germany) and boron suboxide (B_6O) powder from IKTS, Germany. Table 3.1 shows a summary of all the materials and chemicals used for this work. Commercially obtained titanium hydride and boron carbide powders were mixed together by means of a milling technique using desired proportions (detailed calculation in appendix A.1), to produce blended powders that were in turn used for the generation of in situ formed reinforced particulate titanium matrix composites.

3.3 Materials and Characterization

Detailed chemical analysis of the powders as per the manufacturerôs specification shows that titanium powder (99.5% purity, -44ε m) contains the following impurities: O = 0.23wt. %, Fe = 0.033wt. %, C = 0.009wt. %, N = 0.018wt. %, P = <0.0023wt. %, S = <0.0013wt. %, Mn, Cl, Si, Mg = 0.013wt. % (each), Na, Al = <0.013wt. % (each) and H = 237ppm; titanium hydride (99% purity) contains H = 3.7 wt. % and maximum 0.3wt. % N. The average particle size distribution of commercial titanium powder is d_{10} = 15.6 µm, d_{50} = 30.4 µm, d_{90} = 55.1 µm, that of titanium hydride

$_{0}$ = 4.5µm, d_{90} = 9.4 µm, while that of boron carbide based on manufacturerôs specification is d_{10} = 1.6 µm, d_{50} = 4.6 µm, d_{90} = 9.3 µm. The Ti powder used has a larger particle size than titanium hydride because finer powders are not available and communition methods are difficult to use due to the plastic deformation of the Ti particles which makes further particle size reduction very difficult. The particle size distribution for powder materials were analyzed using a Malvern Mastersizer 2000 (Microscientific), with water as a carrier fluid (Fig 3.2).

The powder morphology of the starting powders is given in Fig. 3.1 a, b, c and d. The morphology of the powders was analyzed using Field Emission Scanning Electron Microscopy (FESEM).

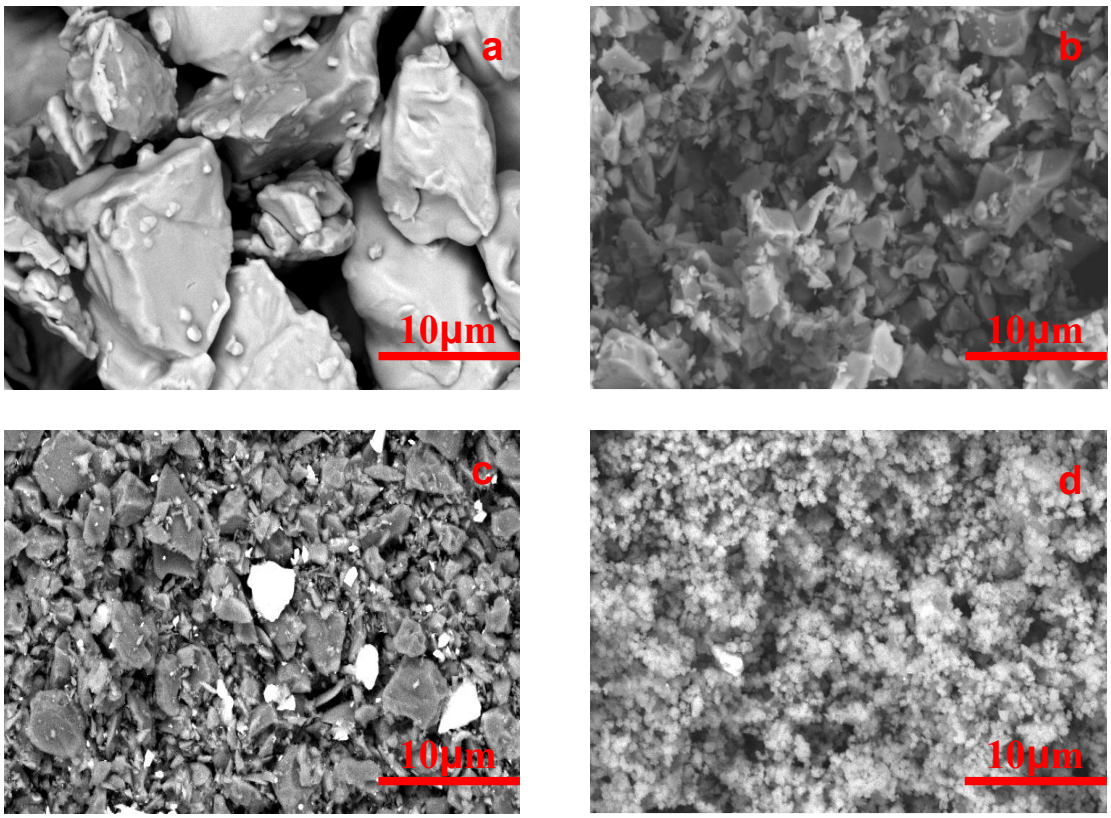

Figure 3. 1: SEM micrograph of (a) titanium (b) titanium hydride (c) boron carbide and (d) boron suboxide powder.

ısed during experimental work.

Material/Chemical	Particle Size d_{50} (µm)	Purity (%)	Supplier
Ti		99.5 (-44ε m)	Alfa Aesar, Germany
TiH_2	1.8	99	Alfa Aesar, Germany
B_4C	4.6	99	Alfa Aesar, Germany
B_6O	2.5	-	IKTS, Germany
Copper Turning			Leco, SA
Alumina boat			Leco, SA
Zirconia Tray			Leco, SA
h-BN rods	-	-	GE Advanced Ceramics
Propan-2-ol			Saarchem
Hexane			Saarchem
Diamond Suspension	9,6,3, and 1		Struers
Diamond Extender(Light blue)			Struers
Absolute Ethanol			Saarchem
Distilled water	-	-	-
Argon	-	UHP	Afrox

For proper understanding of the history and behavior of starting powders, they were subjected to various analyses. Such analysis include Particle size analysis (PSA), X-ray diffraction (XRD) Analysis, Scanning electron microscope (SEM)/ energy dispersive x-ray spectrometer (EDS) analysis, X-ray Fluorescence (XRF) analysis, and thermogravimetric analyser (TGA)/ differential thermal analyser (DTA) analysis etc. The methods and equipments are described below.

3.4.1 Particle size analyzer

The Malvern Mastersizer 2000 particle size analyzer (PSA) was used to determine the particle size and size distribution of the commercially obtained powders and blended powders used in this research. Fig. 3.2 shows the particle size analyzer (Malvern Mastersizer 2000) that was used. The particle size distribution of the starting powders using Malvern Mastersizer is shown in appendix B.

Figure 3. 2: Particle Size Analyzer (Malvern Mastersizer 2000)

XRF)

X-Ray Fluorescence (XRF) spectrometer at element six SA and Council for Geoscience, South Africa, were used to determine quantitatively the elemental composition of starting powders and blended powders.

3.4.3 Thermogravimetric analyzer (TGA)/Differential thermal analyzer (DTA)

TG 92 Setaram Thermogravimetric analyzer (TGA) coupled with a differential thermal analyzer (DTA) in an inert atmosphere (Ultra High Purity argon) was used to study the thermal decomposition of commercially obtained titanium hydride used in this research and it also helps to establish the various temperatures at which chemical changes/ mass changes occurred. The results obtained help choose the conditions for the actual dehydrogenation of titanium hydride in the alumina tube furnace. Fig. 3.3 shows the picture of TGA/DTA machine used in the course of this research.

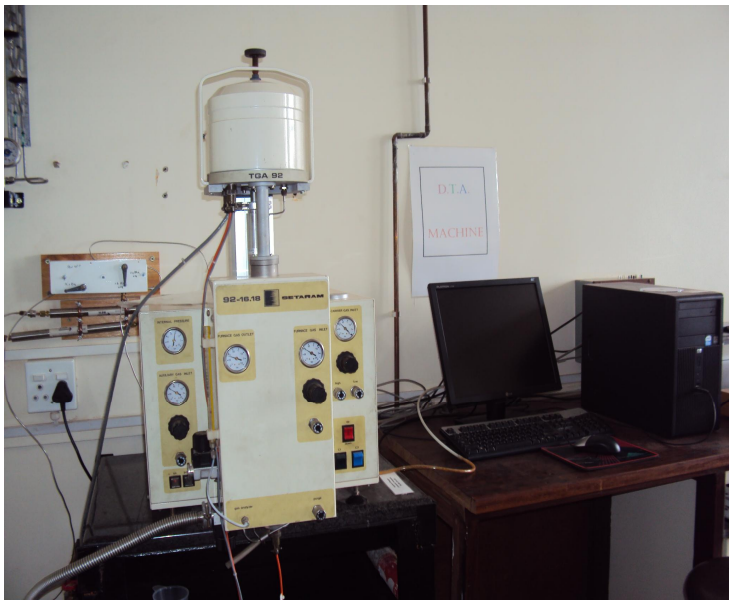

Figure 3. 3: TGA/DTA machine (TG 92 Setaram) (run under argon atmosphere)

A planetary mill, Fritsch Pulversette 6 (PM 100), was used to carry out the wet mixing of titanium hydride and boron carbide powders. The mixing was carried in a 250ml-Tungsten-carbide vessel with alumina balls, either absolute ethanol or propan-2-ol or hexane as a solvent, and a powder to ball ratio of 1:2 . The Planetary mill was operated at a speed of 200 rpm for 4 hours. Fig 3.4 shows the picture of the planetary mill that was used.

Figure 3. 4: Planetary ball mill, Fritsch Pulverisetle PM100

The mixed powders were subsequently dried in a rotary evaporator.

Figure 3. 5: Rotary Evaporator (Heidolph-4010)

3.4.6 Tube furnace/ Oxygen getter furnace

A tube furnace (Elite TSH17/75/150, Elite Thermal Systems) with maximum temperature of 1700^{0}C was used for the dehydrogenation and pressureless sintering of titanium hydride and composites powders. The furnace consists of a central alumina tube with an inner diameter of 69.9mm, outer diameter of 76.2mm and a length of 1200mm. The furnace has a Eurotherm microprocessor that controlled the temperature profile. The furnace temperature was measured by a standard Pt-Rh thermocouple. The tube furnace was modified with the new set up consisting of an oxygen getter tube furnace that preceded the alumina tube furnace and a gas bubbler at the exit of the furnace. The oxygen getter furnace was placed between argon gas cylinder and the tube furnace. The getter furnace consists of a central silica tube (inner diameter of 28-29mm and a length of 50.5-51mm), a microprocessor that controlled the temperature profile (700^{o}C) and a standard removable thermocouple

or. The silica tube was packed with copper turnings, which were kept at 700°C. The purpose of the copper turnings is to trap the small quantity of oxygen present in argon (UHP) gas flowing passing through them before gaining entrance to the main tube furnace, thereby eliminating or reducing the problem of oxidation in the main tube furnace. All the experiments carried out using this machine were done under argon atmosphere. A rectangular alumina boat (72mm x 44mm x 12mm with 2.5mm wall thickness) or a zirconia tray were used as the sample holder are placed at the hot zone area of the tube furnace. The sample holder was surrounded by alumina boats containing commercial pure titanium on either side to prevent any further oxidation from any untrapped oxygen in the inert gas that escaped the oxygen getter furnace. The ends of the alumina tube were sealed using brass enclosures with rubber o-ring. The tightness of the seals was checked using a Gas sniffer leak detector (GasCheck 3000is-intrinsic version only) to determine any gas leaks. Fig. 3.6 shows the tube furnace/oxygen getter furnace used for dehydrogenation and pressureless sintering carried out in this project.

Figure 3. 6: Tube furnace with oxygen getter furnace (Elite TSH17/75/150, Elite Thermal Systems)

A Uniaxial hot press (HP20-2560-FP20 Thermal Technology) was used for hot-pressing and densification of blended powder of TiH_2-B_4C mixture. It consists of a furnace which is heated by a carbon element. The hot-pressing machine has a maximum furnace operating temperature of 2100^oC and can withstand a maximum pushing force (applied force for densification of compacts during hot pressing) of 100 KN. The force is applied through graphite punches uniaxially from the bottom graphite punch. Fig. 3.7 shows the picture of the uniaxial hot press used. h-BN sample cells/crucible was used for all hot pressing experiments. The furnace was evacuated to a pressure less than 300 mtorr and then back filled with ultra high purity argon. Argon was allowed to flow through the furnace during the entire hot pressing process.

Figure 3. 7: Uniaxial hot pressing machine used for the sintering of composites (HP20-2560-FP20 Thermal Technology)

For the hot pressing of blended TiH_2-B_4C mixture, hexagonal-BN material was chosen as a mould. The h-BN rod material was machined into a crucible (Figure 3.8). The piston was a graphite rod of 15mm height coated with layers of h-BN suspension. A 3mm h-BN cylindrical plate was placed between the graphite piston and the sample to avoid any carbon contamination. Fig. 3.8 shows the drawing of the capsule used in this work.

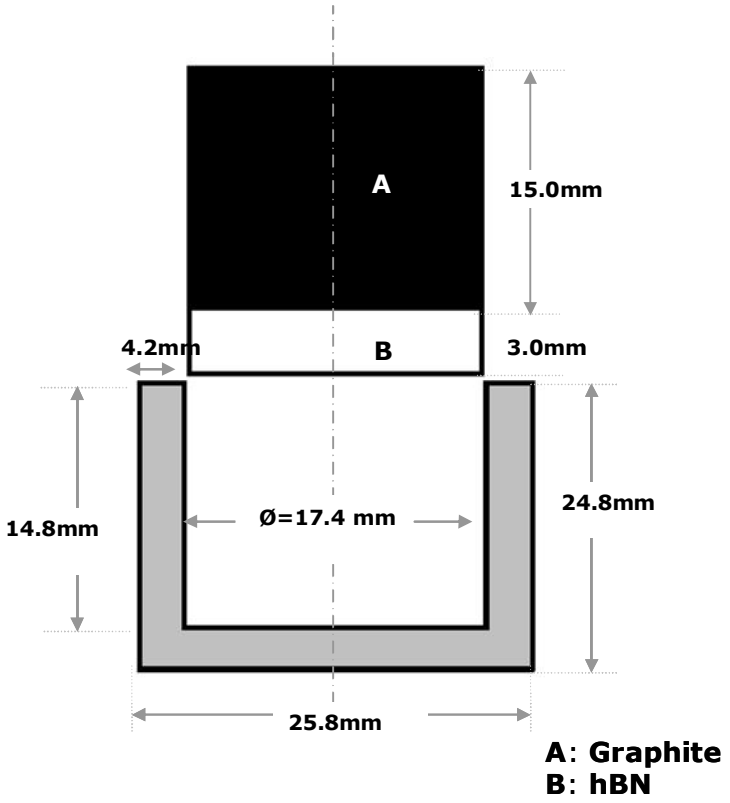

Figure 3. 8: Drawing of capsule used

3.5 Sample preparation

This research intends to produce 10, 20, 40, 60, and 80vol % in situ reinforced particulate TMCs from TiH_2 and B_4C powders. The required stoichiometric amount of the starting powders to obtain for instance, 10vol% reinforced particulate TMC is 98.16wt % TiH_2 and 1.84wt % B_4C. The values were obtained using equation 3.4.

percentage composites are presented in appendix A.1 and equation 3.1-3.4 represents the equation of reactions involved.

$$TiH_2 \rightarrow Ti + H_2 \uparrow \text{----------} \quad (3.1)$$

$$3TiH_2 + B_4C \rightarrow 2TiB_2 + TiC + 3H_2 \uparrow \text{----------} \quad (3.2)$$

$$5TiH_2 + B_4C \rightarrow 4TiB + TiC + 5H_2 \uparrow \text{----------} \quad (3.3)$$

$$(x+5)TiH_2 + B_4C \rightarrow xTi + 4TiB + TiC + (x+5)H_2 \uparrow \text{----------} \quad (3.4)$$

3.5.1 Mixing of TiH_2 -B_4C and Ti-B_6Opowders

Based on the stoichiometric calculation from equation 3.4, the predetermined amount of TiH_2 and B_4C powers required to in situ fabricate 10, 20, 40, 60, and 80 vol. % reinforced particulate TMCs were mixed together in absolute ethanol for 4 hours using the planetary ball mill. A tungsten-carbide chamber with 2mm diameter alumina balls and a powder to ball mass ratio of 1:2 was used. The mixing speed was kept at 200-250rpm. After mixing, the slurry was dried using the rotary evaporator, and subsequently characterized using X-ray powder diffraction to identify the phases present and SEM to confirm the elemental composition and the homogeneity of the admixed powder. In a similar manner, commercial titanium powder was blended together with B_6O powder in the planetary milling machine using 80 vol. % Ti: 20 vol. % B_6O, the slurry was then dried using rotary evaporator.

Starting powders, titanium hydride, titanium, and mixed powders of TiH_2 and B_4C were subjected to compaction to produce samples required for further experiment.

Compaction of titanium and titanium hydride powders was carried out in a uniaxial press using a hardened steel die of diameter 18mm. Cylindrical compacts of about 5mm height were prepared using applied pressure. The pressure was applied gradually and maintained for 1min followed by gradual removal. Compaction graphs of both powders were generated (Fig. 3.9) (detailed data for compaction graphs generation are shown in the appendix A.2). The green body compact of both commercial titanium and titanium hydride showed a green density of 79.3 and 72.1% of theoretical respectively. The green compacts produced at 393MPa pressure were used for subsequent dehydrogenation and pressureless sintering of the converted Ti, while green compacts of commercial Ti were also pressureless sintered in the same manner for comparison.

In a similar manner, the mixed powders of TiH_2 and B_4C (for 10, 20, and 40 vol.% TMCs) were compacted in a uniaxial press using a hardened steel die of diameter of 18mm. Cylindrical compacts of about 4-5mm height were prepared using a pressure of up to 393 MPa. The green body compact produced exhibits green density of about 57% of theoretical. The compacts were further used to carry out pressureless sintering for in situ TMCs fabrication.

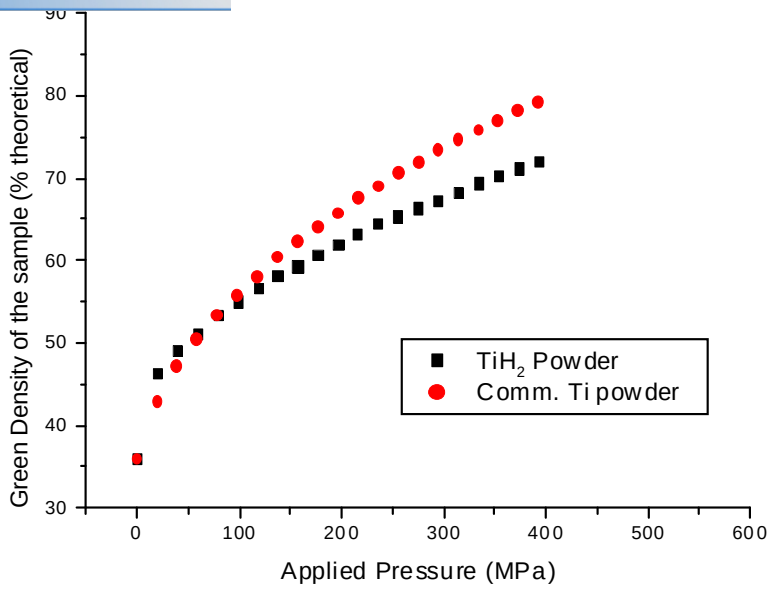

Figure 3. 9: Comparison of the compaction behaviour of as received commercial titanium hydride (TiH_2) and Ti powders

3.6 Sintering and dehydrogenation processing of powders

3.6.1 Pressureless sintering of commercial titanium powder

Compacts produced from commercial titanium powder were pressurelessly sintered at fixed temperatures (1000-1400^{0}C) in an alumina tube furnace. Each compact was placed on a Zirconia tray that was in turn placed in the hot-zone of the furnace. The tray was then surrounded by alumina boats (before and after, in terms of Argon gas flow direction) containing commercially pure titanium on either side to prevent possible oxidation from any untrapped oxygen in the inert gas that escaped the oxygen getter furnace as described in section 3.4.8. The sintering profile comprised a ramp-up stage that was carried at a constant heat rate of 6^{0}C/min up to the sintering temperature. Once the temperature was attained, it was maintained for 90min and the furnace was subsequently allowed to cool to ambient under argon flow at the cooling rate of 6^{0}C/min. The heating cycle is shown in figure 3.10

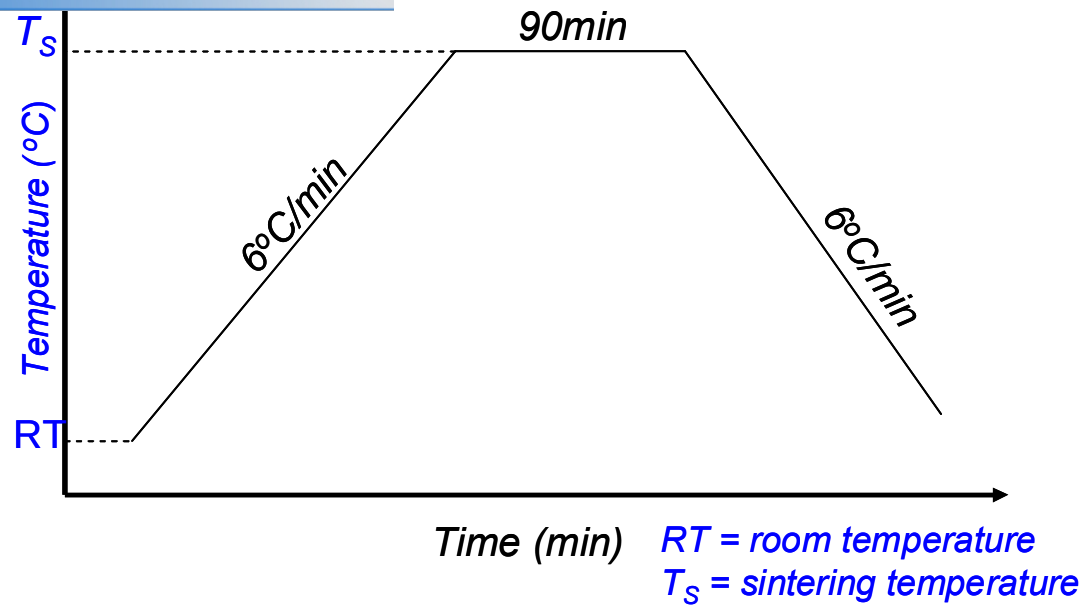

Figure 3. 10: Temperature profile for pressureless sintering of comm. Ti.

3.6.2 Conversion of TiH_2 to Ti through dehydrogenation and pressureless sintering.

For the conversion of TiH_2 to Ti, The dehydrogenation was carried out using both loose powder and compacts. The dehydrogenation temperature was chosen using DTA/TGA literature data (Bhosle et al., 2003; Sandim et al., 2005). Based on these data the loose TiH_2 powder and compacts were dehydrogenated at T_D =680^{0}C and T_D = 715^{0}C respectively in the alumina tube furnace with a constant heat rate of 2^{0}C/min for a dwelling time of 120min. The furnace was subsequently allowed to cool to ambient under argon flow at the cooling rate of 6^{0}C/min. In the case of pressureless sintering of TiH_2, immediately after 120min dehydrogenation dwelling period, the temperature profile was ramped up to a fixed sintering temperature (T_S = 750 to 1400^{0}C at interval of 50^{0}C) at a constant heat rate of 6^{0}C/min, maintained at the fixed T_S for 90min and subsequently allowed to cool to ambient under argon flow at the cooling rate of 6^{0}C/min. Figure 3.13 shows the temperature profile used for both

g of TiH_2 to Ti. The reaction taking place during dehydrogenation is given in equation 3.1

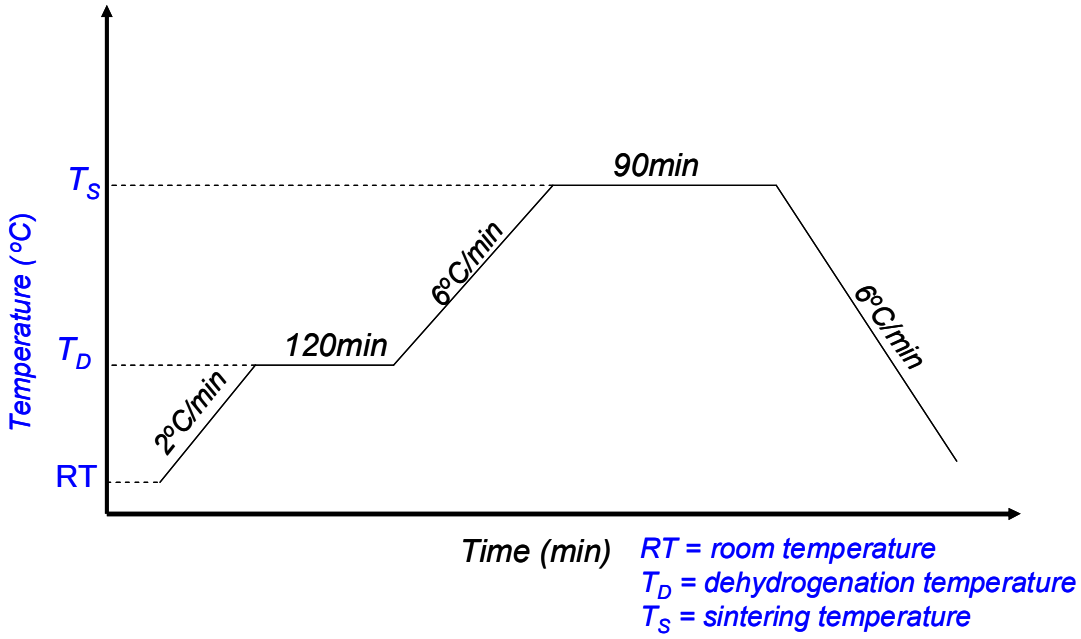

Figure 3. 11: Temperature profile for dehydrogenation and pressureless sintering of titanium hydride compacts

3.6.3 In situ synthesis of TMC through dehydrogenation and pressureless sintering of blended TiH_2-B_4C powder mixtures.

The same temperature profile as in section 3.6.1 (Fig. 3.11) was used to carry out the fabrication of 10, 20, and 40 vol. % in situ formed reinforced particulate TMCs from blended mixture of TiH_2 and B_4C powders using pressureless sintering. The green compact of the blended powders were pressureless sintered in the alumina tube furnace in the same manner as explained in the section 3.4.8 and 3.6. The sintering temperatures considered for the TMCs are 1100, 1200, 1300 and 1400^0C. However, the sintering time was extended from 90 to 120mins so that there would be a longer residence time for reaction. Formation of in situ reinforced particulate TMCs from TiH_2 - B_4C powders through pressureless sintering involves a two stage reaction: TiH_2 first decomposed to Ti and H_2, and Ti subsequently reacts with B_4C to form

egassed. The overall possible reactions that may occur during the sintering process are giving in equation 3.2 and 3.3. When there is excess Ti, the reaction that results to in situ reinforced particulate TMCs from the blended powders is giving in equation 3.4.

3.6.4 In situ synthesis of TMC through hot – pressing of blended TiH2-B4C powder mixtures.

TiH_2-B_4C mixed powders prepared for the fabrication of 20, 40, 60, and 80 Vol. % in situ reinforced particulate TMC were subjected to heat treatment by the hot pressing method, a form of reactive hot pressing (RHP) method. This method, instead of pressureless sintering was used because of the high wt. % B_4C used and the need to achieve an enhanced densification in the final TMCs. Blended powders were used instead of the compact. The desired quantity of blended TiH_2-B_4C powders was put inside the h-BN crucible. This was in turn inserted into the graphite die with insert and punches of the hot pressing machine. The hot press was evacuated to pressures less than 300 mtorr and then back filled with argon. Argon was allowed to flow through the furnace during the entire hot pressing and heating cycle. The furnace was then heated to 715^{o}C at 2^{o}C/min and held at this temperature for 120 minutes. This is to enhance a complete dehydrogenation process. The furnace was subsequently heated to the temperatures, T_{HP} = 1100, 1200, 1300 and 1400^{0}C at 10^{o}C/min and held at this temperature for 120 minutes, within which the pressure was applied and kept constant at 30 MPa for the entire dwelling period. The in situ reactions that lead to the formation of the reinforcements in the Ti matrix is expected to take place within this period. After the dwelling period, the furnace was cooled to room temperature at a cooling rate of 10^{o}C/min. At room temperature the sample cell was removed from the graphite die and the sample was removed from the h-BN crucible for further analysis. Figure 3.12 shows the sintering temperature profile for TMCs. The hot pressed samples were of 18 mm in diameter and 2 to 5 mm in thickness.

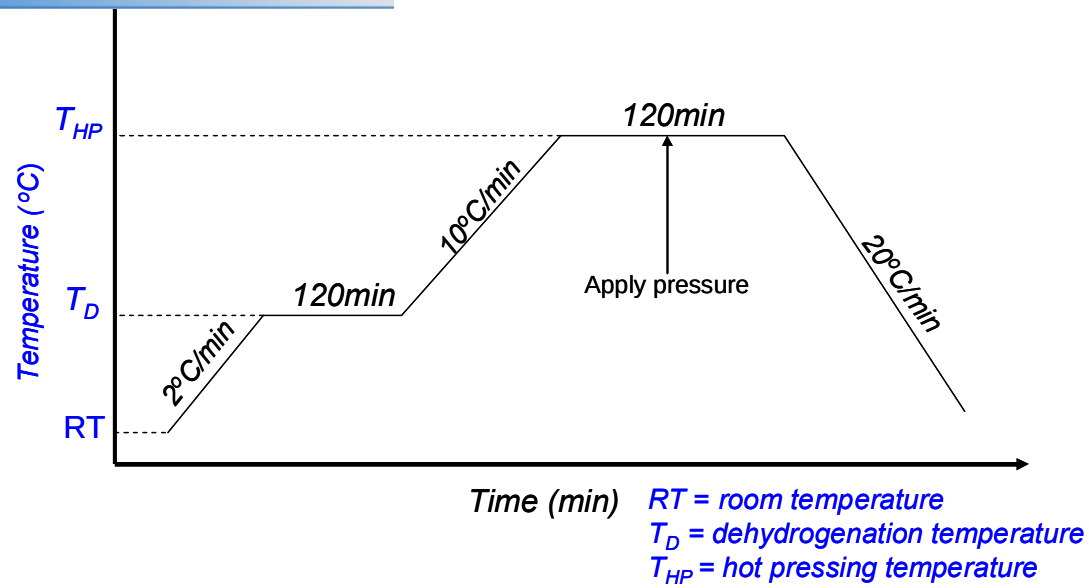

Figure 3. 12: Temperature profile for hot pressing of TiH_2-B_4C mixture to form titanium matrix composites

3.6.5 Nomenclature of pressureless sintered and hot pressed samples

Three forms of heat treatment; dehydrogenation, pressureless sintering and hot-pressing were carried out in this project. TiH_2 was converted to Ti by dehydrogenation, commercial Ti and TiH_2 were pressurelessly sintered, while composites from TiH_2-B_4C mixture were pressureless sintered and hot-pressed under different operating conditions. For easy reference, Ti and TiH_2 materials that were sintered pressureless in this project have been named according to their sintering method, sintering temperature, name of the material, and the sintering time. For instance, **PL**1000**Ti**90 represent commercial titanium that was pressureless sintered at 1000^0C for 90min, while **PL**750**TiH_2**90 represent commercial TiH_2 that was pressureless sintered at 750^0C for 90min.

For the composites fabricated from TiH_2-B_4C mixture, since different volume fraction of reinforcements were in situ formed by means of pressureless and hot-pressed sintering, the referencing was done in accordance to the reinforcements volume

hod, the name titanium matrix composite (TMC), and the sintering temperature. For instance, the sample named 10**PL**TMC**1100** represent a 10vol. % reinforced TMC pressureless sintered at 1100^0C, while 20**HP**TMC**1100** represent a 20vol. % reinforced particulate TMC hot-pressed sintered at 1100^0C.

3.7 Characterization of dehydrogenated and sintered samples

All processed samples were classified into dehydrogenated/pressureless sintered and hot pressed samples. Prior to characterization, hot pressed samples were ground on their surface to remove unwanted h-BN material and decomposed layer. All samples were then cleaned with ethanol and properly dried. The densities of the samples were immediately determined. All the samples were subsequently cross-sectioned into 2 pieces using diamond saw for further analyses. Half cross-sectioned of each samples were used to double check their densities and X-ray diffraction (XRD), while the other half was metallographically prepared for further analysis like, optical microscope (OM), scanning electron microscope (SEM/EDS), as well as the hardness of the polished part of the materials.

3.7.1 X-Ray Diffraction (XRD)

Phase composition of the powders, admixed powders (e.g. mixture of titanium hydride and boron carbide powder used for composites production) and sintered samples was determined using X-ray diffraction analysis. A Philips (PW1710) X-ray diffractometer fitted with monochromatic Cu KŬ radiation set at 40 kV and 20 mA was used to determine the phase composition of powders and sintered samples produced. Scan width (2ɗ) used was between 10^o and 80^o with a step size of 0.02^o. Phase identification was done using Philips Analytical XôPert HighScore® software with an in-built International Centre for Diffraction Data (ICSD) database (version 1.0d, 2003). All desired phases and other peaks were identified by comparing the

s obtained from the database as well as from previous investigation.

3.7.2 Density measurements

The density of samples after dehydrogenation, pressureless and hot pressed sintering was measured using the standard Archimedesô (water immersion) method: The Archimedesô method consisted of the following steps:

i.) Specimen cleaned using isopropanol followed by drying in air at 80^0C for 10minutes. The dry weight of the sample (m_D) was determined using a balance with an accuracy of 0.1mg (used for all the weight measurements).
ii.) Specimen was boiled in distilled water for 3-5hours, so that all trapped air in the pores of the specimen can be displaced.
iii.) The suspended weight of the specimen (m_S) was determined.
iv.) The surface moisture was removed by a light wipe with a damp cloth and the wet weight (m_w) determined.
v.) The procedure was repeated to check consistency of weighing.

For accuracy each mass was determined five times and the mean values were used to determine the bulk density (ρ_S) and the open porosity (P_O) of the samples. Equations 3.5 and 3.6 were used to determine the bulk density and the open porosity respectively.

$$\rho_S = \frac{m_D \rho_{Water}}{(m_S - m_W)} \text{ ---------- (3.5)}$$

$$P_O = \left(\frac{m_W - m_D}{m_W - m_S}\right) x100 \text{ ---------- (3.6)}$$

Where, m_S = suspended mass, m_W = water saturated mass, m_D = dry mass, $\rho_{water} = 1.000 g cm^{-3}$.

Measured densities of titanium matrix composites (TMCs) were compared to the theoretical density, calculated using the volumetric rule of mixtures (ROM).

3.7.3 Polishing of the samples

Due to the extreme ductility of titanium and its alloys that make it prone to mechanical deformation, a three-step polishing method with an automatic polishing machine was used for excellent and reproducible results. The second half of each cross-sectioned sample (as explained in section 3.7) was hot mounted in bakelite powder. Mounted samples were ground to achieve a flat surface and to remove any scratches with specified SiC papers under specified conditions as shown in table 3.2. Ground samples were then polished on a Pan cloth to 1 µm surface using diamond spray and diamond extender to remove surface stress raisers and machining damage such as microcracks and to increase the reproducibility of data, especially, crack size. Samples were then finally polished with OP-S suspension, rinsed with water, ethanol and dried. Table 3.3 shows the summary of the polishing specification and conditions. All polished samples were etched for 5 to 10s with Krollôs reagent (100 ml water, 1-3 ml hydrofluoric acid, and 2-6 ml nitric acid).

rinding.

Surface	Lubricant	Load (N)	Speed (rpm)	Time (min)
240 grit SiC paper	water	25	300	Until plane
320 grit SiC paper	water	25	300	5-10
400 grit SiC paper	water	25	300	5-10
600 grit SiC paper	water	25	300	5-10
800 grit SiC paper	water	30	150	5-10
1200 grit SiC paper	water	30	150	5-10

Table 3. 3: Preparation method for Polishing

Surface	Lubricant	Load (N)	Speed (rpm)	Time (min)
9 μm diamond suspension on TEXPAN Pad	DIALUBE purple extender	35	150	5-10
6 εm diamond suspension on TEXPAN Pad	DIALUBE purple extender	35	150	5-10
3 εm diamond suspension on TEXPAN Pad	DIALUBE purple extender	35	150	5-10
1 εm diamond suspension on TEXPAN Pad	-	35	150	5-10
0.05 εm Nanometer alumina on NAPPAD Pad		35	150	5-10
MD-Chem	OP-S*	35	150	5-10

**Mix 90ml colloidal silica (OP-S) with 10ml hydrogen peroxide (H_2O_2) (30%). Note: During the last 10 seconds of the preparation step with OP-S, the rotating cloth is flushed with water. This will clean the samples, holder and cloth.*

croscopy (SEM)/ Energy Dispersive X-Ray (EDX) and Optical Microscopy

The morphology, elemental compositions as well as the microstructure of the starting powders and sintered samples was determined using A LEO 1525 FE-SEM Scanning Electron Microscope (SEM) coupled with an Oxford link Pentafet Energy Dispersive X-ray (EDS) spectrometer and optical microscopy (Olympus BX41M). SEM/EDX analysis results provide a powerful basis for the acceptance or rejection of some of the phases identified by the XRD.

3.7.5 Hardness (Hv) and measurements

The hardness of dehydrogenated, pressureless and hot pressed sintered samples, after metallographic preparation as described in section 3.9.3 was measured by indentation technique. A Vickerôs indenter (LECO V-100-A2 Vickers Hardness Tester machine), with a load of 5kg and 10kg was used. The diagonal lengths of the indentations (d_1 and d_2 in Fig. 3.16) were used to calculate the hardness of the sample (Hv) in accordance with equation 3.7.

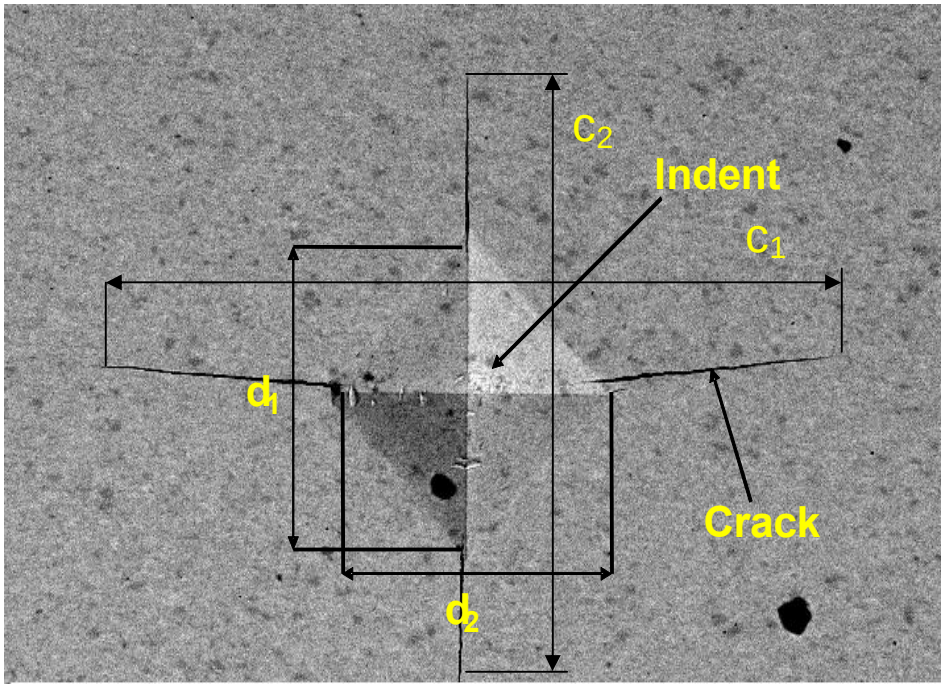

Figure 3. 13: Schematic representations of a Vickers indent.

n length, d_2= horizontal indentation length, d= average indentation length, P is the applied load in Newton (N) and d is the arithmetic mean of the two diagonals in micrometers (μm). Hardness, Hv, is thereby express as

$$H_v = 1854.4 \times \frac{P}{d^2} \text{ ---------- (3.7)}$$

The length of the cracks generated by the indentation (c_1 and c_2), were measured (as shown in Figure 3.16) and used to calculate the indentation fracture toughness (K_{1C}) of the materials, using Anstis equation (3.8).

$$K_{IC} = \xi \left(\frac{E}{Hv} \right)^{1/2} \left(\frac{P}{c^{3/2}} \right) \text{ ---------- (3.8)}$$

where, ξ is the calibration constant (0.016), E is the Young Modulus of Elasticity (GPa) and c the radial crack length (μm) (Anstis *et al.,* 1981).

Chapter Four

4.0 Experimental Results

4.1 Introduction

This chapter presents the results of the characterization of the starting powders, milled TiH_2 and B_4C, dehydrogenated and pressureless sintered TiH_2, pressureless and hot pressed sintered Ti-B_60 and TiH_2-B_4C powder mixtures to form Ti matrix composites (TMC), the microstructure of the sintered samples and mechanical properties of the sintered composites in terms of density and hardness. Discussion of these results and the relationship between densification-to-microstructure-to-property are presented in Chapter 5.

4.2 Characterization of the starting powders.

High purity titanium, titanium hydride, and boron carbide powders obtained from M/S Alfa Aesar (Germany) were used as the starting materials for this research. The phase, elemental composition and detailed chemical analysis of these materials were determined using XRD, SEM and XRF analysis as described in the corresponding section 3.4.2, 3.7.1, and 3.7.4 respectively. XRD result of the commercial titanium and titanium hydride powders have shown that there is only a single phase corresponding to Ti and TiH_2 in each of them respectively, while the pattern of commercially obtained boron carbides shows reflections corresponding to B_4C and few peaks that matched with silicon carbide, SiC. However, further chemical analysis using XRF has shown that the titanium hydride powder contains a small quantity of Nickel, Ni, while boron carbide contains some impurities such as Cu, Ni, Fe, Mn, Cr, K, Si, Al, and Mg.

ressureless sintering of TiH_2.

4.3.1 Dehydrogenation of TiH_2.

The dehydrogenation was carried out using both loose powder and compacts as described in section 3.6.2. The loose TiH_2 powder was dehydrogenated at 680^oC after the dwelling time of 120mins, which shows the significance of dwelling time in achieving pure Ti phase (Table 4.1). The weight change and XRD results reveal that the powder was completely converted into Ti. In the case of TiH_2 green compact, samples were subjected to different dehydrogenation temperatures that started from 680^oC to 715^oC. Within this temperatures range, dehydrogenation time and heating rate was varied (Table 4.1), XRD analysis and weight change measurement indicate that at all other temperatures considered one could detect the presence of TiH_2 except at 715^oC where the compact was completely converted into Ti with a very insignificant trace of Ni. The insignificant Ni peak was noticed up till the sintering temperature of 1000^oC, above which there was no trace of it again. Fig. 4.1 shows the XRD patterns of TiH_2 powder and compact with complete dehydrogenation achieved at 680^oC and 715^oC respectively.

Table 4. 1: Phase composition observed during dehydrogenation of TiH_2 powder and compact.

Sample	*Dehydrogenation condition*			*Phase composition*
	Temperature (^oC)	*Heating rate (^oC/min)*	*Dwelling time (min)*	
1.TiH_2 powder	*680*	*6*	*60*	*TiH_2 ,TiH, Ti*
2.TiH_2 powder	*680*	*6*	*90*	*TiH_2 ,TiH, Ti*
3.TiH_2 powder	*680*	*2*	*90*	*Ti, TiH*
4.TiH_2 powder	*680*	*2*	*120*	*Ti*
5.TiH_2 compact	*680*	*2*	*120*	*TiH_2 ,TiH, Ti*
6.TiH_2 compact	*700*	*2*	*90*	*TiH_2 ,TiH, Ti*
7.TiH_2 compact	*700*	*2*	*120*	*TiH, Ti, Ni*
8.TiH_2 compact	*715*	*2*	*120*	*Ti, Ni*

(b)

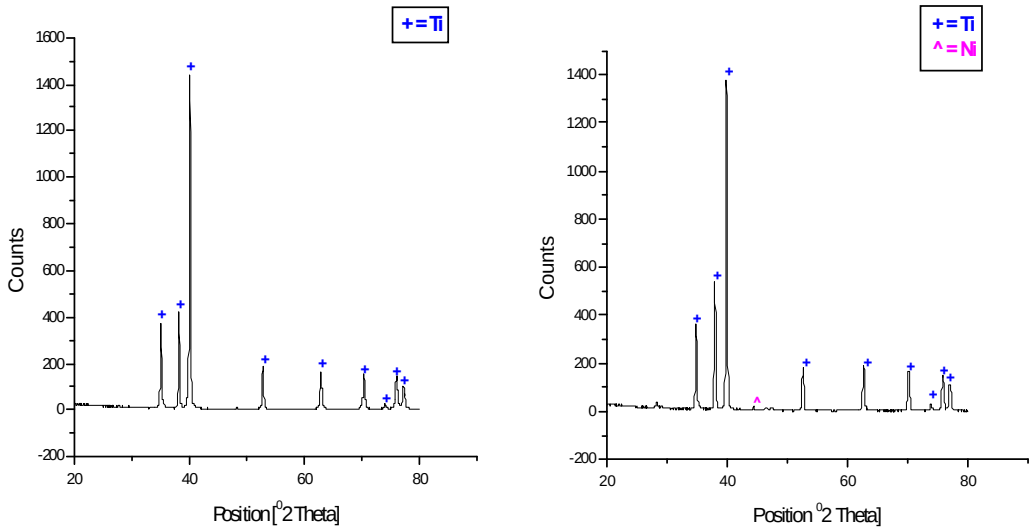

Figure 4. 1: XRD patterns of dehydrogenated (a) TiH_2 powder at 680 °C and (b) TiH_2 compact at 715 °C.

4.3.2 Pressureless sintering of TiH_2 and Ti compact

Pressureless sintering of compacted commercial TiH_2 and Ti was carried out as described in the corresponding section 3.6.1.and 3.6.2 respectively. Sintering temperatures investigated for the two powders ranged from 750 to 1400°C. TiH_2 compact samples were simultaneously dehydrogenated and pressureless sintered over the investigated temperature range. The relative density of pressureless sintered Ti from TiH_2 at 750°C for 90min reached at a heating rate of 6°C /min was 86.74% of theoretical (3.91g/cm^3) (Table 4.2). However, a relative density of 100% of theoretical was obtained at 1200°C, 1300°C and 1400°C for Ti derived from TiH_2. A noticeable densification through pressureless sintering of commercial Ti was observed at sintering temperatures starting from 1000°C (Table 4.2). The densification results of converted TiH_2 are far better compared to 95.00 % of relative density achieved with commercial Ti compact at 1400°C under the same conditions. These results show that TiH_2 based materials start to densify at sintering temperature as low as 750°C, which indicate that Ti produced from TiH_2 has a better sintering

ared to commercial Ti used here. Table 4.2 summaries the density, phase composition and mechanical properties of pressureless sintered (Isothermal sintering time, 90min) samples of commercial Ti and Ti from commercial TiH_2 under the same conditions.

Table 4. 2: Density, phase composition and mechanical property of pressureless sintered (Isothermal sintering time, 90min) sample of comm. Ti and Ti from comm. TiH_2.

Sample	*Sintering Conds.*	*Green density (%)*	*Sintered density (g/cm^3)*	*% Theoretical density*	*Open porosity (%)*	*Phase composition*	*Vickers hardness (Hv)*
PL750**TiH$_2$**90	*750*°C	*72.1*	*3.91*	*86.70*	*12.23*	Ti, Ni	*237±5*
PL800**TiH$_2$**90	*800*°C	*72.1*	*4.02*	*89.14*	*5.99*	Ti, Ni	*243±14*
PL900**TiH$_2$**90	*900*°C	*72.1*	*4.17*	*92.25*	*1.35*	Ti, Ni	*249±28*
PL1000**TiH$_2$**90	*1000*°C	*72.1*	*4.41*	*97.78*	*0.86*	Ti, Ni	*254±33*
PL1000**Ti**90	*1000*°C	*79.3*	*3.67*	*81.37*	*16.85*	Ti	*236±22*
PL1100**TiH$_2$**90	*1100*°C	*72.1*	*4.49*	*99.56*	*0.77*	Ti	*273±24*
PL1100**Ti**90	*1100*°C	*79.3*	*4.01*	*88.91*	*2.62*	Ti	*240±15*
PL1200**TiH$_2$**90	*1200*°C	*72.1*	*4.51*	*100*	*0.45*	Ti	*257±11*
PL1200**Ti**90	*1200*°C	*79.3*	*4.18*	*92.68*	*0.36*	Ti	*251±24*
PL1300**TiH$_2$**90	*1300*°C	*72.1*	*4.54*	*100*	*0.40*	Ti	*262±19*
PL1300**Ti**90	*1300*°C	*79.3*	*4.28*	*94.90*	*0.12*	Ti	*259±10*
PL1400**TiH$_2$**90	*1400*°C	*72.1*	*4.54*	*100*	*0.35*	Ti	*270±31*
PL1400**Ti**90	*1400*°C	*79.3*	*4.30*	*95.34*	*0.12*	Ti	*265±11*

tterns of pressureless sintered commercial Ti at 1200°C and 1400°C for reference purpose, while figure 4.3 shows the XRD patterns of Ti obtained from TiH_2 at pressureless sintering temperatures of 750°C, 1000°C, 1200°C, and 1400°C respectively.

All observed peaks in the XRD patterns of dehydrogenated and pressurelessly sintered samples of TiH_2 are matched with single phase Ŭ-Ti (00-044-1294, ICSD data base). The same was observed for material produced from the commercial Ti powder. Detailed XRD patterns of dehydrogenated and pressurelessly sintered samples at different temperatures investigated are shown in appendix C.

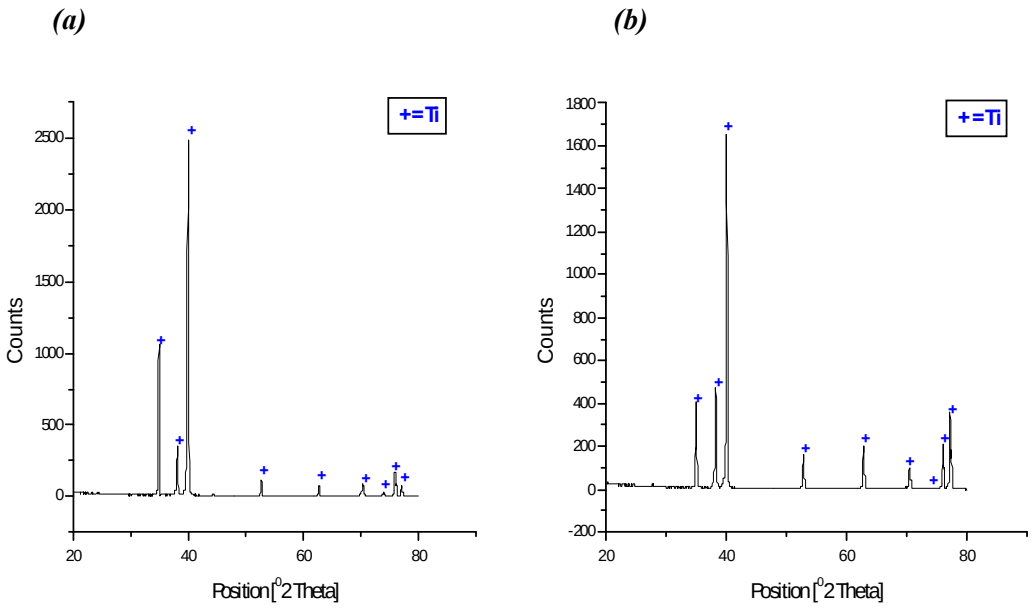

Figure 4. 2: XRD patterns of pressureless sintered comm. Ti at (a) 1200 °C and (b) 1400 °C

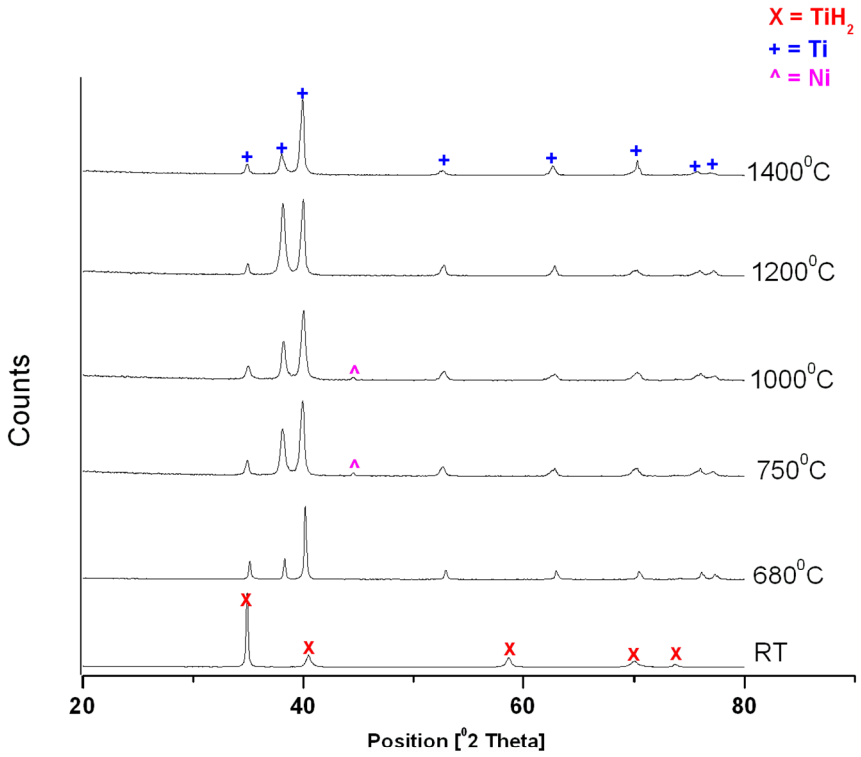

Figure 4. 3: XRD patterns of dehydrogenated and pressureless sintered TiH_2 powder and compacts at various sintering temperatures.

Figure 4.4 shows (a- e) the SEM images of some selected sintered Ti samples produced from TiH_2 after simultaneous dehydrogenation and sintering at the temperatures investigated. The SEM micrograph of sample sintered at 750^{o}C (Fig. 4.4a) has more irregular pores and as the sintering temperature increases to1200^{o}C and 1400^{o}C, the presence of spherical pores could be observed (Fig. 4.4 d-e) respectively. The evolution of microstructure seems to follow the normal pattern of sintering principles. Fig. 4.4f shows the etched microstructure of Ti produced from TiH_2 after dehydrogenation and sintering at 1400^{o}C. The structure shows weaving structure with average particle size of 20ε m. Fig 4.4 (g-h) show the microstructure of the sintered (under the same sintering condition as TiH_2) commercial Ti for the purpose of comparison.

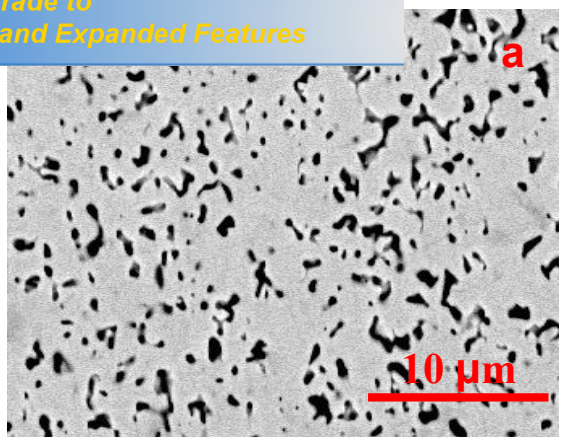

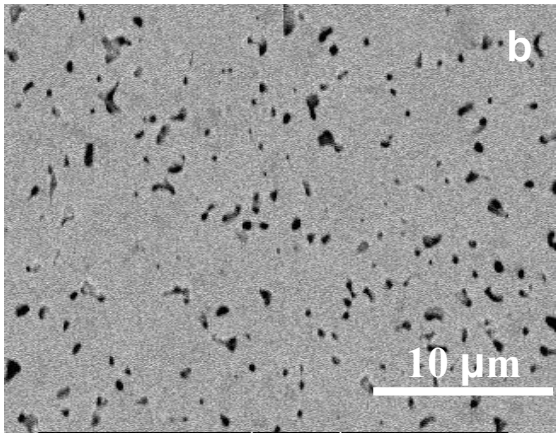

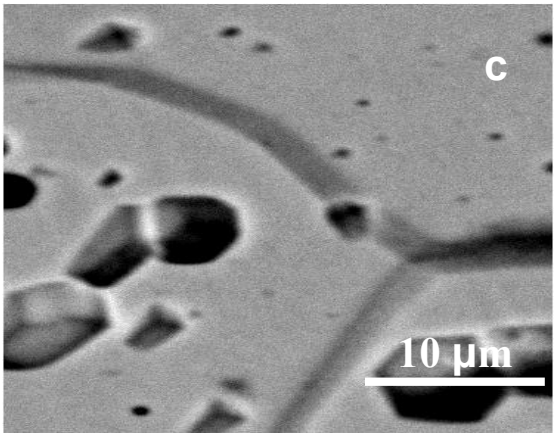

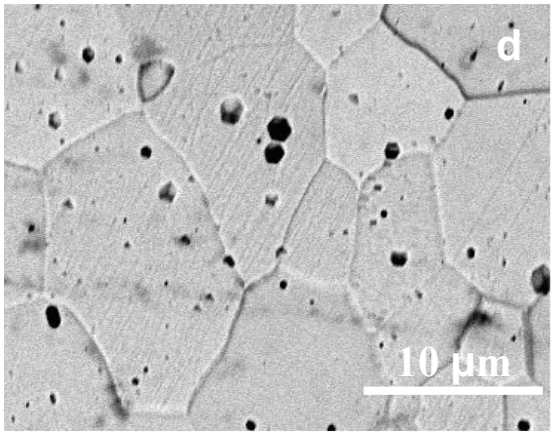

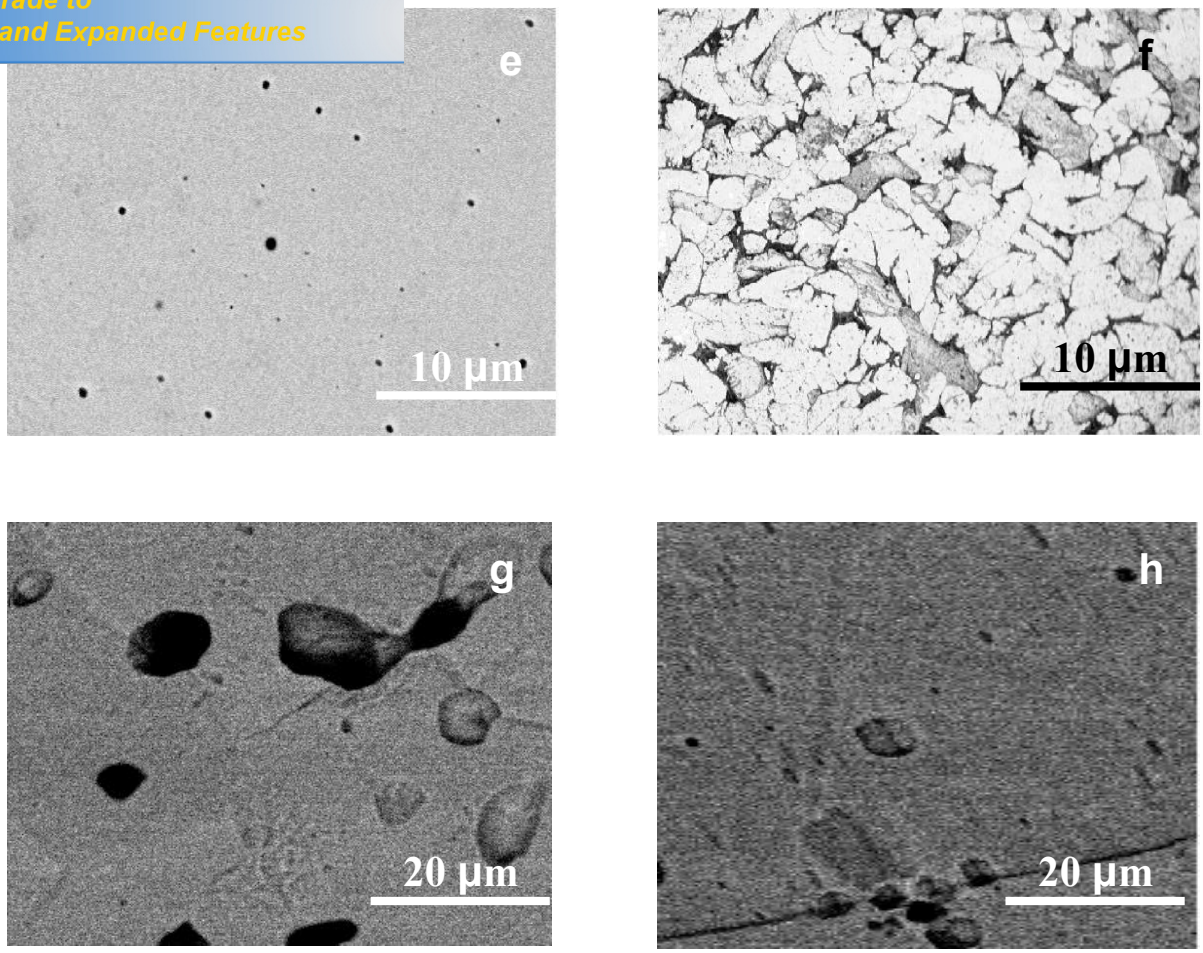

Figure 4. 4: SEM micrographs of as sintered TiH_2 at (a) 750^oC, (b) 900^oC, (c)1000^oC,(d) 1200^oC (e) 1400^oC (f) light micrograph of etched sintered Ti obtained from TiH_2 at 1400^oC; sintered commercial Ti at (g) 1200^oC and (h)1400^oC for reference.

All the EDS of the dehydrogenated and sintered samples of TiH_2 compact confirmed the presence of only Ti without any observed foreign constituent, thus indicating no impurities in the samples produced. Fig. 4.5 shows the EDS of sintered TiH_2 samples at 1400^oC. The EDS analysis of the samples sintered at the other temperatures gave the same results.

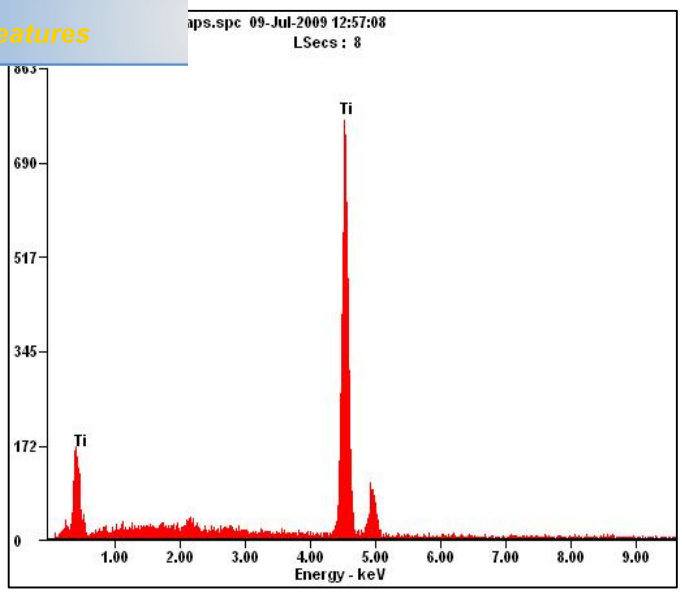

Figure 4. 5: EDS graphs of as sintered TiH_2 samples at(c) 1400^oC

4.4 Mixing and characterization of TiH_2-B_4C powders for titanium matrix composite (TMC)

TiH_2 and B_4C powders were carefully mixed together as described in section 3.5.1 and a homogeneous distribution of the ceramic in TiH_2 matrix was formed. Uniform distribution of this ceramic (B_4C) is expected to further boost uniform distribution of the final reinforcements. The starting powders were so adjusted to synthesize different volume percentage reinforcements (TiC, TiB, and possibly TiB_2), 10, 20, 40, 60, and 80 vol. % in the final titanium matrix composite. Detailed calculations of the stoichiometry amount of TiH_2 and B_4C powders mixed together to form the required composition needed for the formation of the final desired particulate-reinforced TMCs are shown in the appendix A.1. Table 4.3 summarizes the required weight percent of TiH_2, B_4C and volume percent of Ti, TiC and TiB expected in the final TMC. Subsequent mixed powders were characterized to check for the phase, elemental composition and the homogeneity or level of distribution of the mixed

M analysis. Figure 4.6 shows the XRD pattern of the mixed powders for fabrication of different volume percent reinforced TMC.

Table 4. 3: Summary of quantity of mixed powders TiH_2, B_4C and corresponding volume % reinforcements (TiC, TiB) expected in the final TMC Composites.

Material	Reinfs. (Vol %)	Mole Ratio (TiB: TiC)	Ti matrix Vol%	TiB Vol%	TiC Vol%	TiH_2 (wt. %)	B_4C (wt. %)
TiH_2-B_4C	10	4:1	90.00	8.109	1.891	98.16	1.84
TiH_2-B_4C	20	4:1	80.00	16.219	3.781	96.32	3.68
TiH_2-B_4C	40	4:1	60.00	32.438	7.562	92.66	7.35
TiH_2-B_4C	60	4:1	40.00	48.657	11.343	89.03	10.97
TiH_2-B_4C	80	4:1	20.00	64.876	15.124	85.43	14.57

Figure 4.6a shows the XRD patterns of the mixed powder that contain 98.16wt % TiH_2 and 1.84wt % B_4C for the fabrication of 10 vol. % reinforced titanium matrix composite (TMC). The pattern shows reflections that correspond to a single phase TiH_2. However, SEM/EDX analysis of the same sample (Fig.4.7a) shows the presence of B_4C uniformly distributed over the TiH_2 matrix. The inability of XRD to show the presence of B_4C particles in the mixed powder could be attributed to the density difference and the smaller quantity of B_4C (1.84wt %) added to TiH_2 since XRD does not detect material with concentration less than 2-5wt. % in the sample being examined. The same observation was made in the XRD pattern (Fig. 4.6b) and SEM/EDX (Fig.4.7b) for mixed powder prepared for the fabrication of 20 vol. % reinforced titanium matrix composite (TMC). The situation differs for mixed powder prepared for the fabrication of 40, 60, and 80 vol. % reinforced titanium matrix composite (TMC) respectively. The XRD pattern of the mixed powders in these

presence of B_4C (Fig. 4.6c-e). The reason is attributed to the increase in the percentage weight of the B_4C particles in the sample (Table 4.3).

(a)

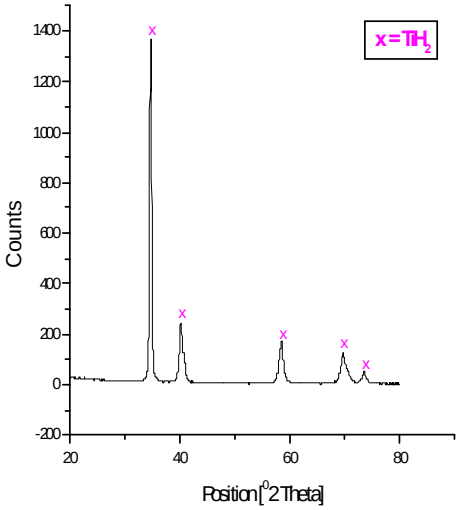

(b)

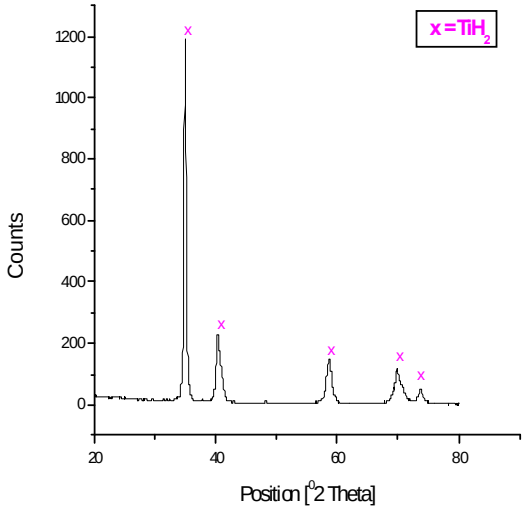

(c)

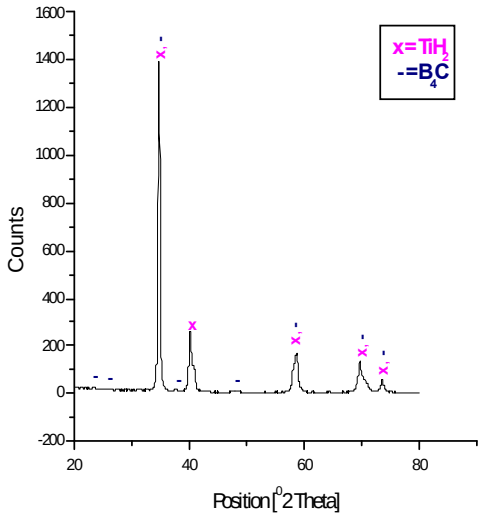

(d)

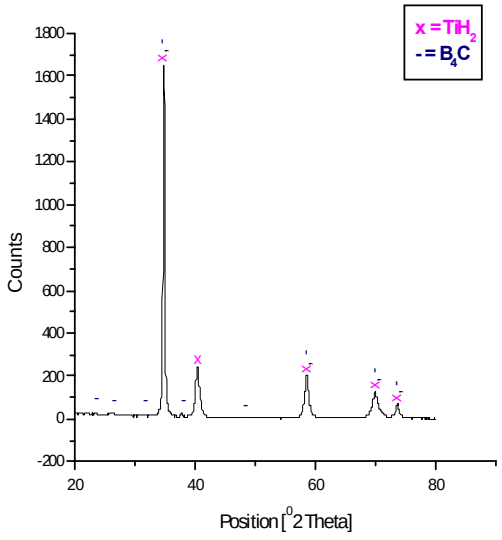

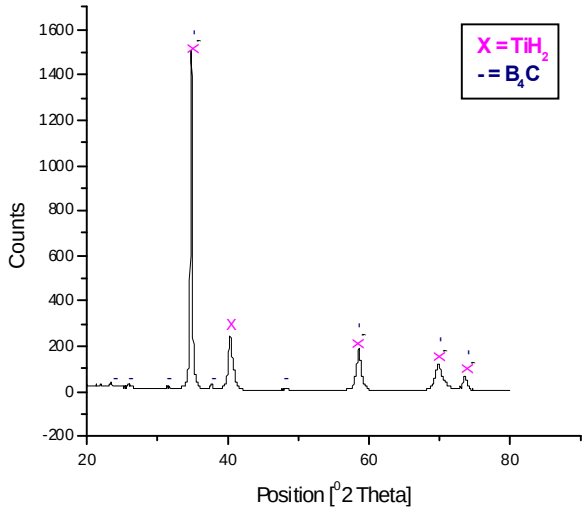

Figure 4. 6: XRD patterns of mixed TiH_2 and B_4C powders at initial state of (a) 10 vol. % reinforced TMC (b) 20 vol. % reinforced TMC of (c) 40 vol. % reinforced TMC and (d) 60 vol. %reinforced TMC (e) 80 vol. % reinforced TMC

own in figure 4.7, reveal in all cases a homogeneous distribution of B_4C in the matrix.

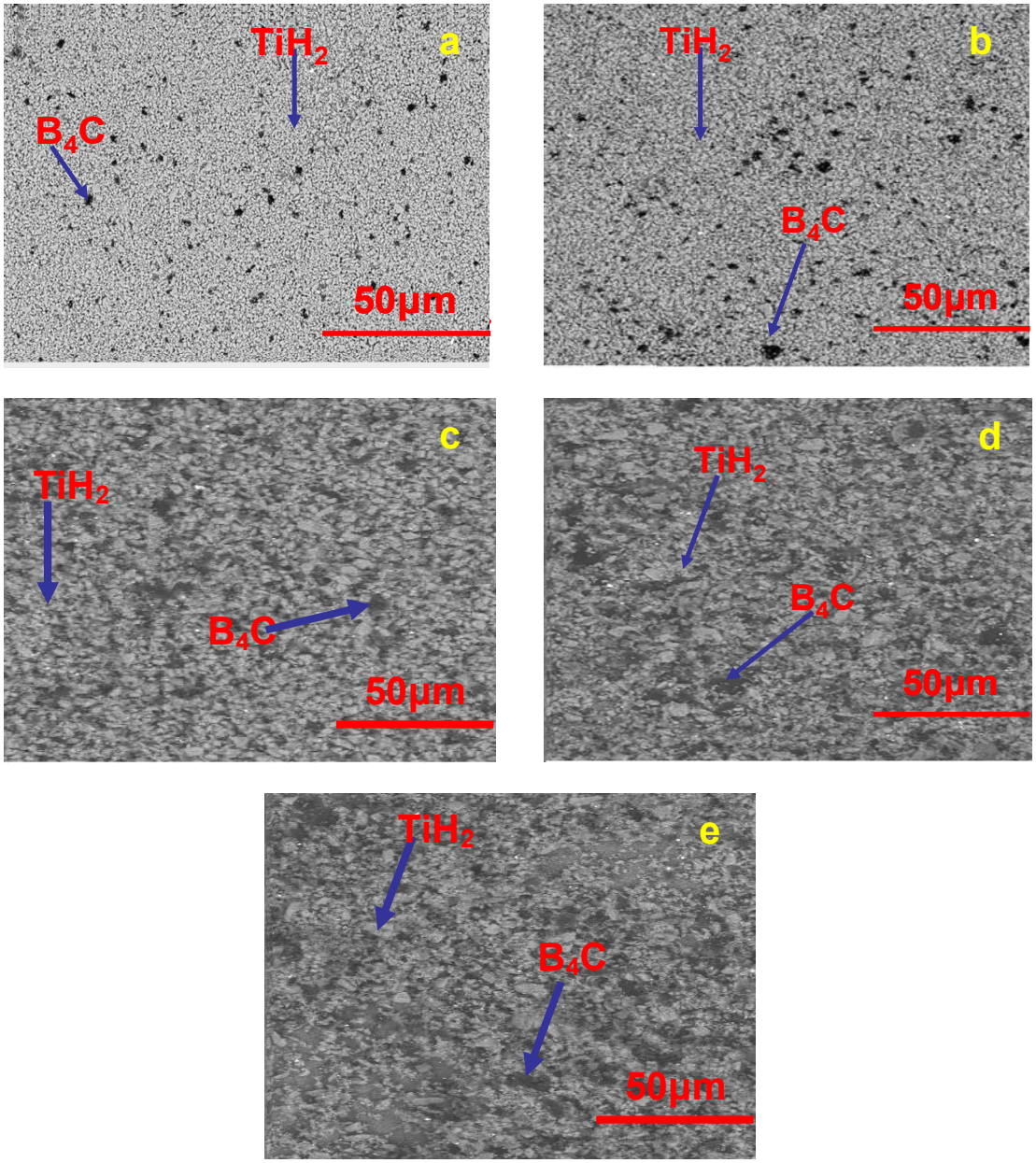

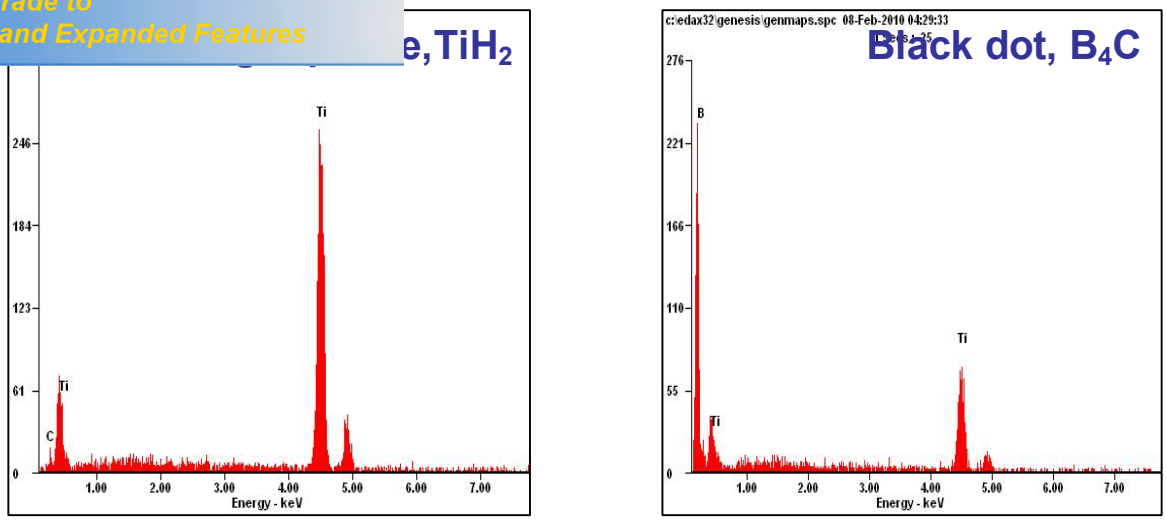

Figure 4. 7: SEM of mixed TiH_2 and B_4C powders (green body) of (a) 10 vol. % reinforced TMC (b) 20 vol. % reinforced TMC (c) 40 vol. % reinforced TMC (d) 60 vol. % reinforced TMC (e) 80 vol. % reinforced TMC; EDX of mixed TiH_2 and B_4C powders (green body) of (a) 10 vol. % reinforced Ti matrix composite.

4.5 In situ synthesis of titanium matrix composite (TMC) from TiH_2 and B_4C powder mixture

In situ synthesis of titanium matrix composites considered in this research is based on the principle of chemical reactions occurring when TiH_2 and B_4C powder mixture is sintered at high temperatures as suggested by Zhang *et al.* (1999) in a similar reaction that involves Ti and B_4C. This process can be considered as in-situ technique of producing TMCs using powder metallurgy method. The expected chemical reactions were as explained in section 3.6.3 with equations 3.1 to 3.4. Two different sintering methods, namely pressureless sintering and hot-pressing were considered in this work.

of TiH_2-B_4C for Ti matrix composites

Cylindrical compacts of 18mm diameter and about 5mm in height were produced from TiH_2-B_4C powder mixtures as described in section 3.5.1 using a hardened steel die. Due to the difficulty involved in the compaction of TiH_2-B_4C powder mixtures and production of compacts intended for the pressureless sintering and synthesis of 20 and 40 vol. % reinforced Ti composites, 3wt. % each of binding agents (stearic acid and polyethylene glycol-PEG) was then added to the powder mixtures. Introduction of these binders enhanced the production of compacts that were subsequently used to carry out the pressureless sintering at different temperatures ranging from 1100-1400^{0}C for an isothermal sintering time of 90min as described in section 3.6.3. Titanium matrix composites with in-situ 10, 20 and 40 vol. % reinforcements were subsequently synthesized and Table 4.4, 4.5, and 4.6 summarize the densities and other properties of the 10, 20 and 40 vol. % reinforced Ti composites respectively.

ness and phase composition of pressureless sintered (isothermal 10vol. % reinforced titanium composites at different sintering temperatures. Assumed theoretical density = 4.54g/cm^3

Sample	*Sintering Condt.*	*Green density (%)*	*Sintered density (g/cm^3)*	*% theoret. density*	*Open Porosity (%)*	*Phase Composition*	*Vickers Hardness Hv-5*	*Reference*
Ti	*1400°C*		*4.54*				*270±31*	*Present work*
*10**PL** TMC **1100***	*1100°C*	*65.6*	*4.42*	*97.36*	*1.9340*	*Ti TiB TiC TiB_2 [a]*	*727±10*	*Present work*
*10**PL** TMC **1200***	*1200°C*	*65.5*	*4.46*	*98.24*	*1.3609*	*Ti TiB TiC Ti_3B_4 [a]*	*746±23*	*Present work.*
*10**PL** TMC **1300***	*1300°C*	*65.6*	*4.48*	*98.68*	*1.4950*	*Ti TiB TiC TiB_2 [a]*	*715±4*	*Present work*
*10**PL** TMC **1400***	*1400°C*	*65.6*	*4.65*	*100*	*0.5552*	*Ti TiB TiC TiB_2 [a]*	*705±19*	*Present work*
Hot Pressing[1)]	*1200°C*		-			-	*581*	*Ni et al., (2006)*

[1)] B_4C particle size 3.5 µm; [a] present in traces

ess and phase composition of pressureless sintered (isothermal forced titanium composites at different sintering temperatures. Assumed theoretical density = 4.55g/cm^3.

Sample	Sintering Conds.	Green density (%)	Sintered density (g/cm^3)	% Theoretical density	Open porosity (%)	Phase composition	Vickers hardness (Hv-5)	Reference
*20**PL**TMC**1100***	*1100°C*	*77.50*	*4.19*	*92.09*	*1.93*	*Ti TiB TiC TiB_2*[a]	*695±21*	*Present work*
*20**PL**TMC**1200***	*1200°C*	*77.50*	*4.26*	*93.63*	*0.71*	*Ti TiB TiC TiB_2*[a]	*754±22*	*Present work*
*20**PL**TMC**1300***	*1300°C*	*77.50*	*4.38*	*96.26*	*0.46*	*Ti TiB TiC TiB_2*[a]	*851±34*	*Present work.*
*20**PL**TMC**1400***	*1400°C*	*77.50*	*4.51*	*99.12*	*0.43*	*Ti TiB TiC TiB_2*[a]	*854±37*	*Present work*

[a] present in traces

ess and phase composition of pressureless sintered (isothermal forced titanium composites at different sintering temperatures. Assumed theoretical density = 4.57g/cm^3

Sample	*Sintering Conds.*	*Green density (%)*	*Sintered density (g/cm^3)*	*% Theoretical density*	*Open porosity (%)*	*Phase composition*	*Vickers Hardness (Hv-5)*	*Reference*
*40**PL**TMC**1100***	*1100^{0}C*	*77.08*	*3.68*	*80.53*	*10.25*	*Ti TiB TiC TiB_2 [a]*	*500±11*	*Present work*
*40**PL**TMC**1200***	*1200^{0}C*	*77.08*	*3.77*	*82.49*	*8.08*	*Ti TiB TiC TiB_2 [a]*	*563±32*	*Present work*
*40**PL**TMC**1300***	*1300^{0}C*	*77.07*	*3.95*	*86.43*	*6.60*	*Ti TiB TiC TiB_2 [a]*	*673±31*	*Present work.*
*40**PL**TMC**1400***	*1400^{0}C*	*77.08*	*4.27*	*93.44*	*0.53*	*Ti TiB TiC TiB_2 [a]*	*858±24*	*Present work*

[a] present in traces

The density of the synthesized Ti composites was measured using Archimedesô method. It can be observed from the above tables that higher densities were obtained by Ti composites with 10vol. % reinforcements than those with 20 and 40 vol. % reinforcements. This difference was probably due to the inclusion of higher amounts of in-situ formed reinforcements (resulting from increased B_4C weight percent) that didnôt sinter well.

Vickers hardness of the pressureless sintered reinforced Ti composites was obtained after 5kg standard load indentation with 10s indentation time as described in section 3.7.5. Higher hardness value was observed in the samples sintered at 1400^{o}C, compared to other sintering temperatures and the Vickers hardness values measured

lightly higher in 40 and 20 vol. % reinforced Ti composites than that of 10 vol. % reinforced Ti matrix composites.

Figure 4.8, 4.9, and 4.10 show the XRD patterns of as sintered 10, 20, and 40vol. % reinforced Ti composites respectively produced at sintering temperature 1100^{o}C, 1200^{o}C, 1300^{o}C, and 1400^{o}C. Analysis of the patterns shows no trace of starting powders (TiH_2 and B_4C), an indication that the titanium matrix reacted well with B_4C. Besides Ti matrix, the major phases observed are TiC and TiB with a trace amount of TiB_2. Only sample 10**PL**TMC**1200** shows a few new reflections that correspond to Ti_3B_4. Also, the peak intensity of the in-situ formed reinforcements increased gradually with increased volume fraction, indicating that the volume fraction of reinforcing phase increases with increasing B_4C content in the starting powder.

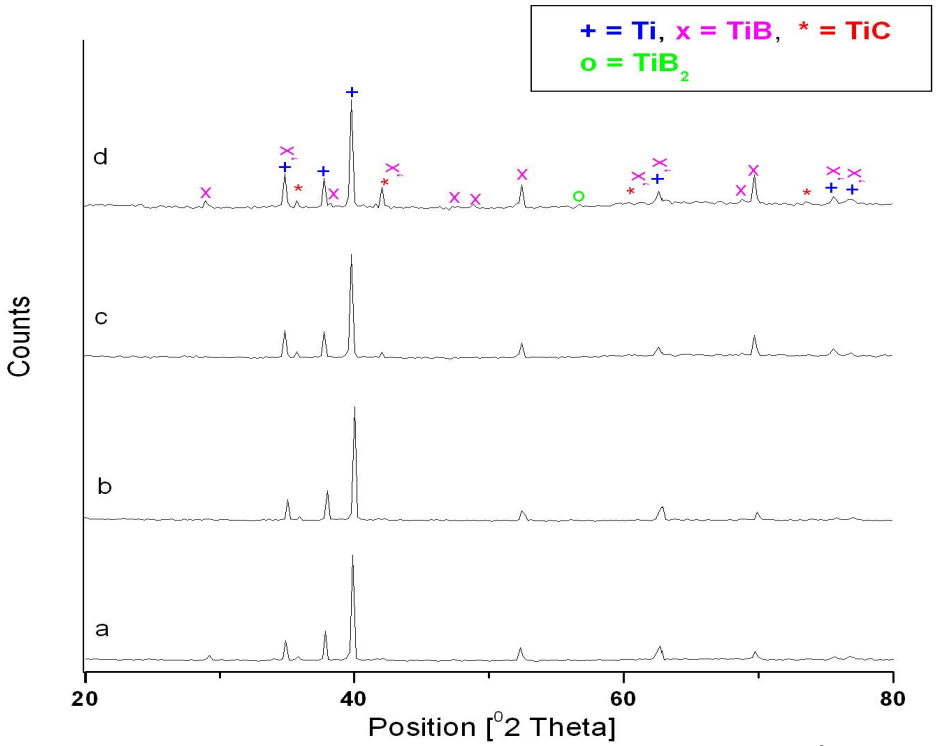

Figure 4. 8: XRD patterns of pressureless sintered 10 vol. % TMC at (a) 1100^{0}C (b) 1200^{0}C (c) 1300^{0}C and (d) 1400^{0}C.

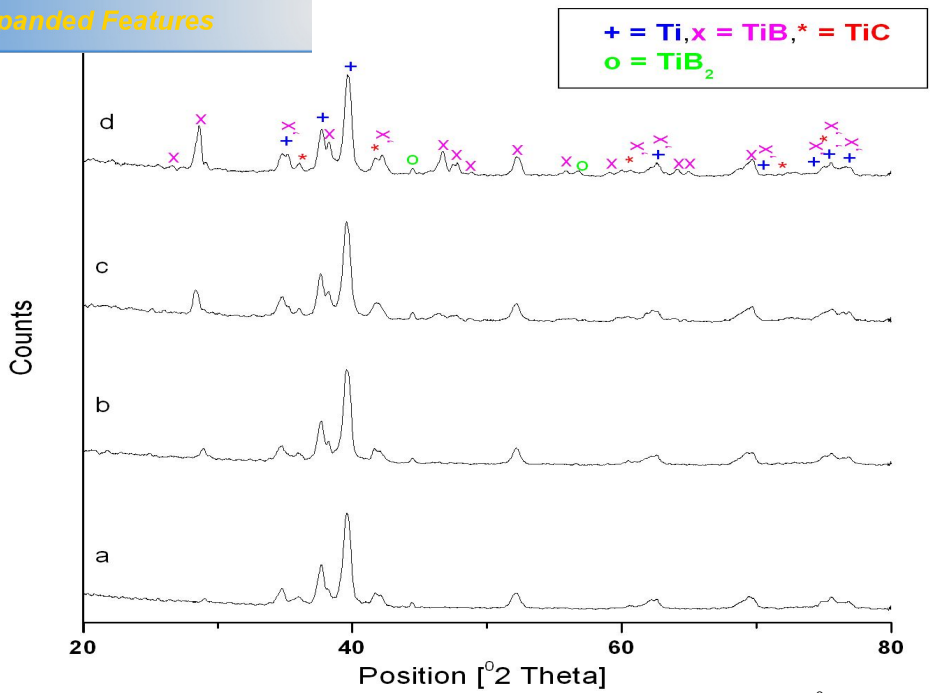

Figure 4. 9: XRD patterns of pressureless sintered 20 vol. % TMC at (a) 1100^0C (b) 1200^0C (c) 1300^0C and (d) 1400^0C.

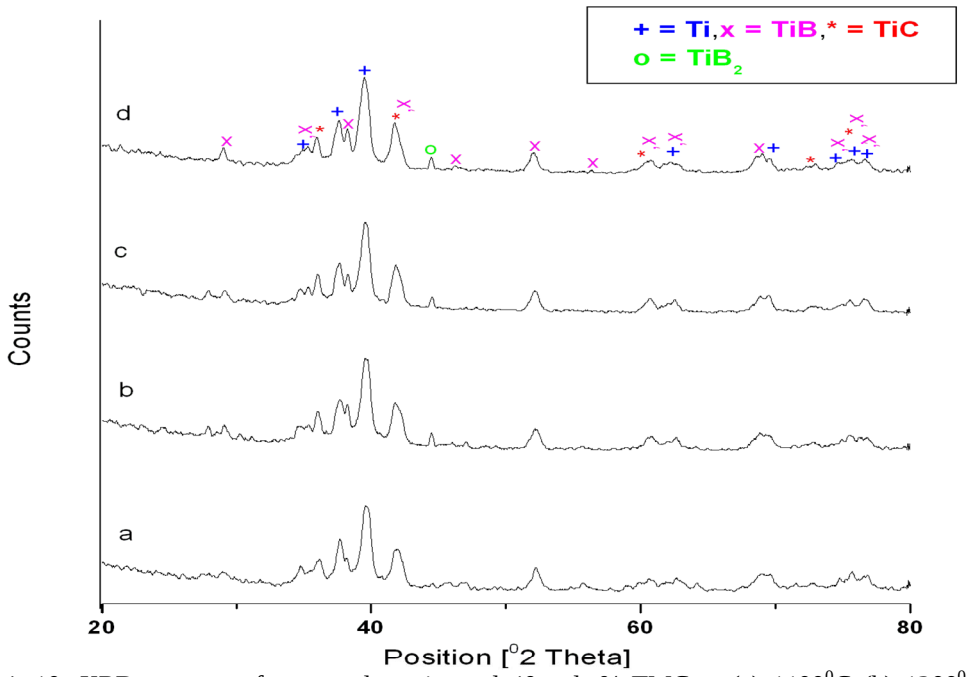

Figure 4. 10: XRD patterns of pressureless sintered 40 vol. % TMC at (a) 1100^0C (b) 1200^0C (c) 1300^0C and (d) 1400^0C.

ow the SEM images of the as-sintered 10, 20 and 40 vol. % reinforced Ti composites samples treated at various sintering temperatures. The micrographs, especially for samples sintered at 1300 and 1400^{o}C (**10PL**TMC**1300**, 10**PL**TMC**1400**, 20**PL**TMC**1300** and 20**PL**TMC**1400**) exhibit clearly two different morphological structures, namely needle and equiaxed shaped inclusions that are uniformly distributed in the titanium matrix. These images may imply that the chemical reaction that leads to the evolution of in-situ reinforcements in the Ti matrix is more pronounced at higher sintering temperatures (1200 to 1400^{o}C). The EDS analysis (Fig. 4.12) shows that the needle shaped structure corresponds to TiB, the equiaxed shaped corresponds to TiC, while the light portion in the compositeôs micrograph correspond to titanium matrix. The reinforcement structures observed in 20**PL**TMC**1300** and 20**PL**TMC**1400** decreased in size and number compared to 10**PL**TMC**1400**. For instance, the TiB reinforcements in 10vol. % reinforced Ti composites have a diameter of 2-8ε m and length of 10-255ε m, while those in the 20vol. % reinforced Ti composites have a diameter of 4-12ε m and length of 11-170ε m.

Unlike the sintered samples of 10vol. % reinforced Ti composites, 20 vol. % reinforced Ti composites and 40 vol. % reinforced Ti composites are characterized by a higher amount of porosity in addition to fibrous or clustered and equiaxed shaped reinforcements that correspond to TiB and TiC respectively (Fig. 4.14 and 4.16). The SEM analysis also revealed that the size and type of TiB reinforcements in the composites changes. For instance, sample 40**PL**TMC**1400** shows few needle shaped TiB compared to what was observed in sample 10**PL**TMC**1400** and 20**PL**TMC**1400**. The reduction in number of needle shaped TiB observed in sample 40**PL**TMC**1400** could be as a results of increased TiB volume fraction.

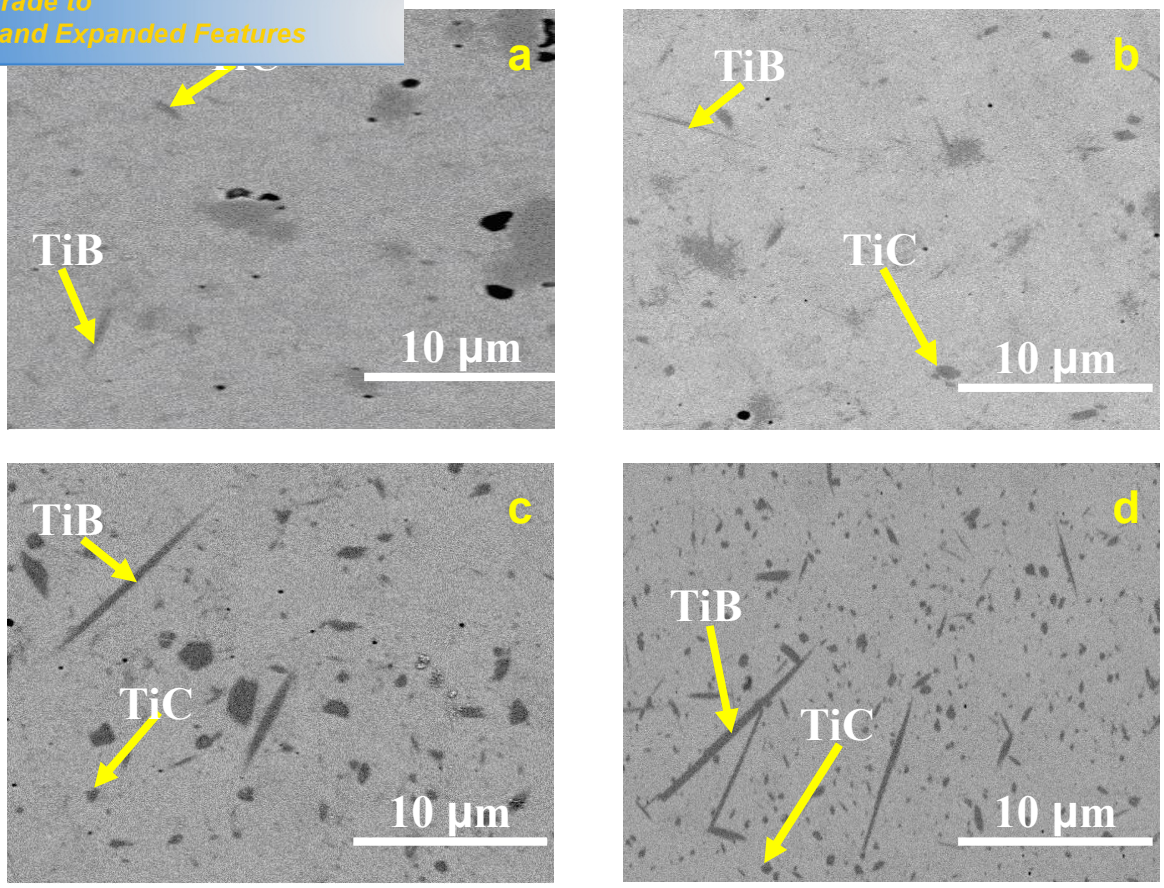

Figure 4. 11: SEM micrographs of pressureless sintered 10 vol. % TMC at (a) 1100^0C (b) 1200^0C (c) 1300^0C and (d) 1400^0C.

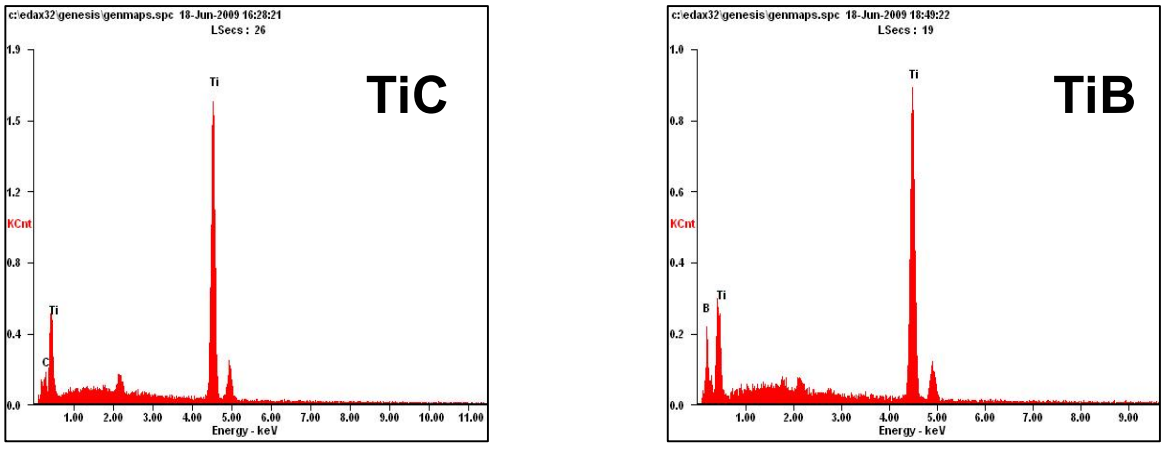

Figure 4. 12: EDS graphs of reinforcements in as sintered sample 10PLTMC1400

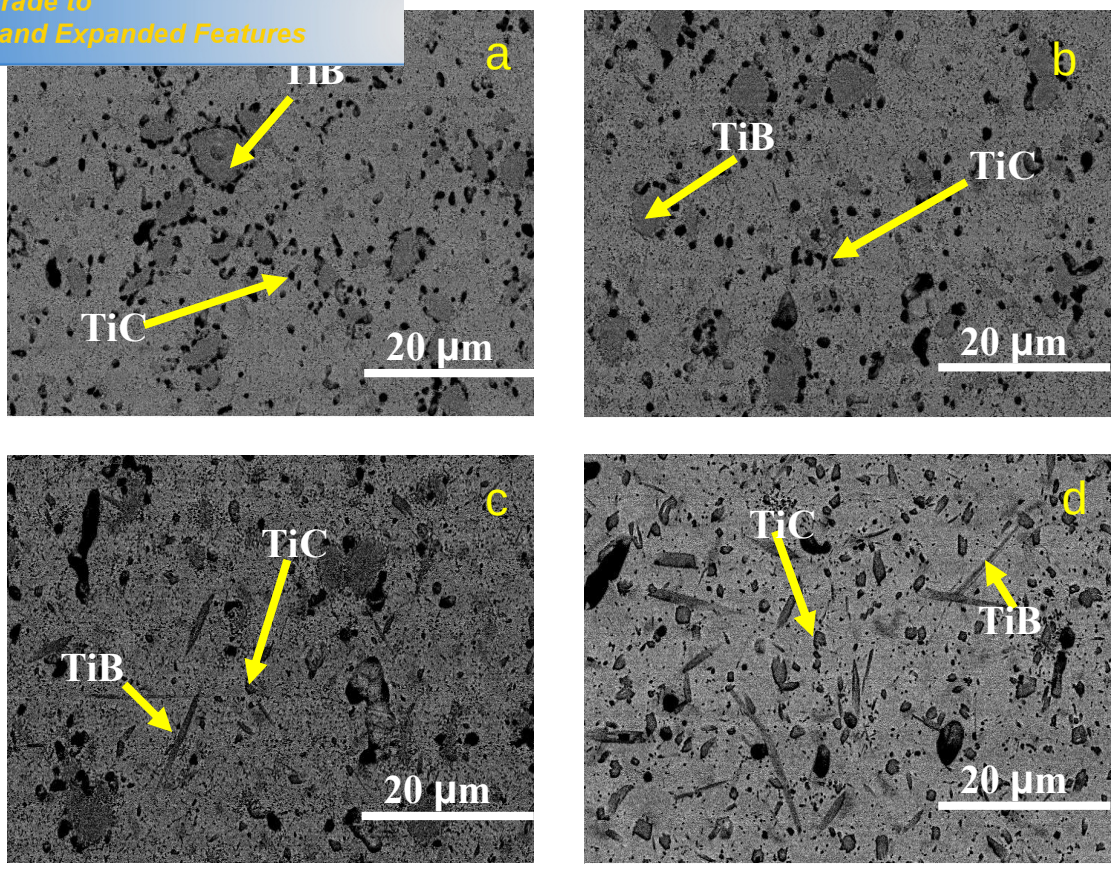

Figure 4. 13: SEM micrographs of pressureless sintered 20 vol. % TMC at (a) 1100^0C (b) 1200^0C (c) 1300^0C and (d) 1400^0C.

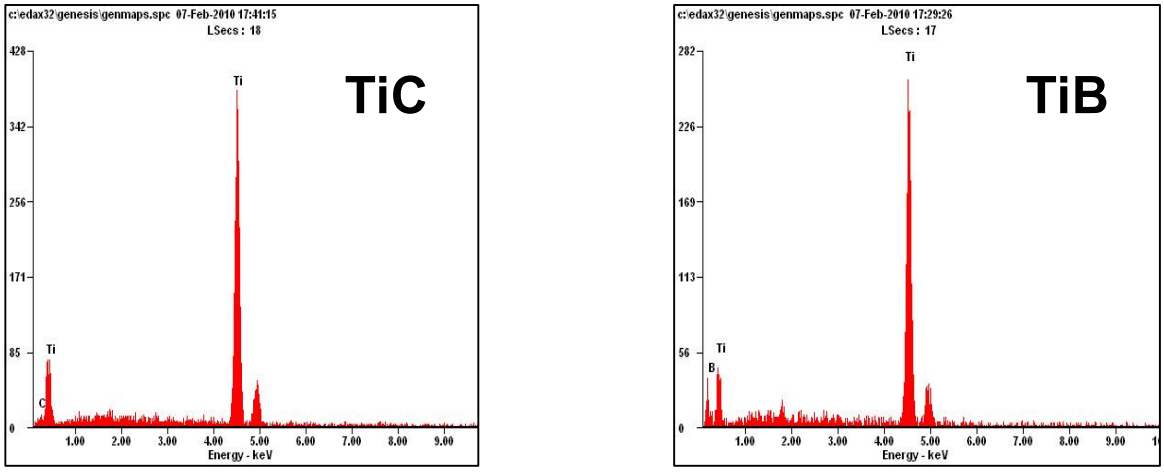

Figure 4. 14: EDS graphs of reinforcements in as sintered sample 20PLTMC1400

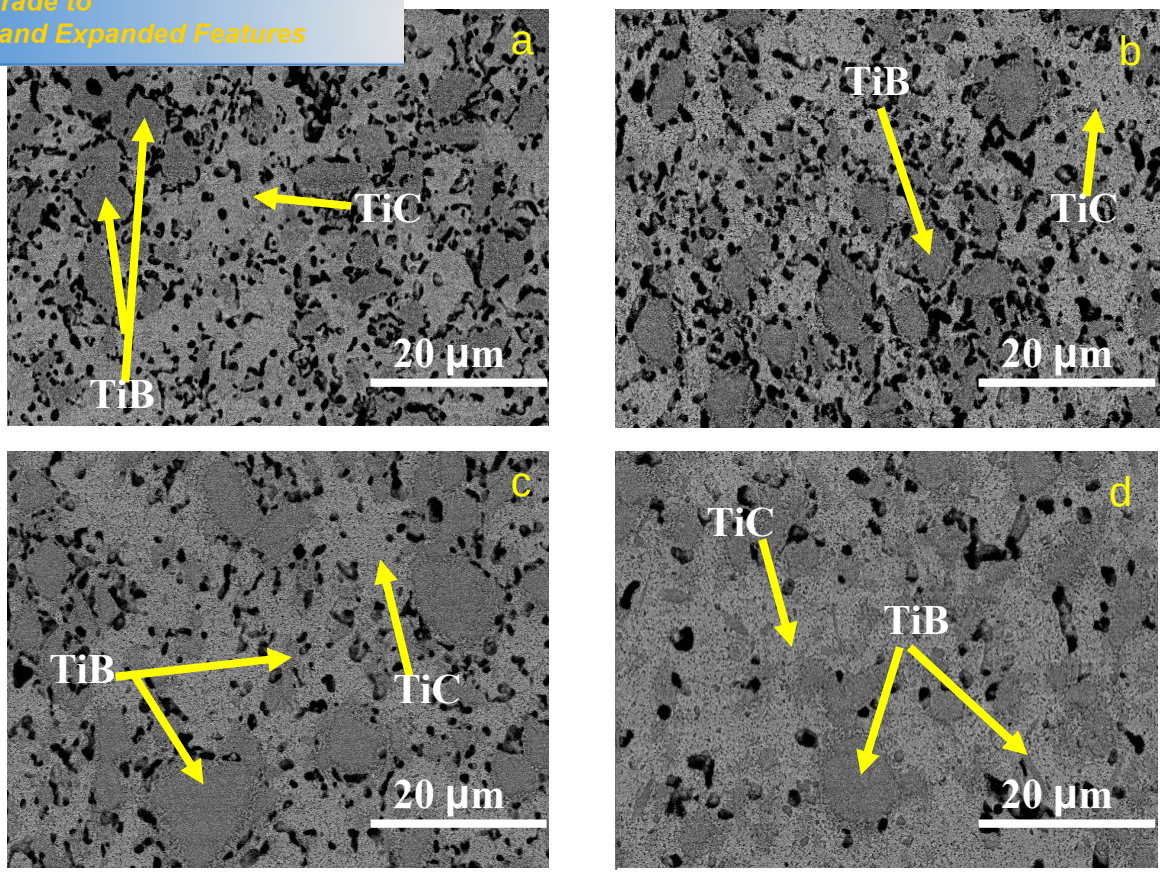

Figure 4. 15: SEM micrographs of pressureless sintered 40 vol. % TMC at (a) 1100^0C (b) 1200^0C (c) 1300^0C and (d) 1400^0C.

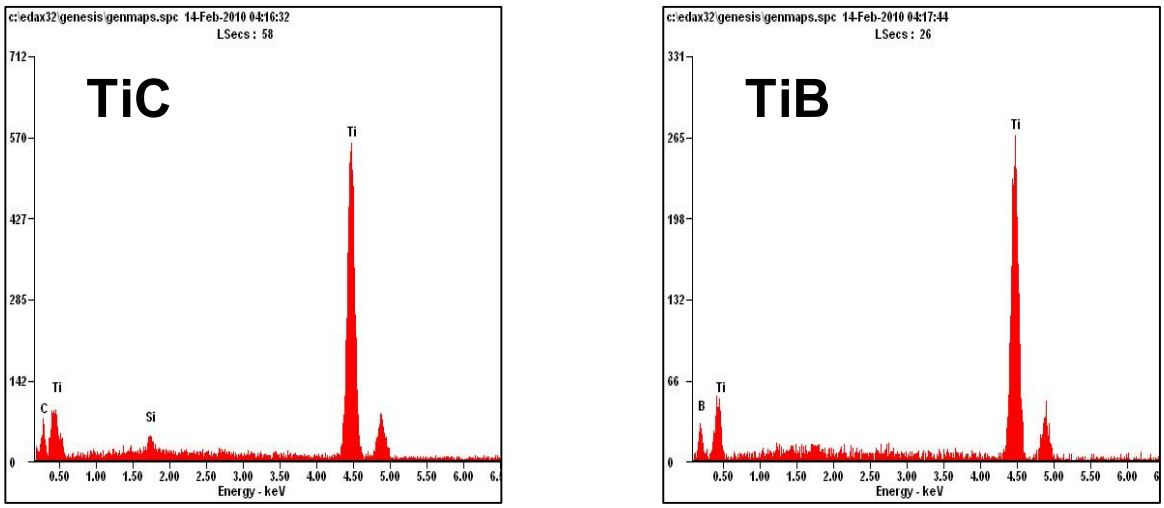

Figure 4. 16: EDS graphs of reinforcements in as sintered sample 40PLTMC1400

Pre-determined stoichiometry amount of TiH_2 and B_4C powders were mixed together and used to fabricate in-situ 20, 40, 60, and 80 vol. % particulate-reinforced titanium matrix composites (TMCs) using hot-pressing method. Different composition of powder mixtures was hot pressed at the selected sintering temperatures (1100, 1200, 1300, and 1400^0C) for 120 minutes under applied pressure of 30 MPa as described in section 3.6.4. This method, instead of pressureless sintering was used because of the higher wt. % B_4C introduced and the need to achieve an enhanced densification in the final reinforced Ti composites. Table 4.7, 4.8, 4.9, and 4.10 summarize densities and mechanical properties of the hot-pressed 20, 40, 60, and 80 vol. % reinforced Ti matrix composites (TMCs) respectively.

Table 4. 7: Density, Vickers hardness and phase composition of hot pressed (isothermal sintering time 120min) 20vol%TMC from TiH_2-B_4C mixture at different temperatures. Assumed theoretical density = 4.55g/cm^3

Sample	*Sintering Conds.*	*Sintered density (g/cm^3)*	*% theoretical density*	*Open porosity (%)*	*Phase composition*	*Vickers hardness (Hv-5)*
*20**HP**TMC**1100***	*1100^{0}C, 30Mpa, 120min at 10^{0}C/min*	*4.48*	*98.46*	*1.78*	*Ti TiB TiC TiB_2*	*921±33*
*20**HP**TMC**1200***	*1200^{0}C, 30Mpa, 120min at 10^{0}C/min*	*4.53*	*99.56*	*0.81*	*Ti TiB TiC TiB_2[a]*	*923±25*
*20**HP**TMC**1300***	*1300^{0}C, 30Mpa, 120min at 10^{0}C/min*	*4.58*	*100*	*0.35*	*Ti TiB TiC TiB_2[a]*	*929±28*
*20**HP**TMC**1400***	*1400^{0}C, 30Mpa, 120min at 10^{0}C/min*	*4.60*	*100*	*0.05*	*Ti TiB TiC TiB_2[a]*	*942±5*

[a] present in traces

s and phase composition of hot pressed (isothermal sintering $_2$-B_4C mixture at different temperatures. Assumed theoretical density = 4.57g/cm^3.

Sample	*Sintering Conds.*	*Sintered density (g/cm^3)*	*% theoretical density*	*Open porosity (%)*	*Phase composition*	*Vickers hardness (Hv-5)*
*40**HP**TMC**1100***	*1100^{0}C, 30Mpa, 120min at 10^{0}C/min*	*4.54*	*99.34*	*1.13*	*Ti TiB TiC TiB_2 [a]*	*1061±14*
*40**HP**TMC**1200***	*1200^{0}C, 30Mpa, 120min at 10^{0}C/min*	*4.59*	*100*	*0.28*	*Ti TiB TiC TiB_2 [a]*	*1073±39*
*40**HP**TMC**1300***	*1300^{0}C, 30Mpa, 120min at 10^{0}C/min*	*4.60*	*100*	*0.25*	*Ti TiB TiC TiB_2 [a]*	*1078±39*
*40**HP**TMC**1400***	*1400^{0}C, 30Mpa, 120min at 10^{0}C/min*	*4.61*	*100*	*0.11*	*Ti TiB TiC TiB_2 [a]*	*1084±36*

[a] present in traces

s and phase composition of hot pressed (isothermal sintering time C mixture at different temperatures. Assumed theoretical density = 4.60g/cm^3

Sample	*Sintering Conds.*	*Sintered density (g/cm^3)*	*% theoretical density*	*Open porosity (%)*	*Phase composition*	*Vickers hardness (Hv)*
*60**HP**TMC**1100***	*1100^{0}C, 30Mpa, 120min at 10^{0}C/min*	*4.28*	*93.04*	*4.40*	*Ti TiB TiC TiB_2 [a]*	*1194±66*
*60**HP**TMC**1200***	*1200^{0}C, 30Mpa, 120min at 10^{0}C/min*	*4.60*	*100*	*0.68*	*Ti TiB TiC TiB_2 [a]*	*1390±48*
*60**HP**TMC**1300***	*1300^{0}C, 30Mpa, 120min at 10^{0}C/min*	*4.65*	*100*	*0.55*	*Ti TiB TiC TiB_2 [a]*	*1414±25*
*60**HP**TMC**1400***	*1400^{0}C, 30Mpa, 120min at 10^{0}C/min*	*4.65*	*100*	*0.28*	*Ti TiB TiC TiB_2 [a]*	*1457±48*

[a] present in traces

ness and phase composition of hot pressed (isothermal sintering iH_2-B_4C mixture at different temperatures. Assumed theoretical density = 4.62g/cm^3

Sample	*Sintering Conds.*	*Sintered density (g/cm^3)*	*% theoretical density*	*Open porosity (%)*	*Phase composition*	*Vickers hardness (Hv)*
*80**HP**TMC**1100***	*1100^{0}C, 30Mpa, 120min at 10^{0}C/min*	*3.11*	*67.32*	*20.39*	*Ti TiB TiC TiB$_2$ [a]*	*232±12*
*80**HP**TMC**1200***	*1200^{0}C, 30Mpa, 120min at 10^{0}C/min*	*3.74*	*80.95*	*14.97*	*Ti TiB TiC TiB$_2$ [a]*	*754±98*
*80**HP**TMC**1300***	*1300^{0}C, 30Mpa, 120min at 10^{0}C/min*	*4.25*	*91.99*	*6.71*	*Ti TiB TiC TiB$_2$ [a]*	*1564±55*
*80**HP**TMC**1400***	*1400^{0}C, 30Mpa, 120min at 10^{0}C/min*	*4.66*	*100*	*0.52*	*Ti TiB TiC TiB$_2$ [a]*	*1602±14*

[a] present in traces

The results obtained show that density of hot-pressed composites samples increased with increasing sintering temperatures. It can be observed that hot pressed composites at 1400^{o}C show better densification compared to other temperatures. The poor densification behavior shown by the samples hot pressed at temperature 1100^{o}C could be connected to the effect of reinforcement inclusion that failed to sinter because it required higher sintering temperature, resulting in the presence of many porosity.

It can also be observed that hot pressed composite samples densify better than pressureless sintered composites materials. For instance, at sintering temperature 1100^{0}C, 20**HP**TMC**1100** achieved 98.46% relative density (4.48g/cm^3) while 92.09% relative density ((4.19g/cm^3) was achieved by 20**PL**TMC**1100**. Full densification was achieved at 1300 and 1400^{0}C by 20**HP**TMC**1300** and 20**HP**TMC**1400** respectively

0**PL**TMC**1400** achieved only 96.26% and 99.12% relative density respectively. Similar tend was observed in the densification behavior of 40vol. % reinforced Ti composites produced by both pressureless and hot press methods. Better densification achieved by hot pressed reinforced Ti composite samples could be attributed to the influence of applied external pressure.

The Vickers hardness test of hot-pressed composite materials was carried out in the same way as pressureless sintered materials by using 5kg load for all indentation period of 10s. The hardness value increased with increasing sintering temperature (Table 4.7, 4.8, 4.9 and 4.10). Sample 80**HP**TMC**1400** has the highest hardness value of 1602Hv. It was observed that higher hardness was achieved in the composites material sintered at 1400^{o}C compared to other sintering temperatures. The difference observed in the hardness value of various sintered composites could be attributed to reduced porosity and increase in the quantity of fine size reinforcements formed. Hot-pressed Ti matrix composites also exhibited better hardness compared to pressureless sintered composites especially at 1400^{o}C. For example, the hardness value of sample 40**HP**TMC**1400** was 1084Hv compared to 858Hv recorded by sample 40**PL**TMC**1400**. This could be connected to the effect of applied pressure used in the hot-pressed materials which in turn reduced the surface area of the initial powder mixture, forming more reinforcement with reduced porosity.

XRD patterns of the hot-pressed 20, 40, 60, and 80vol. % reinforced Ti matrix composites is shown in figure 4.17, 4.18, 4.19 and 4.20 respectively. Analysis of the patterns for all hot pressed composites shows that Ti (matrix), TiC, TiB are the major phases observed with very insignificant peak of TiB_2. These results also confirmed the same observation made in the pressureless sintered composites that in-situ chemical reaction between Ti matrix and B_4C occurs as expected because no trace of the initial starting materials (TiH_2 and B_4C) was observed. The intensity of reinforcementôs peaks increased with increasing temperature (indicating the dependence of sintering reaction that leads to in-situ formation of reinforcements on

with increase in the weight percent of B_4C particles contained in the initial powder mixtures.

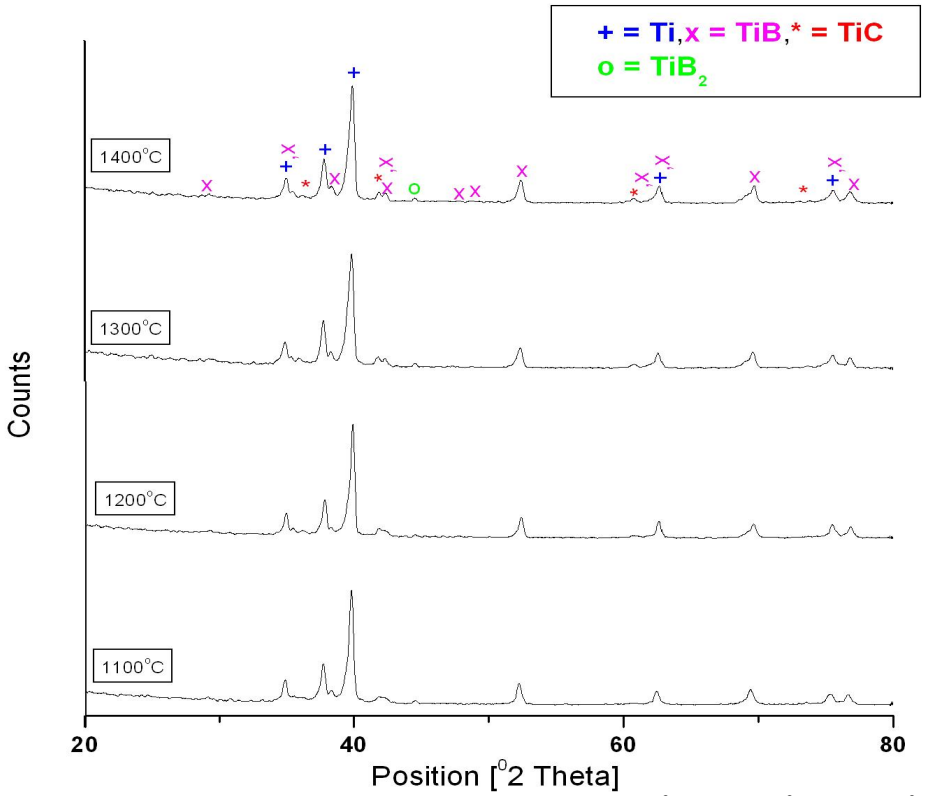

Figure 4. 17: XRD patterns of hot pressed 20 vol. % TMC at (a) 1100^0C (b) 1200^0C (c) 1300^0C and (d) 1400^0C

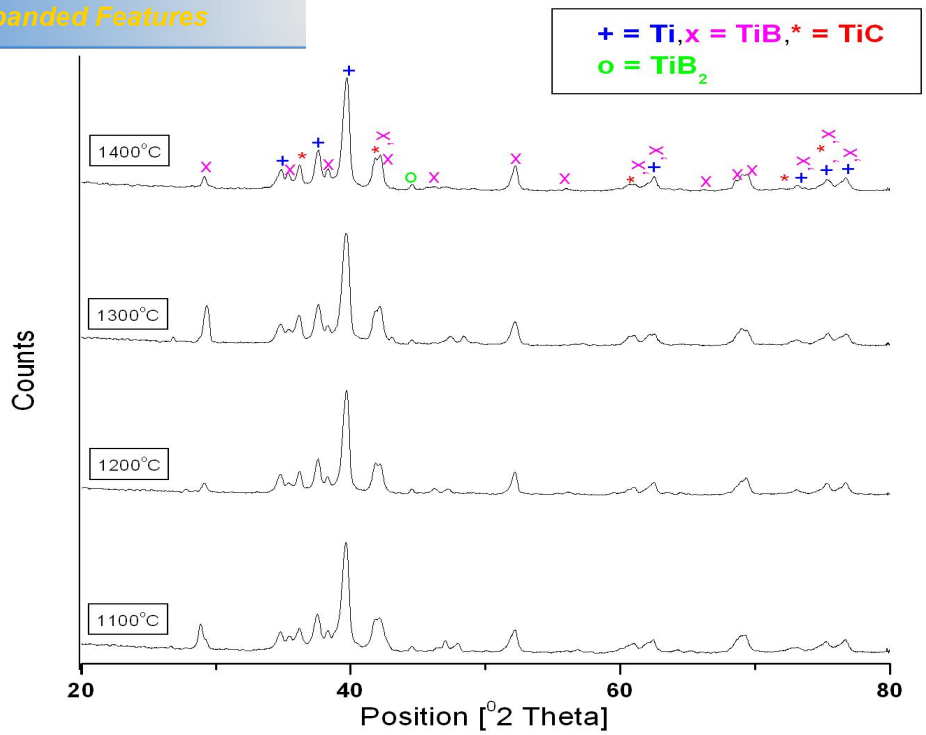

Figure 4. 18: XRD patterns of hot pressed 40 vol. % TMC at (a) 1100^{0}C (b) 1200^{0}C (c) 1300^{0}C and (d) 1400^{0}C

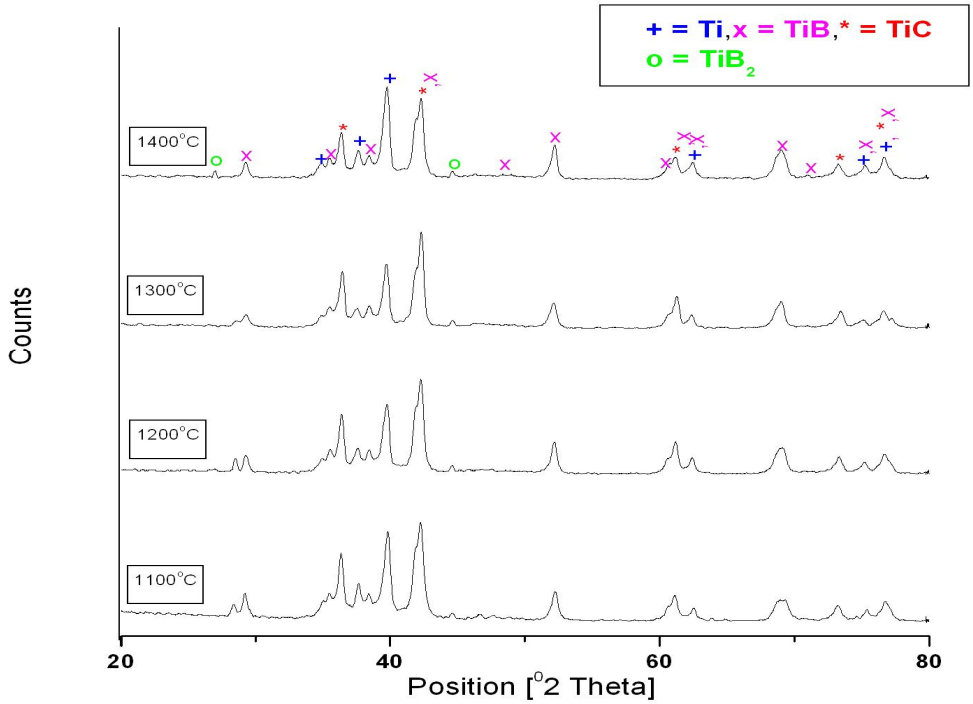

Figure 4. 19: XRD patterns of hot pressed 60 vol. % TMC at (a) 1100^{0}C (b) 1200^{0}C (c) 1300^{0}C and (d) 1400^{0}C

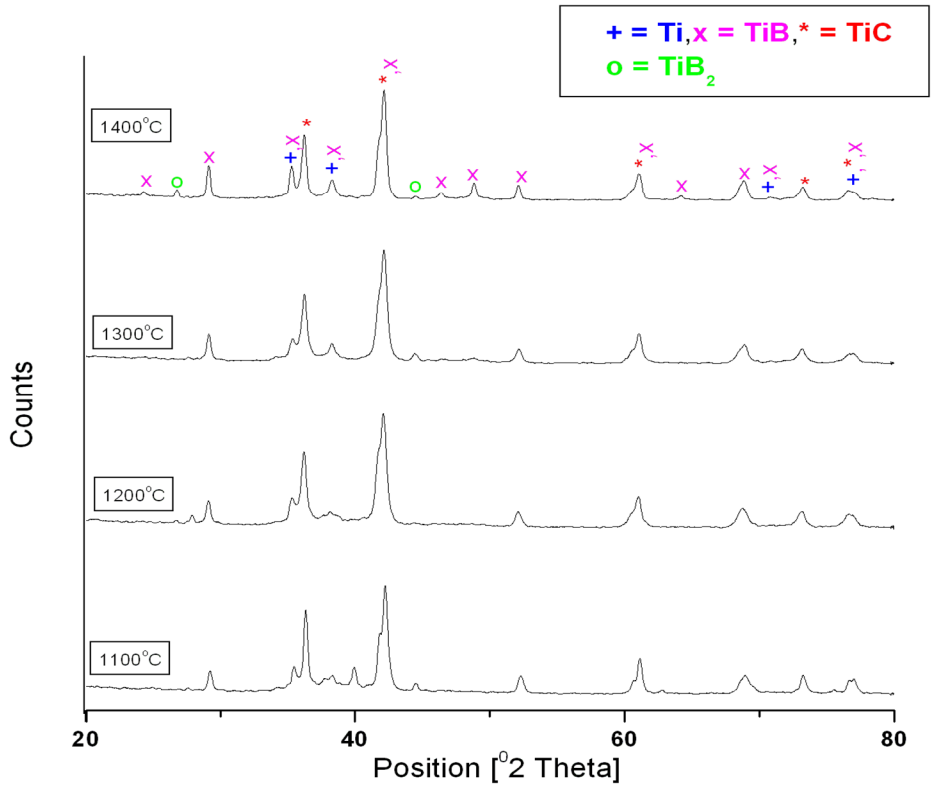

Figure 4. 20: XRD patterns of hot pressed 80 vol. % TMC at (a) 1100^{0}C (b) 1200^{0}C (c) 1300^{0}C and (d) 1400^{0}C

Figures 4.21, 4.23, 4.25 and 4.27 show the SEM images of hot-pressed sintered composites with 20, 40, 60 and 80vol. % in-situ reinforcements respectively. As can be observed from the micrographs the structures of reinforcements are more pronounced at higher sintering temperature 1300^{o}C and 1400^{o}C than 1100^{o}C and 1200^{o}C. For instance, sample 20**HP**TMC**1100** and 20**HP**TMC**1200** show traces of structures that look like needle, clustered and equiaxed in shape; the structures become more pronounced and uniformly distributed over the Ti matrix in the micrographs of sample 20**HP**TMC**1300** and 20**HP**TMC**1400**. EDS analyses (Fig. 4.22) shows that the needle and clustered shaped grains correspond to TiB, equiaxed shaped corresponds to TiC, while the light phase corresponds to titanium matrix. In addition to the needle and equiaxed shaped, a new blocky shaped structure that corresponds to TiB (Fig. 4.24) was observed in all samples with 40vol. %

and size of blocky TiB increased with increased sintering temperature in the 40vol. % reinforced Ti composites, while the amount of needle like TiB decreased. The morphology and size formation of these two identified TiB phases suffer obvious change in their abundance with sintering temperatures and volume fraction of TiB. Sample 60**HP**TMC**1300**, and 60**HP**TMC**1400** are characterized with blocky, reduced needle and equiaxed shaped structures. Sample 80**HP**TMC**1300** and 80**HP**TMC**1400** exhibit mainly blocky and equiaxed shaped with no trace of needle shaped structures. The EDS analyses of the composites (Fig. 4.26 and 4.28) indicate that the blocky shaped structures correspond to TiB while equiaxed shaped correspond to TiC. The microstructures of hot-pressed composites show no apparent porosity like it was observed in the pressureless sintered composites. This can be attributed to the applied pressure.

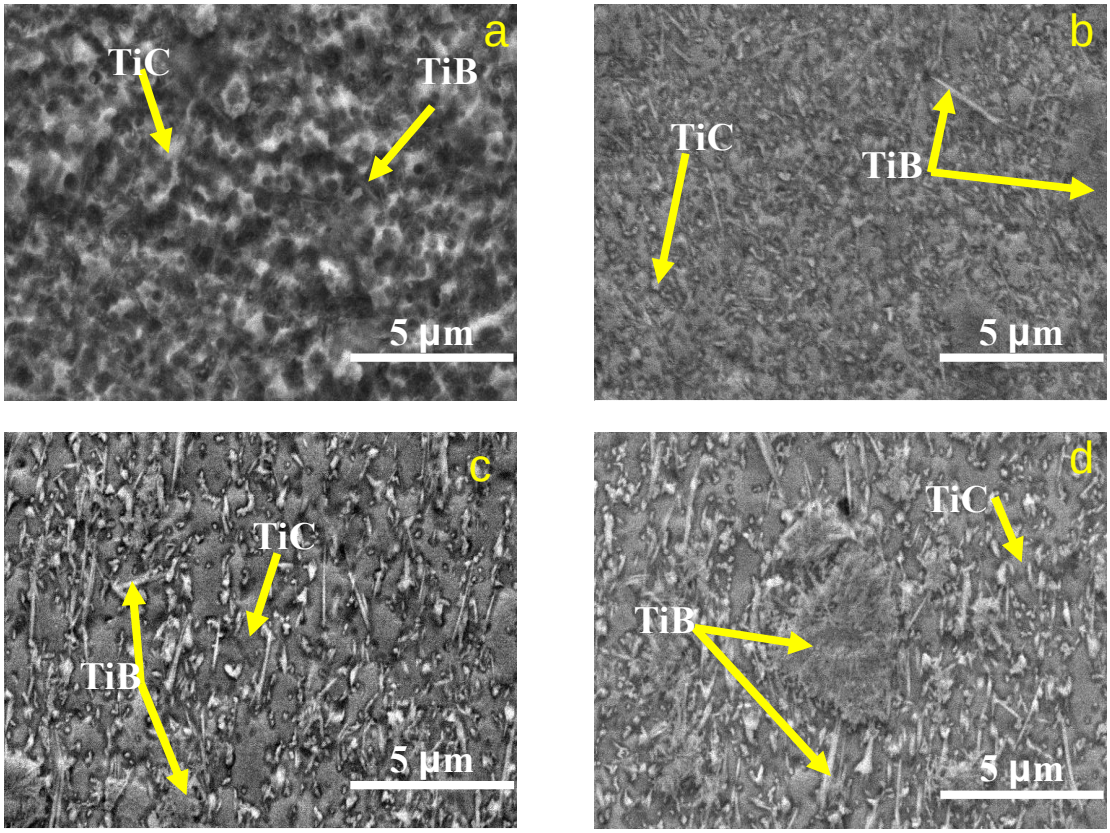

Figure 4. 21: SEM micrographs of hot pressed 20 vol. % TMC at (a) 1100^0C (b) 1200^0C (c) 1300^0Cand (d) 1400^0C.

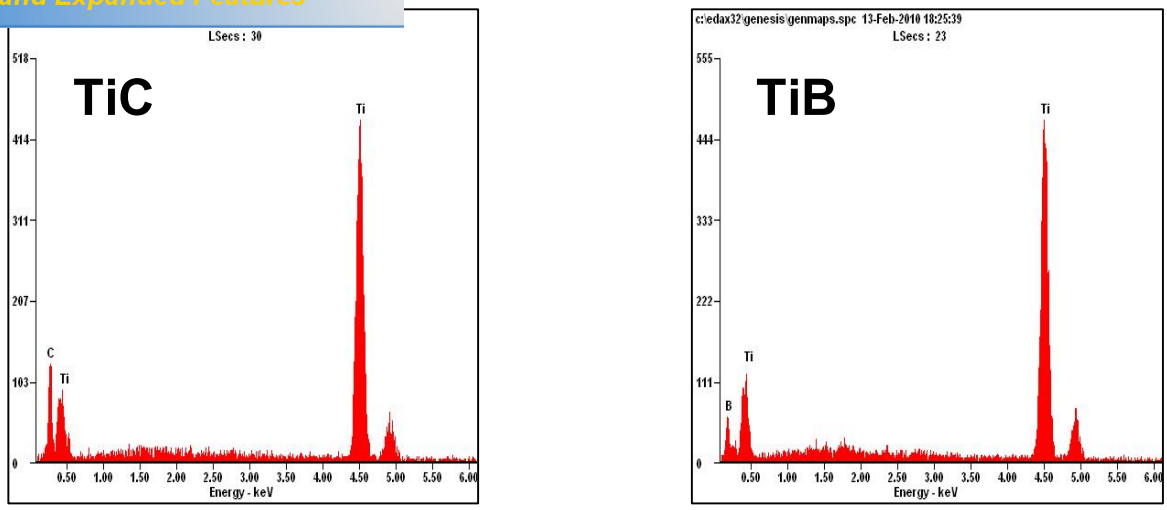

Figure 4. 22: EDS graphs of reinforcements in hot-pressed sample 20**HP**TMC**1400**

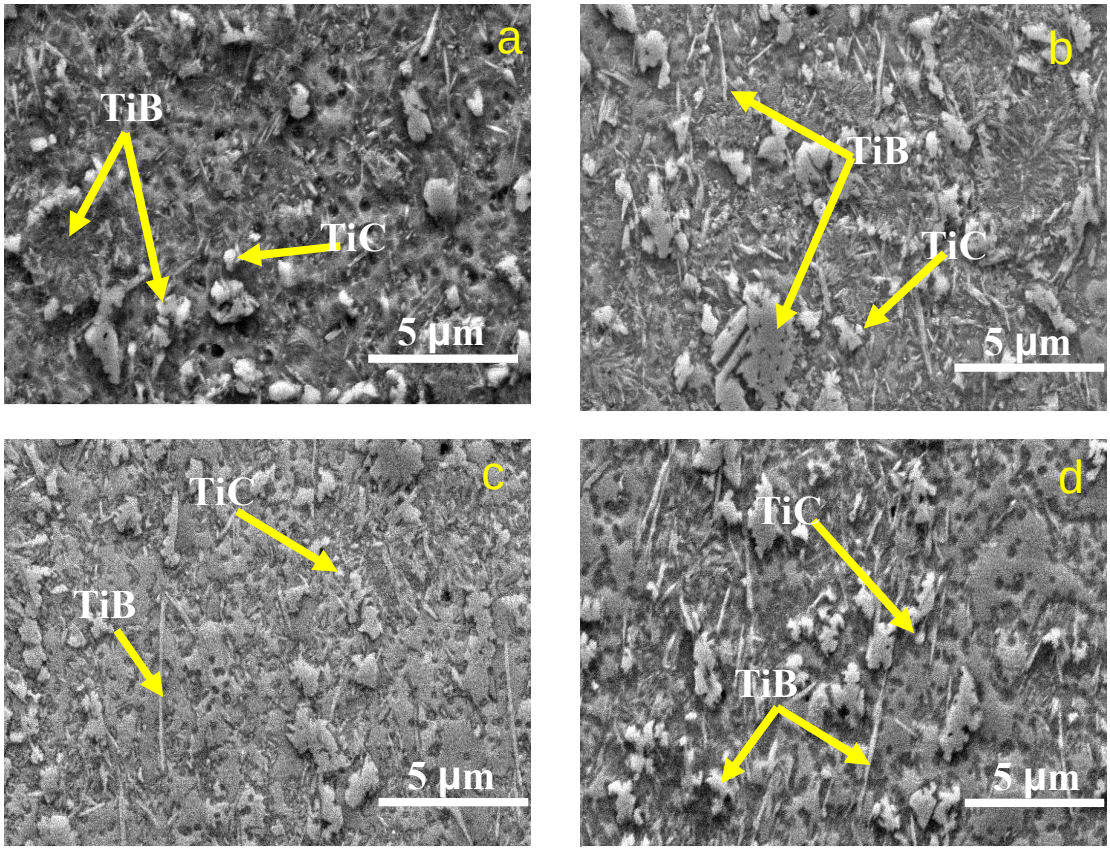

Figure 4. 23: SEM micrographs of hot pressed 40 vol. % TMC at (a) 1100^0C (b) 1200^0C (c) 1300^0Cand (d) 1400^0C.

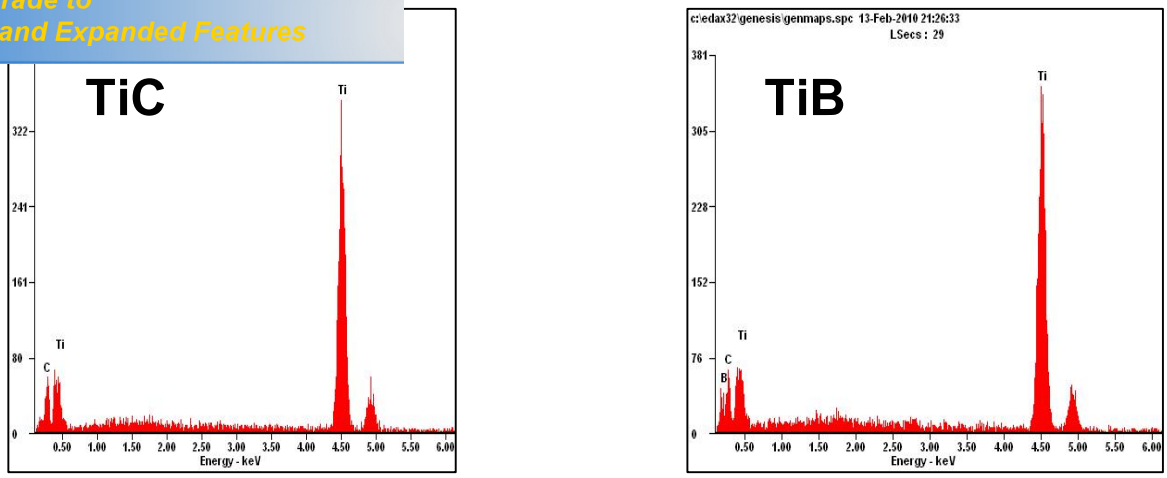

Figure 4. 24: EDS graphs of reinforcements in hot-pressed sample 40HPTMC1400

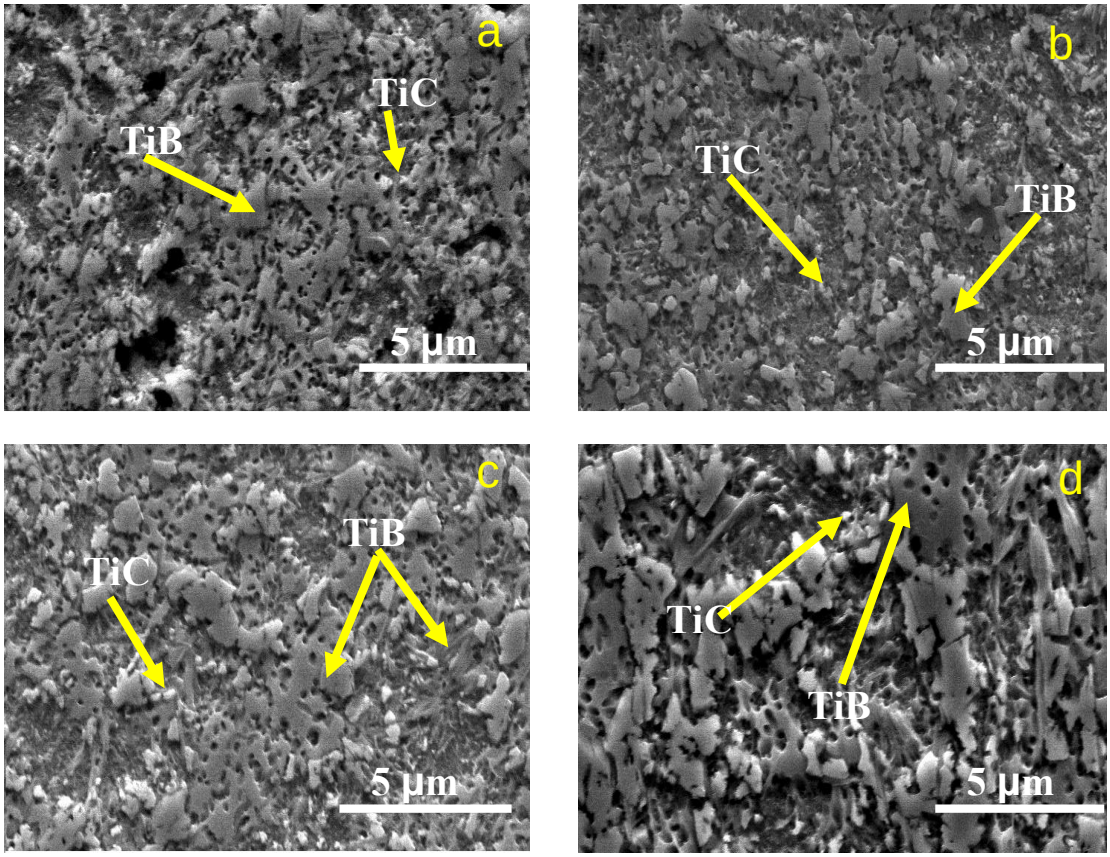

Figure 4. 25: SEM micrographs of hot pressed 60 vol. % TMC at (a) 1100^0C (b) 1200^0C (c) 1300^0Cand (d) 1400^0C.

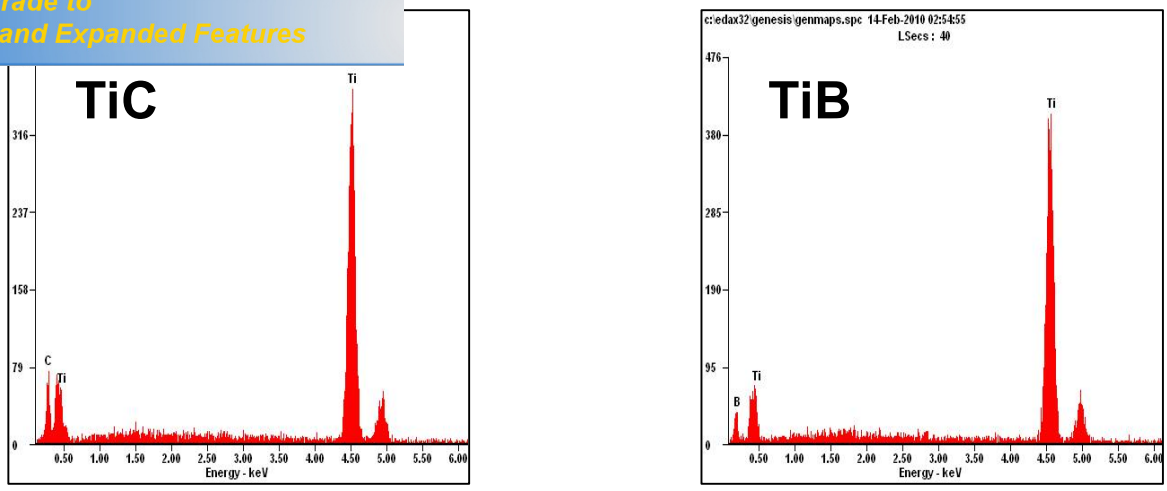

Figure 4. 26: EDS graphs of reinforcements in hot-pressed sample 60**HP**TMC**1400**

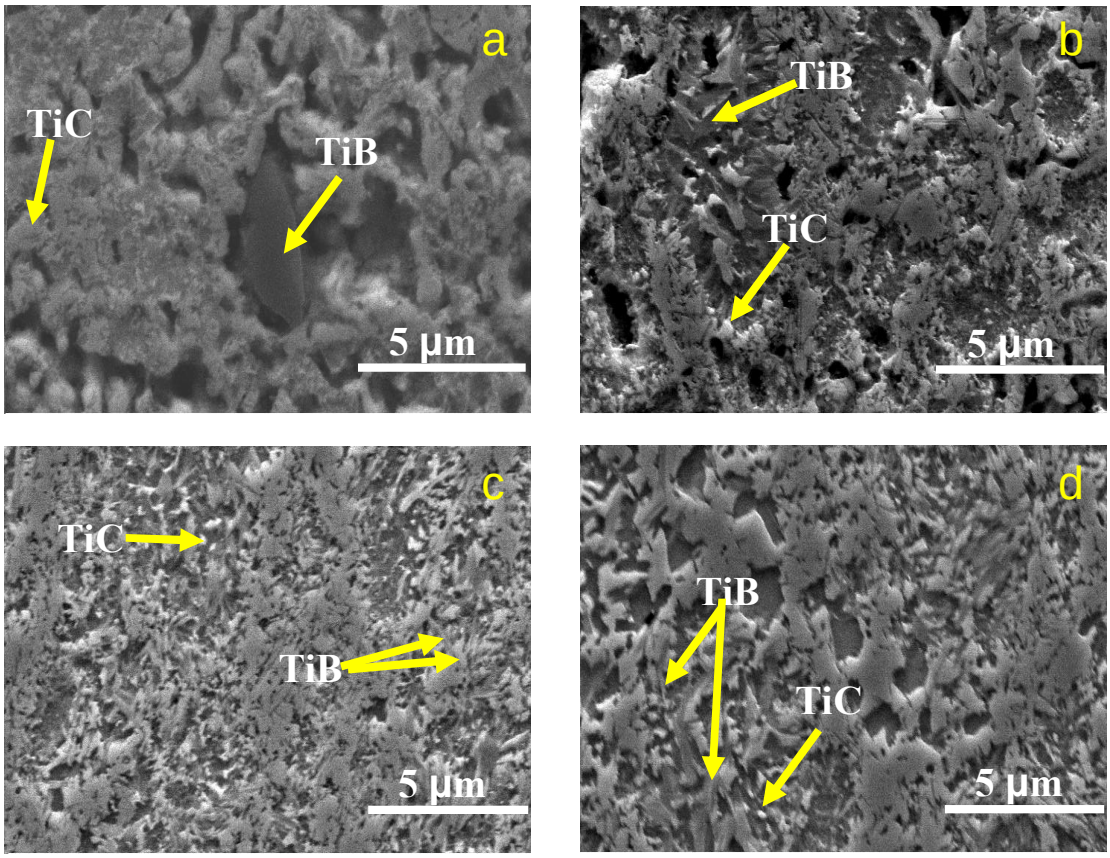

Figure 4. 27: SEM micrographs of hot pressed 80 vol. % TMC at (a) 1100^0C (b) 1200^0C (c) 1300^0Cand (d) 1400^0C.

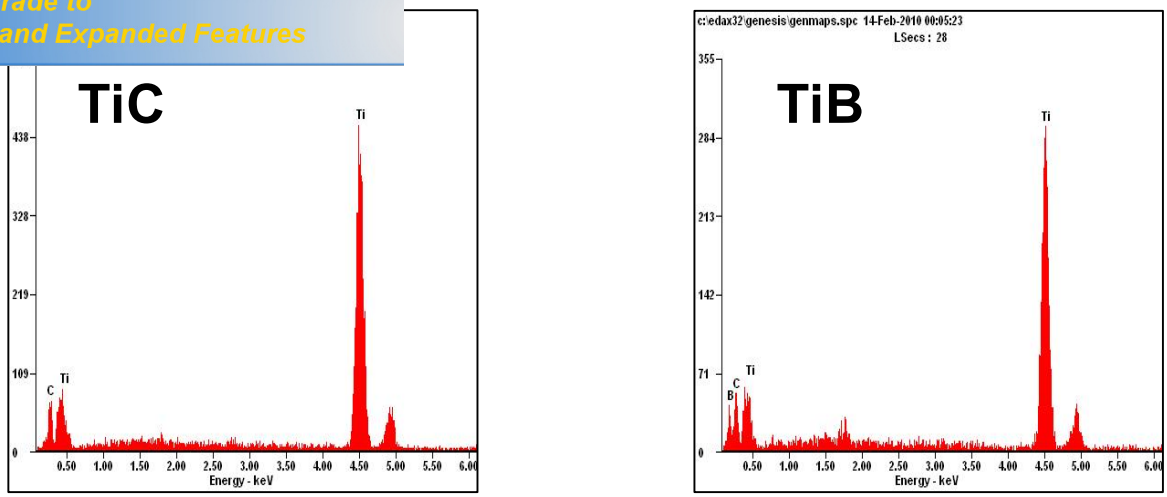

Figure 4. 28: EDS graphs of reinforcements in hot-pressed sample 80**HP**TMC**1400**

4.5.3 Hot-pressing of Ti-B6O for Ti matrix composite

This work also considered the possibility of using B_6O ceramics as a source for the in situ generation of reinforcements (TiB, TiB_2) when Ti matrix and B_6O chemically react during hot pressing at high temperature.

Commercial Ti and B_6O powders were blended together in a planetary milling machine for 10 hours as described in section 3.5.1. The volume fraction of the starting powders was adjusted in such a way to have excess Ti so that Ti matrix composites can be synthesized after the reaction between Ti and B_6O. In the present research, 80 vol. % Ti and 20 vol. % B_6O were blended together to produce the powder mixture that were then used for the hot press sintering. The powder mixture was characterized to check for the phase, elemental composition and the homogeneity of distribution of the ceramic (B_6O) in the Ti matrix using XRD and SEM analysis. Figure 4.29 shows the XRD patterns of the mixed powders used for the fabrication Ti-B_6O composites.

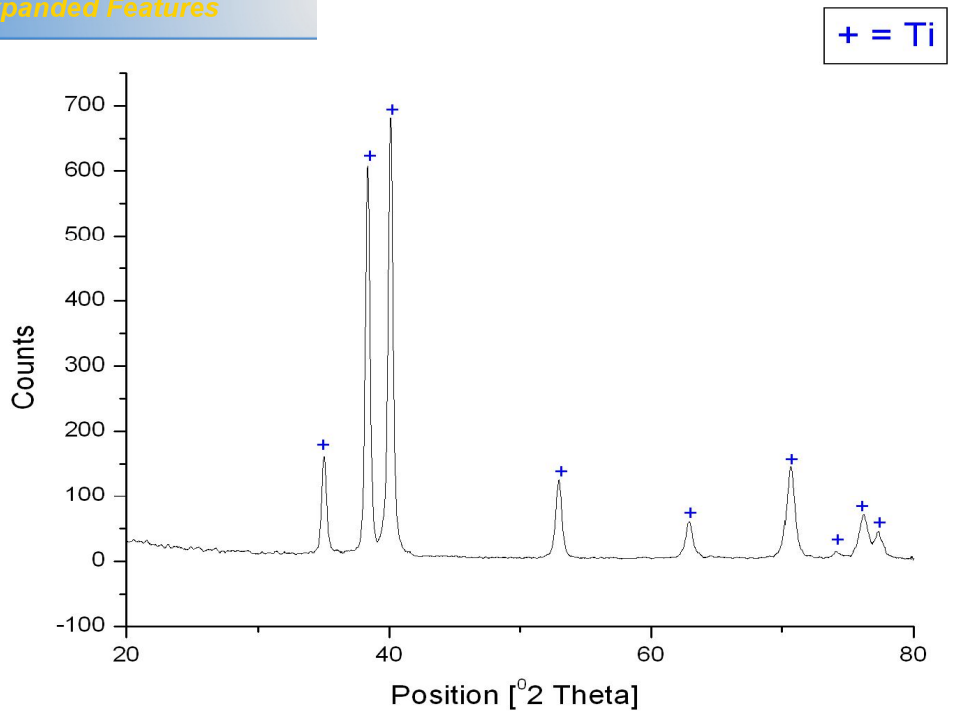

Figure 4. 29: XRD patterns of Ti-B_6O powder mixture (80vol%Ti: 20vol% B_6O) at initial state

The patterns show reflections that correspond to a single phase Ti. However, SEM/EDX analysis of the same sample (Fig.4.30) reveals the presence of B_6O distributed over the Ti matrix. The inability of XRD to detect the presence of B_4C particle in the mixed powder could be attributed to the density difference and the less quantity of B_6O used since the XRD diffractometer does not detect material with concentration less than 2-5wt. % in the sample being analysed.

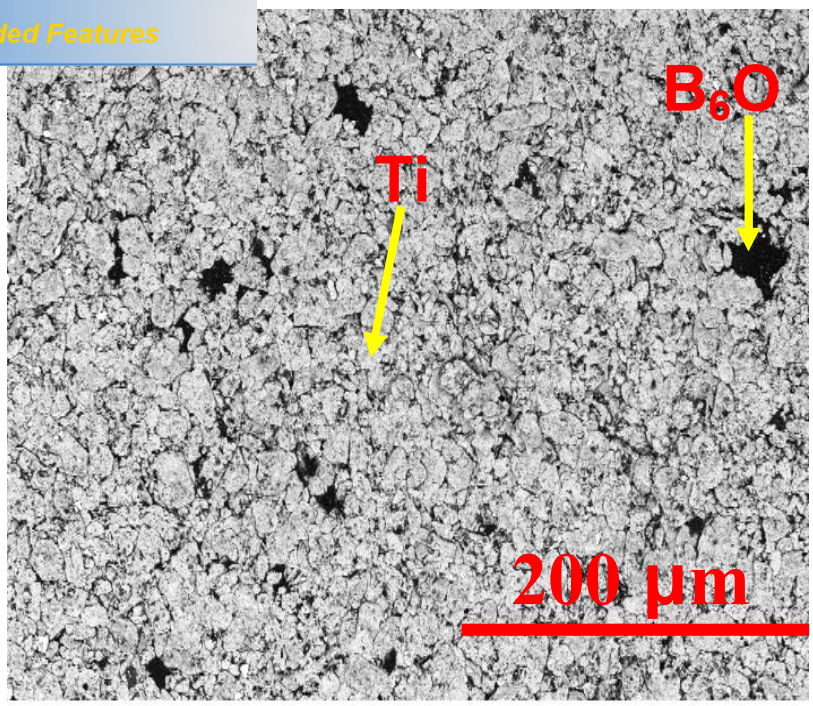

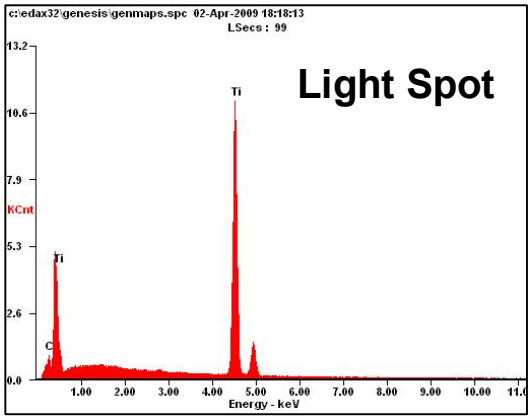

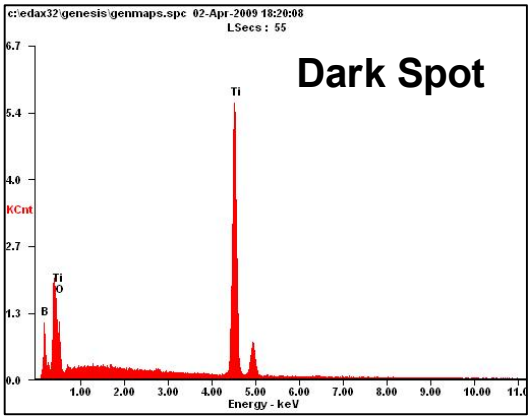

Figure 4. 30: SEM/EDS of Ti-B_6O powder mixture (80vol%Ti: 20vol% B_6O) at initial state

s hot-pressed at various sintering temperatures ranging from 1000, 1100, 1200, and 1300°C for 20 minutes under applied pressure of 50 MPa in argon atmosphere. Table 4.11 summarises densities and mechanical properties of the hot-pressed Ti-B_6O composites synthesized.

Table 4. 11: Density and mechanical properties of Ti-B_6O composites hot pressed at different temperatures (P = 50MPa, t = 20min). Assumed theoretical density = 4.55g/cm^3

Sample	*Sintering Condts.*	*Sintered Density (g/cm^3)*	*% Theoretical density*	*Open porosity (%)*	*Phase composition*	*Vickers Hardness Hv-5*	*Fracture Toughness (MPa.m.$^{0.5}$)*
HP**8Ti2B$_6$O**1000	*1000°C*	*4.25*	*93.41*	*0.36*	*Ti_2O TiB TiB_2*	*888±13*	*10.6±1*
HP**8Ti2B$_6$O**1100	*1100°C*	*4.35*	*95.60*	*0.57*	*Ti_2O TiB TiB_2*	*934±10*	*7.3±2*
HP**8Ti2B$_6$O**1200	*1200°C*	*4.38*	*96.26*	*0.59*	*Ti_2O TiB TiB_2*	*941±31*	*12.7±3*
HP**8Ti2B$_6$O**1300	*1300°C*	*4.47*	*98.24*	*0.18*	*Ti_2O TiB TiB_2*	*924±20*	*10.8±1*

The composite sample hot pressed at 1300°C (**HP**8Ti2B$_6$O**1300**) shows better densification (4.47g/cm^3) compared to (**HP**8Ti2B$_6$O**1000**), (**HP**8Ti2B$_6$O**1100**), and (**HP**8Ti2B$_6$O**1200**). The small difference observed in the densification of the examined samples could be attributed to the effect of sintering temperature.

High measured Vickers hardness values were recorded for the sample hot pressed at 1100-1300°C, while the sample hot pressed at 1000°C (**HP**8Ti2B$_6$O**1000**) had the

xers hardness of the composite materials seems to increase with increasing sintering temperature up to 1200°C, after which the hardness value decreased slightly (this decrease could be as a result of some experimental errors resulting from the indentation points used in calculating the hardness).

XRD patterns of the hot-pressed Ti-B_6O matrix composite are shown in figure 4.31. Analyses of the patterns shows that Ti_2O (matrix) and TiB are the major phases present, although trace amount of TiB_2 was also observed. The results indicate that Ti and B_6O particles do react as expected.

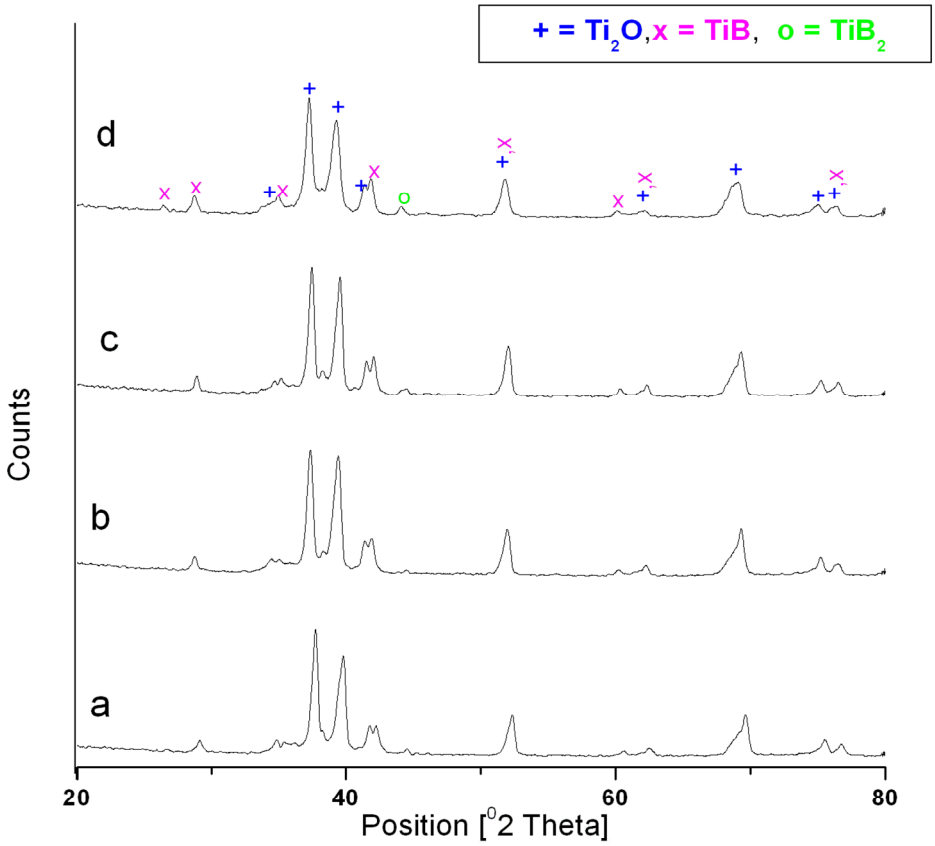

Figure 4. 31: XRD patterns of hot pressed 80Ti -20B_6O composites at (a) 1000°C (b) 1100°C (c) 1200°C and (d) 1300°C.

nages of hot-pressed Ti-B_6O composites heat treated at 1000, 1100, 1200 and 1300^oC respectively. The microstructures analyses of the composite samples, **HP**8Ti2B_6O**1000**, **HP**8Ti2B_6O**1100**, **HP**8Ti2B_6O**1200** and **HP**8Ti2B_6O**1300** look similar in terms of being characterized with traces of needle shaped structure, dark particle spots and a light matrix phase. The EDS analyses (Fig. 4.33) shows that the needle shaped structure corresponds to TiB; the dark spot is predominantly unreacted B_6O particles, while the light phase corresponds to Ti matrix (which XRD shown to be Ti_2O).

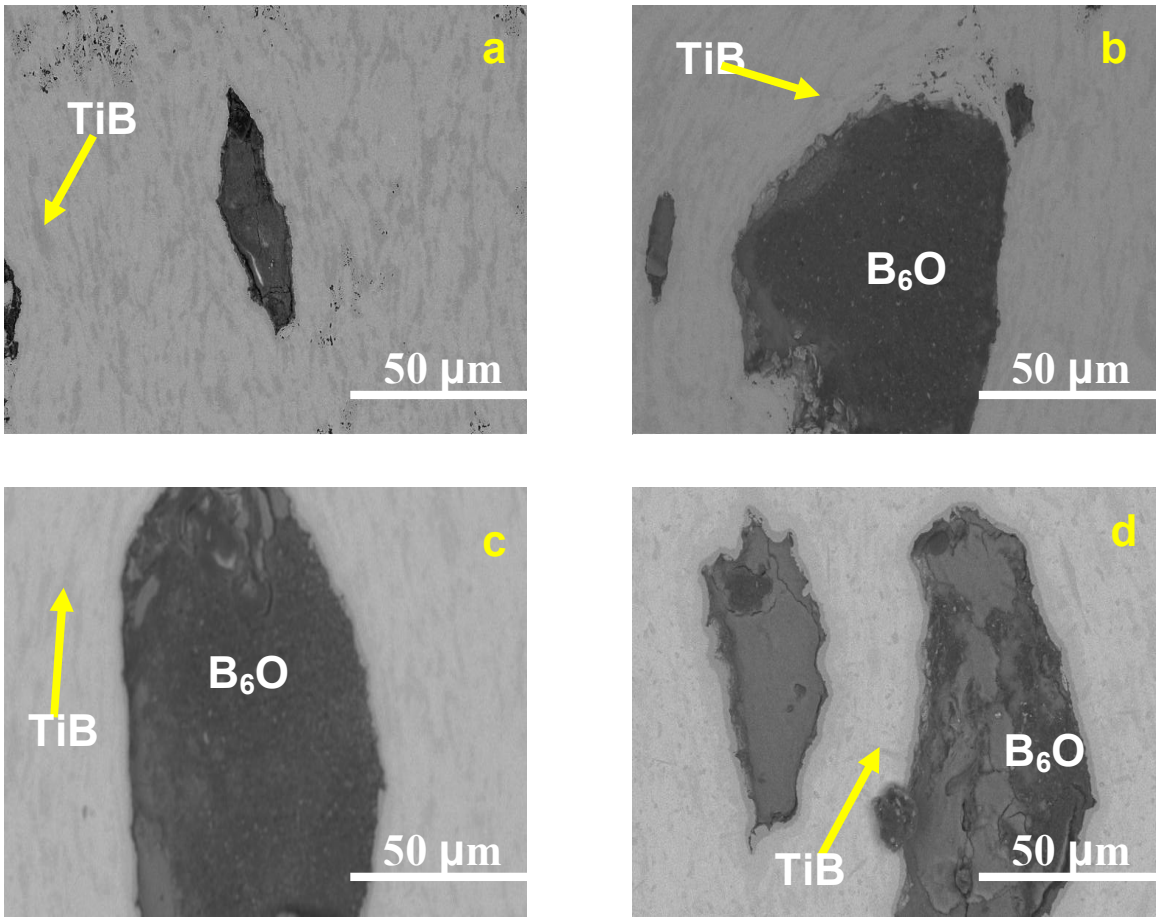

Figure 4. 32: SEM micrographs of hot pressed 80Ti -20B_6O composites at (a) 1000^oC (b) 1100^oC (c) 1200^oC and (d) 1300^oC.

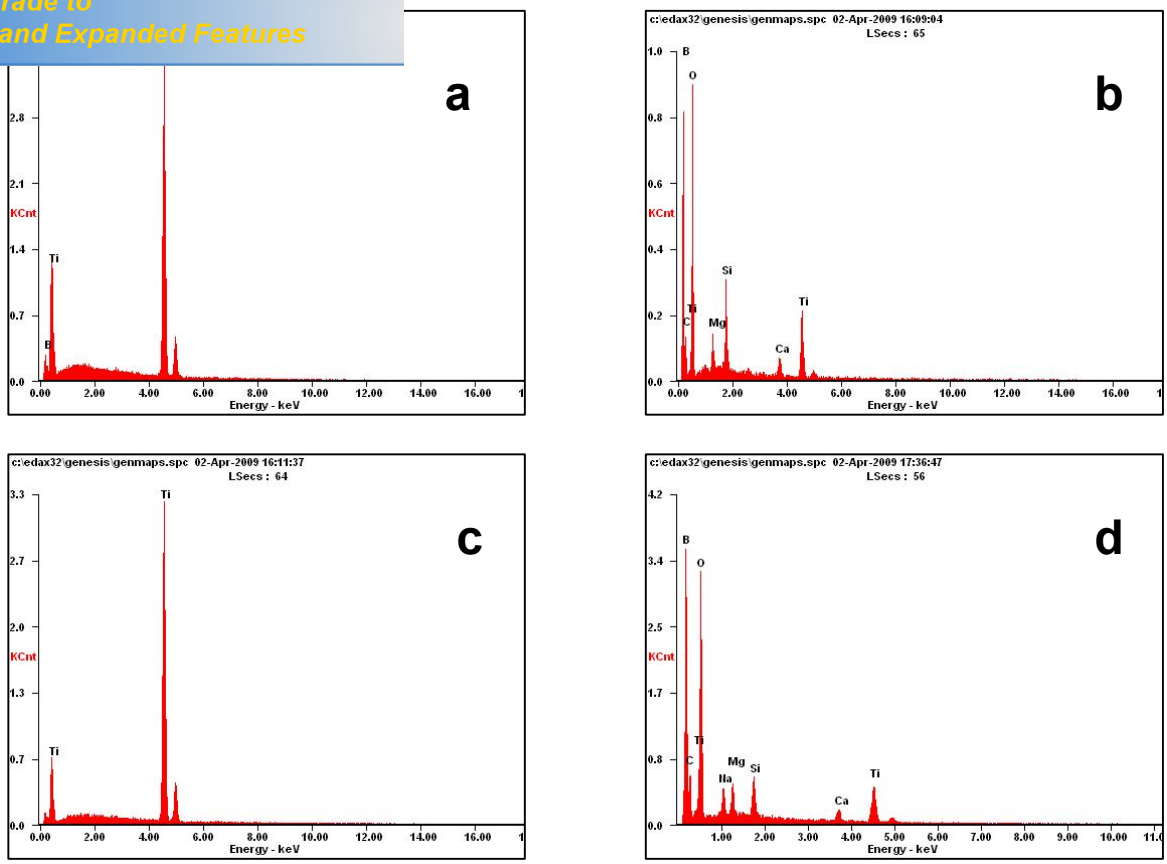

Figure 4. 33: EDS micrographs of hot pressed 80Ti -20B_6O composites heat treated at 1200^oC (a) TiB spot (b) B_6O spot (c) Light Ti matrix phase (d) B_6O aggregate spot

magnification of the dark spot in the SEM micrograph of hot-pressed 80Ti-20B_6O composites. It is clearly shown that a large crack was generated (debonding) at the interface between the Ti_2O matrix and unreacted B_6O aggregates.

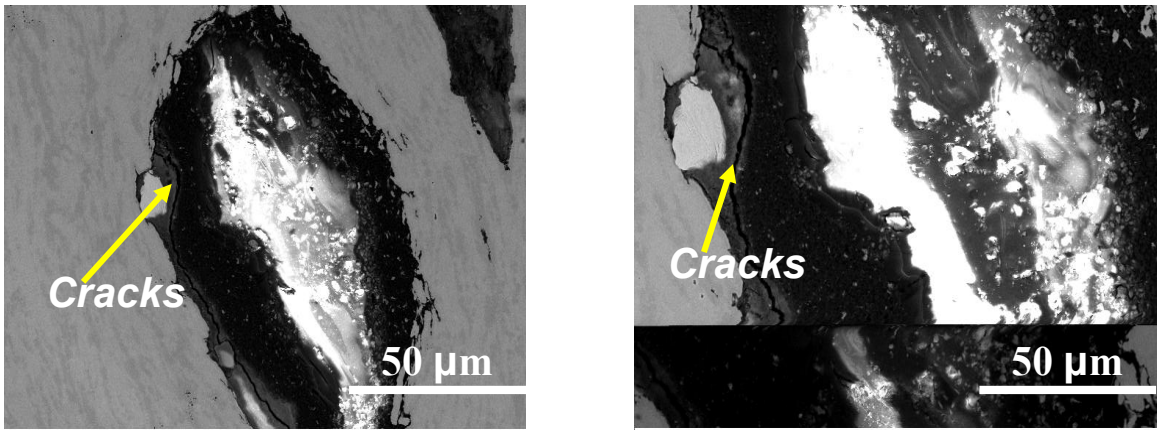

Figure 4. 34: SEM micrographs of hot pressed 80Ti -20B_6O composites at 1000^oC showing cracks around unreacted B_6O particles

micrographs of the Ti-B6O composites hot pressed at 1000, 1100, 1200 and 1300°C respectively. As can be observed, all the composite samples are characterized with much porosity distributed over the Ti matrix but the EDS analysis reveals that some of the pores could be unreacted B_4C aggregate. This could justify the level of densification observed.

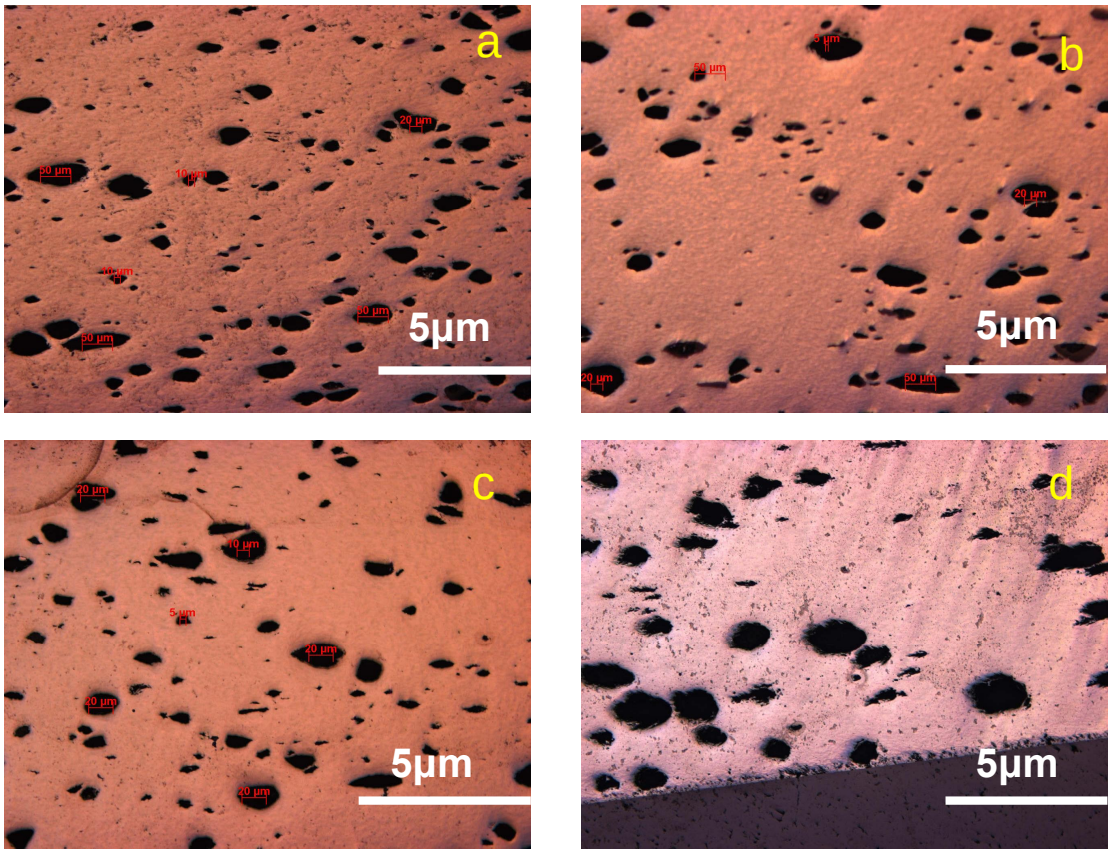

Figure 4. 35: Optical microstructure of hot pressed 80Ti -20B_6O composites at (a) 1000°C (b) 1100°C (c) 1200°C and (d) 1300°C

Chapter Five

5.0 Discussion of results

5.1 Introduction

This chapter discusses the results presented in chapter 4 in terms of the relationship between densification, microstructure, and hardness of the pressureless sintered and hot- press sintered Ti matrix composites.

5.2 Compaction and dehydrogenation behaviour of commercial TiH_2 powder.

Compacts in the form of cylindrical pellets of diameter 18 mm and height 5 mm were produced from Ti and Ti hydride using a uniaxial press at pressures of up to 393 MPa. Figure 5.1 shows the compaction graph generated for both powders in terms of relative density of the green compacts.

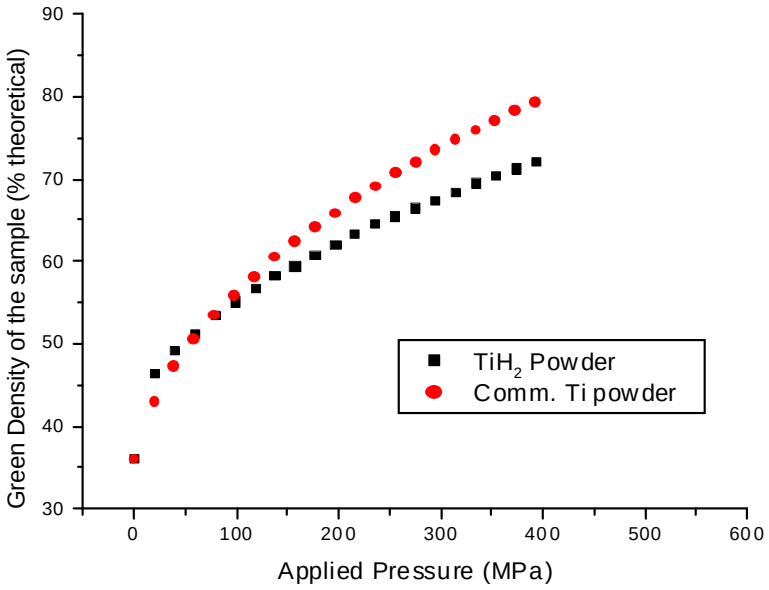

Figure 5. 1: Green density of compacts made from Ti and TiH_2 powders relative to theoretical densities of 4.51g/cm^3 for Ti and 3.91g/cm^3 for TiH_2.

that the porosity of the green compact made from Ti hydride is low but contrary to the report of Robertson and Schaffer (2009), it is not lower than that of Ti compact. However, the relatively high green density (72.12%) achieved by green compact from Ti hydride could be attributed to fragmentation of hydride particles (Ivasishin, *et al.*, 2005; Adams *et al.*, 2008; Ivasishin *et al.*, 2007) and reduced cold welding between hydride particles that allowed more particle rearrangement (Bhosle, *et al.*, 2003). The observed low green porosity in the Ti hydride compact is expected to lead to an increase in the sintered density of hydride compacts, but this would be offset by any porosity created as dehydrogenation occurs during pressureless sintering.

The pressure required to eject the green compact from the die was significantly higher for the Ti powders than for the hydride powders. After compaction at 393MPa, the average of maximum ejection pressure for each compact was 88MPa for Ti and 13MPa for Ti hydride. The results suggest that there is greatly reduced friction and cold welding to the die wall for hydride powder than for the Ti metal powder. This could be attributed to the effect of low deformability of the Ti hydride particles. Reduced cold welding could also be responsible for the lower green strength of Ti hydride compact as was observed during the ejection of the compacts from the die with evidence of broken corners (Fig. 5.2) even at higher compaction pressures (>393MPa).

Figure 5. 2: Macrograph of green compact from TiH_2 powder with broken corner at higher compaction pressure (>393MPa).

Dehydrogenation was carried out using both loose powder and compacts from Ti hydride over temperature ranging from 450 to 715^{o}C in argon controlled tube furnace. The present experimental analyses revealed that the conversion of TiH_2 to Ti is a two-step transformation with the sequence: TiH_2Ÿ TiH_xŸ Ti, where TiH_x is an intermediate phase confirmed through XRD analysis to be TiH (agreed with the report of Bhosle, *et al.*, 2003). Analysis of the XRD results and the mass loss during dehydrogenation indicated that the stoichiometry of the starting Ti hydride is TiH_2. Mass loss due to the release of hydrogen was effectively completed for the loose Ti hydride powder at 680^{o}C for 120min (heating rate of 2^{o}C/min), while that of Ti hydride compact was completed at 715^{o}C for 120min (heating rate of 2^{o}C/min) forming Ŭ-Ti. The reduction in the surface area and the low pore volume for diffusion of hydrogen of Ti hydride powder particles by compaction could possibly be responsible for retardation and consequent higher temperatures required for the dehydrogenation of TiH_2 compact as was observed. This observation agreed with the report of Bhosle, *et al.*, (2003) but the temperature where complete dehydrogenation was achieved for both Ti hydride powder and compact is lower in this study compared to 700 and 800^{o}C respectively reported by Bhosle, *et al.*, (2003). The only

ence could be the lower heating rate of 2°C /min that was used during dehydrogenation in this work as against 20 K/min and 5°C /min used by Bhosle, *et al.*, (2003) and Sandim et al., (2005) respectively. This however confirmed the report of Sandim *et al.*, (2005) that the lower the heating rates the lower is the onset temperature for dehydrogenation.

5.3 Relationship between densification and microstructure.

5.3.1 Pressureless sintered materials

TiH_2 and Ti compacts were pressureless sintered at temperatures between 750°C and 1400°C in argon atmosphere. Summary of the densities obtained for the various sintered materials is given in table 4.1 and it was observed from these results that sintered density increases with increasing sintering temperature (Fig.5.3).

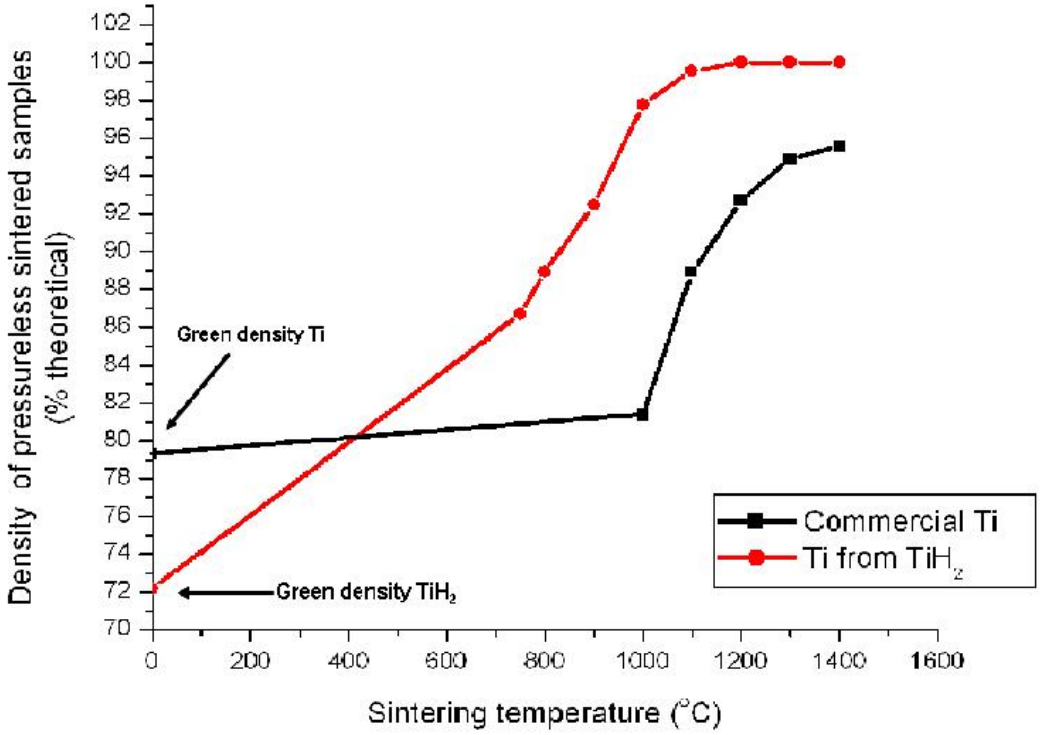

Figure 5. 3: Comparison of relative density of pressureless sintered samples of commercial Ti (44εm) and Ti obtained from TiH_2 against sintering temperature.

density was obtained at 750°C and full densification with theoretical density of 4.51g/cm^3 was achieved for Ti hydride compact sintered at 1200°C , while 95.34% relative density was achieved by sample of commercial Ti sintered at 1400°C (Fig. 5.3). The more rapid densification of TiH_2 compacts (as shown in figure 5.3) despite the observed lower green density relative to commercial Ti compacts could be attributed to lower grain size of TiH_2, as well as enhanced mobility of Ti atoms and contribution to densification which results from more vacant active sites created after hydrogen removal. Fragmentation of hydride particles during compaction as reported by Bhosle, *et al.*, (2003) and Robertson and Schaffer, (2009) could probably make an additional contribution.

The present study achieved a density of 3.91g/cm^3 at 750°C for sintering time of 90min while Bhosle, *et al.*, (2003) that used nanoscale particles under vacuum recorded a density of 4.48 g/cm^3 at the same temperature but with sintering time of 120min. The difference in density could be as result of nanoscale particles and longer sintering time used. At 1400°C, the present study achieved better sintered density of 4.54g/cm^3 (full densification) with very little porosity compared to sintered relative density of 88.2% with swelling observed by Robertson and Schaffer, (2009). The higher density of 4.54g/cm^3 recorded compared to theoretical density 4.51g/cm^3 could be as a result of the contribution of Ni impurities observed during the chemical analysis of the starting TiH_2 powder, however some literature also recorded the theoretical density as 4.54g/cm^3.

SEM micrograph analysis of as sintered sample **PL**750**TiH$_2$**90 at 750°C (Fig. 5.4) can be seen to exhibit high level of porosity suspected to be caused mostly by the porosity of the green Ti hydride compact. This could possibly be regarded as evidence to justify the lower relative density obtained. As the sintering temperature increases the availability of more active and vacant site in the compact enhanced Ti atoms mobility and bonding of its particles, which then resulted in drastically reduced porosity

n in the samples sintered at 1200 to 1400°C (Fig. 5.4a-d). This observation agreed well with the report of Bhosle, *et al.*, (2003) and Robertson and Schaffer, (2009) and the low porosity noticed in sample **PL**1400**TiH$_2$**90 despite better densification has been attributed to the effect of pores left after removal of hydrogen at lower sintering temperature (Robertson and Schaffer, 2009).

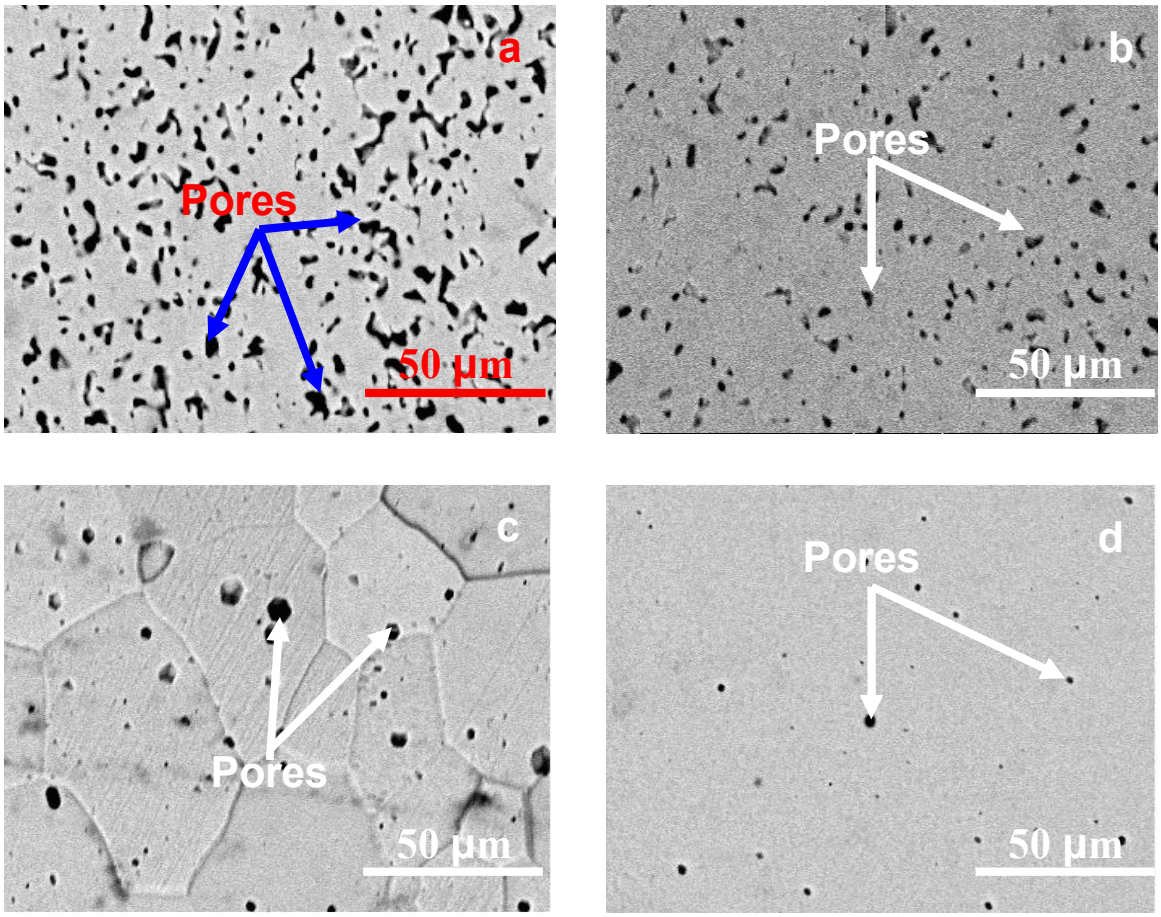

Figure 5. 4: SEM micrographs of the sintered TiH_2 at (a) 750°C, (b) 900°C, (c) 1200°C, (d) 1400°C.

Titanium matrix composites with various in-situ formed reinforcements (TiC, TiB, and very little TiB_2) were produced from TiH_2 and B_4C powder mixtures through powder metallurgy using pressureless sintering and hot-pressing methods. The higher sintering temperatures considered (1100, 1200, 1300, and 1400°C) result in chemical

rmation of the reinforcements (TiC, TiB orTiB_2) in Ti matrix. Figure 5.5 and 5.6 show the Ti-B and Ti-C phase diagrams respectively with dotted lines indicating the temperature region under consideration and the possible phases that can form as a result of interaction between Ti and B_4C. For the Ti-B system, it is considered that the reaction between Ti and B would result in the formation of three kinds of borides, i.e., TiB, TiB_2 and Ti_3B_4 (Zhang *et al.*, 1999). From the Ti-B binary phase diagram (Fig. 5.5), the TiB phase is preferentially formed in the Ti rich area because TiB_2 phase can not be in the equilibrium with Ti (Tjong and Ma, 2000; Cai *et al.,* 2006). Figure 5.6 shows Ti-C binary diagram showing the phase that can form within the temperature region under consideration is TiC (or Ti_2C), most probably TiC_{1-x} where x is ~0.92.

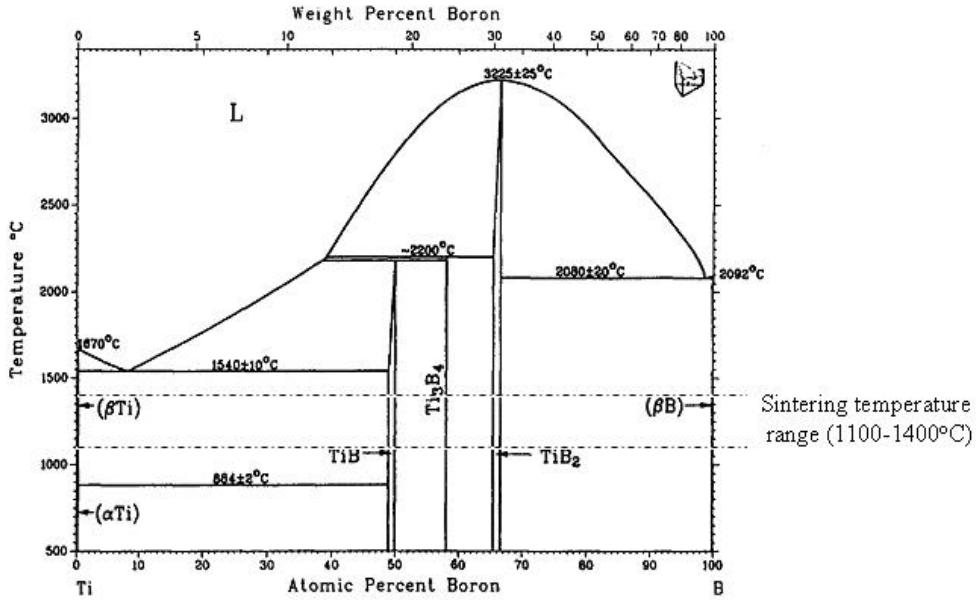

Figure 5. 5: Phase diagram of Ti-B system (Source: Gorsse et al., 98). The dotted parallel lines represent the sintering temperature region under consideration

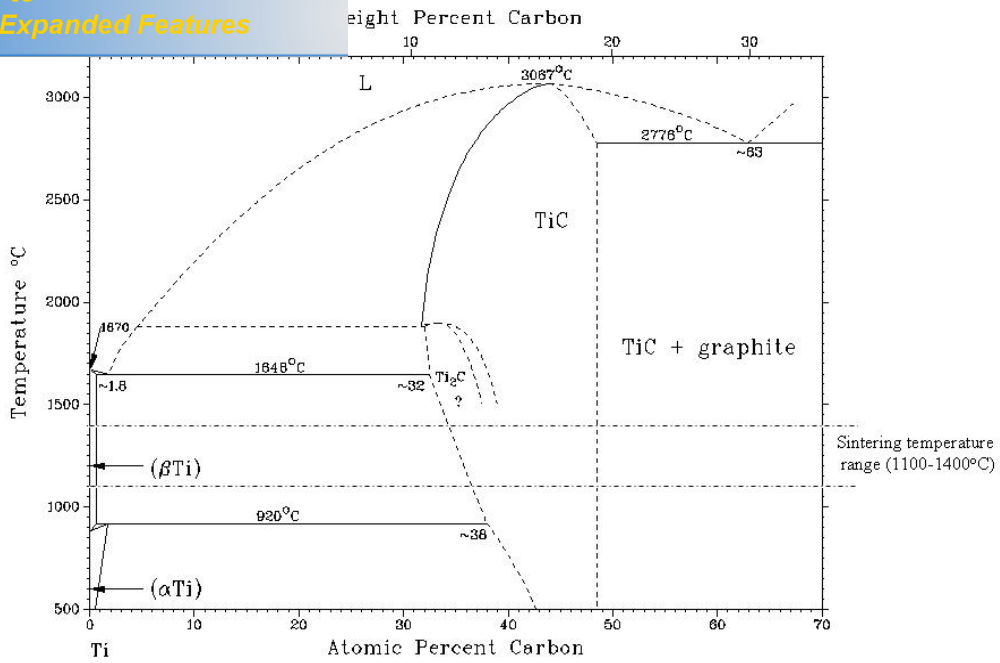

Figure 5. 6: Phase diagram of Ti-C system (Source: Vallauri et al., 2008) the dotted parallel lines represent the sintering temperature region under consideration

The study undertaken here shows that the reaction between Ti and B_4C after dehydrogenation occurs above 1000°C as reported by Liang *et al.*, (2008) because the SEM/EDX analysis of the sintered composite samples (as would be shown later) shows trace amount of the microstructures of the expected reinforcements at the sintering temperature 1100 ^{0}C, thus indicating that the reaction really occurred within the reported range. Although the Ti-B phase diagram indicates that TiB forms at lower temperature, while that of TiC become pronounced at 800 ^{0}C (Kim et al, 2001) but Lu and Li (2008) reported that the reaction between Ti and B_4C does not occur even at 900 ^{0}C and in another report, the reaction between Ti and B_4C according to the DTA report of Liang *et al.*, (2008) occurs around 1093 ^{0}C. All this information and arguments forms the basis of the chosen temperatures range for the present research work.

XRD patterns of all the composites presented in chapter four show that the major phases present are Ti matrix, TiB and TiC with very low amount of TiB_2. This locally

react only slowly with the excess Ti due to the low diffusion coefficient involved.

This observation confirmed that there was a chemical reaction between B_4C particles and Ti matrix (slightly above 1000^oC) that formed from TiH_2 after dehydrogenation. This observation agreed well with the information in the equilibrium phase diagram of Ti-B and Ti-C as shown in figure 5.5 and 5.6 and also with the available literatures (Zee *et al.*, 1991, Ma *et al.*, 2007, Radhakrishna Bhat *et al.*, 2002, Ni *et al.*, 2006, and Tjong and Ma, 2002). However, there was apparent shift noticed in the Ti major peak of composites produced in this work compared to the pure Ti peaks. Based on the literature, similar shifts were observed in the XRD pattern of Ti composites produced by Zee *et al.* (1991), Ma *et al.* (2007), Radhakrishna Bhat *et al.* (2002), Ni *et al.* (2006), and Tjong and Ma (2002).

Ma *et al.* (2007) and Zee *et al.* (1991) reported that the reaction between Ti and B_4C to prepare in situ (TiB+TiC)/Ti composites cannot proceed completely, and some C and B always dissolve in the Ti matrix during preparation causing the corresponding observed peak shift. Zee *et al.* (1991) explained further that when C dissolved in Ti matrix, it expand its unit cell by increasing both lattice parameters ***a*** and ***c*** and that B also expands the Ti lattice but to a lesser extent. Therefore, the shift observed in the Ti peak of the present study could be attributed to the same reason give above.

In the present study, Ti matrix composites with 10, 20, 40, 60, and 80 vol. % in-situ formed reinforcements (TiC + TiB) were fabricated: 10, 20, and 40vol. % reinforced Ti composites by pressureless sintering method and 20, 40, 60, and 80vol. % reinforced Ti composites by hot-press sintering method as described in chapter three. To understand and properly explain the densification behaviour of these composites, it is necessary to consider the effect of sintering temperature and different volume fraction of reinforcements (inclusions) in-situ formed in the Ti matrix composites.

hip between the sintering temperature and the relative density obtained for the sintered Ti matrix composites using pressureless sintering. As can be seen, the relative density of the sintered composites increases gradually with increasing sintering temperature. For instance, up to 1400°C only the pure Ti from TiH_2 and the material with 10 vol. % of reinforcing component could be sintered to density higher than 99%. This is clear evidence that the reinforcing components retard the sintering process. This could be expected because TiC and TiB can only sinter at temperature higher than 1500°C (Tian *et al.*, 2008).

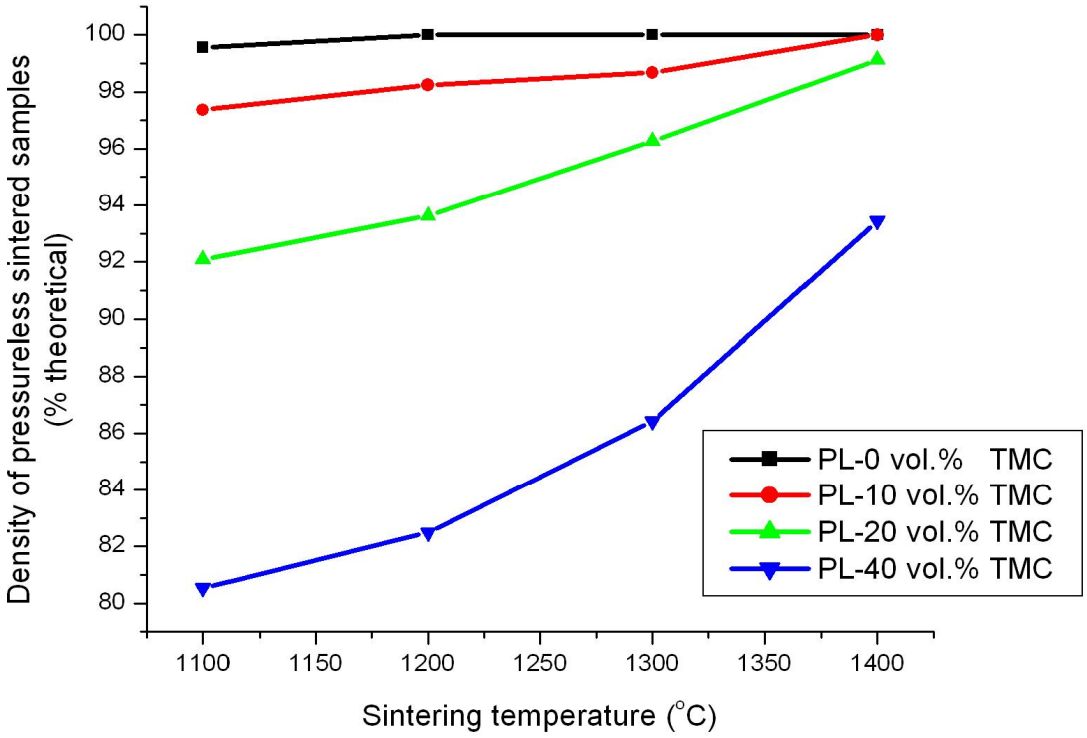

Figure 5. 7: Density of pressureless sintered Ti matrix composites as a function of sintering temperature.

The morphological evolution and transformation of in-situ formed reinforcements (inclusions) as observed in the SEM micrographs (Fig. 5.8, 5.9, 5.10) showed good evidence to support the densification behaviour shown above. For instance, the micrograph of 40**PL**TMC**1100** (Fig. 5.10a) and 20**PL**TMC**1100** (Fig. 5.9a) are

pores than were observed in sample10**PL**TMC**1100** (Fig. 5.8a) because of the presence of large amount of unsintered in-situ formed reinforcing components relative to the Ti matrix. At 1400^{o}C, the SEM of the sintered samples (Fig. 5.8b, 5.9b, and 5.10b) shows an improvement in densification (reduced porosity) that could be attributed to reduction in retardation influence of reinforcing component on the sinterability of the composites.

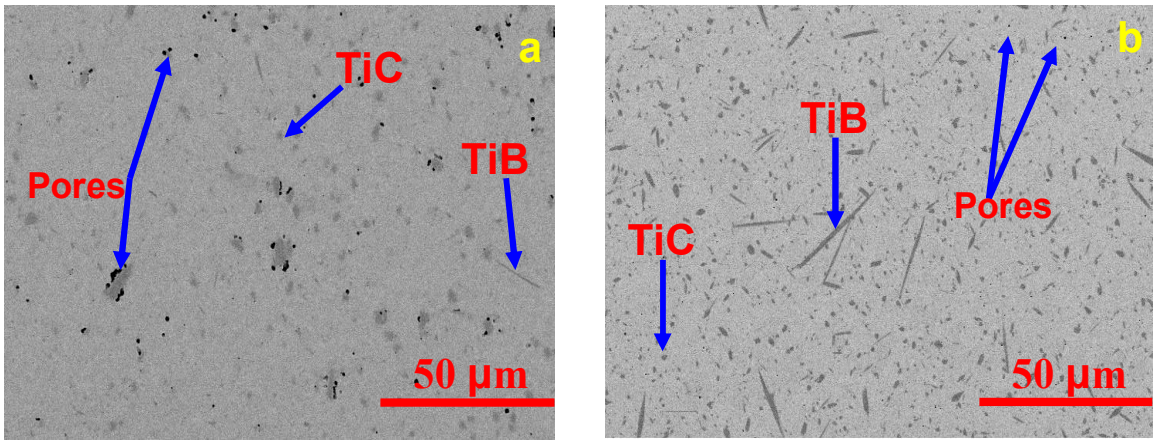

Figure 5. 8: SEM micrographs of 10vol. % reinforced Ti matrix composites at (a) 1100^{0}C (b) 1400^{0}C

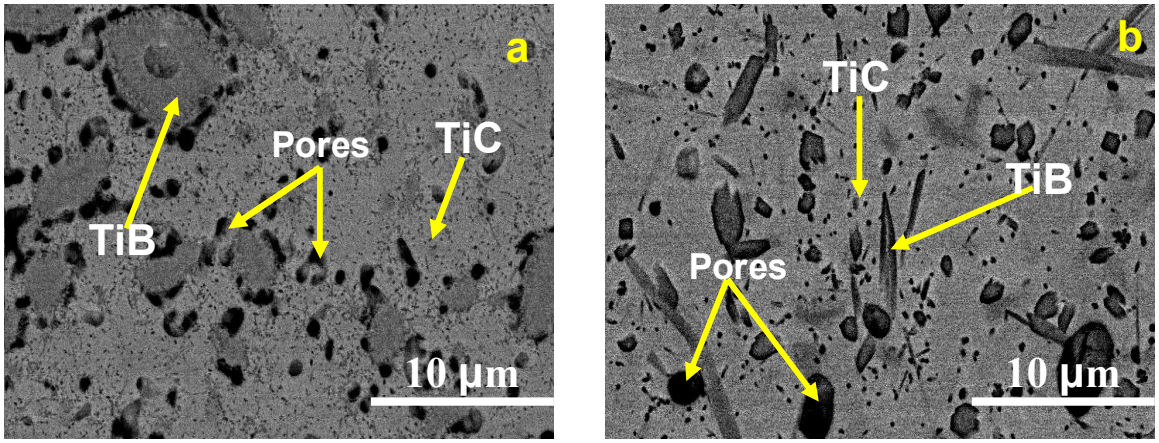

Figure 5. 9: SEM micrographs of 20vol. % reinforced Ti matrix composites at (a) 1100^{0}C (b) 1400^{0}C

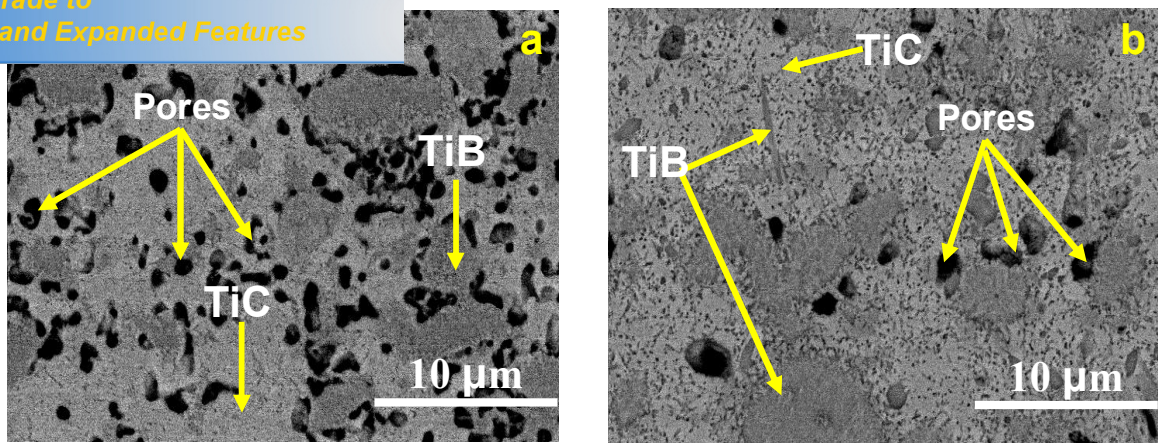

Figure 5. 10: SEM micrographs of 40vol. % reinforced Ti matrix composites at (a) 1100^0C (b) 1400^0C

Analysis of the morphology change observed in the microstructure of these composites relative to change in temperature shows that at low temperature, only small precipitates of equiaxed shaped reinforcing components was observed. At temperature above 1200^oC, the morphology of the composite was characterized with needle like TiB and larger TiC particles. The influence of volume fraction shows that increasing volume content of in-situ formed reinforcements leads to reduction in the amount of needle shaped TiB while more equiaxed TiB was formed.

Figure 5.11 shows the relative densities of pressureless sintered Ti matrix composites as a function of the volume fraction of in-situ formed reinforcements (inclusion). It can be observed from this figure that relative density of the sintered Ti matrix composites decreased with increasing volume fraction of reinforcing phase. Only samples treated at 1400^oC shows increase in relative density up to 10vol. % inclusion, after which the relative density decreases with increasing volume fraction of inclusion.

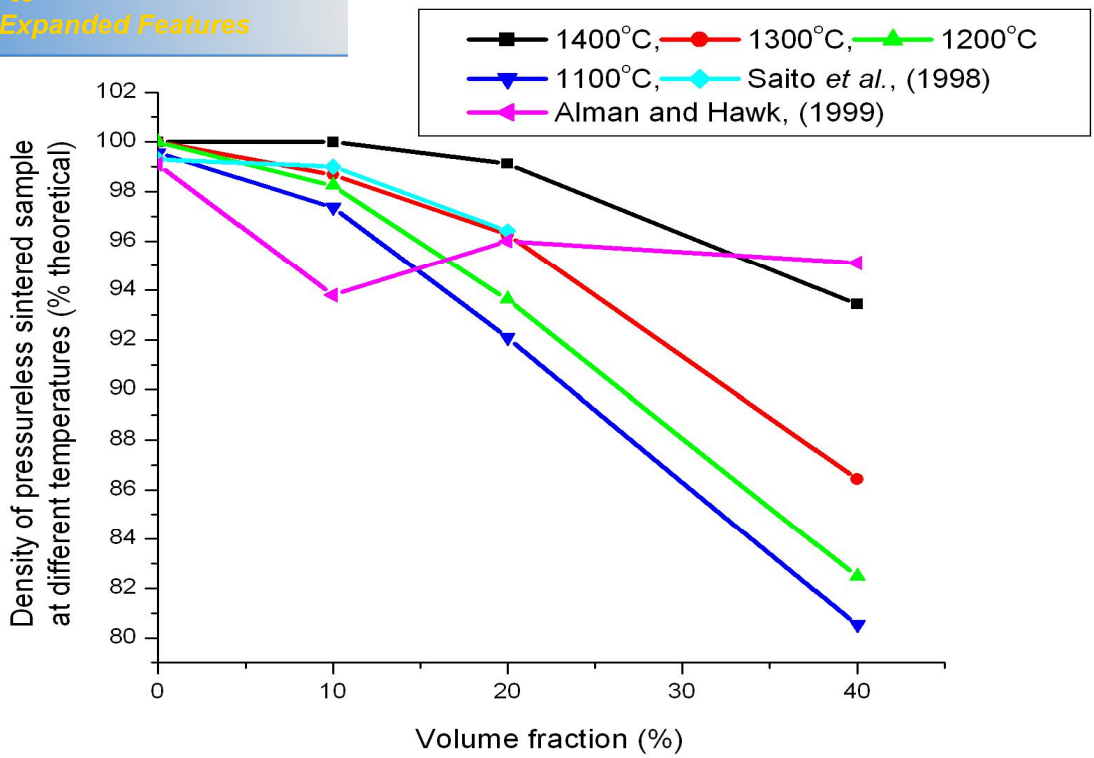

Figure 5. 11: Density of pressureless sintered Ti matrix composites as a function of volume fraction (%) of in-situ formed reinforcements (TiC + TiB).

These results shows that the relative density of Ti matrix composite produced decreases with increasing volume fraction of inclusion. This observation, as shown in figure 5.11 agreed well with findings of Saito, *et al.*, (1998) and Alman and Hawk, (1999). Composites produced in this study, especially at higher temperature (1400^{o}C) showed higher densification compared to the literature data (Fig. 5.11). The reduced densification that characterized composites samples with more than 10vol. % inclusion could be attributed to negative effect of large differential sintering rate that exists between Ti matrix and inclusion region. As can be seen in figure 5.9a and 5.10a, the observed pores formed round the region of strong bonded inclusions that require higher sintering temperature compared to Ti matrix. This differential sintering rate is suspected to develop some stress field at the interface of Ti matrix and inclusions, generating pores that lower the densification of the composites. Therefore,

mposites with higher volume fraction reinforcements attaining full densification compared to sample with zero and 10 volume fraction inclusions obviously reflects the influence of reinforcements on the densification of Ti matrix composites.

5.3.2 Hot pressed composite materials

The pressureless sintering results have shown that composites with 20 and more vol. % reinforcing components could not be densified by pressureless sintering method. Therefore, hot pressing was used to densify the materials with up to 80 vol. % (TiC + TiB) inclusions.

Densification behaviour of these hot-pressed composites was investigated putting into consideration the influence of sintering temperature, as well as volume fraction of the in-situ formed reinforcements. Figure 5.12 shows the relationship between the sintering temperature and the corresponding relative density of hot-pressed Ti matrix composites produced. Besides the fact that the relative density of the hot-pressed materials increased gradually with increasing sintering temperature, a greater improvement in the densification compared to pressureless sintered composites was achieved. The improvement in densification shown by hot-pressed composites can only be attributed to the effect of applied external pressure.

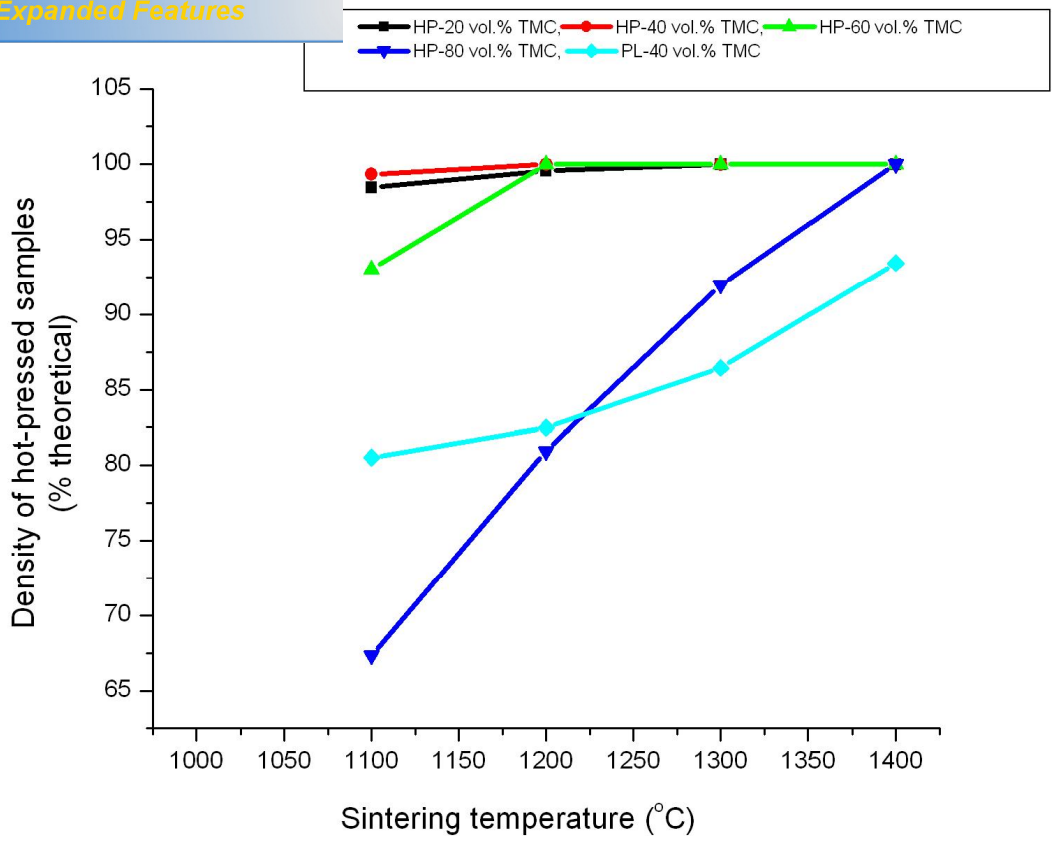

Figure 5. 12: Density of hot-pressed Ti matrix composites as a function of sintering temperature

These better densifications could be justified with the observations made from the SEM analyses of the corresponding samples (Fig. 5.13-5.16). The micro structural analysis of samples hot-pressed at 1100°C, as can be seen in fig. 5.13a, 5.14a, 5.15a and 5.16a for materials with 20-80vol. % of reinforcements phase are characterized with considerably reduced porosity but also by a changed morphology of the in-situ formed reinforcements compared to what was observed in pressureless sintered composites samples (Fig. 5.8a, 5.9a, and 5.10a). Figure 5.13b, 5.14b, 5.15b and 5.16b showed the SEM micrographs of hot-pressed sample at 1400°C with practically no pores while the quantity of in-situ formed reinforcements increased tremendously compared to what was obtainable in the corresponding pressureless sintered materials. Analysis of the morphology change in the structure of reinforcements shows that at low temperature (1100°C), small precipitates of needle and equiaxed

of TiC particles were produced. At higher temperature (1200-1400°C), the microstructures of the composites exhibits large amount of needle shaped TiB and few amount of blocky TiB especially for composites with 20-40vol. % inclusions. Above 40vol. % up to 80vol. %, more blocky TiB with low or no needle shaped TiB, and increased TiC particles were formed.

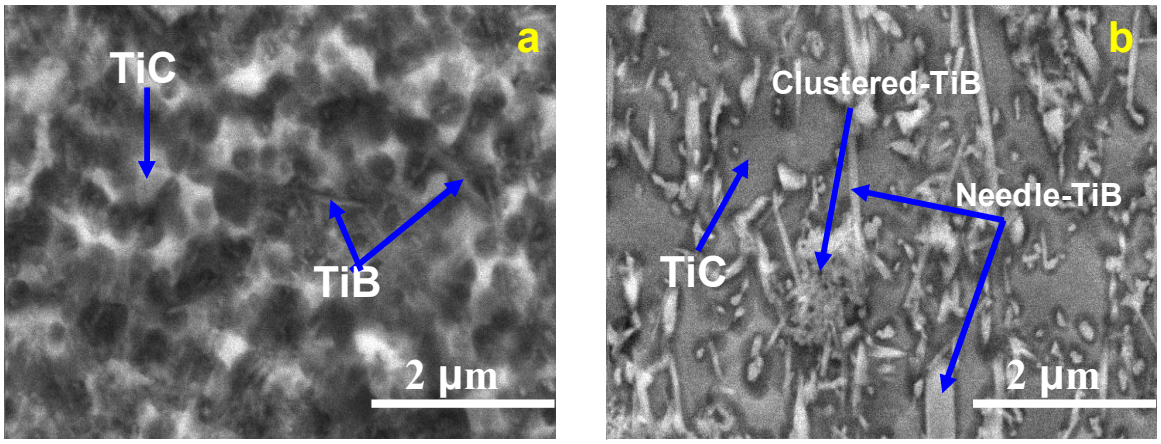

Figure 5. 13: SEM micrographs of hot-pressed 20vol. % reinforced Ti matrix composites at (a) 1100^{0}C (b) 1400^{0}C

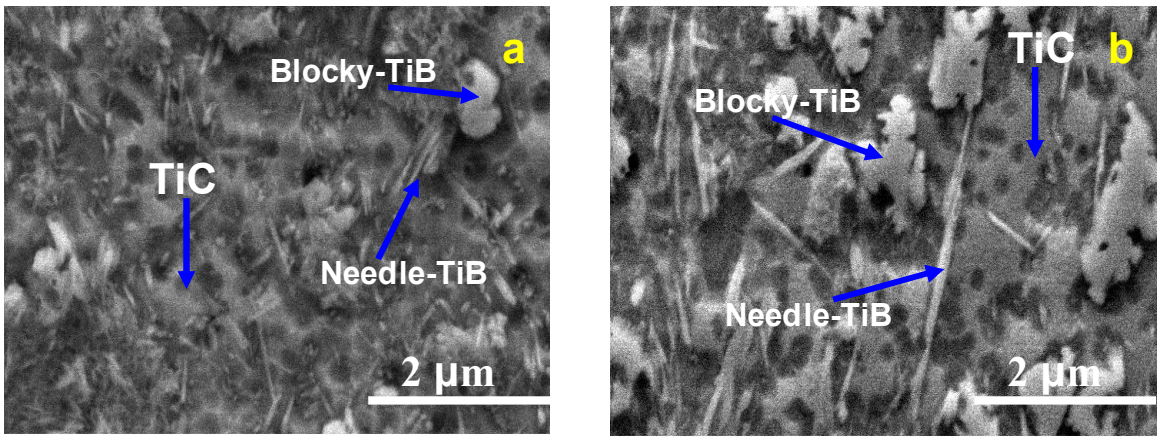

Figure 5. 14: SEM micrographs of hot-pressed 40vol. % reinforced Ti matrix composites at (a) 1100^{0}C (b) 1400^{0}C

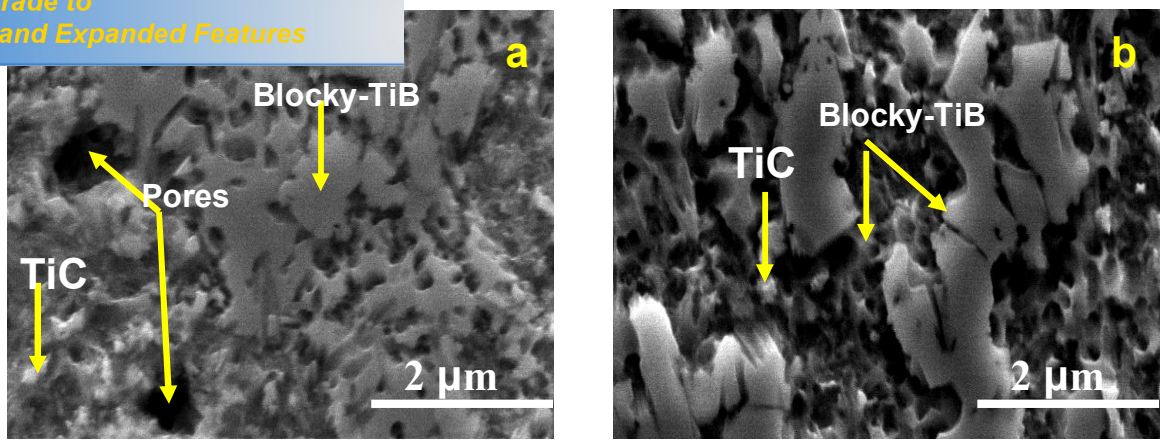

Figure 5. 15: SEM micrographs of hot-pressed 60vol. % reinforced Ti matrix composites at (a) 1100^0C (b) 1400^0C

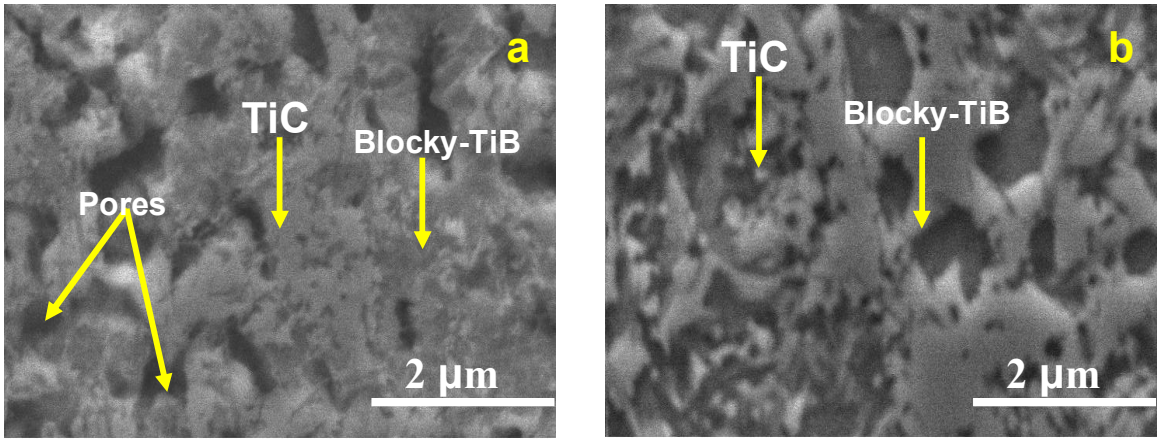

Figure 5. 16: SEM micrographs of hot-pressed 80vol. % reinforced Ti matrix composites at (a) 1100^0C (b) 1400^0C

The morphology change observed agree quite well with the findings of Tsang *et al.*, (1997) that the size and amount of blocky TiB increases and the amount of needle-type TiB decrease with increasing volume fraction of TiB. SEM micrographs of composites sample with 40 vol. % and above reinforcements (Fig. 5.14-5.16) obviously characterized with uniformly distributed blocky and needle shaped TiB structures as well as equiaxed TiC structures. The micrographs of hot-pressed materials with 60 and 80 vol. % (Fig. 5.15, 5.16) are generally characterized with blocky TiB, few scattered TiC, no needle shaped TiB and no presence of porosity. This analysis showed that there was reduction in the needle shaped TiB as the volume fraction of TiB increases.

Figure 5.17 shows the relative densities of hot-pressed Ti matrix composites as a function of the volume fraction of in-situ formed reinforcements (inclusion). It can be seen from the figure that the densification of the composite materials as hot-pressed at 1100°C increased gradually with increasing volume fraction of inclusion up to 40 vol. %, after which the relative density decreased. At 1400°C, constant full densification with over 99% relative density was achieved in the composites 20-80vol. % reinforcing components.

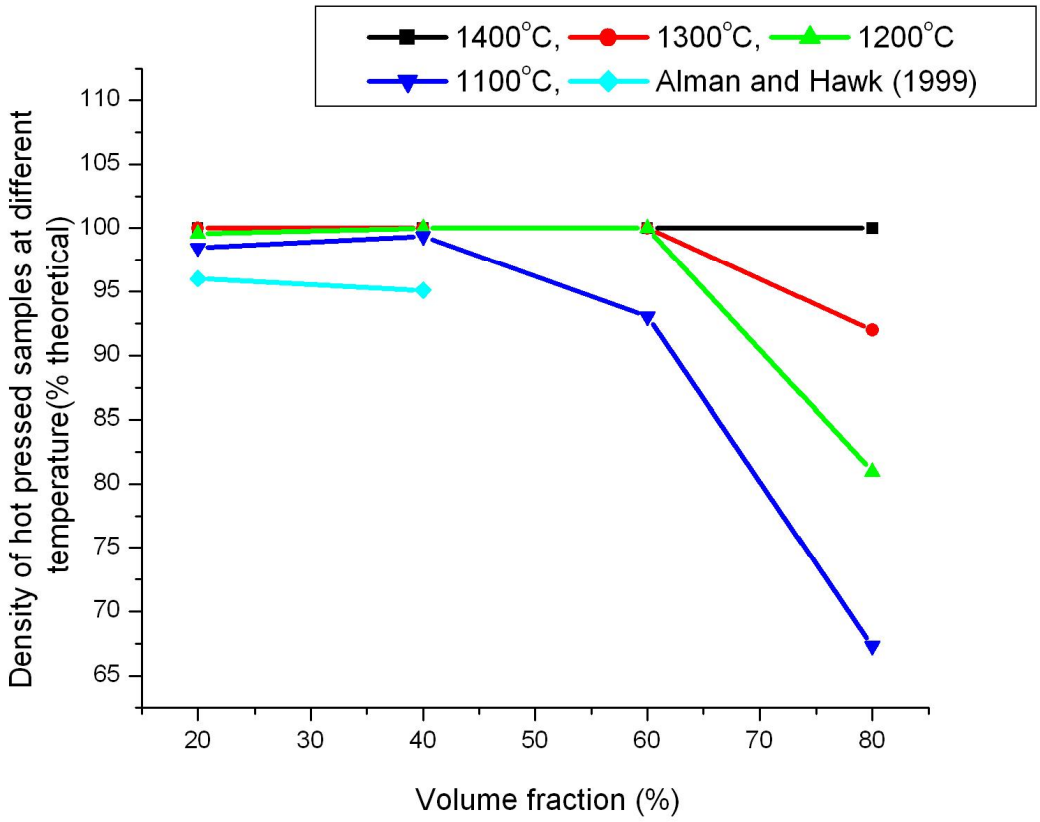

Figure 5. 17: Density of hot-pressed Ti matrix composites as a function of volume fraction (%) of in-situ formed reinforcements (TiC + TiB)

The results show that the applied pressures improved the density for the whole range, but the increase is not enough for complete densification at high volume content of reinforcing elements. The observation in the present study could not be compared

use the available data (from Alman and Hawk, 1999) didnâ consider inclusion beyond 40vol. %. Their results agreed with the observation under pressureless sintering but are not consistent with the observation derived for the hot-pressed samples. However, the general assessment shows that composites produced in this study densified much better than what is available in known literature.

5.4 Relationship between hardness and microstructure

Hardness is the property of a material that enables it to resist plastic deformation, penetration, indentation, and scratching. Therefore, hardness is important from an engineering standpoint because resistance to wear by either friction or erosion, by steam, oil, and water generally increases with hardness. In this work, pure Ti from TiH_2 and commercially sourced Ti were pressureless sintered in argon atmosphere as described in chapter three. Vickers hardness measurement in the present study was carried out using a standard 5kg load for an indentation time of 10s as described in section 3.7.5.

Sintered pure Ti derived from TiH_2 at 1100^{o}C yielded higher Vickers hardness of 273Hv compared to 240Hv achieved by sintered commercial Ti. Figure 5.18 shows the effect of sintering temperature on the Vickers hardness of both sintered samples. Vickers hardness measurement on the pure Ti from TiH_2 increases with temperature up to 1100^{o}C, above which the hardness remain constant taking into account the errors. Hardness of a metal depends on relative density, interstitial content and grain size (Zadra *et al.*, 2008); but the slight Vickers hardness increase recorded for pure Ti from Ti hydride could be attributed to the higher densification of pure Ti from TiH_2 as earlier discussed.

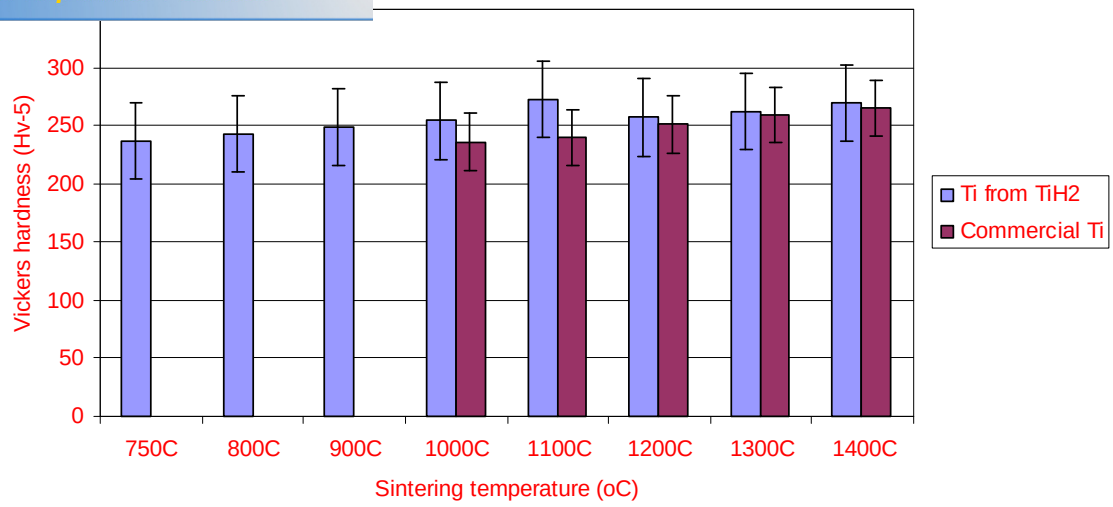

Figure 5. 18: Vickers hardness (Hv_{-5}) of pressureless sintered Ti from TiH_2 and commercial Ti against the sintering temperature.

In comparison with literature data, figure 5.19 reveals that pure Ti produced in the present study achieved higher Vickers hardness compared to the two different grades of commercial Ti sintered by Zadra *et al.*, (2008). Apart from the higher densification considered to have enhanced the hardness of pure Ti, other factor such as temperature duration, cooling rate, sintering methods and small amount of impurities could possibly be connected to the difference in hardness as earlier reported in the work of Rocha *et al.*, (2006).

Figure 5.4 shows the SEM micrographs of sample **PL**750**TiH$_2$**90 and **PL**900**TiH$_2$**90 that are characterized by high porosity which could be attributed to the lower hardness value of 237 and 249Hv respectively, while at 1100 and 1400 ^oC, the porosity in sample **PL**1100**TiH$_2$**90 and **PL**1400**TiH$_2$**90 is reduced drastically leading to enhanced densification which in turn boosted the hardness value of 273 and 270Hv respectively.

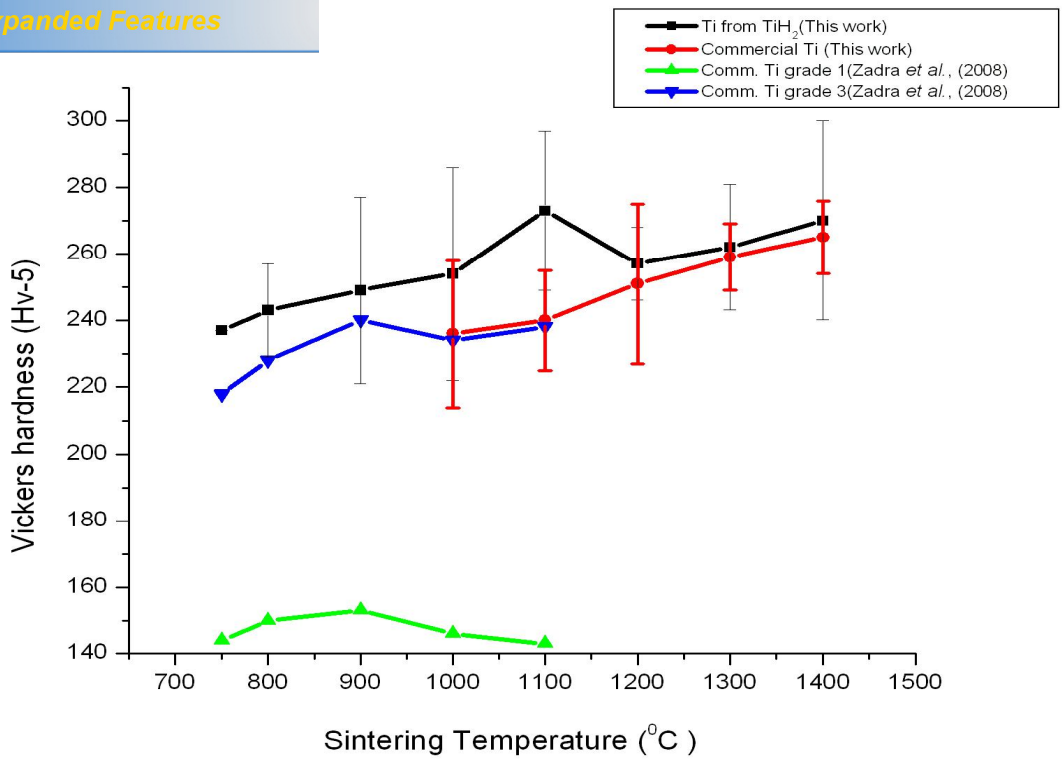

Figure 5. 19: Comparison of the Vickers hardness of as sintered pure Ti from TiH_2, and commercial Ti carried out in this work against the commercial Ti of different grades sintered by Zadra *et al.*, (2008).

In a similar manner, Vickers hardness of pressureless sintered and hot-pressed titanium matrix composites (TMCs) with different vol. % reinforcements was measured after metallographic preparation. Most of the relevant literature on Ti matrix composites did not to specify the hardness of their composites materials produced. However, the Vickers hardness measurement of Ti matrix composites produced in the present study shows higher hardness compared to available data in the literature.

Figure 5.20 compared the Vickers hardness of as sintered pure Ti from TiH_2 with pressureless sintered and hot-pressed Ti matrix composites produced at 1400 ^{o}C. Typical indents are shown in figure 5.21.

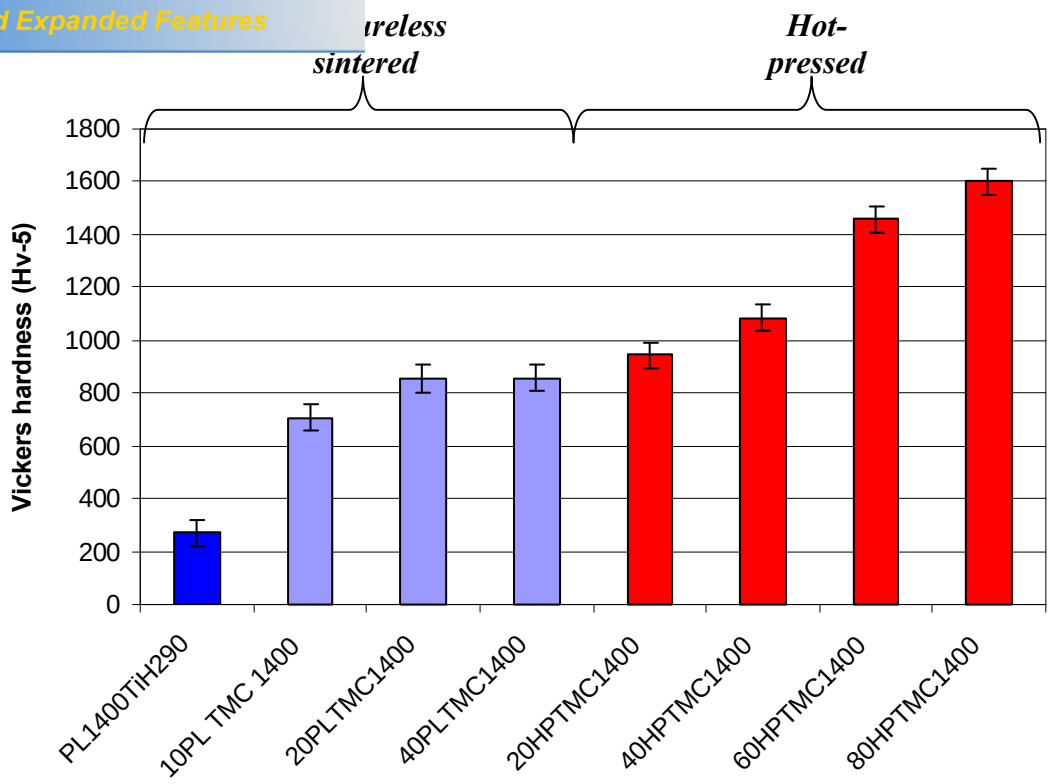

Figure 5. 20: Graph comparing the hardness of pressureless sintered and hot-pressed composites at 1400^{o}C in argon atmosphere. Hardness values were measured using 5kg load.

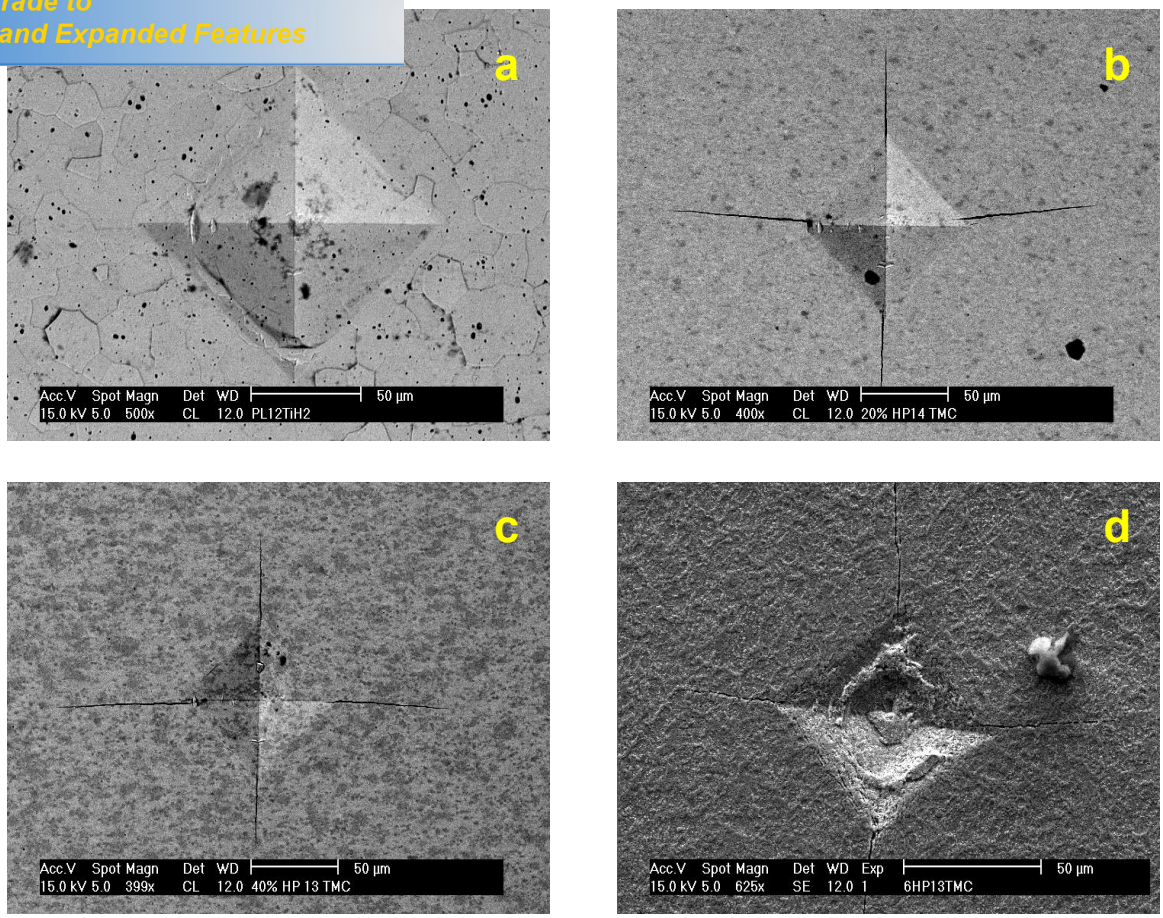

Figure 5. 21: SEM image of sample (a) **PL**1200**TiH$_2$**90 (b) 20**HP**TMC**1400** (c) 40**HP**TMC**1300** (d) 60**HP**TMC**1300** showing an indent made using 5kg load.

As can be seen in figure 5.20, the Vickers hardness of the Ti composites produced increased with increasing volume fraction of the in-situ reinforcements formed. 10vol. % reinforced Ti matrix composite for instance yielded a measured Vickers hardness that is about 3 times higher than that of pure Ti produced from TiH_2. This difference could be attributed to the intrinsic hardness values of reinforcing (TiB and TiC) phasesô in-situ formed after pressureless sintering and hot pressing of the powder mixtures used. The difference shown (Fig. 5.21) in the indentation of sample **PL**1200**TiH$_2$**90 and other Ti matrix composites is also an evidence that the pure Ti sample is not as hard as the composite materials that contain reinforcements but could have a much higher fracture toughness.

The variation in Vickers hardness of composites produced has been linked mainly with change in the content of reinforcing phases present; therefore, figure 5.23 and 5.24 presented the variation of Vickers hardness with the volume fractions of reinforcement in-situ formed using pressureless sintering and hot pressing method respectively. As can be seen in both figures, the gradient of hardness between pure Ti (unreinforced) and 10 vol. % reinforcementôs content is very high compared to others because of the interstitial interaction of C and B atoms that diffused into the Ti matrix. From figure 5.22, composite samples sintered at 1400^{o}C show a progressive increase in the hardness value with increased volume fraction over the investigated range. The hardness increase between 20 and 40 volume fraction (%) is just about 0.5%. At 1200 and 1300 ^{o}C, the hardness increased with volume fraction up to 20vol. %, above which the hardness decreased sharply. At 1100^{o}C, the hardness value of sintered composites decreased gradually with increased volume fraction of reinforcements. The reason for this behavior could be attributed to the reduced density due to retardation of densification by the inclusions. This process is more pronounced at lower sintering temperatures. This figure also shows that the hot-pressed samples exhibit higher hardness than pressureless sintered composites due to better densification achieved.

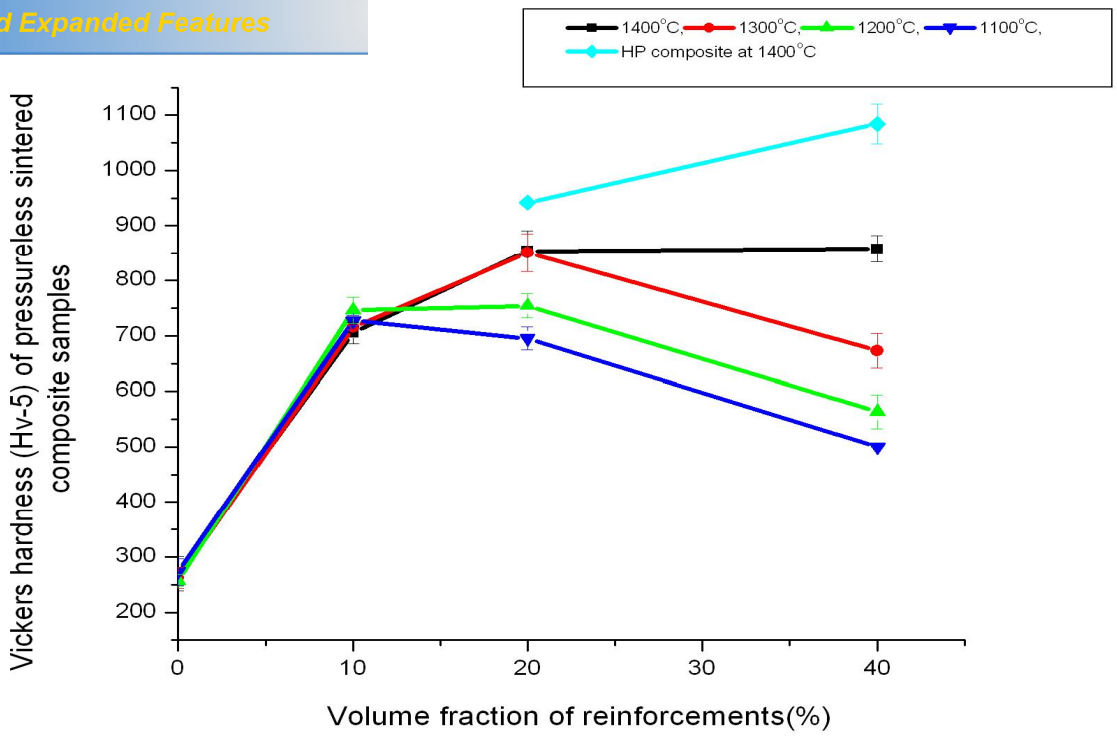

Figure 5. 22: Vickers hardness (Hv-5) of pressureless sintered Ti matrix composites as a function of volume fraction (%) of in-situ formed reinforcements (TiC + TiB)

The hardness of hot-pressed composites at 1300 and 1400 ^{o}C increased gradually with increased volume fraction over the range investigated (Fig. 5.23). The situation differed from the composites hot-pressed at 1200 and 1100 ^{o}C because increase in hardness with increasing volume fraction was noticed up to 60% volume fraction, above which the hardness decreased sharply due to incomplete densification.

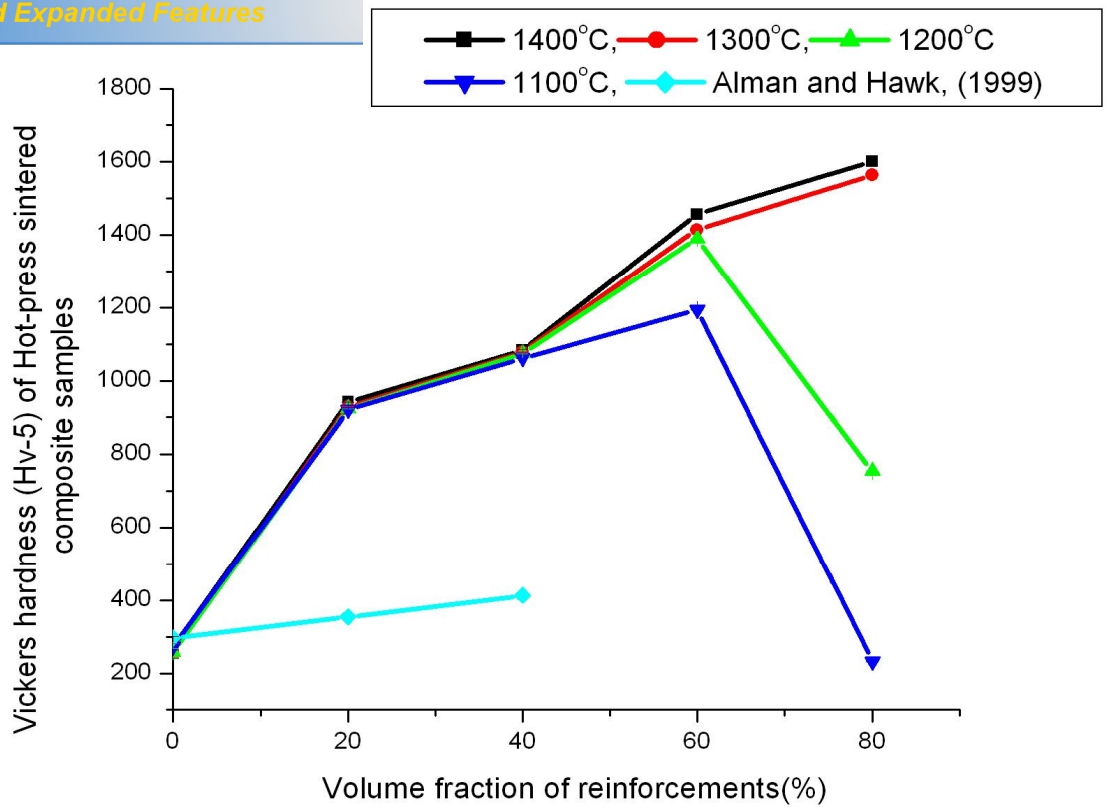

Figure 5. 23: Vickers hardness (Hv-5) of hot-press sintered Ti matrix composites as a function of volume fraction (%) of in-situ formed reinforcements (TiC + TiB)

It is clear from figure 5.24 that the Vickers hardness value obtained for Ti matrix composites in this work is higher than what is available in the literature. This difference shows that utilization of the reaction between Ti matrix produced from TiH_2 and B_4C powder mixtures using in-situ technique will produce Ti matrix composites with good densification and attractive mechanical properties such as hardness.

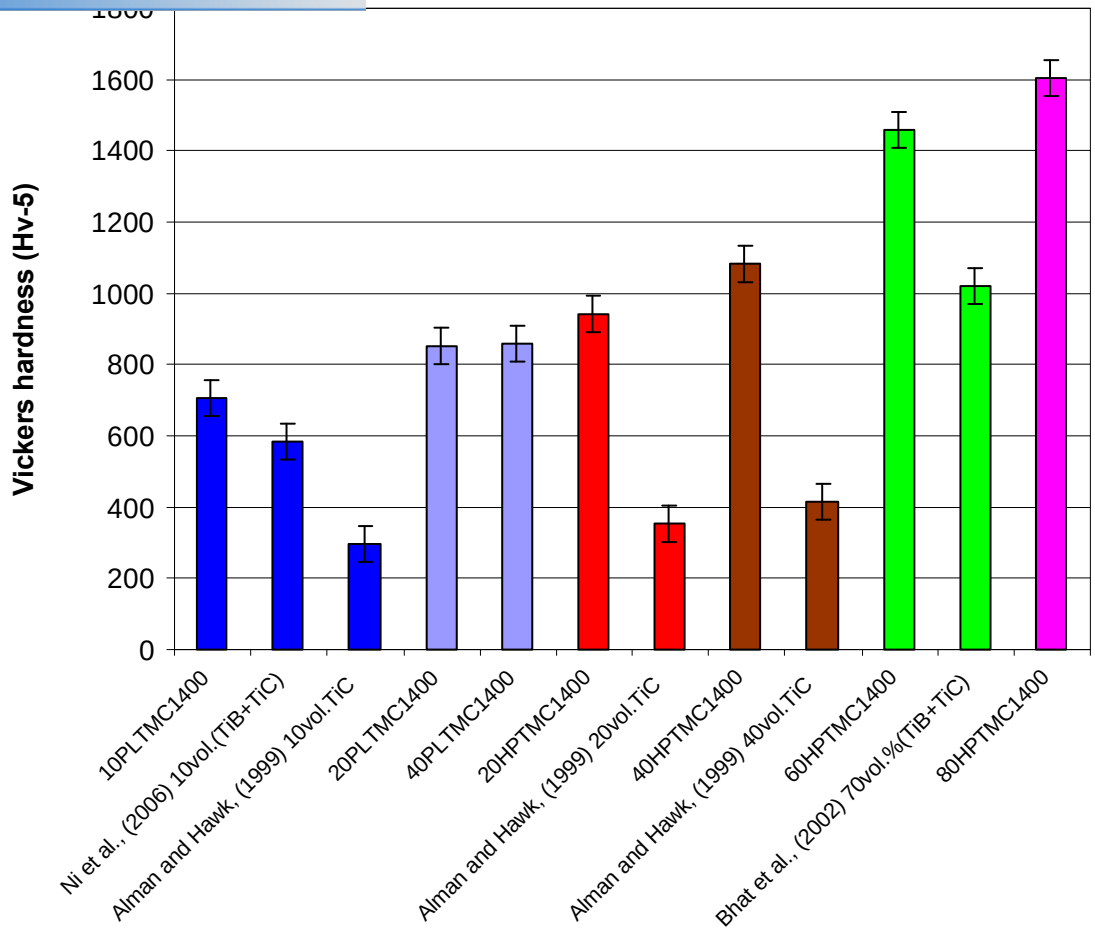

Figure 5. 24: Comparing Vickers hardness values of composites s obtained in this work and those obtained by other researchers.

Figure 5.25 compared the fracture toughness of the Ti matrix composites produced in this work with those available in the relevant literature. Fracture toughness measurement in this work was carried out using 5kg load as described in chapter three. The fracture toughness of the sintered pure Ti from TiH_2 could not be measured through the indentation technique used because the indentation macrograph obtained (Fig. 5.21) shows no crack length. This in principle can be regarded as a sign of having much higher fracture toughness. Even if the method used gives result, it may not be adequate values due to the expected higher ductility of Ti. However, the data can be used to rationalize a trend of the change in the fracture toughness.

Although the fracture toughness of the sintered and hot-pressed Ti matrix composites produced in this work is lower compared to that of titanium and titanium alloy (Ti-6Al-4V), the values obtained compared quite well with similar materials produced in the literature. For instance, sample10**PL**TMC**1400** and 40**HP**TMC**1400** show fracture toughness of 4.1MPa.$m^{1/2}$ and 5.3MPa.$m^{1/2}$ respectively, while Barsoum *et al.* (1993) and Brodkin *et al.* (1996) reported fracture toughness of 4-5, 5.6 and ~6MPa.$m^{1/2}$ for titanium matrix composites (TMCs) they produced using the reaction between Ti and B_4C at different ratio of 3:1, 4:1 and 6:1. The phase composition of their composites includes TiB_2, TiC, and Ti_3B_4. The fracture toughness of the Ti matrix composites produced increased with increasing content of reinforcement, which also agreed with the report of Dubey and Soboyejo (1997) that fracture toughness depends on the composition and contents of reinforcements, while its improvement depends on the change in reinforcement morphology and the quantity that occurs during the heat treatment. Composite materials produced by Dubey and Soboyejo (1997) shows highest fracture toughness because they contained Ti alloy (Ti, Al, Fe) and TiB as reinforcements. The results show the disadvantage of the reaction sintering method. Due to the strong interaction of Ti with the reinforcing components, dissolution of B and C occur in the Ti matrix reducing the ductility of Ti strongly. Perhaps in the future, it has to be investigated if the use of Ti alloys for the production of TMC can overcome this problem.

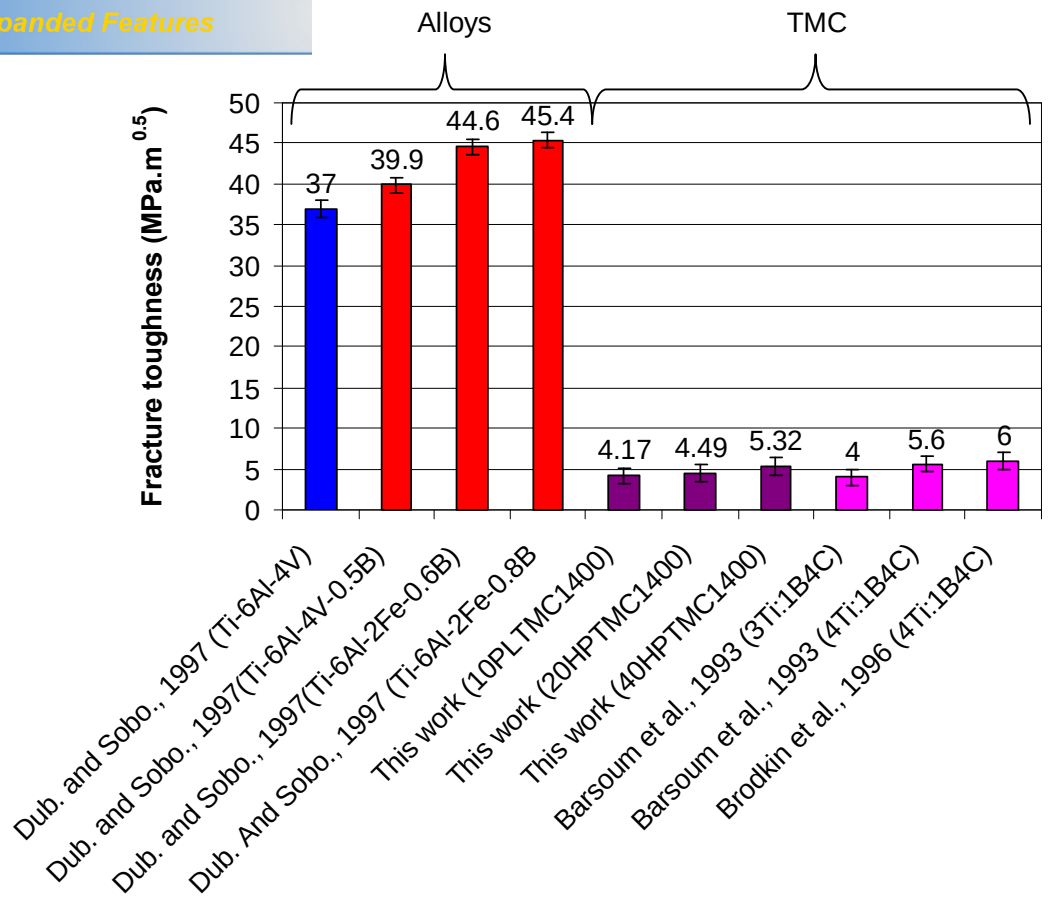

Figure 5. 25: Comparing the fracture toughness of some selected Ti matrix composites produced with those obtained from the literature by different author.

5.5 Ti-B_6O composites

An attempt was also made to produce titanium matrix composites from commercial Ti and B_6O (ceramic) with the major aim of forming the reinforcing particles through in-situ reaction between the two starting materials. The Ti-B_6O powder mixtures were hot presses over temperature ranging from 1000 and 1300^{o}C. Detailed results were presented in chapter four.

show that the major phases present in the composite produced from Ti-B_6O are TiB, TiB_2 with Ti_2O as the matrix. The equation of reaction is this case is represented as:

$$8Ti + B_6O \rightarrow 6TiB + Ti_2O \text{ ----------5.1}$$

$$5Ti + B_6O \rightarrow 3TiB_2 + Ti_2O \text{ ----------5.2}$$

The densification behaviour of the composites produced is encouraging but the material is not as dense as the hot-pressed composite produced from TiH_2-B_4C powder mixture. At 1000°C, relative density of 93.41% was obtained by sample **HP**8Ti2B_6O**1000** while at 1300°C near full densification with relative density of 98.24% was attained by sample **HP**8Ti2B_6O**1300**. This shows that further increase in temperature would possibly produce a fully densified composite like those obtained from TiH_2-B_4C.

SEM analysis of these samples shows traces of a needle shaped structure and many black spot (Fig. 5.26a) that EDS analyses revealed to be TiB and unreacted B_6O respectively. Presence of high levels of porosity at lower temperature could justify the densification observed, whereas many of what looks like pores in the sample hot-pressed at 1300°C (Fig. 5.27b) are unreacted B_6O aggregates (EDS analyses). The presence of unreacted B_6O shows that the reaction was not complete and this may be connected to high melting and sintering temperature required for B_6O relative to the matrix or the formation of passivating layers, which lead to a limited generation of reinforcement (TiB) particles formed in the structure. Highest Vickers hardness of 941Hv was achieved but the fracture toughness (12.7MPa.$m^{0.5}$) is better than 5.327MPa.$m^{0.5}$ recorded by Ti matrix composite (40**HP**TMC**1400**).

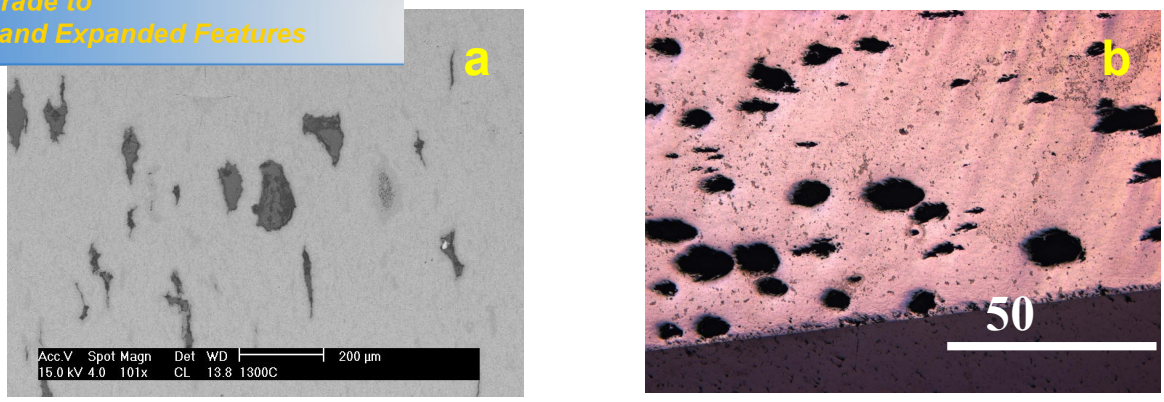

Figure 5. 26: Hot-pressed sample **HP**8Ti2B_6O**1300** (a) SEM micrograph (b) Optical micrograph

Based on these findings, the type of composite materials and the intent area of application (due to the influence of oxygen) would play a major role before considering using Ti-B_6O system as starting materials.

As shown in table 4.11, the fracture toughness of hot-pressed Ti-B_6O composites changes with sintering temperature, as well as the composition of the reinforcements formed. Although there is no consistency in the values obtained. For instance, sample **HP**8Ti2B_6O**1000** has fracture toughness of 10.6MPa.$m^{1/2}$ while that of sample **HP**8Ti2B_6O**1100** is 7.3MPa.$m^{1/2}$.

In comparison, hot-pressed Ti-B_6O composites shows higher fracture toughness compared to pressureless and hot-pressed Ti-B_4C composites produced. For instance, sample **HP**8Ti2B_6O**1300** show fracture toughness of 10.8MPa.$m^{1/2}$ compared to 5.3MPa.$m^{1/2}$ shown by sample 40**HP**TMC**1400**. The observed difference could be attributed to difference in composition and contents of reinforcements, as well as reinforcementôs morphology and the quantity that occur during the heat treatment (Dubey and Soboyejo, 1997). This claim is substantiated with the observation from the XRD (Fig. 4.31, page 116) and SEM (Fig. 4.32, page 117) analysis of Ti-B_6O composites that shows the presence of Ti_2O, TiB, TiB_2 and unreacted B_6O phases against Ti, TiC and TiB phases detected in Ti-B_4C composites.

Chapter Six

6.0 Conclusions and Recommendations

The cost of production and presence of certain impurities in titanium powder has made its use in the fabrication of titanium matrix composites a serious challenge. This research looked into the possibility of producing Ti matrix composites from titanium hydride (TiH_2) and boride ceramics (B_4C and B_6O) using in-situ technique.

In this study, titanium hydride powder was compacted into cylindrical pellets that were further used to produce pure Ti through dehydrogenation and pressureless sintering. Different composition of TiH_2-B_4C powder mixtures produced composites with 0 to 80 vol. % reinforcing (TiB + TiC). The power mixtures and compacts were used to produce in-situ reinforced Ti matrix composites through pressureless sintering and hot pressing methods at various temperature ranges (1100-1400^oC) under argon atmosphere. The hot-pressing was carried out with the application of 30MPa for 120min in case of TiH_2-B_4C mixture. Composites produced were characterized, density measured and metallographically prepared before hardness and fracture toughness were determined.

Based on the experimental results and findings discovered in the present research, the following conclusions were made:

1. Green compacts produced from TiH_2 powder show lower green density with low ejection force compared to commercial Ti powder. These observations may be connected to the reduced cold welding between TiH_2 particles and between the wall of the compaction die and TiH_2 particles. This can be attributed to the fact that TiH_2 particles are less easily deformed and less reactive than Ti metal powder.

2. Conversion and pressureless sintering of TiH_2 powder and compacts to pure Ti was successfully carried out under argon atmosphere. It was established that dehydrogenation temperature decreases with decreasing heating rates. Reduction in surface area of TiH_2 powder particles by cold compaction was found to retard dehydrogenation of compacts and results in higher temperature for complete removal of hydrogen. Mass loss due to the release of hydrogen was effectively completed after dehydrogenation of loose hydride powder at 680^{o}C for 120min and hydride compact at 715^{o}C for 120min forming Ŭ-Ti. The dehydrogenation is finished at temperatures far below the temperature of intensive sintering.

3. Full densification of pressureless sintering pure Ti from TiH_2 was achieved at 1200^{o}C for an isothermal sintering period of 90min. The more rapid densification of pure Ti from TiH_2 in comparison to commercial Ti was primarily attributed to lower grain size of TiH_2 powder. Presence of very low or no impurities, as well as creation of more vacant sites that enhanced the mobility of Ti atoms after hydrogen removal may also contribute to the enhanced densification observed.

4. Particulate-reinforced Ti matrix composites with different composition of in-situ formed reinforcements were successfully fabricated from TiH_2 and B_4C powder mixtures using pressureless sintering and hot-pressing methods as against the common practice of using Ti and B_4C powder mixtures. Observed XRD and SEM analysis shows that (TiB + TiC)/Ti composites with different volume content of reinforcements were produced.

5. XRD analysis of all the synthesized composites confirmed that Ti and B_4C reacted after removal of hydrogen and it was shown that Ti matrix, TiB

ajor phases present with small amount of TiB_2. There was a shift noticed in the major Ti peak; this was suspected to be a result of small amounts of C and B that dissolve in Ti matrix during the preparation process. This confirmed the report of Ma *et al.*, (2007) that the reaction between Ti and B_4C powder to produce in situ (TiB + TiC)/Ti composites cannot proceed to completion. This is probably the reason for the strongly reduced toughness observed even when a low amount of reinforcing elements is present.

6. SEM/EDS analysis shows that in-situ formed reinforcements contain needle and blocky type of TiB and equiaxed shaped TiC. The amount of reinforcements formed increases with increased amount of B_4C used in the starting powder mixtures. It was also established that the amount of needle-type TiB decreases and the size and amount of blocky-type TiB increases with increasing volume fraction of TiB. This observation confirmed an earlier report of Tshang *et al.*, (1997).

7. Dense materials and improved Vickers hardness enhanced by in-situ reinforcements and applied external pressure was achieved by the hot-pressed composites especially those treated at 1400 ^{o}C compared to the pressureless sintered composites under the same conditions and to relevant literature. The densification is generally influenced by sintering temperature, volume content of the reinforcements and the applied external pressure. Generally, Ti matrix composites produced in the present study show higher Vickers hardness values compared to available data in the literature. The hardness of the composites was found to depend on the volume fraction of the reinforcements present. Although the fracture toughness obtained is low, it compared quite well with reported results in the literature.

ns of reinforcing elements strongly reduce the fracture toughness of the composite from 30-70Mpa.$m^{0.5}$ found for pure titanium to a value below 5-6 Mpa.$m^{0.5}$. This is the disadvantage of this reaction sintering route. The interaction results in some solution of B and C in the Ti matrix resulting in this strongly reduced toughness.

9. Composites produced from Ti-B_6O show the presence of TiB and TiB_2 in a Ti_2O matrix. Unreacted B_6O particles were discovered; this may be responsible for very small amount of TiB reinforcement formed, which in turn makes its properties incomparable with those fabricated from TiH_2 and B_4C powder mixtures.

Findings of this study therefore established that Ti matrix composites with high density and appropriate physical and mechanical properties can be produced from titanium hydride and boron carbide powders using in-situ technique that involves pressureless sintering and hot-pressing. It has been established that Ti matrix composites produced through this route will give rise to a better quality (less or no impurity) and above all, less expensive composites that will gain wide acceptability and application in multi faceted industrial areas as enumerated in the literature (Yamada, 1996, Christoph and Manfred, 2003; Seagle, 1995; Larsson *et al.*, 1996). However, there is need for further investigations on the composites produced before the products could be considered for commercialization. On this basis, the following suggestions are considered necessary for future research on the developed composite materials using TiH_2 and B_4C powders as starting materials:

1. Comprehensive study of mechanical properties of Ti matrix composites developed in this study is very essential for extensive comparison with properties of Ti matrix composites produced using commercial Ti and B_4C

perties may include elastic modulus, tensile strength, ductility, fracture toughness, wear, and creep behavior.

2. There is a need for further work on the detail reaction mechanism and kinetics of reaction between B_4C and Ti particles as the knowledge will facilitate better understanding of the science involved in the production of the TMCs. There is no literature on this aspect so far.

Abdallah, M. M. (1996) Corrosion of titanium and zinc alloy in Dead Sea water, Anti-Corros. Methods Materials, 43 (1), pp. 17ï 22.

Abkowitz, S. and Weihrauch, P. (1989) *Trimming the Cost of MMCs*. Advanced Materials and Processes, volume.136, Issue 1, July, pp. 31-34.

Abkowitz, S., Abkowitz, S. M., Fisher, H. and Schwartz, P. J. (2004) *Cerme Ti discontinuously reinforced Ti-matrix composites: Manufacturing, properties, and applications.* JOM, 56(5), pp.37-41

Abkowitz, S., Weihrauch, P. and Abkowitz, S.M. (1993) *Particulate-Reinforced Titanium Alloy Composites Economically Formed by Combined Cold and Hot Isostatic Pressing.* Industrial Heating, 60(9), pp. 32-37.

Adams, J., Duz, V. and Moxson, V. (2008). *Powder Metallurgy Processes for Producing Titanium Alloy Products from Hydrogenated Titanium Powder*, *Proceedings TMS2008: Materials Processing and Properties*, 1, pp. 363-367.

Alman, D. E. and Hawk, J.A. (1999) *The abrasive wear of sintered titanium matrix–ceramic particle reinforced composites.* Wear 225ï 229, pp.629ï 639.

Anstis, G., Chantikul, P., Lawn, B. and Marshall D. (1981): ñA Critical Evaluation Indentation Techniques for Measuring fracture Toughness: I, Direct Crack Measurementsò, *Journal of Ceramic society*. Vol 64, pp. 533-8.

Barsoum, M.W. and Houng, B. (1993) *Transient plastic phase processing of titanium-boron-carbon composites.* Journal of the American Ceramic Society, 76, pp.1445-1451.

Bashkin, I.O., Kolesnikov, A.I. and Adams, M.A. (2000) *Pressure effect on the hydrogen vibrations in g-TiH and g-ZrH.* J Phys Condens Matter, 12, pp. 4757ï 65.

Bejamin, J.S. (1970) *Dispersion-strengthened superalloys by mechanical alloying.* Metall. Trans. 1, pp. 2943ï 2951

Bejamin, J.S. (1976) *Mechanical alloying.* Sci. Am. 234, pp. 40-48

(1974) *Mechanism of mechanical alloying*. Metall. Trans, volume 5, Issue 8, pp.1929-1934.

Bhosle, V., Baruraj, E. G., Miranova, M. and Salama, K. (2003) *Dehydrogenation of Nanocrystalline TiH_2 and Consequent Consolidation to form Dense Ti*. Metallurgical and Materials Transactions A, volume 34A, pp. 2793-2799.

Boyer, R., Welsch, G. and Collings, E.W. (1994) *Materials properties handbook: Titanium alloys, the materials information society*, ASM International, Materials Park.

Brodkin, D., Kalidindi, S.R. and Barsoum, M.W. (1996) *Microstructural evolution during transient plastic phase processing of titanium carbide-titanium boride composites.* Journal of the American Ceramic Society, 79, pp.1945-1952.

Cai, L., Zhang, Y., Shi, L., Yang, H. and Xi, M (2006) *Research on Development of In Situ Titanium Matrix Composites and In Situ Reaction Thermodynamics of the Reaction System*. Journal of University of Science and Technology Beijing, Volume 13, Number 6, pp. 551.

Chandran, K.S., Panda, K.B. and Sahay, S.S. (2004) *TiB_w-Rinforced Ti Composites: Processing, Properties, Application Prospects, and Research Needs.* JOM (Journal of Material Science and Engineering), May 2004 edition, pp.42-48.

Chen, J., Geng, Z. and Chin, B.A. (1989) *High temperature ordered intermetallic alloys III*. Materials Research Society Symposium Proceedings, volume 133, pp. 447.

Christodoulou, L., Parrish, P.A and Crowe, C.R (1988) *High Temperature/High Performance Composites.* Mater.Res.Soc.Symp.Proc.120, pp.29

Christodoulou, L., Parrish, P.A. and Crowe, C.R. (1988a). *XD titanium aluminide composites*. Materials Research Society Proceedings, volume 120, F.D. Lemkey, S.G. Fishman, A.G. Evans, and J.R. Strife, eds. Pittsburgh, Pa.: Materials Research Society, pp. 29-34.

red Peters (2003) ‘õTitanium and Titanium alloys: Fundamentals and Applicationsõõ WILEY-VCH Verlag GmbH and Co KGaA. Germany. ISBN 3-527-305, pp. 34-43.

Chu, M.G. and Premkumar, M.K. (1993) *Mechanism of TiC formation in Al/TiC in situ metal-matrix composites.* Metallurgica and Materials Transactions A, volume 24, No 12, pp. 2803-2805.

Crane, R. L., Chattoraj, S. C. and Strope, M.B. (1971) *Room-temperature polymorphic transition of titanium hydride.* Journal of the Less-Common Metals, 25(2), pp. 225-7.

Dariel, M.P., Frage, N., and Levin, L. (2002) *A novel approach for the preparation of B4C- based cermets.* International Journal of Refractory Metals & Hard Materials 18, pp. 131-135

Dearnley, P.A. and Roberts, K.A. (1990) in Proceeding of Conference on Processing Pacific Resources, Auckland (University of Auckland, New Zealand), pp. 477.

Dillon, A.C., Gilbert, K.E.H., Alleman, J.L., Gennett, T., Jones, K.M. and Parilla, P.A. (2001) *Carbon nanotube materials for hydrogen storage.* In: Proceedings of the 2001 DOE hydrogen program review, NREL/CP, pp. 570ï 30535.

Dubey, S. and Soboyejo, W.O. (1997) *Deformation and Fracture Properties of Damage Tolerant In-situ Titanium Matrix Composites.* Applied Composite Materials 4, pp. 361-374.

Emura, S., Hagiwara, M. and Kawabe, Y. (1996) *Titanium ’95 Science and Technology*, ed. P.A. Blenkinsop, W.J. Evans, and H.M. Flower (London: The Institute of Materials, 1996), pp. 2714-2721.

Froes, F.H. and Suryanarayana, C. (1993) *Powder Processing of Titanium Alloys.* Rev. Particulate Mater., Issue 1, pp. 223-75.

Frommeyers, G., Beer, S. and Oldenburg. K.V. (1994) *Microstructure and mechanical properties of mechanically alloyed Intermetallic Mg_2Si-Al*

er Metallkunde/Materials Research and Advanced Techniques, volume 85, Issue 5, pp. 372-377

Gai, G, Yang, Y., Jin, L., Zou, X., and Wu, Yunxin (2007) Particle shape modification and related property improvements. Powder Technology, Article in press. Doi:10.1016/j.powtec.2007.11.026.

Gilman, P.G., Bejamin (1983) *Mechanical alloying*. Annual Review of Materials Science, volume 13, pp. 279-300

Godfrey, T.M.T., Wisbey, A., Goodwin, P.S., Bagnall, K. and Ward-Close, C.M. (2000) *Microstructure and tensile properties of mechanically alloyed Ti-6Al-4V with boron additions.* Materials Science & Engineering, A: Structural Materials: Properties, Microstructure and Processing (2000), A282 (1-2), pp. 240-250.

Gorsse, S. and Miracle, D.B (2003) *Mechanical Properties of Ti-6Al-4V/TiB Composites with Randomly Oriented and Aligned TiB Reinforcements*. Acta Materialia 51, pp. 2427-2442.

Gorsse, S., Chaminade, J. P. and Le Petitcorps, Y. (1998) *In situ preparation of titanium base composites reinforced by TiB single crystals using a powder metallurgy technique.* Composites Part A, 29A, pp.1229-1234.

Grosgogeat, B, Reclaru, L, Lissac, M. and Dalard, F. (1999) *Measurement and evaluation of galvanic corrosion between titanium/Ti–6Al–4V implants and dental alloys by electrochemical techniques and auger spectrometry*, Biomaterials 20, pp. 933ï 941.

Hagiwara, M., Arimoto, N., Emura, S., Kawabe, Y. and Suzuki, H.G. (1992) *Mechanical properties of Particulate Reinforced Titanium-Based Metal Matrix Composites Produced by the Blended Elemental PIM Route.* Transactions of the Iron and Steellnstitute (/SIJ) International, Vol. 32. No. 8, pp. 909-916.

Han, Z. Zhao, H. Chen, X.F. and Lin, H.C. (2000) Corrosion behaviour of Tiï 6Alï 4V alloy welded by scanning electron beam, Mater. Sci. Eng. A277, pp. 38ï 45.

A. and Lavernia, E.J. (1991) *Particulate Reinforced Metal Matrix Composites- a review.* Journal of Materials Science 26, pp. 1137-1156.

Ivasishin, O.M., Savvakin, D.G., Bielov, I.S., Moxson, V.S., Duz, V.A., Davies, R. and Lavender, C. (2005) *Microstructure and properties of titanium alloys synthesized from hydrogenated titanium powders.* Materials Science and Technology, volume 4, pp.151-158.

Ivasishin, O.M., Savvakin, D.G., Moxson, V.S., Duz, V.A and Lavender, C. (2007) Proc. Cong. on *'Ti-2007 science and technology'*, Kyoto, Japan, 2007, The Japan Institute of Metals, pp.757-760.

Jackson, M and Dring, K (2006) *A review of advances in processing and metallurgy of titanium alloys*. Material Science and Technology, Vol.22, No 8, pp.881-887.

Jianxin, D. and Junlong, S. (2009) *Microstructure and mechanical properties of hot-pressed B_4C-TiC-Mo ceramic composites.* Ceramics International 35, pp. 771-778.

Johnson, T.P., Brooks, J.W. and Loretto, M.H. (1991) *Mechanical properties of a Ti-based metal matrix composite produced by a casting route*. Scripta Metallurgical Materialia, volume 25, issue 4, pp. 785-789

Kang, E.S. and Kim, C.H. (1990) *Improvement in Mechanical Properties of TiB_2 by the Dispersion of B_4C particles*. Journal of Materials Science 25, pp. 580-584.

Kim, Y.-J., Chung, H. and Kang, S.J.L. (2001) *In situ formation of titanium carbide in titanium powder compacts by gas-solid reaction*. ELSEVIER, Composites (Part A: applied and manufacturing), Part A32, pp. 731-738.

Knacke, O., Kubaschewski, R. and Hesselman, R. (1991) *Thermodynamical properties of inorganic substances.* Second edition, Springer, Berlin.

Konitzer, D.G. and Loretto, M.H. (1989) *Microstructural assessment of Ti6A14V-TiC metal-matrix composite.* Acta Metallurgica, volume 37, issue 2, pp. 397-406

008) *An Experiment Study on Ultrasonic Machining of Pure Titanium Using Designed Experiments.* Journal of the Braz. Soc. of Mech. Sci. & Eng. Vol. XXX, No. 3, pp. 231-238

Kumar, R.S., Cornelius, A.L., Pravica, M.G., Nicol, M.F., Hu, M.Y. and Chow, P.C. (2007) *Bonding changes in single wall carbon nanotubes (SWCNT) on Ti and TiH2 addition probed by X-ray Raman scattering.* Diam. Relat. Mater, 6(4ï 7), pp.1136ï 9.

Larsson, C. Thomsen, P. Aronsson, B. O. Rodahl, M. Lausmaa, J. Kasemo, B. (1996) *Bone response to surface-modified titanium implants: studies on the early tissue response to machined and electropolished implants with different oxide thicknesses*. Biomaterials, 17, pp 605- 10.

Lederich, R.J., Soboyejo, W.O. and Srivatsan, T.S. (1994) *Preparing damage tolerant in-situ titanium matrix composites.* Journal of Metals, volume 46, pp. 68-71.

Levin, L., Frage, N. and Dariel, M.P. (2000) *A novel approach for the preparation of B_4C-based cermets.* International Journal of Refractory Metals & Hard Materials 18 , pp. 131-135

Li, D.X., Ping, D.H., Lu, Y.X. and Ye, H.Q. (1993) *Characterization of the microstructure in TiB-whisker reinforced Ti alloy matrix composite*. Materials Letters, volume 16, Number 6, pp. 322-326

Liang, Y.H., Wang, H.Y., Yang, Y.F., Du, Y.L. and Jiang, Q.C. (2008) *Reaction Path of the Synthesis of TiC-TiB_2 in Cu-Ti-B4C System*. International Journal of Refractory Metal & Hard Materials 26, pp. 383-388.

Lin, Y., Zee, R. H. and Chin, B. A. (1991) *In situ Formation of Three-Dimensional TiC Reinforcements in Ti-TiC Composites*. Metallurgical Transactions A: Volume 22A (April), pp. 859.

Liu, G., Zhu, D. and Shang, J.K (1993) *Temperature Dependence of Fracture Toughness in TiC-Particulate Reinforced Ti-6Al-4V Matrix Composite.* Scripta Metallurgical et Materialia, vol.28, pp. 729-732.

D.G. (1990) *The effect of matrix reinforcement reaction on fracture in Ti-6Ai-4V-base composites*. Metallurgical Transactions A: Volume 21, Issue 6, June 1990, pp. 1579-1587.

Lu, C.J. and Li, Z.Q. (2008) *Structural evolution of TiH_2-B_4C during ball milling and subsequent heat treatment*. Journal of Alloys and Compounds 444, pp.198-201

Lu, L., Lai, M.O., Niu, X.P. and Ho, H.N. (1998) *In situ formation of TiB_2 reinforced aluminium via Mechanical alloying.* Zeitschriftfuer Metallkunde/Materials Research and Advanced Techniques, volume 89, issue 8, pp. 567-572.

Lu, W., Zhang, D., Zhang, X., Wu, R., Sakata, T. and Mori, H. (2001) *Microstructural Characterization of TiC in in situ synthesized titanium matrix composites prepared by common casting technique*. Journal of Alloys and Compounds 327, pp. 248-252

Lu, W.J., Zhang, X.N., Zhang, D., Wu, R.J., Bian, Y.J. and Fang, W.P. (1999) *Growth mechanism of reinforcement in in situ processed TiC/Ti composites*. Jinshu Xuebao /Acta Metallurgical Sinica. Volume 35, Issue 5, pp. 536-540P.

Ma, F., Lu, W. and Qin, J. (2007) *Hot deformation behavior of in situ synthesized Ti composite reinforced with 5 vol. % (TiB + TiC) particles.* Journal of Materials Science, 42, pp. 6901-6906.

Ma, Z.Y., Tjong, S.C. and Geng, L. (2000) *In-situ Ti-TiB metal–matrix composite prepared by a reactive pressing process*. Scripta Materialia., volume 42, No. 4, pp.367ï 373

Madtha, S., Lee, C. and Ravi Chandran, K.S. (2008) *Physical and Mechanical Properties of Nanostructured Titanium Boride (TiB) Ceramic.* Journal of American Ceramic Society, 91 [4], pp. 1319ï 1321

Merzhanov, A.G. (1990) *Combustion and plasma synthesis of high temperature materials*, edited by Z.A. Munir and J.B. Holt (VCH Publishers, NY).

nd Froes, F.H. (1998) *Production and application of low cost titanium powder products.* International journal of powder metallurgy (Princeton, New Jersey), volume 34, Issue 5, pp.45-53

Ni, D.R., Geng, L., Zhang, J. and Zheng, Z.Z. (2006) *Effect of B_4C on Microstructure of in situ titanium matrix composites prepared by reactive processing of Ti-B_4C system,* Scripta Materialia 55, pp. 429-432.

Nukami, T. (1998) *The growth of TiC particles in an Al matrix*. Journal of Materials Science letters, volume 17, Number 4, pp. 267-269 (3).

Numakura, H. and Koiwa M. (1984) Hydride precipitation in titanium. *Acta Metallurgica*, 32(10), pp.1799-1807.

Odwani, A.A. Tabtabaei, M. A. Nabi, A. A. (1998) Performance of high chromium stainless steels and titanium alloys in Arabian Gulf seawater, Desalination 120, pp. 78ï 81.

Ogwu, A.A. and Davies, T.J. (1996) *The Densification and Mechanical Properties of a TiC and TiB_2 Hardmetal Sintered with a Reactive Alloy Binder.* Phys. Stat. Sol. (A) 153, pp. 101-116.

Padurets, L.N. and Shilov, A.L. (1997) *Limiting composition and thermal decomposition of titanium hydride.* Russ J. Inorg. Chem, 42(8), pp.1135.

Panigrahi, B.B, Godkhindi, M.M, Dasa, K, Mukunda, P.G. and Ramakrishnan, P. (2005*) Sintering kinetics of micrometric titanium powder. Journal of materials.* Science and Engineering A 396, pp. 255ï 262.

Panigrahi, B.B. (2007): *Sintering behaviour of Ti–2Ni and Ti–5Ni elemental powders.* Material Letters 61, pp. 152-155.

Peng, T.C., Bowden, D.M. and Sastry, S.M.L. (1989) *Advances in powder metallurgy IV* (eds. Gassbarre, T.G and Jandeska, W.F.) 387 MPIF, Princeton, NJ, pp.127-141.

Radhakrishna Bhat, B.V., Subrahmanyam, J. and Bhanu Prasad, V. V. (2002) *Preparation of Ti-TiB-TiC & Ti-TiB composites by in-situ reaction hot pressing*. Material Science and Engineering A 325, pp. 126-130.

ess for Producing Particulate-Reinforced Titanium Matrix Composites, Patent files 22 September 1994, Indian Patent Office (New Delhi), No 1181/DEL/94.

Ranganath, S. (1997) *A Review on Particulate-reinforced Titanium Matrix Composites.* Journal of Materials Science 32, pp. 1-16.

Ranganath, S. and Subrahmanyam, J. (1991) *Impact response of AI_20_3 and AI_20_3-TiB_2 ceramic composites.* Journal of Mater. Sci. Lett.10, pp. 1297.

Ranganath, S., Roy, T. and Mishra, R.S. (1996) *Microstructure and deformation of TiB + Ti_2C reinforced titanium matrix composites.* Materials Science and Technology, volume 12, Issue 3, pp. 219-226

Ranganath, S., Roy, T. and Mishra, R.S. (1996) *Steady state creep behaviour of particulate-reinforced titanium matrix composites*. Acta mater, volume 44, No. 3, pp. 921-935, 1996

Ranganath, S., Vijayakumar, M. and Subrahmanyam, J. (1992) *Combustion-assisted synthesis of Ti-TiB-TiC composite via the casting route.* Materials Science and Engineering, A149, pp. 253-257.

Ravichandran, G., Tong, W., Christman, T. and Vreeland Jr., T. (1995) *Processing SiC-particulate reinforced titanium-based metal matrix composites by shock wave consolidation*. Acta Metallurgica Materialia, volume 43, issue 1, pp.235-250.

Ravichandran, K.S. and Panda, K.B. (2002) *Titanium composites with TiB whiskers*. Advanced Materials Processes. Volume 160, Isssue 10, pp.59-62.

Rawers, J.C., Wrzesinski, W.R., Roub, E.K. and Brown, R.R. (1990) *TiAl-SiC composites prepared by high temperature synthesis*. Materials Science and Technology, Volume 6, Issue 2, February 1990, pp. 187-191

Reilly, J.J. and Wiswall, R.H. (1974*) Formation and properties of iron–titanium hydride.* Inorg Chem, 13(1), pp.218ï 22.

Robertson, I.M and Schaffer, G.B. (2009) *comparison of sintering of titanium and titanium hydride powders.* Institute of Materials, Minerals and Mining, published by Maney, pp. 1-9.

Henriques, G. E. P. and Nobilo, M. A. A. (2006) *Vickers hardness of cast commercially pure titanium and Ti-6Al-4V alloy submitted to heat treatments*. Braz Dent J, vol. 17, No. 2, pp.126-129.

Sahay, S.S., Ravichandran, K.S., Atri, R., Chen, B. and Rubin, J. (1999) *Evolution of microstructure and phases in in situ processed Ti-TiB composites containing high volume fractions of TiB whiskers*. Jour0nal of Materials Research., volume 14, Issue 11, pp. 4214-4223**.**

Saito, T (2004) *The Automotive Application of Discontinuously Reinforced TiB-Ti Composite*. 2004 May JOM, pp.30-34.

Saito, T. (1995). *A cost-effective P/M Ti matrix composite for automobile use.* Advanced Performance Materials, (Kluwer Academic Publishers, Boston - Netherlands), 2, pp. 121-144.

Saito, T., Furuta, T. and Yamaguchi, T. (1993a). Proceedings 3rd International SAMPE Symposium (Tokyo: SAMPE, 1993), pp. 1810-1807.

Saito, T., Furuta, T. and Yamaguchi, T. (1993b). *Recent Advances in Titanium Metal Matrix Composites*, ed. F.H Froes and J. Storer (Warrendale, PA: TMS, 1995), pp. 33-44.

Saito, T., Takamiya, H. and Furuta, T. (1998). *Thermomechanical properties of P/M titanium metal matrix composites*. Materials Science and Engineering, A243, pp. 273-278.

Sandim, H. R. Z, Morante, B. V, and Suzuki, P. A. (2005) *Kinetics of thermal decomposition of titanium hydride powder using in-situ high-temperature X-ray diffraction (HTXRD)*. Materials Research, Vol.8, No 3, pp. 293-297.

Schmidt, H. Konetschny, C. and Fink, U. (1998) Electrochemical behaviour of ion implanted Tiï 6Alï 4V in ringerôs solution. Mater. Sci. Technol.14, pp 592ï 598.

Seagle, S.R. (1996) The state of the USA titanium industry in 1995, Mater. Sci. Eng. A213, pp 1ï 7.

n, S.K. and Borovinskaya, I.P. (1978) *Review Self-Propagating High Temperature Synthesis*. Sov. Pow. Met. Ceram. 17, pp. 424.

Shang, J. K. and Ritchie, R. O. (1990) *Monotonic and Cyclic Crack Growth in a TiC-Particulate-Reinforced Ti6Al-4V Metal-Matrix Composite.* Scripta Metallurgical Materialia, vol.24, pp. 1691-1694.

Smith, P.R. and Froes, F.H. (1984) *Developments in titanium metal matrix composites*. Journal of Metals, Volume 36, Issue 3, March 1984, pp. 19-26.

Soboyejo, W.O., Lederich, R.J. and Sastry, S.M.L. (1991) *High performance composites for the 1990s,* (eds. Das, S.K., Ballard, C.P., and Marikar, F.) TMS, Warrendale, PA, pp.127-141.

Soboyejo, W.O., Lederich, R.J. and Sastry, S.M.L. (1994) *Mechanical behavior of damage tolerant TiB whisker-reinforced in situ titanium matrix composites.* Acta Metallurgical Materialia. Vol. 42, No. 8, pp. 2579-2591.

Subrahmanyam, J., Vijayakumar, M. and Ranganath, S. (1989) *Thermochemistry of self-propagating high temperature synthesis of titanium diboride composites*, Met. Mater. Process. 1, pp. 105ï 112.

Subrahmanyam, J., Vijayakumar, M. and Ranganath, S. (1996) *On the In Situ Formation of TiC and Ti_2C Reinforcements in Combustion- Assisted Synthesis of Titanium Matrix Composites*. Metallurgical and Materials Transactions A, Vol. 27A, pp.237.

Swain, M.V. (1994) in: Chan, R.W., Haasen, P. and Kramer, E.K., Materials Science and Technology, volume 11, Weinhelm VCH, Verlagsgesellschaft mbh, pp. 183.

Thompson, M.S. and Nardone, V.C. (1991*) In-situ-reinforced titanium matrix composites*. Materials Science and Engineering, A144, pp.121-126.

Tian, Y.S, Chen, C.Z., Chen, L.B. and Liu, J.H. (2005) *Wear properties of alloyed layers produced by laser surface alloying of pure titanium with B_4C and Ti mixed powders*. Journal of Material Science 40, pp. 4387-4390.

Wang, D.Y. and Chen, C.Z. (2008) *Analysis of the growth morphology of TiB and the microstructure refinement of the coatings fabricated on Ti-6Al-4V by laser boronizing*. Journal of Crystal Growth and Design, vol. 8, No.2, pp. 700-703.

Tjong, S.C. and Ma, Z.Y. (2000) *Microstructural and Mechanical Characteristics of In Situ Metal Matrix Composites*. Materials Science and Engineering, 29, pp. 49-113.

Tong, X.C. (1998) *Fabrication of in situ TiC reinforced aluminum matrix composites Part I Microstructural Characterization*. Journal of Materials Science, volume 33, Issue 22, pp.5365-5374

Tong, X.C. and Fang, H.S. (1998) *Al-TiC Composites in situ–processed by ingot metallurgy and rapid solidification technology: Part I. Microstructural Evolution.* Metallurgical and Materials Transaction A, volume 29A, pp. 875-891.

Tong, X.C. and Fang, H.S. (1998) *Al-TiC Composites in situ–processed by ingot metallurgy and rapid solidification technology: Part II. Mechanical Behavior* Metallurgical and Materials Transaction A, volume 29A, pp. 893-902.

Tong, X.C., Shen, N.F. and Liu, B.C. (1995) *The structure of a rapidly solidified Al-Fe-Ti-C alloy***.** Journal of Materials Science 30, pp. 3680 3689

Tsang, H.T., Chao, C.G. and Ma, C.Y. (1996) *"Thermochemical calculation and mechanical properties of boride-reinforced Ti MMC produced by combustion synthesis"*, Scripta Materialia, Vol.35, No.8, pp. 1007-1012.

Tsang, H.T., Chao, C.G. and Ma, C.Y. (1997) *Effects of volume fraction of reinforcement on tensile and creep properties of in-situ TiB/Ti MMC.* Scripta Materialia, Vol. 37, No. 9, pp. 1359-1365.

Vallauri, D, Atias Adrian, I. C. and Chrysanthou, A. (2008) *TiC-TiB_2 Composites-A review of phase relationships, processing and properties*. Journal of the European Ceramic Society 28, pp. 1697-1713.

Merlini, M., Wang, Z. and Saxena, S.K (2008) *Phase stability of TiH2 under high pressure and temperatures.* International Journal of Hydrogen Energy, 33, pp. 6667-6671.

Villars, P and Calvert, L. D (1991) *Pearson's Handbook of Crystallographic Data for Intermetallic Phases,* 2nd edition. Ohio: ASM International, Metals Park.

Wang, M., Lu, W., Qin, J., Ma, F., Lu, J. and Zhang, D. (2006) *Effect of Volume Fraction of Reinforcement on Room Temperature Tensile Property of In Situ (TiB + TiC)/Ti Matrix Composites*. Materials and Design 27, pp. 494-498.

Wang, T., Eichhorn, F., Grambole, D., Grotzschel, R., Herrmann, F Kreissig, U. and Moller, W. (2002) *A new Ti/H phase transformation in the H^{+2} titanium alloy studied by x-ray diffraction, nuclear reaction analysis, elastic recoil detection analysis and scanning electron microscopy.* Journal of Physics: Condensation Matter, 14**,** pp. 11605ï 11614

Woo, O. T., Weatherley, G. C., Coleman, C. E. and Gilbert, R.W. (1985) *The Precipitation of gamma-deuterides (hydrides) in titanium. Acta Metallurgica*, 33(10), pp.1897-1906.

Xu, D., Lu, W.J., Yang, Z.F., Qin, J.N. and Zhang, D. (2005) *In Situ Technique for Synthesizing Multiple Ceramic Particulate Reinforced Titanium Matrix Composites (TiB + TiC + Y_2O_3)/Ti*. Journal of Alloys and Compounds 400, pp.216-221.

Yamada, M. (1996) An overview on the development of titanium alloys for non-aerospace application in Japan, Mater. Sci. Eng. A213, pp 8ï 15.

Yamada, S; Hirao, K., Yamauchi, Y. and Kanzaki, S. (2003) *High Strength B_4C-TiB_2 Composites Fabricated by Reaction Hot-Pressing.* Journal of the European Ceramics Society 23, pp. 1123-1130.

Yang, Z.F., Lu, W.J., Xu, D., Qin, J.N. and Zhang, D. (2006) *In situ synthesis of hybrid and multiple-dimensioned titanium matrix composites.* Journal of Alloys and Compounds 419, pp. 76-80.

1996) *Titanium '95 Science and Technology*, ed. P.A. Blenkinsop, W.J. Evans, and H.M. Flower (London: The Institute of Materials, 1996), pp. 2755-2762.

Yu, S.Y., Brodrick, C.W. Ryan, M.P. and Scully, J.R. (1999) Effects of Nb and Zr alloying additions on the activation behaviour of Ti in hydrochloric acid, J. Electrochem. Soc. 146 (12), pp 4429ï 4438.

Zadra, M, Casari, F, Girardini, L and Molinari, A (2008) *Microstructure and mechanical properties of CP-titanium produced by spark plasma sintering*. Powder Metallurgy, Vol. 51, No 1, pp. 59-65.

Zee, R., Yang, C., Lin, Y. and Chin, B. (1991) *Effects of boron and heat treatment on structure of dual-phase Ti-TiC*. Journal of Materials Science, Volume 26, Issue 14, July 1991, pp. 3853-3861.

Zhang, G.J., Jin, Z.Z. and Yue, X.M. (1999) *Reaction synthesis of TiB_2-SiC composites from TiH_2-Si-B_4C.* Materials Letters 25, pp. 97-100.

Zhang, H. and Kisi, E.H. (1997) *Formation of titanium hydride at room temperature by ball milling.* J. Phys Condens Matter, 9, L185.

Zhang, X., Lu, W., Zhang, D. and Wu, R. (1999) *In Situ Technique for Synthesizing (TiB + TiC)/Ti Composites.* Scripta Materialia Vol. 41, No. 1, pp. 39-46.

Zhu, S.J., Lu, Y.X., Wang, Z.G. and Bi, J (1993) in: *Antonio Miravete (Ed), Proceedings of the Ninth Internation Conference on Composite Materials* (ICCM/9), Vol.1, University of Zaragona and Woodhead Publishing Limited, pp. 549.

www.efunda.com/materials/alloys/titanium/titanium.cfm, 2008

Appendix A: *Calculation of Stoichiometric amount of TiH_2 and B_4C powder*

Based on the report of the work done by Ranganath et al., (1992) on the possible chemical reactions between Ti and B_4C particles, the similar reactions that can occur if Ti is replaced by TiH_2 include:

$$5TiH_2 \rightarrow Ti + 5H_2 \uparrow \text{----------} (1)$$

$$Ti + 5H_2 \uparrow + B_4C \rightarrow 4TiB + TiC + 5H_2 \uparrow \text{----------} (2)$$

Therefore,

$$5TiH_2 + B_4C \rightarrow 4TiB + TiC + 5H_2 \uparrow \text{----------} (3)$$

Then when there is excess xTi in form of $(x+5)$ TiH_2, equation 3 becomes

$$(x+5)TiH_2 + B_4C \rightarrow xTi + 4TiB + TiC + (x+5)H_2 \uparrow \text{----------} (4)$$

Analytically, equation 3 implies that 5moles of TiH_2 will react with 1mole of B_4C to form 4moles of TiB, 1mole of TiC plus $5H_2$ that goes off. Since 1mole of TiH_2 $= 47.88 + 2(1.01) = 49.9g$, this implies that 5moles of TiH_2 = $49.9 * 5 = 249.5g$ while I mole of B_4C = $4(10.81) + 12.01 = 55.25g$

Therefore, for there to be a complete reaction,

$$\Rightarrow 249.5gTiH_2 + 55.25gB_4C \rightarrow 4TiB + TiC + 5H_2 \uparrow \text{----------} (5)$$

…t (%) of reinforcements (TiB and TiC) and Ti matrix expected in the final titanium matrix composite (TMC):

This research intends to produce 10, 20, 40, 60, and 80vol % in situ reinforced particulate TMCs from TiH_2 and B_4C powders. The required stoichiometric amount of the starting powders to obtain for instance, 10vol% reinforced particulate TMC, in accordance with equation 4 is 98.16wt % TiH_2 and 1.84wt % B_4C and the detailed calculation shown below:

The parameters used include: density of TiH_2, $\rho_{TiH_2} = 3.91g/cm^3$; density of B_4C, $\rho_{B_4C} = 2.51g/cm^3$; density of Ti, $\rho_{Ti} = 4.51g/cm^3$; density of TiB, $\rho_{TiB} = 4.56g/cm^3$ and density of TiC, $\rho_{TiC} = 4.99g/cm^3$

To have TMC with 10vol. % reinforcements (TiB + TiC) implies that Ti matrix is the remaining 90vol. %. The composite is expected to consist of $xTi + 4TiB + TiC$, where xTi is the matrix and 4TiB + TiC are the reinforcements. Based on equation 4, the amount of TiB in the composite is 4moleTiB = 4*(47.88 + 10.81) = 234.76g. Then the volume of TiB in the composite is

$V_{TiB} = \frac{Mass}{Density} = \frac{234.76}{4.56} = 51.48245614cm^3$, and

$V_{TiC} = \frac{Mass}{Density} = \frac{59.89}{4.99} = 12.00200401cm^3$. The total volume of reinforcements,

$V_R = 51.48245614 + 12.00200401 = 63.48446015cm^3$

Since both reinforcements are to have a total volume fraction of 10% composite, then the percentage of each will be

(i) $Vol\%TiB = \frac{51.48245614}{63.48446015} * 10\% = 8.109457971\%$

(ii) $Vol\%TiC = \frac{12.00200401}{63.48446015} * 10\% = 1.890542029\%$

(iii) $Vol\%Ti = ?$

composite is, V_{xTi} then the total volume of the composite will be $V_T = V_{xTi} + 63.48446015$

This implies that $\frac{51.48245614}{V_T} * 100 = 8.109457971\%$ TiB, then

$$V_T = \frac{51.48245614}{8.109457971} = \frac{12.00200401}{1.890542029} = 634.8446015 cm^3$$

Therefore, $V_{xTi} = 634.8446015 - 51.48245614 - 12.00200401 = 571.3601413 cm^3$.

Similarly, the total mass of the total Ti in the composite will be

$$M_{xTi} = V_{xTi} * \rho_{Ti} = 571.3601413 * 4.51 = 2576.834237 g$$

Then, the number of moles of Ti in the composite will be

$$n = x = \frac{2576.834237}{47.88} = 53.8185931 \approx 54 moles$$

Therefore, for 10vol. % reinforced Ti, the stoichiometry equation 4 can now be written as

$$(54+5)TiH_2 + B_4C \rightarrow 54Ti + 4TiB + TiC + 59H_2 \uparrow ----------(6)$$

This implies that 59moles TiH_2 plus 1mole B_4C is required to achieved 90vol. %Ti (matrix) and 10vol. % reinforcements (TiB + TiC) composite. Then, 59moles $TiH_{1.924}$ = $59 * (47.88 + 1.01 * 2) = 2944.1 g$ and 1mole B_4C = $55.25 g$ which translate to 98.16wt % TiH_2 and 1.84wt % B_4C. The same procedure was used to obtain the percentage weight of TiH_2 and B_4C required for other volume fractions accordingly.

d compaction graphs generation.

Titanium and titanium hydride powder were compacted into cylindrical pellets as explained in chapter three. The data obtained using displacement die gauge was used to generate the compaction graphs in terms of relative density of the green compacts and the applied pressures. The data for both powders are shown below:

Table A 2. 1 : Compaction data for titanium powder

TITANIUM POWDER, -44µm

Mass of compact(M):4.929g

Diameter of die(D):18mm=1.8cm

Thickness of the compact(h):5mm=0.5cm

Volume of the compact=1.272345025cm^3 obtained from V = ´ (D^2/4)h

Density of the sample(mass/volume)=3.93g/cm^3, while theoretical density is 4.53g/cm^3

Applied force (KN)	Applied pressure (MPa)	Gauge Displacement (mm)	Thickness of compact (mm)	Thickness of compact (cm)	Volume (cm^3)	Green compact density (g/cm^3)	Green compact theor. density (%)
0	0	0	11.84	1.184	3.013	1.636	36.11
5	19.649	1.9	9.94	0.994	2.53	1.948	43
10	39.293	2.8	9.04	0.904	2.301	2.142	47.28
15	58.939	3.38	8.46	0.846	2.153	2.289	50.53
20	78.585	3.85	7.99	0.799	2.033	2.424	53.51
25	98.232	4.2	7.64	0.764	1.944	2.535	55.96
30	117.878	4.5	7.34	0.734	1.868	2.639	58.26
35	137.524	4.78	7.06	0.706	1.797	2.743	60.55
40	157.171	4.99	6.85	0.685	1.743	2.828	62.43
45	176.817	5.18	6.66	0.666	1.695	2.908	64.19
50	196.464	5.35	6.49	0.649	1.652	2.984	65.87
55	216.11	5.52	6.32	0.632	1.608	3.065	67.66
60	235.756	5.65	6.19	0.619	1.575	3.13	69.09
65	255.403	5.79	6.05	0.605	1.54	3.201	70.66
70	275.049	5.91	5.93	0.593	1.509	3.266	72.1
75	294.695	6.02	5.82	0.582	1.481	3.328	73.47
80	314.342	6.12	5.72	0.572	1.456	3.385	74.72
85	333.988	6.21	5.63	0.563	1.433	3.44	75.94
90	353.634	6.29	5.55	0.555	1.412	3.491	77.06
95	373.281	6.38	5.46	0.546	1.39	3.546	78.28
100	392.927	6.45	5.39	0.539	1.372	3.593	79.32

TITANIUM HYDRIDE POWDER, TiH_2, 1-7MICRON

Mass of compact(M):3.921g

Diameter of die(D):18mm=1.8cm

Thickness of the compact(h)t:5mm=0.51cm

Volume of the compact=1.2980cm^3
obtained from V = ´ (D^2/4)h

Density of the sample (mass/volume)=2.822g/cm^3, while theoretical density is 3.91g/cm^3

Applied force (KN)	Applied pressure (MPa)	Gauge Displacement (mm)	Thickness of compact (mm)	Thickness of compact (cm)	Volume (cm^3)	Green compact density (g/cm^3)	Green compact theor. density (%)
0	0	0	10.93	1.093	2.7817	1.41	36.06
5	19.649	2.44	8.49	0.849	2.1607	1.815	46.42
10	39.293	2.94	7.99	0.799	2.0335	1.928	49.31
15	58.939	3.24	7.69	0.769	1.9571	2.003	51.23
20	78.585	3.56	7.37	0.737	1.8757	2.09	53.45
25	98.232	3.78	7.15	0.715	1.8197	2.155	55.12
30	117.878	3.98	6.95	0.695	1.7688	2.217	56.7
35	137.524	4.16	6.77	0.677	1.723	2.276	58.21
40	157.171	4.3	6.63	0.663	1.6873	2.324	59.44
45	176.817	4.44	6.49	0.649	1.6517	2.374	60.72
50	196.464	4.58	6.35	0.635	1.6161	2.426	62.05
55	216.11	4.71	6.22	0.622	1.583	2.477	63.35
60	235.756	4.82	6.11	0.611	1.555	2.522	64.5
65	255.403	4.91	6.02	0.602	1.5321	2.559	65.45
70	275.049	5	5.93	0.593	1.5092	2.598	66.45
75	294.695	5.08	5.85	0.585	1.4888	2.634	67.37
80	314.342	5.17	5.76	0.576	1.4659	2.675	68.41
85	333.988	5.26	5.67	0.567	1.443	2.717	69.49
90	353.634	5.33	5.6	0.56	1.4252	2.751	70.36
95	373.281	5.4	5.53	0.553	1.4074	2.786	71.25
100	392.927	5.47	5.46	0.546	1.3896	2.822	72.17

Appendix A.3: Theoretical density calculation

It is important to estimate the theoretical density of the composites formed after sintering of the admixed powders in order to ascertain the densification obtained from the pressureless and hot pressing techniques. It was assumed that the reaction between Ti and B_4C was complete, TiC, TiB and Ti are the only formed phases and no significant amount of TiB_2 forms during the sintering reaction. The theoretical density is determined from the expression;

$$Theoretical...density = \frac{100}{\left(\frac{wt\%Ti}{\rho_{Ti}}\right)+\left(\frac{wt\%A}{\rho_{A}}\right)+...}$$

ρ_A= *density of the resulting sintered phases (TiB and TiC)*

The parameters used include: density of TiH_2, $\rho_{TiH_2} = 3.91 g/cm^3$; density of B_4C, $\rho_{B_4C} = 2.51 g/cm^3$; density of Ti, $\rho_{Ti} = 4.51 g/cm^3$; density of TiB, $\rho_{TiB} = 4.56 g/cm^3$ and density of TiC, $\rho_{TiC} = 4.99 g/cm^3$.

listribution of starting powders:

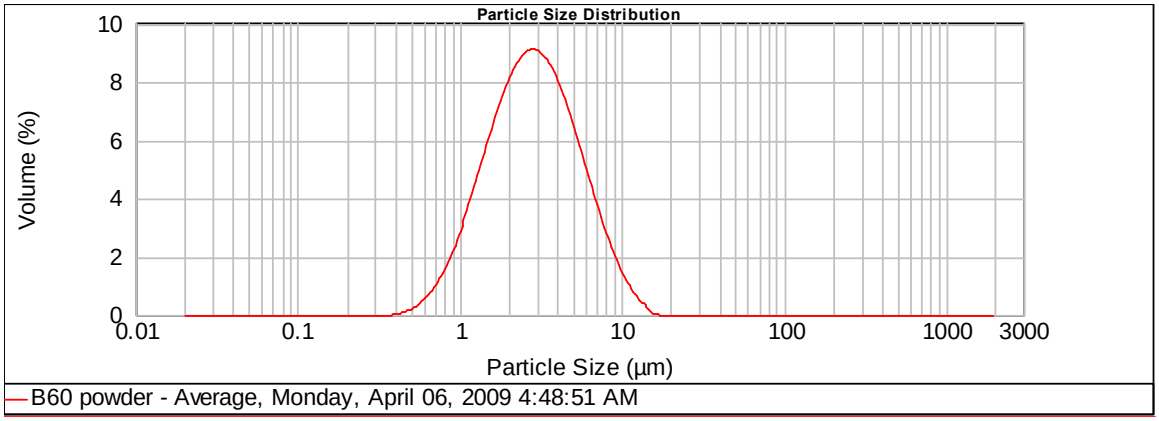

Figure B. 1: Particle size analysis of Pure B_6O powder: d (0.1) = 1.214µm, d (0.5) = 2.819 µm, d (0.9) = 6.440µm

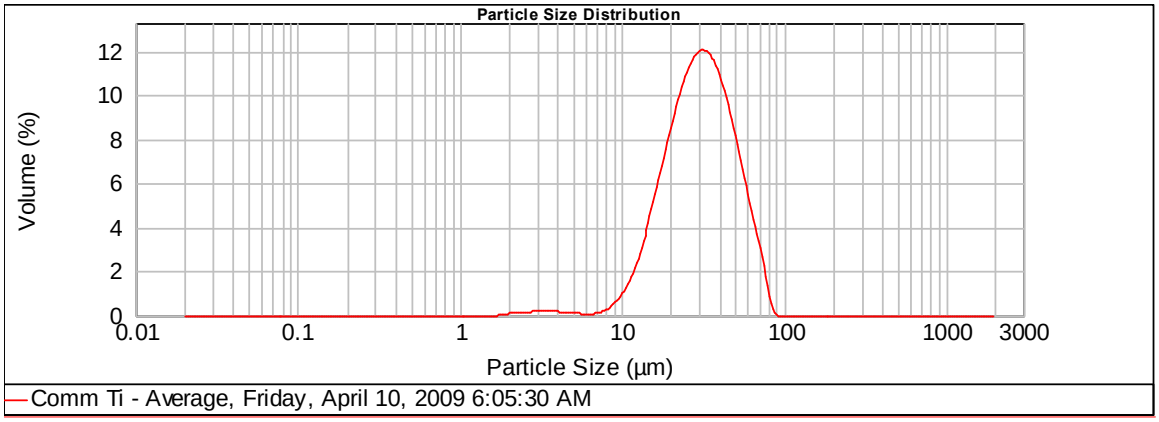

Figure B. 2: Particle size analysis of commercially obtained titanium, Ti-powder: d (0.1) = 15.672µm, d (0.5) = 30.492µm, d (0.9) = 55.166µm

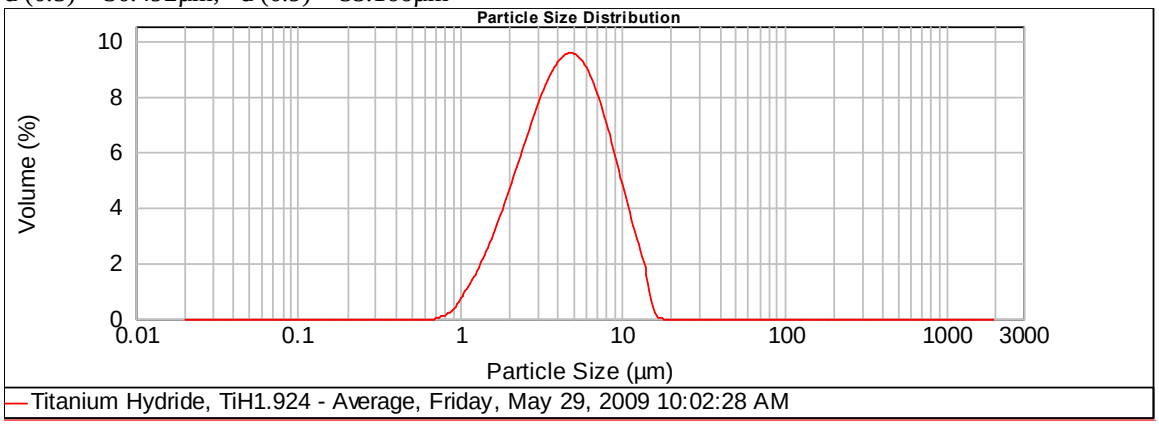

Figure B. 3: Particle size analysis of commercially obtained titanium hydride powder: d (0.1) = 1.925 µm, d (0.5) = 4.473 µm, d (0.9) = 9.409 µm

of used starting powders and sintered samples:

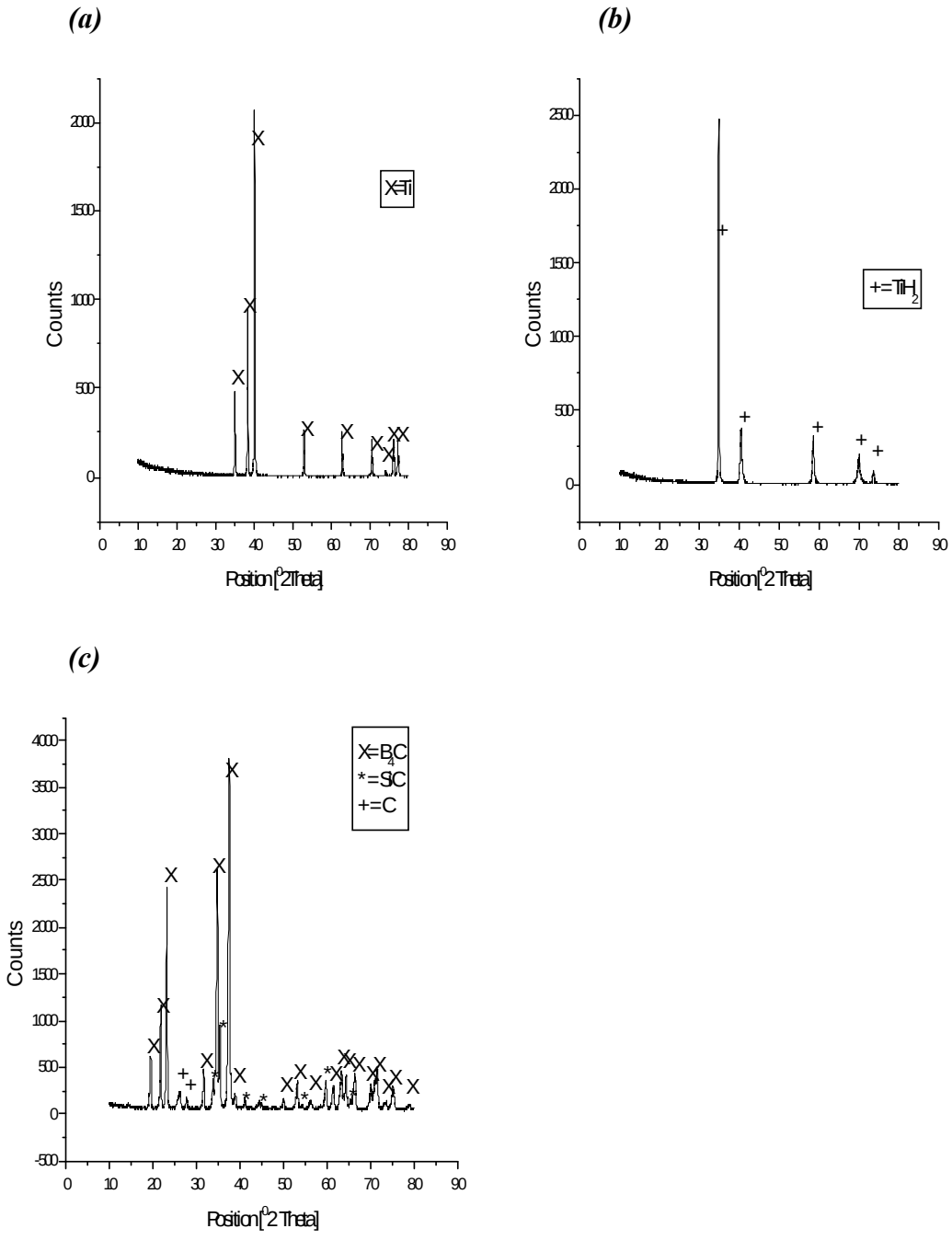

Figure C. 1: XRD patterns of (a) titanium (-44ε m), (b) titanium hydride and (c) boron carbide powder

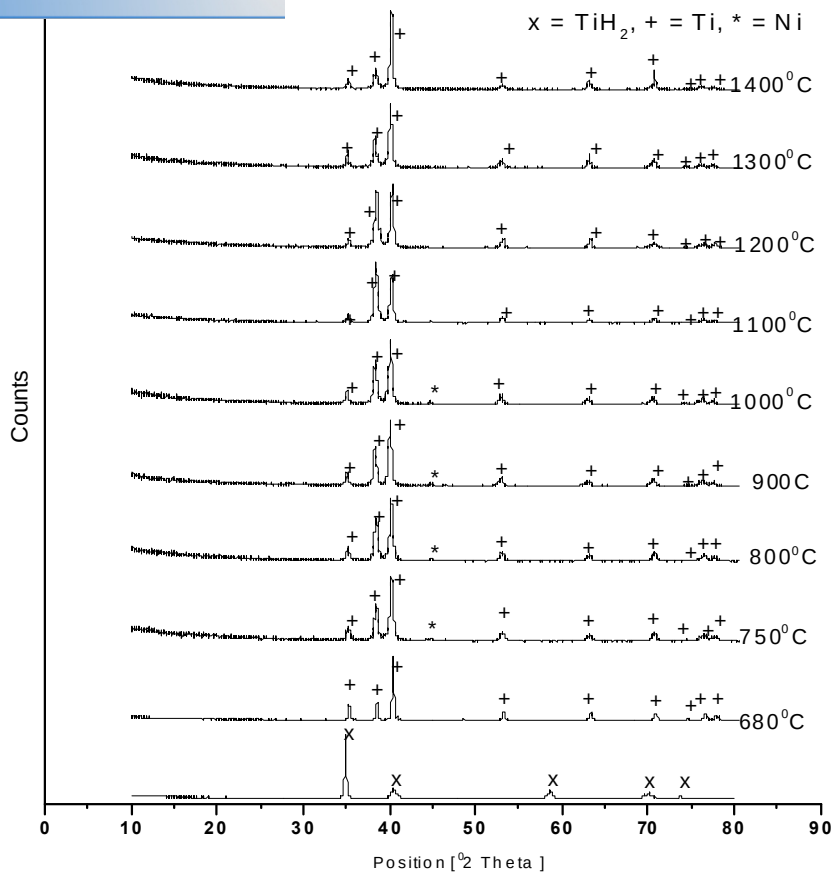

Figure C. 2: XRD patterns of dehydrogenated TiH_2 sample at different temperatures

Appendix D: *SEM micrographs of sintered and hot pressed samples*

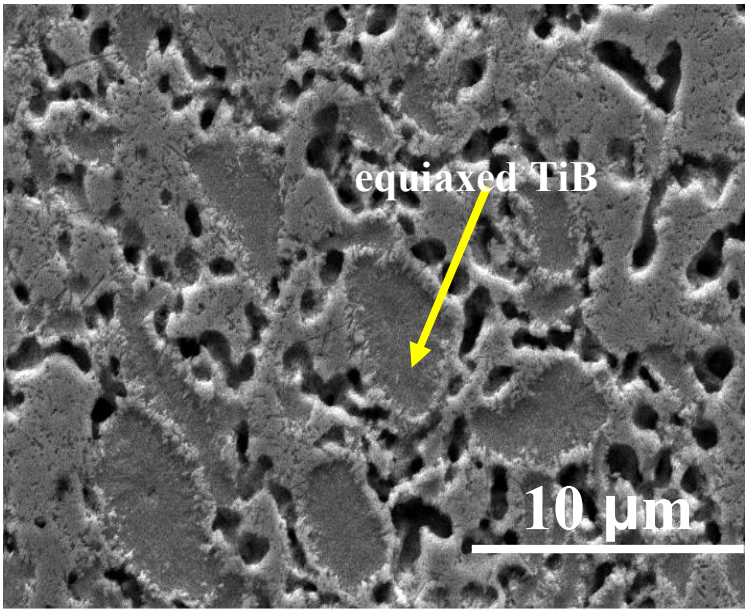

Figure D. 1: SEM (SE) image of the pressureless sintered sample 40PLTMC1200 showing equiaxed TiB and porosity

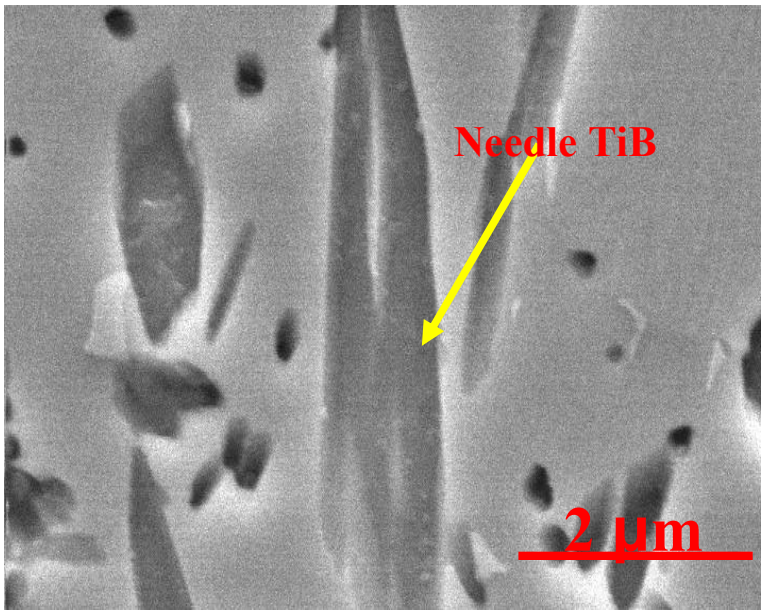

Figure D. 2: SEM (SE) image of the pressureless sintered sample 40**PL**TMC**1400** showing TiB formed

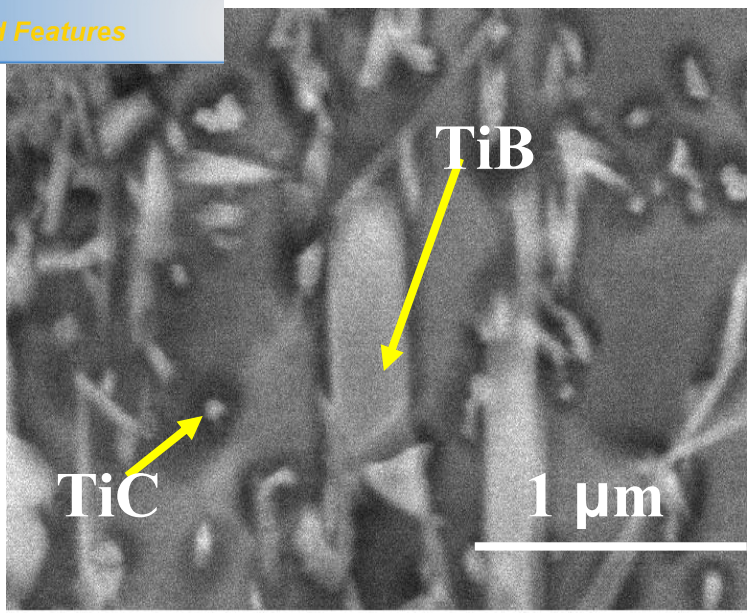

Figure D. 3: SEM image of hot pressed sample 20**HP**TMC**1400** showing different sizes of TiB and TiC formed

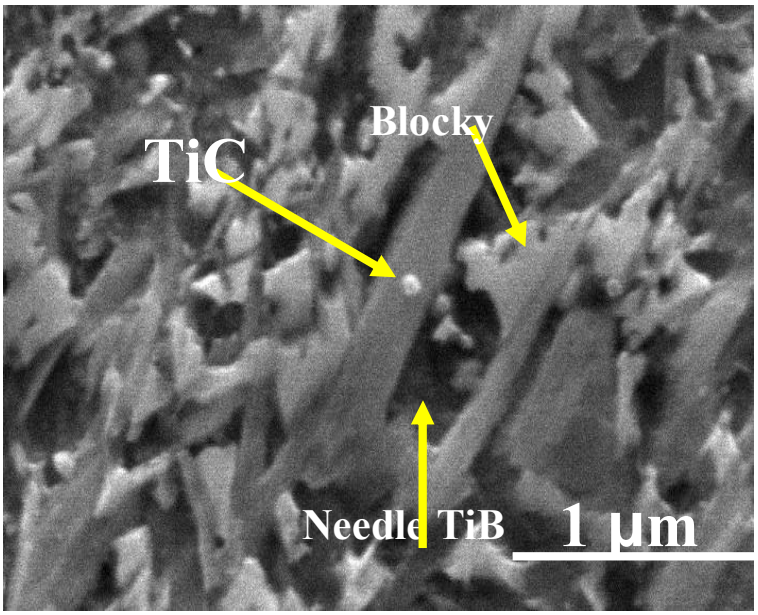

Figure D. 4: SEM image of hot pressed sample 40**HP**TMC**1400** showing types of TiB formed

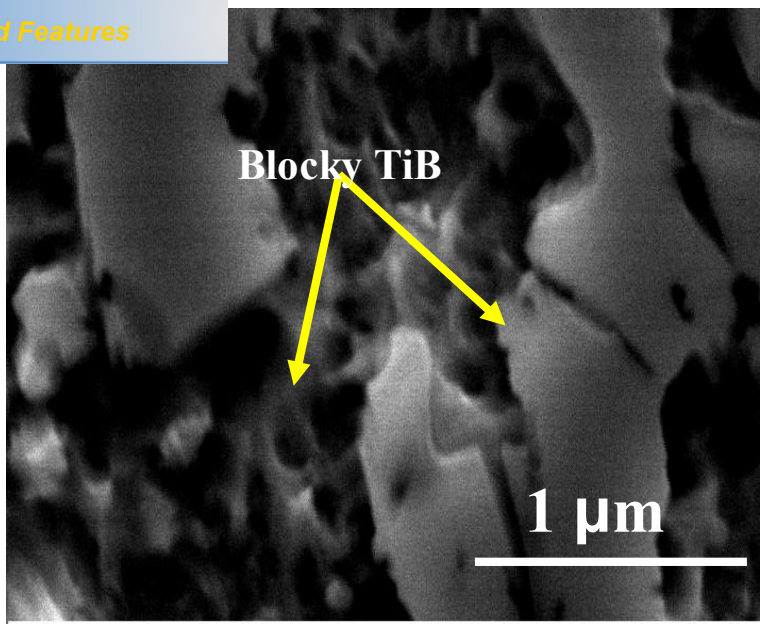

Figure D. 5: SEM image of hot pressed sample 60**HP**TMC**1400** showing higher magnification of blocky TiB formed